TALLINN UNIVERSITY OF TECHNOLOGY
DOCTORAL THESIS
31/2018

Modeling and Implementation of Linear Energy Prediction for Energy Harvesting in Intermittently Powered Wireless Sensor Nodes

FAISAL AHMED

TTÜ PRESS

TALLINN UNIVERSITY OF TECHNOLOGY
School of Information Technologies
Thomas Johann Seebeck Department of Electronics

This dissertation was accepted for the defence of the degree of Doctor of Philosophy in Electronics and Telecommunication on MAY 10th, 2018.

Supervisor: Professor Yannick Le Moullec
Thomas Johann Seebeck Department of Electronics
Tallinn University of Technology, Tallinn, Estonia

Co-supervisors: Senior Research Scientist Paul Annus
Thomas Johann Seebeck Department of Electronics
Tallinn University of Technology, Tallinn, Estonia

Senior Research Scientist Gert Tamberg
Department of Cybernetics, Division of Mathematics
Tallinn University of Technology, Tallinn, Estonia

Opponents: CNRS Research Director Jean-Philippe Diguet
French National Centre for Scientific Research, LAB-STICC/UBS
Lorient, France

Associate Professor Sébastien Bilavarn
Polytech Nice Sophia
Sophia-Antipolis, France

Defence of the thesis: JUNE 15th, 2018, Tallinn

Declaration:
Hereby I declare that this doctoral thesis, my original investigation and achievement, submitted for the doctoral degree at Tallinn University of Technology has not been submitted for any academic degree.

Faisal Ahmed --
signature

European Union
European Social Fund
Investing in your future

ISSN 2585-6898 (publication)
ISBN 978-9949-83-269-9 (publication)
ISSN 2585-6901 (PDF)
ISBN 978-9949-83-270-5 (PDF)

TALLINNA TEHNIKAÜLIKOOL
DOKTORITÖÖ
31/2018

Katkendliku toitega traadita sensorsõlmede energiakorje tulemuse lineaarne ennustus, modelleerimine ja rakendused

FAISAL AHMED

TTÜ KIRJASTUS

Contents

LIST OF PUBLICATIONS

The work of this thesis is based on the following publications. Copies of these publications can be found in the appendix of the thesis.

1. **Faisal Ahmed,** Yannick Le Moullec, Paul Annus, Syed Ashad, “Analytical Evaluation of Indoor Energy Harvesting Technologies for WSNs with FYPSIM Framework”, In Proceedings of the International Conference on Industrial Informatics and Computer Systems (CIICS), Sharjah, March 2016; pp. 1–6. (ETIS 3.11)
2. **Faisal Ahmed,** Tauseef Ahmed, Yar Muhammad, Yannick Le Moullec, Paul Annus, “Operating Wireless Sensor Nodes without Energy Storage: Experimental Results with Transient Computing”, MDPI Electronics, Vol. 5, No. 4, 2016. (ETIS 1.1).
3. **Faisal Ahmed,** Gert Tamberg, Yannick Le Moullec, Paul Annus, “Dual-Source Linear Energy Prediction (LINE-P) Model in the Context of WSNs”, MDPI Sensors, Vol. 17, No.7, 66, 2017. (ETIS 1.1).
4. **Faisal Ahmed,** Yannick Le Moullec, Gert Tamberg, Paul Annus, “Autonomous Wireless Sensor Networks: Implementation of Transient Computing and Energy Prediction for Improved Node Performance and Link Quality”, (2018). (ETIS 1.1). [Revised-version submitted to The Computer Journal, Oxford Academic; currently under (minor) revision]
5. **Faisal Ahmed,** Gert Tamberg, Yannick Le Moullec, Paul Annus, “Adaptive LINE-P: An Adaptive Linear Energy Prediction Model for Wireless Sensor Network Nodes ”, MDPI Sensors, Vol. 18, No. 4, 2018. (ETIS 1.1).

---

1 For readers unfamiliar with the Estonian research classification:

ETIS 3.1: Articles/chapters in books published by the publishers listed in Annex (including collections indexed by the Thomson Reuters Book Citation Index, Thomson Reuters Conference Proceedings Citation Index, Scopus)

ETIS 1.1: Scholarly articles indexed by Web of Science, Science Citation Index Expanded, Social Sciences Citation Index, Arts & Humanities Citation Index and/or indexed by Scopus (excluding chapters in books)

OTHER RELATED PUBLICATIONS

I. **Faisal Ahmed,** Yannick Le Moullec, Paul Annus, “FYPSim: Evaluation Tool for Solar-based Energy Harvesting for WSNs," Int'l Journal of Bioelectromagnetism, 17(2), 75–86, (2015). (ETIS 1.2).

II. **Faisal Ahmed,** Yannick Le Moullec, Paul Annus, “FYPSIM: An Estimation Framework for Energy Harvesting and Energy Prediction for WSNs'', IEEE ICCE-TW 2016, May 2016. (ETIS 3.1)

III. Tauseef Ahmed, **Faisal Ahmed,** Yannick Le Moullec, “Optimization of Channel Allocation in Wireless Body Area Networks by Means of Reinforcement Learning”, 2016 IEEE Asia Pacific Conference on Wireless and Mobile (APWiMob), Bandung, 2016, pp. 120-123. (ETIS 3.1)

AUTHOR'S CONTRIBUTION TO THE PUBLICATIONS

The author's main contributions to the papers are briefly described in what follows. Note that this section describes the role of the author of this PhD thesis; the scientific contributions are described in the introductory chapter later on in the thesis.

I. The author of this PhD thesis proposed the hybrid energy harvesting model where three energy sources are combined and their sum is multiplied by an efficiency coefficient. The author designed and developed the system-level framework named FYPSim in Matlab. The author analyzed the experimental results with the help of his supervisors. These results illustrate the capabilities of FYPSIM to deal with different energy sources such as RF, solar, and thermal with different sensor nodes. The author has written a significant part of the paper with the guidance and feedback of his supervisors.

II. The author of this PhD thesis is the main contributor of this paper. In this paper, he designed, implemented, and verified the practical feasibility of transient computing with three energy harvesting sources on a non-volatile wireless sensor node. The author performed all the simulation and practical experiments under the guidance of his supervisors. The author has written a significant part of the paper with the advice of his supervisors.

III. The author of this PhD thesis proposed the so-called LINE-P (all cases) energy prediction model. The author also conducted a comparative analysis of the LINE-P model against the state-of-the-art with suggestions from his supervisors. The author gathered real data sets (energy profiles) from reliable sources, thereafter deployed them into FYPSim and then conducted the experiments. Based on the results analysis, the author illustrated that the proposed LINE-P model is more accurate than state-of-the-art models. The author has written a significant part of the paper using his supervisors' advice.

IV. The author of this PhD thesis proposed the novel idea behind this paper. He suggested to combine two different modalities, namely transient computing and the above-mentioned LINE-P energy prediction model. In this paper, the author (in cooperation with an intern student) generated all the results based on the real implementation of a peer-to-peer network application. This combined transient computing and energy prediction approach improved the system (node)'s performance and as well as the link quality, while communicating with its peer node. The author has written a significant part of the paper with the advice and feedback of his PhD supervisors.

V. The author of this PhD thesis proposed the Adaptive LINE-P (all cases) model. This is an extension of the above-mentioned LINE-P (all cases) model and addresses the so-called fixed parameter weighting factor issue by incorporating a dynamic parameter based on the energy source condition (e.g. weather). In addition, the author also proposed an energy profile compression technique based on the Hann kernel (sampling theory) to accommodate the limited memory of the WSNs sensor node. With the help of his supervisors, the author designed and performed the experiments. The author has written a significant part of this paper under the supervision and guidance of his supervisors.

Abbreviations

Explanations of the abbreviation used in the thesis.

AESA	Accurate Solar Energy Allocation
ARR	Average-Receiving Rate
CTPL	Compute Through Power Loss Utility
CRC	Cycling Redundancy Check
EH	Energy Harvesting
EWMA	Exponential Weighted Moving Average
Elia	Belgium's electricity transmission system operator
EP	Energy Prediction
FRAM	Ferroelectric RAM
FYPSIM	Faisal Yannick Paul Simulator
IoT	Internet of Things
IEEE	Institute of Electrical and Electronics Engineers
LINE-P	Linear Energy Prediction
MAC	Medium Access Control layer
MSE	Mean Square Error
MAE	Mean Absolute Error
PHY	Physical layer
Pro-Energy	PROfile Energy prediction model
Pro-Energy-VLT	PROfile Energy prediction model Variable-Length TimeSlot
PG&E	Pacific Gas and Electric Company
QoS	Quality of Service

QoE	Quality of Experience
QL-SEP	Q-Learning
RF	Radio Frequency
RSA	Rivest, Shamir, and Adleman
RX	Receiving
SDG&E	San Diego Gas & Electric Company
SCE	Southern California Edison Company
SRRL	Solar Radiation Research Laboratory
TC	Transient Computing
TX	Transmitting
TI	Texas Instrument
TEG	Thermoelectric Generators
UD-WCMA	Universal Dynamics Weather Conditioned Moving Average
WSN	Wireless Sensor Network
WCMA	Weather Conditioned Moving Average
WLAN	Wireless LAN
WBAN	Wireless Body Area Network

INTRODUCTION AND MOTIVATION

Recent research and development in the field of Internet of Things (IoT) remarkably changed the entire scenario of the integration of the physical domain with internet-based computer networks. In particular, IoT is concerned with the interconnection and integration between computers and so-called smart devices (“things”). Back in 2008, the U.S. National Intelligence Council’s forecast was that *”by 2025 Internet nodes may reside in everyday things –food packages, furniture, paper documents, and more*” [1]. This trend in the emergence of IoT, including wireless sensor networks (originally known as ‘smart dust’), has since then been confirmed; recent reports indicate that “The global Internet of Things (IoT) market is projected to grow from $2.99T in 2014 to $8.9T in 2020, attaining a 19.92% compound annual growth rate (CAGR).” [2].

Generally, the term IoT can be seen as building upon the concept of wireless sensor network (WSN). They can sense data and then gather it, and afterwards send it to the network via a sink (also known as gateway) [3]-[6]. Significantly, WSN is considered as one of the enabling technologies for the realization of the IoT. These low power devices are essentially miniaturized radio communication units with some physical quantity measurement capabilities. They are applicable in a very wide range of scenarios, including but not limited to, e-health, environment, industry, military, etc. However, the life span of the WSNs nodes depends on their energy storage capacity (e.g. battery source), and this limited energy is one of the most significant constraints for the successful deployment of IoT/WSN applications.

The incredible growth of the IoT provides solutions to various problems. At the same time, the IoT raises some concerns as well; for instance, in [7] it is expressed that the global electricity consumption of IoT devices had exceeded 615 TWh in 2013 and that this demand will further increase up to 1140 TWh by 2025, which will be the 6% of the total electricity consumption in the world. In addition, based on statistics [7], it is expected that there will be 23 billion battery-powered IoT devices in 2025. Thus, the production of batteries for the IoT will put an extra load of 2 TWh in 2025.

Given these challenges, energy harvesting (EH), also known as energy scavenging, has recently gained strength in the fields of renewables and sustainability, especially in the context of fully autonomous WSNs nodes with application to the IoT.

In relation to the above, EH is one of the explored solutions for powering WSN nodes and/or for extending their life span. EH is a process that extracts energy from one source (typically from the environment) and converts it to another type (in our context, electric energy) [8]. There are numerous energy-harvesting technologies proposed in the literature such as radio-frequency (RF), thermal, vibration, thermoelectric, piezoelectric, wind, and solar [9]-[10]. Generally, solar energy harvesting is more efficient than the other technologies. Research has shown that energy harvesting is not capacity–limited as compared to non-rechargeable batteries; thus, WSN nodes can potentially operate for a very long time [11]. EH can be used either as an alternative to batteries or other energy storage sources (such as super-capacitors) or cascaded with them and is highly beneficial [12]. Besides, for further increasing the life-span of WSN nodes, various solutions have been presented in the literature; for instance, energy-aware protocols and duty-cycling [13]-[16], task scheduling, transient computing (Publication 2), energy prediction (Publication 3), data prediction [17], and mobility cut down the power usage, if such solutions have sufficiently low overheads [18]. In Chapter 1 of this PhD thesis, the author gives a general introduction of a typical WSN node and its architecture; thereafter, the author discusses the energy harvesting technologies and the related modeling and the contribution in terms of the hybrid energy-harvesting model.

Transient computing (TC) is an emerging approach that can be used to deal with the intermittent nature of EH. The fundamental idea behind TC is to stop (in the ideal case, to pause) and to restart (in the ideal case, to resume) the WSN node activities depending on the available energy. This approach can even eliminate the battery energy source and drive WSN nodes directly from the energy harvester. This kind of approach is especially suitable for applications which do not require 24/7 monitoring or that are tolerant to delays and/or errors. In this work, a TC mechanism has been implemented by means of a non-volatile microcontroller. In short, in case of low energy, a WSN node stops operating and saves an image of its configuration and data. Afterwards, if energy is again available then the image is restored and the node proceeds operating. Nevertheless, such autonomous (battery-less) devices bring new dynamics and challenges to programmers and computer architects [19], in particular regarding the various ways of the backup process depending on the application requirements, e.g. when to save the microcontroller state/data and how much of that state/data to save [20]-[23]. In the literature, TC mechanisms exploit two main types of non-volatile memory technologies, namely flash or more recently ferroelectric RAM (FRAM). In addition, two types of TC approaches have been proposed in the literature, namely hardware-driven and software-driven [24]-[27].

As of today, the most power hungry component is still the radio's chip of the WSNs node (Publication 4). Thus, appropriate power and energy management of the WSNs node's operations, especially of the radio transmission/reception based on the estimated energy availability could be the most effective way of saving energy. Therefore, the accuracy and the robustness of the prediction model are essential when the operations of WSNs node are optimized and rely on the estimated energy [26]. Thus, energy prediction is expected to be a precious tool to estimate the energy available in the near future and to guide WSN nodes to make decisions related to their operations. To turn this assumption into reality, numerous estimation approaches have been proposed in the literature. However, their accuracy and reliability is still questionable. Typically, solar and wind are uncontrollable sources of energy, thus their accurate prediction is quite challenging, especially for longer time-period horizons.

There has been approaches for TC and prediction models proposed in the literature on an individually basis. This PhD work presents a novel idea that combines these two modalities simultaneously to improve the system performance and link quality. For this, in Chapter 2 the author firstly assesses the practical feasibility of energy harvesting combined with TC on an FRAM-based WSN node. Next, the author describes the proposed linear energy model (LINE-P). Finally, the author presents the joint implementation of TC and LINE-P in a peer-to-peer network. The results show that the implementation of combined modalities improves the system performance (node), the link quality, and increases communication stability by 50%.

Apart from that, this PhD work is based on four other contributions, namely, i) 'FYPSIM' a system-level framework which allows the rapid exploration of design alternatives; ii) 'LINE-P' a mathematical modeling of dual energy sources which is highly accurate, adaptable and of low complexity in terms of computational power;

iii) 'Adaptive LINE-P', i.e. an extension of LINE-P; iv) a compression technique that reduces the memory overheads by approximately 75% in a wireless node.

It is noted that most of the existing prediction models are somewhat limited because they consider a fixed weighting parameter [26] based on the shorter time-period horizon [8], [26]-[30]. Thus, in Chapter 3 of this PhD thesis, the author addresses such issues by proposing Adaptive LINE-P. This proposed model is based on variable-length time slots (in contrast to [31]) and considers an adaptive weighting parameter depending upon the energy profiles (in contrast to [26]). The accuracy of the estimation results yielded by the proposed model is up to 90%. Furthermore, the author proposes a compression method that reduces the energy profiles by 4 and reduces the memory overhead in the WSN node by 50%.

The problem statement and research questions related to the above are formulated in what follows.

PROBLEM STATEMENT AND RESEARCH QUESTIONS

Over the last few years, significant research advances have been made in the field of TC and EP under the umbrella of EH. However, these advances have mostly been done independently from each other. Thus, there are still various open issues that need to be addressed, specifically in the context of autonomous WSN nodes. In relation to above, the major issues addressed in this work are:

Firstly, identifying suitable energy harvesting mechanisms to power the WSN nodes; secondly, dealing with the intermittent nature of EH sources (including power loss) by means of the simultaneous exploitation of EH and TC; and thirdly managing the available energy and in turn reducing the adverse effects of power losses by means of EP in addition to EH and TC.

More specifically, this research work seeks to answer the following four main research questions:

1. How to rapidly evaluate the feasibility of existing and emerging energy harvesting technologies in the context of WSNs/IoT and what kind of models are sufficient to enable the above?
2. How to combine and implement the concepts of EH and TC in WSN nodes and what are the practical possibilities and limitations of such a joint approach?
3. How to design an EP model that can be used with several types of EH sources and how to reduce its computational overhead so that it can be implemented on a resource-constrained WSN node? In addition, how to further improve the EP model in terms of adaptability and reduced memory overhead?
4. How to combine and exploit EH, TC, and EP to make the best use of the available energy, i.e., control the quality of service of the application executing on a WSN network that include a WSN node solely powered by EH?

In the following author have identified the novelty in this PhD work.

STATEMENT OF NOVELTY

A first novel aspect in this PhD work is the proposed FYPSIM framework, which enables to rapidly determine the feasibility of EH sources for WSN nodes.

Furthermore, in order to deploy accurate and reliable energy predictors, the proposed LINE-P and Adaptive LINE-P prediction models bring significant benefits to the design and implementation of WSN nodes. The author proposes both energy prediction and energy profile compression methods as well as FYPSIM (simulator) tool in the domain of WSN nodes.

In particular, the author illustrates that utilizing the proposed multiple energy sources based algorithms and compression technique increases the WSN node performance and prolong its life by harvesting the energy from the environment and making best use of it thanks to the accurate estimates, as well as reduces the memory overheads by around 75%. Furthermore, the combination of EH with TC and EP improves the reliability and link quality, as illustrated for a peer-to-peer wireless communication.

The work that has been conducted in relation to the above questions has resulted in the contributions that are summarized in what follows.

CONTRIBUTION OF THIS PhD THESIS

The contributions described in this PhD thesis and detailed in the appended publications comprises five parts:

A. A system-level framework, named FYPSim, has been designed and implemented. FYPSim provides support for modelling not only various single EH technologies (solar, thermal, RF, etc.) but also hybrid EH technologies, a feature lacking in most WSN frameworks. Experiments conducted with FYPSim illustrate how the framework can be used to evaluate various EH sources (indoor solar, airflow, and RF) for powering WSN nodes from different vendors (Dresden AVR, Atmel ATmega, SenseNode, and WiSense) under varying activity rates.

B. The feasibility to operate WSN nodes without energy storage has been evaluated by means of an experimental setup. The setup comprises various EH sources (RF, solar, thermal, or hybrid) and several wired and wireless sensor nodes; TC has been implemented on a non-volatile node (FRAM-based). Among other things, the experimental results show that EH combined with TC in the non-volatile WSN node is indeed feasible thanks to the implementation of Texas Instrument's Compute Through Power Loss mechanism that allows pausing and resuming the node's operation depending on the available energy.

C. A new EP model, LINE-P (for Linear Energy Prediction), has been proposed and evaluated. LINE-P builds upon sampling and approximation theory and features a so-called symmetrical kernel. LINE-P is suitable for dual EH sources and various data time intervals, as opposed to previous models that are only recommended for a particular data time interval. LINE-P also enables adjusting/resizing the kernels, which makes it compatible with solar powered WSNs, a feature generally lacking in existing solar-based prediction models. The simulation results on real-life energy datasets show that the prediction accuracy is up to ca. 98% for LINE-P for solar energy, and up to ca. 96% for wind-based prediction, while keeping the computational overheads acceptable.

D. A TC-based scheme used to reduce the adverse effects of power losses in WSN nodes that operate solely on EH has been proposed and implemented. LINE-P EP model (contribution C. above) is integrated in the scheme to manage the energy by allowing firing communication tasks only if sufficient and stable energy is predicted. The scheme has been evaluated for a peer-to-peer wireless setup. The results illustrate that the combined TC and EP modalities require only 15% of the node's memory and that the LINE-P (Case-II)'s accuracy is up to 98% for consistent weather and up to 90% for inconsistent weather. In addition, the results illustrate that the proposed approach yields an average receiving rate up to 94.6%.

E. The last contribution is Adaptive LINE-P that addresses the fixed weighting parameter issue, found in most EP models, by calculating adaptive weighting parameters based on the stored energy profiles. In addition, a profile compression method is proposed to reduce the memory requirements. The simulation results on real-life energy datasets indicate that Adaptive LINE-P accuracy is up to 90-94% and that the profile compression method can reduce memory overheads by 50%.

The above contributions are reflected in the appended research papers, as shown in Table 1.

Table 1. Relation between the research papers and the contributions

Contribution	Paper I	Paper II	Paper III	Paper IV	Paper V
A	✓	✓			
B		✓		✓	
C			✓	✓	
D				✓	✓
E					✓

THESIS OUTLINE

This PhD thesis comprises an introduction, three chapters and a conclusion.

Chapter 1

This chapter describes the general architecture of a WSN node and its operations. Afterwards, EH technologies are discussed. Finally, the proposed hybrid EH modelling and framework are introduced (they are described in further details in Publication 1).

Chapter 2

This chapter introduces the concept of TC and its various types, as well as the related state-of-the-art. This chapter discusses the various energy prediction models along with the related state-of-the-art, based on the different time-period horizons. Further details about EP, the assessment of the proposed model, and the results can be found in Publications 2 and 3. In addition, the chapter introduces the combined implementation of TC and EP; further details can be found in Publication 4.

Chapter 3

This chapter describes Adaptive LINE-P, i.e. the extension of the LINE-P model, which addresses the fixed parameter-weighting factor by proposing an adaptive weighting factor based on the stored energy profile. Thereafter, the author discusses the energy profile compression technique which provides a solution for explicitly low memory sensor node. Further details can be found in Publication 5.

The last chapter comprises various points, namely a conclusion of the PhD work, a summary of the claims, and a few suggestions for future work.

1. WIRESLESS SENSOR NODES AND EH MODELLING

This chapter gives a general overview of a typical WSN node and its architecture, afterwards presents some background information on EH technologies, and then introduces the author's contribution regarding the modelling of EH and in particular hybrid EH.

Regarding EH modelling, various simulators have been proposed in the literature to explore the feasibility of an EH-powered WSN before its actual deployment. Thus, this chapter also discusses the comparison between the proposed framework named FYPSim and WSN simulators. Further detailed information relevant to the main contribution can be found in Publication 1.

With the advent of the IoT, the design and implementation of WSNs and WSN nodes is getting a lot of attention from both the scientific community and the industry, in particular with respect to their energy efficiency. Generally, a sensor node can be seen as a small embedded system or electronic component that contains various elements such as a microcontroller, an RF module, an energy storage device (if needed), a power management mechanism (hardware circuit and/or software function), a possible energy harvester, and the sensor itself (e.g. for temperature, humidity, etc.), as generically represented in Figure 1. The basic function of the sensor node lies in data acquisition, data processing and data communication. Usually, a sensor node is implemented on a resource-constrained platform; it has limited computational power, memory, battery capacity, and communication bandwidth.

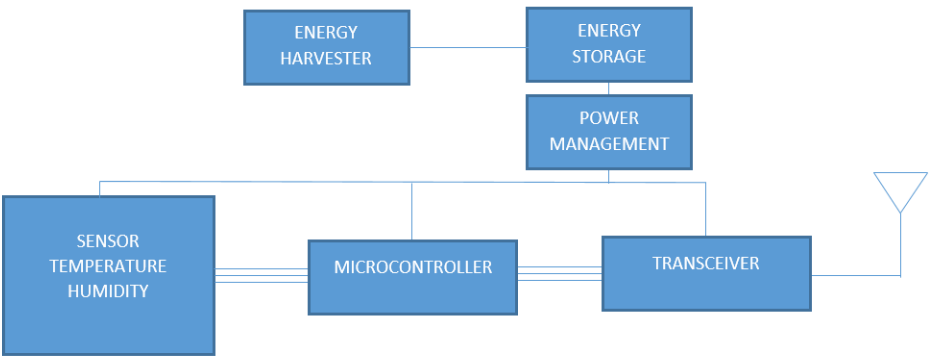

Figure 1. Generic block diagram of a wireless sensor node.

A single sensor node only performs basic tasks (sense and transmit the data). The combination of multiple such sensor nodes, together with central node(s) such as a coordinator and gateway constitutes a wireless sensor network [3]-[4], [32]-[33], as shown in Figure 2.

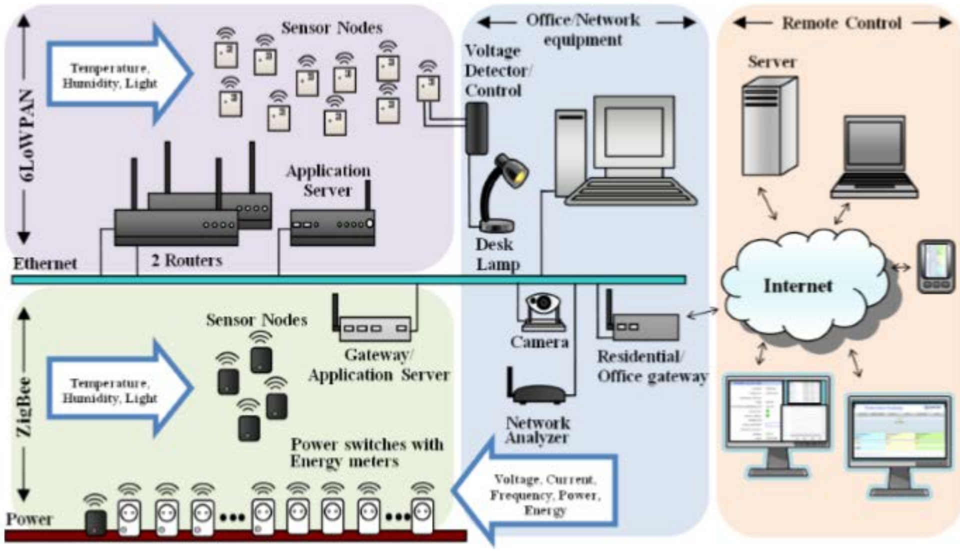

Figure 2. The concept of wireless sensor network [36].

Research in WSNs include many issues ranging from the development of the node's hardware, the protocol design, to the energy management [34]. WSNs are a key enabler for a vast range of applications, ranging for instance from environmental monitoring to healthcare [3]. WSNs significantly gained strength and more attention in the field of healthcare applications, especially in terms of fully autonomous devices.

An example of the latter is the next-generation sensor nodes for mHealth, which include so-called biostamps [35], i.e. thin and stretchable tattoo-like sensors that can replace bulky traditional sensors. Such biostamps are used for measuring e.g. body temperature, UVA/B exposure, lactate, pH, and glucose levels. In order to make these convenient and autonomous, they should feature both wireless communication and, of special interest for this work, energy harvesting capabilities such as the flexible thermoelectric generator (TEG) shown in Figure 3.

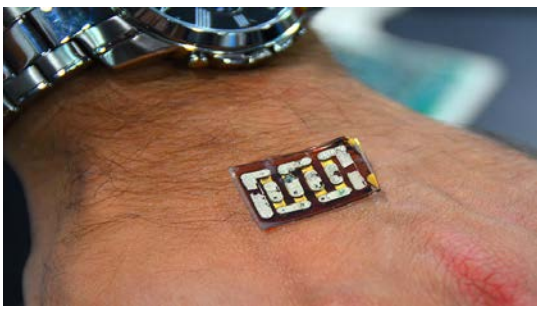

Figure 3. Prototype of a flexible thermoelectric generator (TEG). Source: North Carolina State University's Centre for Advanced Self-Powered Systems of Integrated Sensors [37].

Typically, sensor nodes are powered by a battery source; if the battery becomes depleted, the node will not be able to operate (so-called "dead" from a wireless communication perspective). Although batteries can be replaced or recharged, this is quite often an expensive, time consuming and sometimes nearly impossible task, especially for large-scale networks or remote application (e.g. glacier or in space). Despite some improvements in battery technologies during the past few years, energy is still the biggest constraint when designing and operating WSNs node. Therefore, different techniques and various ways of reducing the energy consumption have been proposed in the literature to increase the lifetime of the nodes. Nevertheless, providing additional energy to the nodes remains highly desirable and can be achieved by means of EH. In an EH-powered WSN node, the energy source (e.g. solar, thermal, etc.) can be connected to the rechargeable battery or super capacitor or, in some cases, be used to directly WSN node (a.k.a. autonomous or battery-less WSN node). However, one of the significant drawbacks of EH is that such sources typically (although not always) exhibit intermittent patterns, e.g. changing weather conditions will impact the energy collected by means of a solar panel.

1.1 Energy Harvesting and WSN nodes

Nowadays EH is getting more and more popular among the researchers and in the industry since it provides additional energy which can solve, or at least alleviate, the capacity issue of battery sources. EH extracts the energy from the environment or other mechanisms and converts that energy into electric energy. EH plays a vital role to extend the lifetime of WSN nodes; an example of a WSN node architecture including EH capabilities is shown in Figure 4.

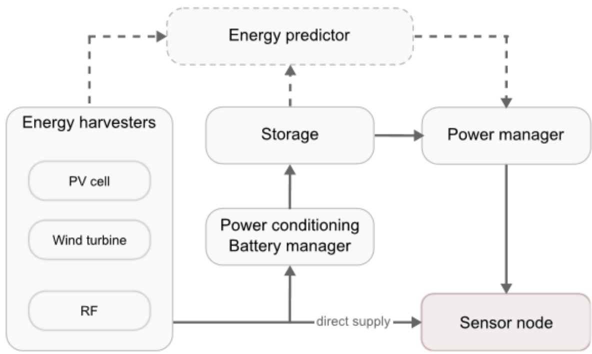

Figure 4. Block diagram of energy harvesting architecture in a WSN node [41].

As can be seen in Figure 4, one or several energy sources can be used; the latter case is known as hybrid EH. The bold lines in the figure represent the energy paths. In one path, energy flows from the energy harvester(s) through a power conditioner and battery manager block before reaching the energy storage. The energy then flows through a power manager that delivers it to the WSN node. In another path, the energy flows directly to the WSN sensor node.

The harvested energy is dependent upon the efficiency of the harvester, its orientation (if solar), location, or some other aspects such as weather, time or machine activity [38]. Generally, EH is an explored technology and is successfully deployed in many applications, especially where size does not matter [39]. Furthermore, in some application, EH provides directly power to sensor node with no power source (battery) [40], as also indicated by the direct supply path in Figure 4.

However, EH is intermittent in nature [41], and thus, completely relying on EH could be the cause of disruptions or delays in the application's operations. While this is not acceptable in time critical applications, it may be acceptable in others (e.g. in delay tolerant networks).

Given the above, three issues of special interest have been explored in this work. The first one is that of evaluating the feasibility of using a single or hybrid EH source for powering a given WSN. This issue and the related EH modelling is further discussed in this chapter (Section 1.3) and in Publication 1.

The second one is that of managing power losses due to the intermittent nature of EH, especially when used as the sole energy source. This issue is further discussed in Chapter 2 and Publications 3 and 4.

The third one, illustrated by the dashed box and dashed lines in Figure 4, is that of predicting the available energy to better control the WSN node operations. This issue is also further discussed in Chapter 2 and Publications 3 to 5.

However, before looking more closely to the above issues, various EH technologies are briefly introduced in Section 1.2.

1.2 Energy Harvesting Technologies

Numerous EH technologies exist, but this chapter covers only the most relevant ones in the context of WSN nodes such as solar, thermal, wind, RF and acoustic. These EH driving low power embedded devices are discussed in several survey papers such as [42].

EH and renewable energy have a wide range of potential applications. For example, various EH WSNs have implemented in the past like Trio [43] and Prometheus [44].

Figure 5 shows different types of energy harvesting technologies.

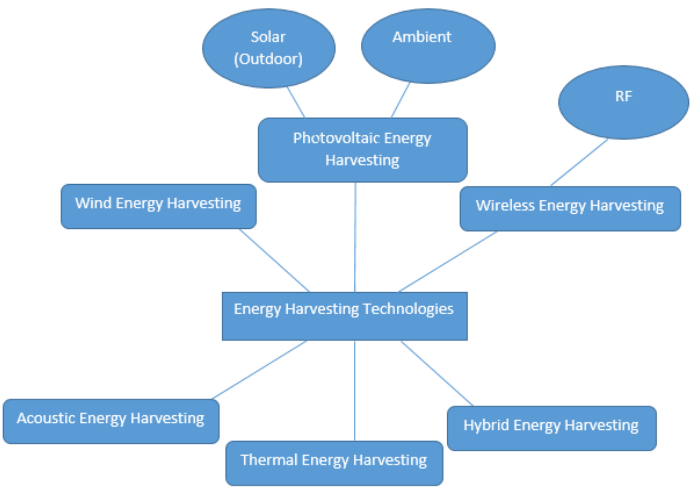

Figure 5. Overview of the numerous energy harvesting technologies.

1.2.1 Photovoltaic (PV) EH is the process of converting incoming photons from sources such as outdoor or ambient (indoor) light into electricity. A PV energy harvester consists of semiconducting materials: n-type and p-type. Typically, PV EH provides higher power output as compared to other harvesting technologies; it is applicable also for the large-scale WSN networks. However, it is light or environment dependent. The power efficiency depends upon the material and orientation as well [45]. Some prototypes of PV harvester are presented in [46]-[48].

1.2.2 Thermal EH is the process of creating electric energy from a temperature difference using a thermoelectric generator (TEG). A TEG is a thermopile formed by p-type and n-type semiconductor, placed between a hot and a cold plate and connected in series [49].

1.2.3 Wireless EH

RF energy harvesting is the process of converting electromagnetic waves into electricity by means of a rectifying antenna, or rectenna. Energy can be harvested from either ambient RF power from sources such as radio and television broadcasting and mobile phone transmitters and microwave or from EM (electromagnetic) signals generated at a specific wavelength. Another possible solution is to use a dedicated RF transmitter to generate power as per the requirements. However, the RF efficiency depends on the distance and between the RF transmitter and the harvester. In particular, a useful application of RF EH is to wake up sensor nodes from deep sleep state upon request (aka wakeup node). Examples of implementations of wireless energy harvesting techniques for WSNs are available in [50]-[52].

1.2.4 Wind EH is the process of converting energy from wind into electrical energy. A (small size) wind turbine is used to power WSN nodes. However, efficient design of small-scale wind energy harvester is still an ongoing research effort. Some examples of wind energy harvesting designed for WSNs are available in [53]-[54].

1.2.5 Acoustic EH is the method that transform the higher and continuous acoustic waves from the environment into electrical energy through a transducer. The received acoustic emissions may be of the type longitudinal transverse, bending and hydrostatic waves from low to high frequencies [55]. Usually, it is used where power is not available, for e.g. remote areas [56, 55]. However, the efficiency of harvester acoustic power is low [41].

1.2.6 Hybrid EH is the combination of two or more harvesting technologies, for example solar (PV) with RF and thermal or the other way around. The main idea behind hybrid EH is to use uncorrelated energy sources that can complement one another so as to increase the probability of uninterrupted energy supply. However, the power management of each harvester consume energy itself.

Literature on EH systems is still largely related to extensive simulation studies. Most of the works focus on the system building, efficiency and viability of EH mechanisms [57].

Evaluating the WSNs node behaviour, network performance and practical feasibility, can be carried out via a WSNs simulator (framework). In what follows, a comparative analysis of WSNs simulators is briefly discussed.

In addition, the author proposed a hybrid model for energy harvesting (RF, solar, thermal) based on combined ambient (indoor) energy sources. The author also proposed a battery management circuit, with low power current consumption, which is cascaded with the energy storage device and the energy harvester. The detailed description of the author’s contribution can be found in Publication 1.

cascaded with the energy storage device and the energy harvester. The detailed description of the author's contribution can be found in Publication 1.

1.3 WSNs Simulator

The author proposed a system-level framework (testbed) designed to rapidly evaluate the operating feasibility of the WSNs node based on various functionality of simulator, for instance, WSNs nodes power consumption, practicability with single and hybrid energy harvester (a feature is lacking in other simulators), energy prediction models and energy storage support. In relation to the above, Table 2 shows the comparison between the proposed framework and the state-of-the-art. The following table illustrates that only GreenCastalia, WSNSim and HarvWSNet provide the source code, [58] in order to evaluate the WSNs node behaviour, network performance and practical feasibility, before working on the WSNs node implementation. On the contrary, the proposed FYPSim covers the aspects which are required for the coarse-grain but rapid exploration of design alternatives.

Table 2. Illustration of the supported features in selected WSN simulators.

Tools	Code Availability	Energy Prediction Models	Storage Model	Hybrid Harvester model	Power Consumption model	Compression technique
Green Castalia [59]	✓		✓	✓	✓	
SensEH [60]			✓		✓	
WSNSim [61]	✓		✓		✓	
[62]			✓		✓	
[63]			✓		✓	
HarvWS Net [64]	✓		✓	✓	✓	
[65]			✓		✓	
[66]			✓		✓	
FYPSim (This work)		✓	✓	✓	✓	✓

exploration of design alternatives and thus relatively coarse-grain models of the harvesters are used.

As an example, let's consider a RF-EH that converts higher AC voltages to DC voltages at short distances. A model for an RF to DC voltages is as follows:

$$V = 2\ [G_{ant}\lambda / 4\pi\ d\ (2R_e\ [Z_{rec}].P_{rf}\ (1{+}Q_{rf}^{\ 2}))^{1/2}\text{-}V_F] \qquad (1)$$

where V is the DC output voltage, Gant is the gain of the antenna, d is the distance, Re [Zrec] is the reactance, Prf is the power, Qrf is the quality factor and VF is the forward voltage.

Other energy harvester models, such as solar and thermal, used in FYPSim have been discussed in Publication 1 (Appendix A).

In addition, FYPSIM includes a hybrid energy harvesting setup model, which is lacking in most WSN simulators. For this, the author proposed a hybrid energy-harvesting model with a single power management circuit.

More information about the hybrid EH circuit and the above model and the battery management system can be found in Publication 1.

Experiments have been conducted to explore the behaviours of various sensor nodes such as Dresden AVR, Atmel Atmega, SenseNode and WiSense, which are evaluated at three different states i.e. idle, sleep and active modes, and their current consumption based on the hybrid harvester with battery source and super capacitor.

Four cases, corresponding to various activity rates have been considered; they are classified into the following way:

CASE A: In this case the nodes are always in the sleep mode, as a result the energy consumption is minimal. However, the author found that, for the selected hybrid EH setup, this case is not feasible for Dresden AVR node which has a higher consumption than the other nodes.

CASE B: In this case, the author changed the scenario and kept the sensor nodes active for every 1 s out of 60 s, which is applicable in e.g. a health monitoring system, temperature monitoring, etc. Based on the experimental results (see Publication 1), the number of feasible combinations is similar to case A; and again Dresden AVR node, with the selected hybrid EH setup, is not feasible at this activity level due to its higher current consumption.

CASE C: The author made this case to have more active time than in previous cases, namely every 1.6 s out of 60 s, which is applicable in more intensive sensing and signal processing activities. Results (see Publication 1) illustrates that the nodes consume more energy as compared to the previous cases, and only WiSense node is feasible with the selected hybrid EH setup.

CASE D: This case can only be considered where continuous monitoring is required on an e.g. 24/7 basis, which is suitable for extremely critical applications such as surveillance, disaster monitoring etc. The experiments show that no solution is appropriate for the selected hybrid EH setup.

An extract of the results found in Publication 1, is given in Table 3.

Table 3: Hybrid Energy Harvester powered different sensor nodes cascaded with a 3.75V Supercapacitor.

Sensor Nodes	Case A Idle =0s Active =0s Sleep=300s Total Time =300s	Case B Idle =5s Active =5s Sleep=290s Total Time =300s	Case C Idle =8s Active =8s Sleep=284s Total Time =300s	Case D Idle =0s Active =300s Sleep=0s Total Time =300s
Dresden AVR Idle Active Sleep	Current Consumption (A) 3.24 97.2 -1.5	Current Consumption (A) 163.13 4953.96 -4858.26	Current Consumption (A) 262.26 7868.01 -7772.31	Current Consumption (A) 3240 97200 -97104.3
Atmel ATmega Idle Active Sleep	Current Consumption (A) 0.19 5.83 89.86 ✓	Current Consumption (A) 2.34 70.45 25.24 ✓	Current Consumption (A) 3.64 109.22 -13.52	Current Consumption (A) 129.6 3888 -3792.3
SenseNode Idle Active Sleep	Current Consumption (A) 0.06 1.94 93.75 ✓	Current Consumption (A) 1.85 55.51 40.18 ✓	Current Consumption (A) 2.92 87.66 8.03 ✓	Current Consumption (A) 142.56 3207.6 -3111.9
WiSense Idle Active Sleep	Current Consumption (A) 0.03 0.97 94.72 ✓	Current Consumption (A) 1.38 41.55 54.14 ✓	Current Consumption (A) 2.19 65.90 29.79 ✓	Current Consumption (A) 81 2430 -2334.3

In conclusion, the author has shown how a designer can estimate and evaluate the feasibility of hybrid energy harvesting by using FYPSim for various nodes, here cascaded with a supercapacitor.

1.4 Chapter Summary

In this chapter, the author discussed the background and presented the architectural overview of a generic wireless sensor node, in particular its limited life time due to energy storage constraints. This lead to discuss a variety of energy harvesting technologies.

Next, an example of the models used in FYPSim has been presented and the proposed model for hybrid energy harvesting has been introduced.

Some selected results illustrate how the framework can be used to explore the feasibility of EH for various WSN nodes.

Publication 1 presents additional EH models and results for both Li-Ion battery and supercapacitor. In addition, the paper also presents a single power management system for hybrid energy harvester which was designed and simulated with LT spice. The operating principle of this management system depends on the battery voltage, if it drops below a threshold then the circuits starts harvesting energy. The details can be found in the Publication 1.

During this initial phase of the PhD work, the author observed that the concept of TC was emerging as a potentially valuable approach to deal with some of the challenges associated with EH. Thus, the focus of the remainder of the work is on TC in combination with EP, as discussed in the next chapter.

2. TRANSIENT COMPUTING, LINEAR ENERGY PREDICTION, AND THEIR JOINT IMPLEMENTATION

This chapter covers the following topics:

- An overview of transient computing, its benefits, constraints, and state-of-the-art, as well as a summary of the TC implementation initially conducted on a single WSN node powered by means of EH.
- A brief introduction to energy prediction and related state-of-the-art, a summary of the proposed linear energy prediction model (LINE-P) which is based on sampling theory, and finally its comparison with the state-of-the-art in terms of estimation error, time complexity and space (memory) requirements.
- A description of the proposed mechanism that deploys two modalities (TC and EP) in a combined way on a non-volatile sensor node (TI MSP430FR5739 + CC2500), and thereafter the assessment of the performance and link quality of a peer-to-peer setup powered by means of a solar energy harvester.

2.1 Transient Computing

The concept behind TC is to dynamically stop/pause and restart/resume computation (and communication) operations depending on the available energy. In the context of this work, TC is a useful mechanism to deal with power losses that result from either a depleted battery/supercapacitor and, of special interest, when operating a WSN node directly from an energy harvester without any energy storage (i.e. no battery or supercapacitor).

The integration of EH and TC in wireless sensor nodes enables the design of highly energy constrained, battery-less systems that operate only as a function of their environment [68, 69]. Thus, TC can not only minimize the size of the sensor node but also its mass, complexity, and cost [39, 70]. Such TC-enabled battery-less sensor nodes can also be used in environments where the electrochemical properties of the batteries are incompatible with safety requirements, such as in certain space applications.

In practice, this concept is enabled by the use of microcontrollers that include non-volatile memory (e.g. flash or more recently FRAM). When a power loss occurs, the TC mechanism takes a snapshot (i.e. saves the state and/or data of the microcontroller), and thereafter, when the power reaches back the operating threshold, the last saved snapshot is restored and the operation is continued from where it was interrupted [67]. The registers of the microcontroller are saved upon imminent power failure (typically detected by means of a threshold voltage) and restored when the power is again available, as shown in Figure 6 [71].

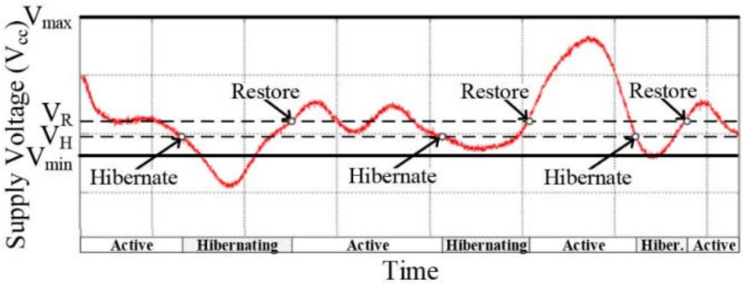

Figure 6. Illustration of the operation of a transient computing system [67].

In this example, the node hibernates when the supply voltage goes down to VH, i.e. a snapshot of the state/data of the microcontroller is saved in non-volatile memory before the supply voltage goes below Vmin. Once the supply voltage goes above VR, the snapshot is restored and the node goes back to the active mode.

In order to operate TC systems continuously and efficiently, they require sufficient energy for the executing the tasks. However, in case of low energy the node will be shut down until energy is again available. The time interval between shut down and wakeup or vice versa depends on the input power source [39].

In relation to above operations, researchers have identified some challenges in the design of transiently powered systems [36, 39]:

1. Transient systems are unable to control the time when they are on since this only depends on the available input power.
2. Between on and off operations, the system is shut down and peripherals are off. Supposing that the application requires several on and off conditions, the non-volatile memory (NVM) have to save the system state between the on and off conditions.

The above challenges are already significant when the TC system includes a single node. The situation is even more complex when the number of sensor nodes are expanded and transformed into a WSN or has to performed bi-directional communication. In Publication 4, the author faced some more challenges while implementing the peer-to-peer network based on TC (Note: these have been addressed in the last part of Chapter 2).

1. The WSN node is supposed to update its peer that the communication is no longer possible in case of low energy and just before the system (node) enters the shut-down mode.
2. The employed TC mechanism does not directly support the radio configuration since the registers of the radio chip cannot be directly saved to FRAM.
3. Re-establishing the communication when there is again enough available energy requires the implementation of an additional mechanism.

The author addresses the above issues by proposing to combine two modalities, namely TC and EP, to better deal with EH-powered nodes. Moreover, works on EH systems are often limited to single node networks [57]. Thus, when the nodes are added up in a network, they can perform data processing in a more powerful manner [72]. The author used a peer-to-peer setup for the assessment of the combined TC and EP approach. The detailed information can be found in Publication 4.

Before going into some of the details of the proposed approach, what follows summarizes the state-of-the-art of TC.

Mementos was the first TC approach presented by Ransford et al. [21]. It shifts general computing into an interruptible model which can deal with intermittent power off phases via a checkpointing mechanism. This mechanism saves and restores the data and instruction to and from flash memory in case of power fluctuations. However, this concept increases the overall execution time.

Afterwards, DINO (“Death Is Not an Option”) [24] adds a mechanism which helps insuring consistency between volatile and non-volatile data even when in the presence of frequent interrupts. In addition, another novelty in DINO is to use a FRAM-based microcontroller rather than one based on flash memory. The overhead in terms execution time lies between 1.8x to 2.7x.

Significantly, Hibernus [20] reduces the number of checkpoints by replacing the periodic checkpointing by an ad-hoc technique that is triggered only when the supply voltage decreases below a given threshold. As compared to Mementos, Hibernus reduces the execution time and energy overheads by 76%-100% and 49%-79%, respectively.

QuickRecall [25] introduces a new concept that saves all the instructions, data and state into FRAM (unified approach where the RAM is not used). This potentially reduces the execution time and energy consumption since no data have to be transferred between the FRAM and the RAM. QuickRecall can reduce the program execution time by up to 4.5x as compared to other methods and allows operations to be performed in short on-time slots of 5 ms (vs. 15 ms in other approaches).

Balsamo et al. [23] developed a new TC method called “power neutral” operation. In this method, the microcontroller’s frequency is dynamically adapted against the input power source. Their results illustrates that such a power-neutral method can extend operations for 4%-88% further with a 21% acceleration in application execution.

Hibernuss++ [67] proposes a dynamic adaptation of the hibernate and restore thresholds based on the fluctuation in energy and the system load properties. Results show that Hibernuss++ reduces energy consumption by 16% and accelerate the application excecution time by 17% as compared to other techniques. However, this approach requires additional circuitry.

HarvOs [64] is a series of code instrumentation strategies deployed at compile-time and adapting the execution of the program at run-time as a function of the remaining energy. The approach allows transiently powered devices to complete a given workload with 68% fewer checkpoints on average and the number of required checkpoints rests only 19% far from the ideal solution.

ARM mbed support presented in [73] integrates TC approaches into the mbed OS. It enables multiplatform and TC as a service above IoT application protocols. The paper illustrates the feasibility of the approach by implementing it on a low power microcontroller with flash memory operating from only 1 mF additional capacitance.

Bhatti et al. [74] present a selective policy for efficient state retention that dynamically indicates the unallocated space and only saves to flash memory. In addition, [75] implements an “Allocated State” policy on different memories, i.e., FRAM and Flash. This policy was implemented on both technologies; Figure 7(a) and 7(b) illustrate that the cost for saving is proportionally reduced with the size of allocated memory, as compared to saving the entire memory (up to 85.1% reduction when memory usage is 18%).

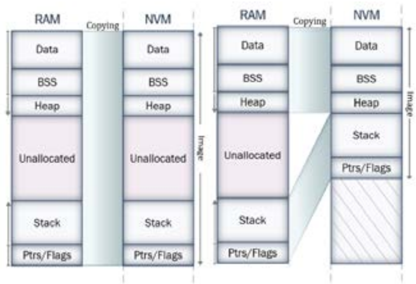

(a) Complete State *(b) Allocated State*

Figures 7. Illustration of the state of memory with NVM and Flash [74].

Furthermore, by employing this kind of concept on flash memory, it was observed that it is less effective in terms of saving times and energy, as shown in Figure 8(c) and 8(d), as compared to the case with FRAM (Figure 8(a) and 8(b)); the penalty being largely due to the erasing process for the flash memory.

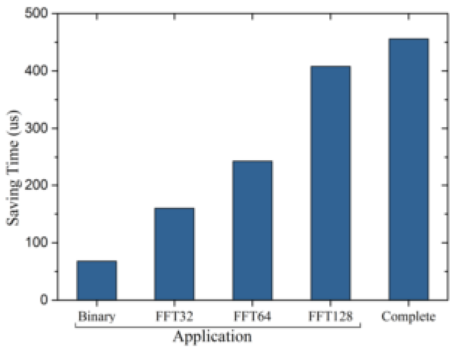

(a) Saving time (FRAM)

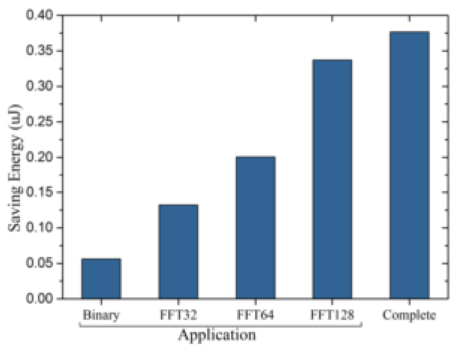

(b) Saving energy (FRAM)

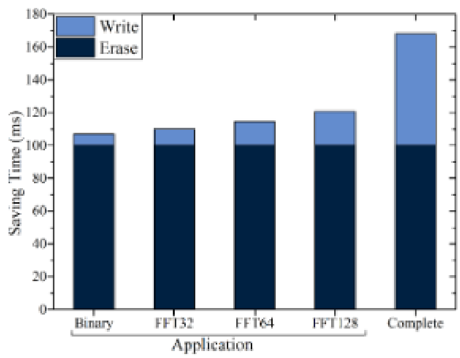

(c) Saving time (Flash)

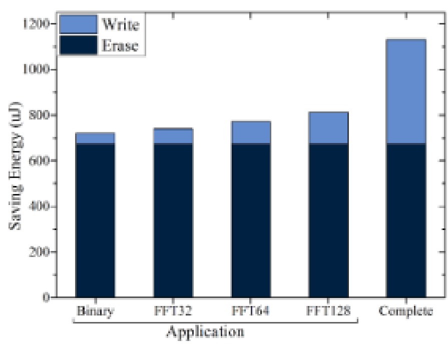

(d) Saving energy (Flash)

Figure 8: Time and energy overheads between FRAM (a and b) and flash memory (c and d) [74].

In [75], incremental work in checkpoint is proposed to minimize the size of the checkpoint updates in the secondary storage. The approach can be categorized in three different techniques, namely i) records modification in the RAM only, ii) avoid computational overhead by binding variables to program paths, and updating the relevant variables, iii) do not require program path to variable binding, rather it efficiently indicates modified memory locations using a Hash of Hashes (HoH) approach.

In [76], the authors present WISPCAM, a wireless camera that is powered from harvested RF energy and supports data-transfer from non-volatile memory using RFID. The system has an energy storage capacity (a 6 mF super capacitor) to enable a single photo to be shot and stored in NVM. In case of energy failure, the system does not fail as the photo is stored in NVM and supercapacitor will be charged later again. In relation to the above, in [77], the authors propose a similar kind of system, which will not performed until there is at least 80µF energy in the capacitor. Monjolo [78], presents a similar approach to [76] in home, whereby a current clamp around a main cable harvests energy via induction and charges a 500 µF capacitor.

Usually, TC is demonstrated on a microcontroller (most of them without wireless connectivity feature) and the literature still lacks reports on experiments with wireless-enabled sensor nodes.

TC provides the support for extending the life span of the WSNs without adding an energy storage device. Thus, this innovative concept effectively reduces the physical size of the node and alleviates the limited energy capacity constraints. However, TC is more suitable for those applications where permanent operation or monitoring is not mandatory.

The combination of EH and TC is still a least explored area. The harvested energy is intermittent and possibly leaving the node without power and thus TC operates the node by pausing and resuming its operations depending upon the harvested energy.

The purpose of this section is to share some of experimental results obtained when three EH sources such as solar, thermal and RF are used to power an FRAM-based node with a TC mechanism without energy storage, as well as the assessment of the practicability of TC for WSNs.

In relation to the above, the author selected a FRAM-based microcontroller (MSP-EXP430FR5739) kit combined with a CC2500 radio chip, both from Texas Instrument. Thereafter, author modified the CTPL (Compute through Power Loss Utility) library, in order to implement TC mechanism. In particular, the CTPL library contain numerous functions for deploying the mechanism, as shown in figure 9 (Publication 2).

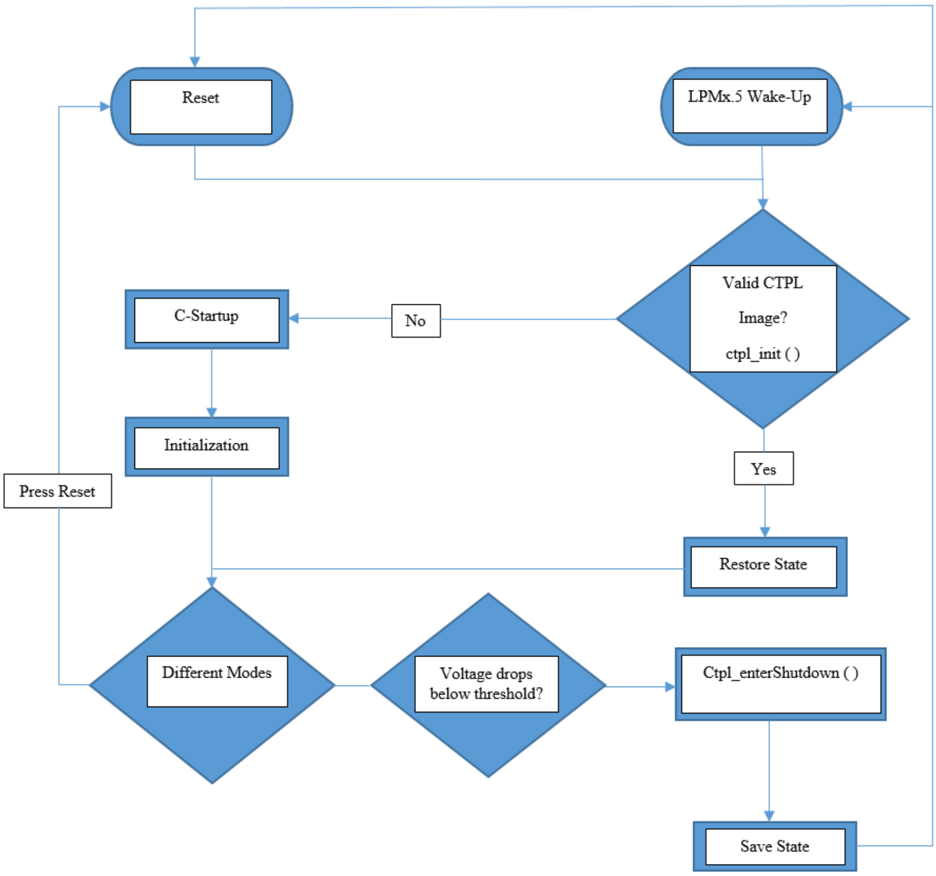

Figure 9: Texas Instrument's Compute through Power Loss Utility strategy used for implementing TC (Publication 2).

The block diagram of the experimental setup can be seen in Figure 10, which illustrates that the microcontroller (MSP430FR5739 kit) is cascaded with either a DC power supply (non EH mode) or with an energy harvesting kit (DC2080A) and as well as solar panel (PRT-13781) through selector (switch). Here, the operating principle is that in case of the voltage goes below a threshold voltage i.e. 2.5 V, the ctpl_enterShutdown () function is triggered and thereafter the state and data of the microcontroller are saved (Publication 2).

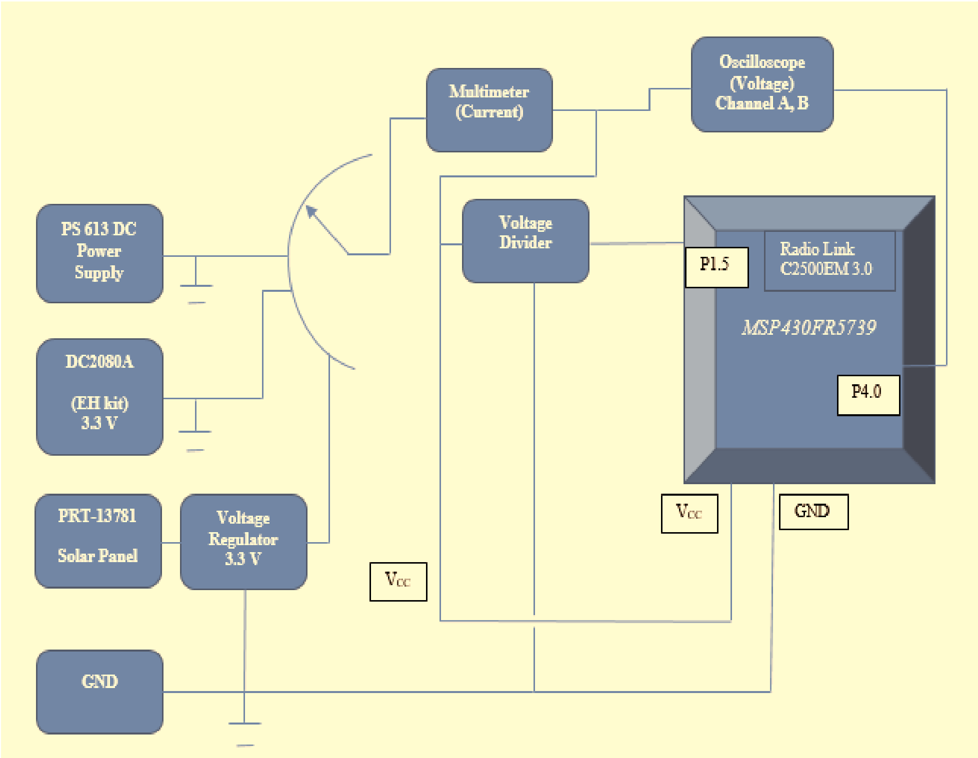

Figure 10: Block diagram of the experimental setup to implement TC mechanism (Publication 2).

The results illustrates that the solar energy source is able to power and operate the nodes (see Table 4 Publication 2). However, the RF and TEG module were not satisfying the power requirements of the nodes (the results can be found in Publication 2).

Table 4. 1st and 2nd rows: measured voltage and current for the MSP-EXP430FR5739+CC2500 used as a transmitter. 3rd and 4th rows: measured voltage and current for the MSP-EXP430FR5739+CC2500 used as a receiver, with the larger solar panel (13.5 x 11.2 cm).

	Case I (Outdoor Light)	Case II (Indoor Light)	Case III (Sharp lamp Indoor Light)
Light Intensity [LUX]	5.36K	1.46K	9.98K
Voltage [V] and Current [mA] without radio	3.06 2.46	3.10 2.00	3.5 2.16
Voltage [V] and Current [mA] with radio	3.0 20.0	3.09 22.0	3.5 22.16
Voltage [V] and Current [mA] without radio	3.0 2.16	3.10 2.00	3.5 2.16
Voltage [V] and Current [mA] with radio	2.91 19.98	3.09 22.0	3.5 22.16

More information and results can be found in (Publication 2).

Now that the principles of TC have been introduced and that the first contribution related to EH and TC have been summarized, the discussion moves to the state-of-the-art related to EP and the proposed linear energy prediction model.

2.2 Energy Prediction and Proposed LINE-P (Linear Energy Prediction) model

EH, aided by energy prediction (sometimes also referred to as energy estimation), has led to a service-oriented infrastructure supporting a broad range of applications such as IoT, cyber physical system, by optimizing the energy consumption and balancing the traffic load to increase the node lifetime.

Some researchers argue that energy prediction is quite a mature topic; however, only few energy prediction models provide sufficient accuracy, reliability and robustness. In fact, EP in the context of autonomous WSNs is still a least explored area. In particular, EP can be considered as an alternate solution [31], which can control certain operations of the WSNs nodes. The accurate prediction is very essential, especially in the domain of autonomous WSNs nodes, where operations are dependent on the estimation of the available energy [26]. EP is quite useful for WSNs that predict the energy in the near future over short (a few minutes) and medium (a few hours) terms, and that thereafter execute the tasks based on the estimated energy, which minimizes the wastage of energy and reduces the computation overhead [41].

This section discusses various state-of-the-art EP models that have been proposed in the literature. It is to be noted that among the research community, the two most popular sources are solar and wind energy harvesters.

The classification of the EP models falls into two categories, i) fixed weighting parameter based EP models and ii) adaptive EP models that calculate their weighting parameter based on the stored energy profile.

Most of the EP models are based on a fixed weighting parameter, here represented by (α). Normally, this factor is tuned at the beginning of the experiment to ensure the closest estimation; however, this is the biggest constraint because a tuned parameter (α) affects the accuracy of the estimation under significant varying conditions, such as for example, inconsistent weather. Thus, this approach is incompatible with e.g. solar powered WSNs because each solar panel contains different and unknown series of parameters such as orientation or even dust [26].

In [28], the authors presented an exponentially weighted moving-average (EWMA) EP model; it is widely used in solar energy estimation based on an exponentially weighted moving–average filter [79]. EWMA considers that the harvested energy of the current day time-slot is identical to the observed energy at the same time on the previous days. The amount of energy available during the past days is maintained as a weighted average, in which the contribution of previous data is exponentially decaying. This algorithm is able to both exploit the periodic cycle in solar energy and to adapt to seasonal variations, but leads to significant prediction errors in case of inconsistent weather, i.e., when sunny and cloudy days occur on alternative basis [41].

To address the above issue, Piorno et al. [80] proposed the EP model named Weather-Conditioned Moving Average (WCMA). In particular, WCMA is estimating with 20% less errors than EWMA, especially in an inconsistent weather.

In [81] the authors proposed a parameterized specification and the computation of an optimal online controller. In addition, to compute the solution of a linear program (LP) in a multiparametric fashion and transfer most of the associated overhead to an offline computation. This approach based on low computational complexity. Evidently, the actual control action compute in approximately in 2 ms and consume low power.

In [82] the authors compared and discussed various solar energy prediction models. In particular, author identify that neural network based algorithm is unable to adapt the changes but the WCMA and EWMA presents much higher performance in terms of estimation and as well as adaptation. In addition, they required less computation and memory, in order to implement in WSNs. Simulation results prove that the most efficient predictors is highly accurate and kept the fluctuations with real profile not more than 10%.

In [83], the authors exploit the EWMA model and proposed and extension which keeps track of the solar energy observed in the previous days. The presented algorithm is designed and developed for the short-term varying weather conditions. They proposed a scaling factor which adjusts the next value. After each slot, scaling calculates the ratio between the harvested energy during the current timeslot and the estimated energy for the same timeslot. As a result, the proposed algorithm yields improved latency and throughput in the network.

In [84], the authors addressed the issue of EH prediction for real-time embedded systems (RTES). They contend that accurate estimation of the energy in future is crucial for RTES, as the performance of optimization techniques is based on harvesting estimation. Therefore, they investigated three techniques in real time series prediction (regression analysis, moving average and exponential smoothing) and found that regression has the best prediction within a time horizon of 1 second. The proposed model aims is to yield the best system performance with the energy harvesting constraints. However, although this approach works well, it is not meant for medium-term prediction horizon-periods.

Generally, it is assumed that the right estimation for the near future energy intake are available to the system, either by simply looking at the past records [85] or by utilizing any low computation energy predictors [86]. Information about the behaviour of energy sources over short and medium time interval is often needed to optimize the system, and some solutions even rely on it to work well [87].

In [88], the authors presented a new approach that run the sensor node through solar and wind energy harvesting techniques. They observed that when estimating energy possibility at timescales between 3 hours to 3 days, using forecasting data provides better accuracy than if estimating the energy based on previous data. They explained that the reason for the unsatisfactory performance of traditional predictors is that the weather patterns are inconsistent. Thus, they developed a model for solar panel and wind turbine, which converts the weather forecast data into energy predictors. In addition, they showed the system increased ability as compared to existing strategies.

Although several EP models have been proposed in the literature, there remain a need to develop a model that would exhibit both sufficient accuracy and low computational complexity. Thus, the author of this PhD thesis proposed a dual–source (solar and wind) LINE-P (linear energy prediction) model based on sampling operators. The aim was to construct a predictor that on the one hand is good for approximation of smooth trends and on the other hand, it is not so sensitive to fluctuations. In this approach, the author used some elements of approximation and sampling theory. This contribution, presented in details in Publication 3, is summarized in what follows.

2.2.1 Mathematical Model of LINE-P (all cases)

Generally, in the literature (see above for some examples), most of the prediction models as designed for solar or wind energy harvesters as an energy source at two different time-period horizons, for instance shorter and medium, and they are highly dependent on the past records. Because of this, their estimation results contain more errors when rapid changes occur in the weather conditions. On the contrary, the proposed symmetrical kernel-based LINE-P model estimates the values on three different data time intervals, namely shorter, medium and longer, and the estimations errors are less even in inconsistent weather conditions. In addition, LINE-P is compatible with dual-source (solar and wind) energy harvesters.

This chapter highlights another issue, i.e. most of the prediction models are based on a fixed weighting factor, which is incompatible with the varying properties (e.g. orientation) of solar panel powered WSN nodes. The author of this thesis addresses the above issue by using symmetric kernels, which have simple computation of the dot product in a potentially infinite dimensional feature space by means on the kernel function. In particular, symmetric kernels have a simpler structure than non-symmetric kernels.

The goal of the author is to develop a generic mathematical model for dual-source (solar and wind) energy harvester, such as [89]-[90], that estimates energy accurately at different time intervals. To validate LINE-P estimations, the author used real energy profiles (data sets) of energy provider companies for photovoltaic panels and wind turbines, available in [91]-[92], respectively.

LINE-P (Case-I)

The proposed LINE-P (Case-I) model is expressed as follows; note that the detailed derivation and further two more cases are presented in Publication 3.

The samples $f_l(l = 1, \dots, k)$ are from the k previous days. The parameter vector b defines a symmetric kernel and the parameter vector a, where $a_k = 0$ for $k \leq 0$, generates a one-sided kernel with the corresponding sampling operator

$$(S_{PREDI;\mathrm{b}} f)(j) \coloneqq \sum_{k=1}^{m} b_k f(j-k) + \sum_{k=-m}^{0} b_k\, f_l(j-k) + CDIF_{PREDI;\mathrm{a;b};l}(j)$$

where the correction term $CDIF_{PREDI;\mathrm{b}}$ is in Equation (2),

$$CDIF_{PREDI;a;b;l}(j) \coloneqq CT_{PREDI;a;b} \left(\sum_{k=1}^{n} a_k f(k-i) - \sum_{k=1}^{n} a_k\, f_l(j-k) \right), \quad (2)$$

with the multiplier $CT_{PREDI;\mathrm{b}}$ as:

$$CT_{PREDI;a;b} \coloneqq \sum_{k=-m}^{0} b_k \,. \quad (3)$$

LINE-P (Case-II)

This performs energy prediction based on few samples. In addition, this case is dependent on only one variable a, as shown in (4).

$$(S_{PREDII;a} f)(j) \coloneqq \sum_{k=1}^{m} a_k f(j-k). \quad (4)$$

LINE-P (CASE-III)

The third case is very similar to Case-I, the only difference is in $CT_{PREDIII;\mathrm{b}}$ as shown in (5) with the multiplier $CT_{PREDIII;\mathrm{b}}$

$$CT_{PREDIII;b} \coloneqq \frac{\sum_{k=-m}^{0} b_k}{\sum_{k=1}^{m} b_k}. \quad (5)$$

What follows presents some of the results related to the evaluation of the performance of the LINE-P model based on the solar and wind energy profiles against the state of the art models in terms of : (i) Graphical representations, (ii) Time complexity, and (iii) Space (memory) requirements. The full set of results can be found in Publication 3.

2.2.1.1 Graphical representation (Error comparison of the models for solar energy profiles)

This subsection provides some results which were not included in Publication 3 due to space constraints. Typically, mean square error (MSE) and mean absolute error (MAE) have been considered for comparing the error of each of the models. In order to evaluate the errors, a solar-based (SDG&E) dataset (see Figure 11 and 12) has been used. In addition, the author considered a medium interval (61 slots) in 24 hours. Figures 11 and 12 show that LINE-P (all cases) yields the lowest errors as compared to the other models.

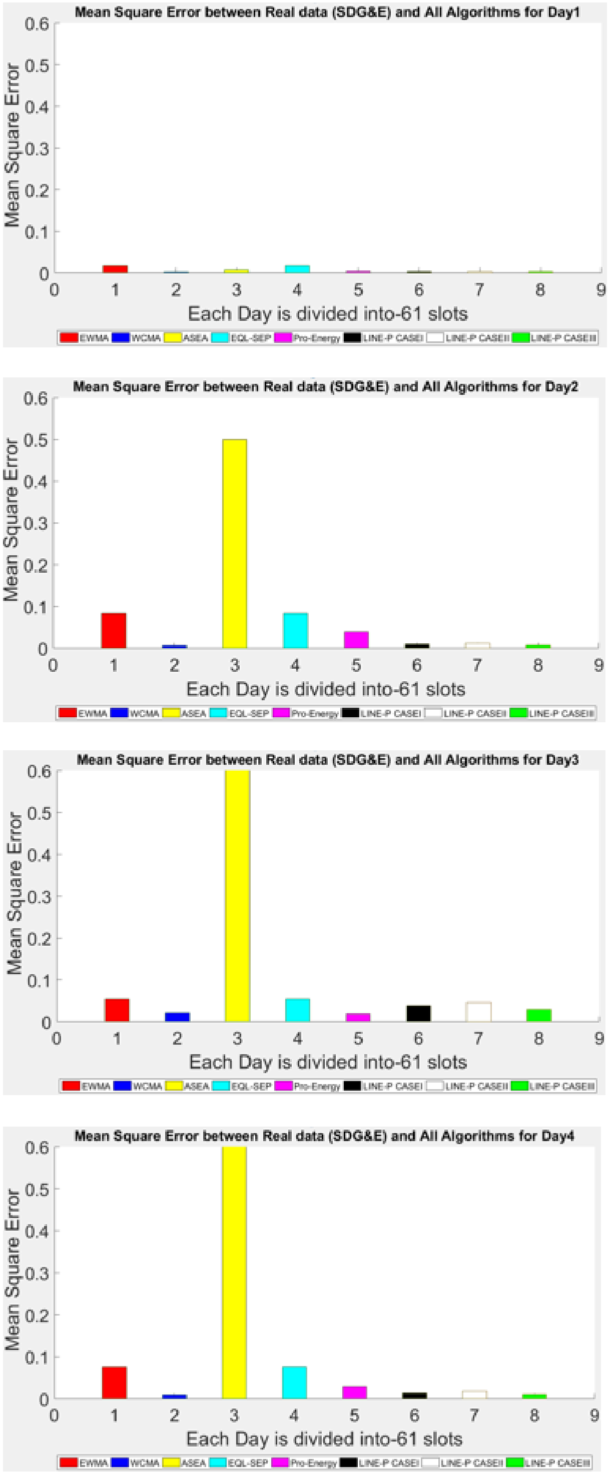

Figure 11. Average MSE for 4 days for all prediction models for solar energy.

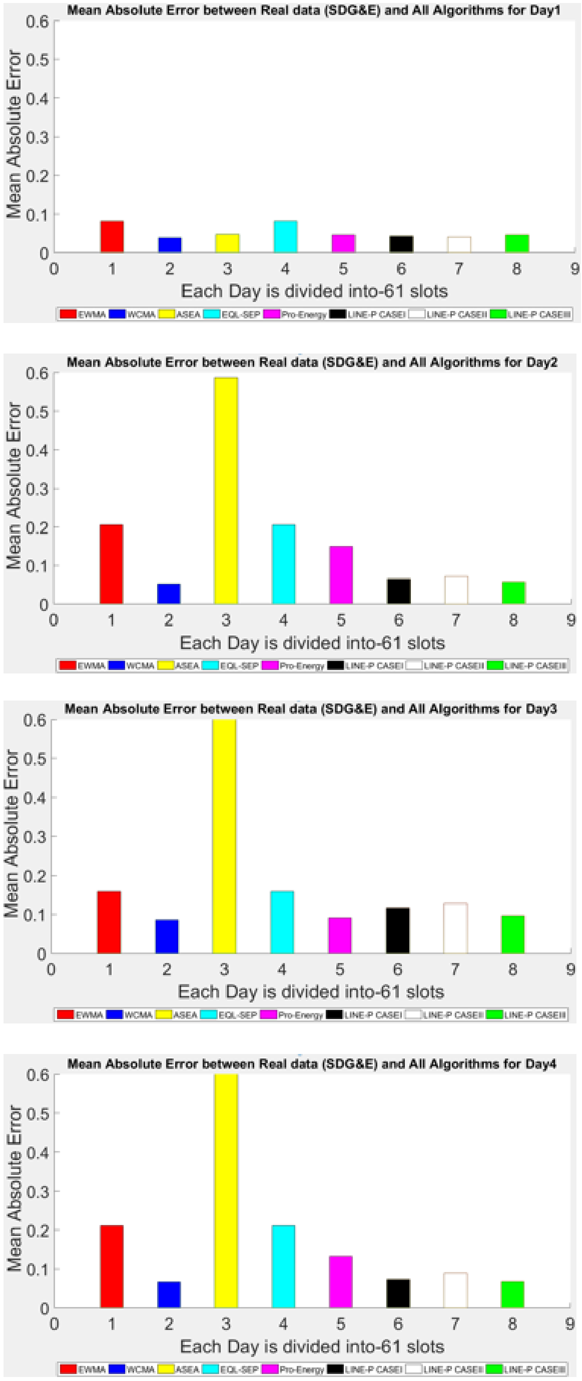

Figure 12. Average MAE for 4 days for all prediction models for solar energy.

The previous section compared the performance of all models for solar energy; in what follows, the author compares the performance of LINE-P and Pro-Energy for wind energy since only Pro-Energy is multi-source (i.e. which can be applied to the wind profile as well).

2.2.1.2 Graphical representation (Error comparison of the models for wind energy profiles)

In this assessment, the author used a shorter data interval of 96 slots in 24 hours from Elia dataset [92]; the results shown in Figure 13 confirm that LINE-P performs better than Pro-Energy. MSE and MAE are used to compare the prediction errors of Pro-energy and LINE-P (all cases). The results shown in Figure 13 and 14 are for four consecutive days (datasets). The results show that in general the prediction errors of LINE-P (all cases) are lower than that of Pro-Energy, however, WCMA also yield less error on certain specific cases. Thus, it is concluded that LINE-P (all cases) prediction values are very close to real data, especially Case-III.

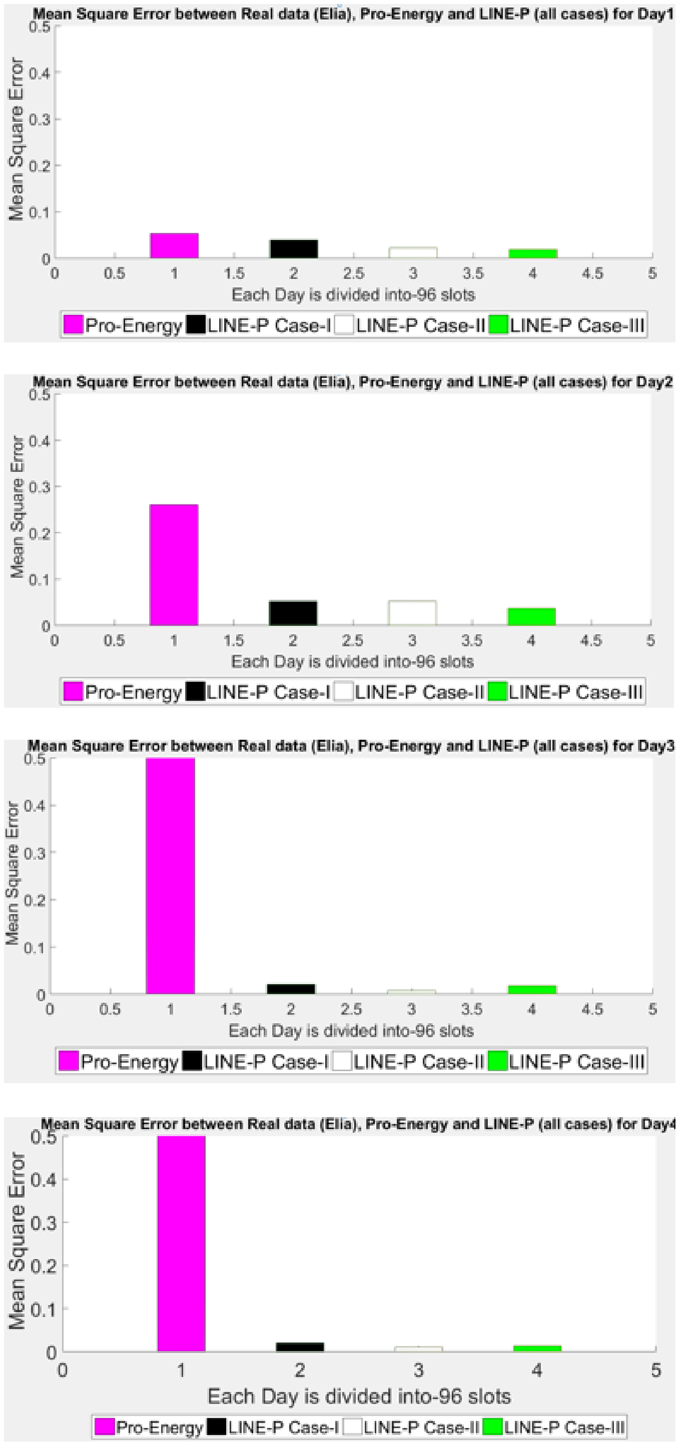

Figure 13. Average MSE for 4 days for Pro-Energy and LINE-P (all cases) for wind energy.

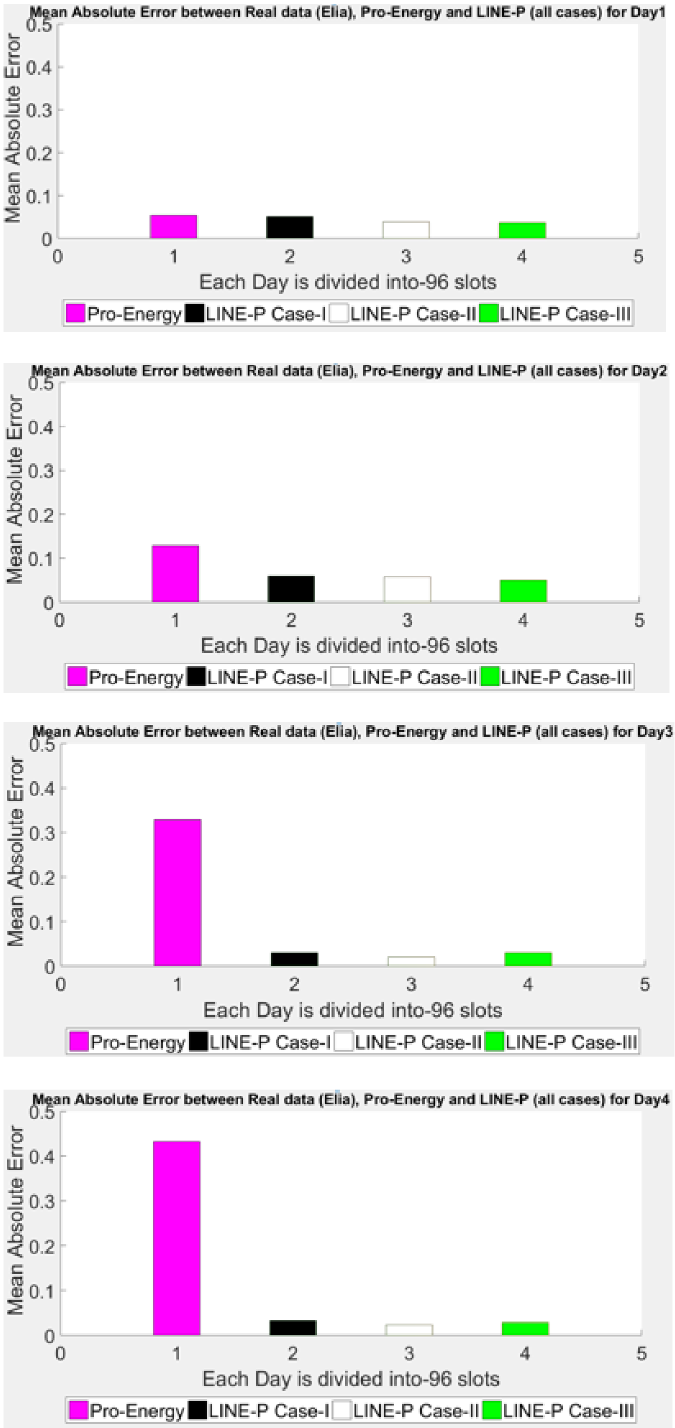

Figure 14. Average MAE for 4 days for Pro-Energy and LINE-P (all cases) for wind energy.

2.2.1.3 Time Complexity of the EP models

The time complexity and Big-O notations for all prediction models are compared. ASEA and EWMA have constant complexity (O(2)), whereas WCMA and Pro-Energy have quadratic complexities ($O(n^2)$ and $O((k+1)^2)$, respectively). QL-SEP and LINE-P (all cases) have linear complexity (O(n) and O(m)).

Considering both the prediction performance of all models and their respective complexities, it can be said that the proposed LINE-P approach offers the best trade-off, i.e. equivalent or better prediction accuracy than the best existing models at a lower complexity. This means that LINE-P is a good candidate for embedded implementation on resource-constrained platforms such as WSN nodes/coordinators where CPU usage and energy consumption are critical.

Table 5. Time Complexity of LINE-P (all cases) and the other prediction models. Note: In some models, we consider m and k times rather than n times (see Publication 3 for more details).

Prediction Models	Time Complexity T(n)	Big-O Notation O(n)
EWMA	$T(n) = 2$	$O(2)$
ASEA	$T(n) = 2$	$O(2)$
WCMA	$T(n) = k(n^2 + 1)$	$O(n^2)$
Pro-Energy	$T(n) = (k + 1)^2 n$	$O((k + 1)^2)$
QL-SEP	$T(n) = (4n + 2)q$	$O(n)$
LINE-P Case-I	$T(n) = 2(nk + m)+1$	$O(n)$
LINE-P Case-II	$T(n) = n$	$O(n)$
LINE-P Case-III	$T(n)=m(2k+ 1) + 1$	$O(m)$

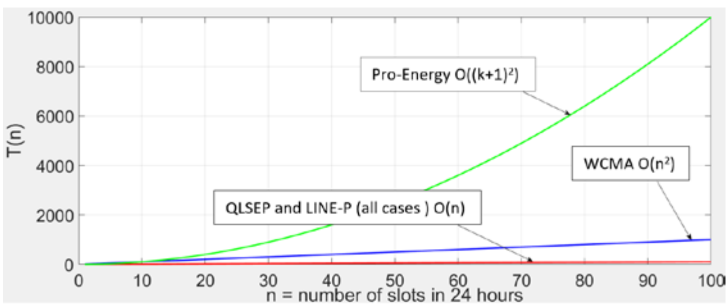

Figure 15. Illustration of the time complexity of LINE-P (all cases) as compared to the state-of-the-art.

2.2.1.4 Comparison of Space (Memory) Requirements

The proposed LINE-P model performs well as compared to the other models in terms of prediction error, and at the same time has small memory requirements. A higher number of slots N means higher memory overhead for a given predictor. For instance, assuming N = 48 and D (previous days) = 20, WCMA requires almost 4 kB of memory to store the matrix N·D for an energy prediction [34]. On the contrary, LINE-P (Case-I) and (Case-III) only require N = 13 and D = 4. Similarly, LINE-P (Case-II) only requires N = 8 and D = 1. Thus, LINE-P models' memory overheads are approximately 90% and 70% lower than for WCMA and Pro-Energy models, respectively (see Publication 3 for more details).

The above results show that the proposed LINE-P model, especially Case-III, is up to 90% accurate, has lower time complexity in three different time intervals and requires less space (memory) than the other EP models.

Now that the proposed LINE-P model has been summarized, the next contribution of this PhD work is introduced. The remainder of this chapter is organized as follows. In section 2.3, the author discusses the novel concept of combining the two previous modalities (TC and EP) simultaneously. Thereafter, their impact on a WSN node and as well as on peer-to-peer network powered by means of a solar energy harvester is discussed.

2.3 Combination of Transient Computing and Energy Prediction Modalities

Generally, with the increasing number of users, WSN nodes, and wireless and wired traffic, significant research efforts are also required to improve and ensure the quality of service, quality of experience and reliability of the applications.

In this section, the author summarizes the proposed approach for combining two different modalities, TC and EP, simultaneously in the context of WSNs for stable and reliable communication.

The literature discusses and suggests TC and EP as separate modalities in relation to WSNs; however, and to best of our knowledge, no work exploits TC and EP simultaneously specifically for WSN nodes; only one work considered this merging concept as a future work [71]. The main purpose of this part of this work is to deploy this combined approach and to evaluate its impact in terms of performance, adaptability and robustness. The remainder of this chapter summarizes the related key issues and results; the details thereof can be found in Publication 4.

Firstly, the author addresses issues related to the design and implementation of TC and EP together. Initially, it is needed to decide which energy source and prediction model to take into consideration. We have shown in Publication 2 that in our setup the solar energy harvesters is the best to operate the wireless nodes. Moreover, the existing prediction models are dependent on relatively large amounts of past values; however, these are unfeasible in real implementations because of the limited memory of the WSN nodes. Furthermore, another issue is related to the connectivity of the nodes, i.e. how to re-establish the connectivity of the sensor nodes after a power failure using TC?

In the first part of this thesis, the author assessed the practical feasibility of TC on a single node by using three energy harvesters (RF, thermal and solar) as detailed in

Publication 2. As shown in Figure 15, that approach is re-implemented in this part of the work, but this time both with a programmable power supply for controlled experiments and a solar panel for real-life experiments. Moreover, one of the three cases of LINE-P, i.e. Case-II, has been selected since it performs energy prediction based on a single variable and less memory space is required for the implementation of the combined TC and EP. In addition, the author implemented a peer-to-peer setup where the two modalities are integrated and evaluated in terms of link quality features such as jitter, packet receiving ratio and energy consumption. The details can be found in Publication 4; the key results are summarized in what follows.

2.3.1 Impact of EP on a TC-based WSN node

In this subsection, the behaviour of the system is evaluated with three cases: without energy prediction as well as with 5 and 10 minutes energy prediction. LINE-P (Case-II) model estimates the next value based on the six previous values (slots). Therefore, a 1-minute prediction is based on 6-minutes data; similarly, a 5-minutes prediction is based on the last 30-minutes (half an hour), and a 10-minutes prediction is based on the last hour, respectively.

Note: In the following figures of this section, the estimated energy and Vcc were recorded at every 30 seconds by the node. In particular, if the estimated energy goes above 2.9 V, then the system starts the communication (in the figure, ‘1’ means start communication), otherwise it stops it (‘0’ means stop communication).

2.3.1.1 Behaviour of the System Without Energy Prediction

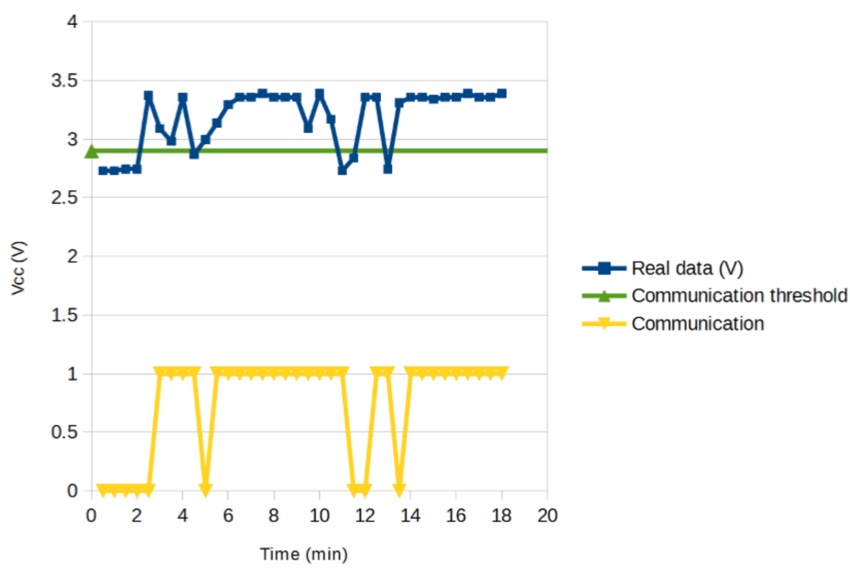

Figure 16. Behaviour of the system without energy prediction (Publication 4).

Figure 16 illustrates that the system performs communication by considering the current Vcc value. The system is adaptive and sensitive against the fluctuations. For example, the communication is stopped at 11:00 and 13:00 although the voltage increases again just after the loss.

2.3.1.1 Behaviour of the System with a 5-Minutes Energy Prediction

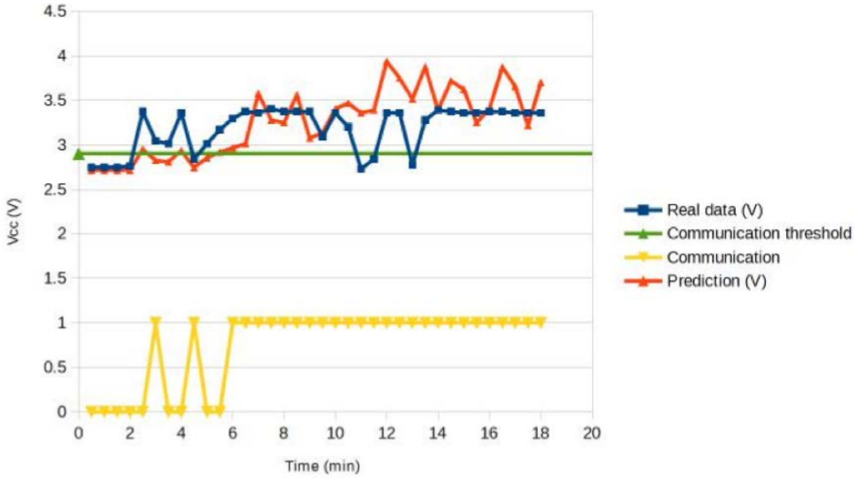

Figure 17. Behaviour of the system for 5-minutes energy prediction (Publication 4).

Figure 17 shows that the communication time is longer since prediction time is higher. The voltage drops at 11:00 and 13:00, but despite that, the system continues to communicate. Therefore, by deploying EP, the system is more robust and stable against the energy variations; however, the system is less adaptive because the prediction time is increased.

2.3.1.2 Behaviour of the System with a 10-Minutes Energy Prediction

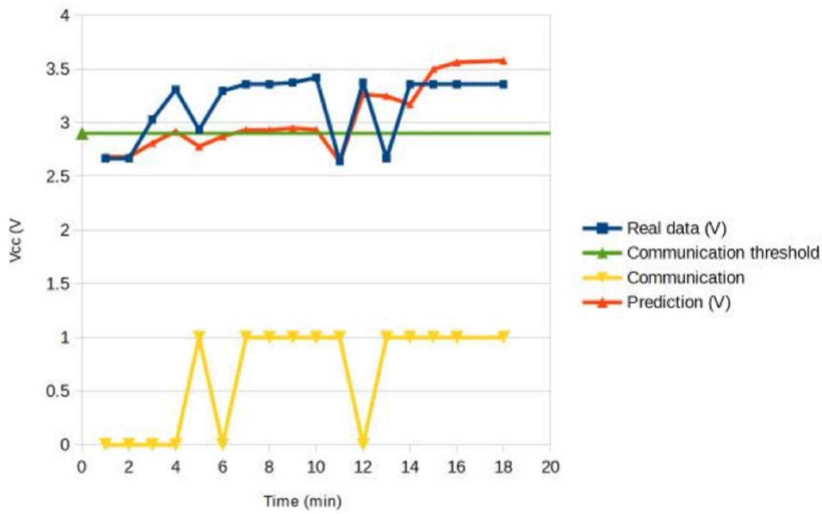

Figure 18. Behaviour of the system for 10-minutes energy prediction (Publication 4).

In this third case, the experiment shows long and stable communication although the energy prediction is very close to communication threshold and a decrease of a few millivolts would stop the communication. However, the waiting time for a stable communication is longer than in the previous case, as shown in Figure 18 at 13:00. Therefore, this specific case illustrates that for such a long prediction time, the system is not adaptive enough.

Through the various experiments and observations, the author found that too short or too long slots are not beneficial for the energy prediction model in order to achieve stability in the communication. In addition, numerous parameters, for instance communication threshold, sampling period, prediction time, and the energy harvester capacity play a vital role to develop a stable system.

2.3.1.3 Evaluation of link quality and reliability of the peer-to-peer Network

The performance of the peer-to-peer setup at certain distances has been assessed by considering three features, namely jitter, ratio of packets transmission, and energy consumption. Though ensuring reliability and link quality could be essential in some applications, in the present environment (temperature monitoring case), this is not very critical. Tables 6 and 7 show the jitter, average receiving rate and other metrics for the link quality and system (node) performance; the details can be found in Publication 4.

Table 6. Peer-to-peer setup performance based on the average receiving rate at various distances (Publication 4).

Distance (m)	Jitter (ms)	Average receiving rate (%)	Power Consumption (mW)
0.3	20.9	94.6	66.7
1	20.9	94.6	66.7
3	20.9	94.6	66.9
6	20.9	94.6	70.2

An important observation is that the implementation of both modalities into the peer-to-peer setup does not affect power significantly; as shown in Tables 6 and 7, the differences in power consumption of the node is very low. In addition, deploying TC and LINE-P (Case-II) model improves the link quality and system stability. The setup's performance and reliability is illustrated by the fact that 94.6% packets were received successfully, as shown in Table 6.

Table 7. Power consumption of the node without TC and LINE-P modalities at various state (Publication 4).

State	Current Consumption (mA)	Power Consumption (mW) at Vcc = 3V
Idle	2	6
Linking	20	60
Communicating	20	60

The experiments illustrate that by adding EP in the TC-based system, the WSN node can estimate the near future energy and based on that amount the node can take the decision to operate further or suspend the operation. However, without EP, TC performs the task based on the instantaneous energy only, neither estimating the availability of energy nor performing the tasks accordingly for e.g. decreasing energy. In this hardware-based implementation, the author also observed that if the voltage decreases sharply for e.g. 4.9 volts/s or more, then the TC mechanism will not be triggered. Similarly, the energy prediction model has its own limits e.g. in highly inconsistent weather.

2.4 Chapter Summary

In this chapter, the author has covered the methodologies of TC and EP, including some background information and state-of-the-art.

The first part explained the TC-based mechanism, its impact and implementation with various energy harvesters as a source. These detailed in Publication 2 where the author exploited TI's CTPL API to implement a TC mechanism similar to that of Hibernus [20].

The second part was related to proposed LINE-P (Linear energy prediction) model for dual source (solar and wind) energy harvester. The author summarized how LINE-P is based on the sampling theory, and how it estimates the energy on the next time-slots. This part also highlighted that LINE-P (all cases) is less complex and requires less information of the past records in order to predict the energy comparatively to the other energy prediction models. The details can be found in Publication 3.

The third part presented the novel idea that combines the two modalities simultaneously. In particular, the benefits of this combining concept were illustrated on a peer-to-peer setup. The details can be found in Publication 4.

3. ADAPTIVE LINE-P (all cases) AND ENERGY PROFILE COMPRESSION TECHNIQUE

This chapter covers the following topics:

- The proposed enhancement of LINE-P, named Adaptive LINE-P model, to address the fixed weighting parameter issue.
- The proposed energy profile compression technique, which can be integrated in any energy prediction model.

In this chapter, the author recalls the limitation shared by most of the prediction models such as IPRO-Energy [8], QL-SEP [27], EWMA [28], PRO-Energy [29], ASEA [30], WCMA [80], and LINE-P (all cases) (Publication 3), i.e., they estimate energy based on a fixed weighting parameter. Such solutions are not always feasible in practical deployments since energy harvesters such as solar panels each have a different set of parameters such as orientation, dust, etc. [26]. Thus, the author suggests an adaptive weighting factor based on the stored energy profiles. The proposed Adaptive LINE-P predicts the energy over three different time-period horizons, i.e. shorter, medium and longer and uses variable-length timeslots. In addition, the proposed model improves the prediction accuracy and minimizes the error between the harvested energy and stored profiles as compared to other non- adaptive, adaptive and variable time-slot EP models.

The remainder of this chapter is organized as follows. First, in the next section, the author discusses the state-of-the-art related to the non-adaptive and adaptive EP models. The proposed Adaptive LINE-P is discussed in Section 3.1. Thereafter, the proposed compression technique is presented in Section 3.2. Its integration with different EP models and their comparative analysis is discussed in Section 3.3. A conclusion is drawn in Section 3.4 and the chapter summary is given in Section 3.5.

In what follows, the author discusses the state-of-the-art regarding fixed kernel parameter, variable length time slots and adaptive (a.k.a dynamic) EP models.

3.1 Non-Adaptive Energy Prediction Models

3.1.1 IPro-Energy

IPro-Energy is an extension of the Pro-Energy model. IPro-Energy has two additional features; first, it uses a weighted profile (WP) technique to counter inconsistent weather. Second, the model estimates energy with low computational complexity and as well as relatively small execution time with low storage data [8]. In addition, IPro-Energy has higher accuracy energy estimation and the implementation of the IPro-Energy on sensor nodes is expected to be feasible without great effort. The results presented in [8] indicate that IPro-energy predictions are 78% accurate for the short term and 50% for medium term prediction horizon.

3.1.2 Pro-Energy-VLT (Variable-length timeslots)

Pro-Energy-VLT is an extension of Pro-Energy which combines energy predictor with timeslots of variable lengths that increases the robustness of the algorithms. In [95], the authors proposed a perceptually important point (PIP) technique to calculate the variable size timeslots such as 30, 60 and 90 minutes, as compared to their original design, which was fixed to a 30 minutes data interval [95]. The authors of Pro-Energy – VLT discussed a case study and assessed the practical feasibility of a hardware implementation with real-life solar and wind energy profiles and as well as publicy-available traces. The authors claim that Pro-energy-VLT improves the prediction accuracy, while reducing the memory and the energy overhead of energy forecasting by 67% and 40%, respectively [95].

3.2 Adaptive Energy Prediction Model

Here, the author discusses the adaptive weighting factor based EP models, which are dependent on the stored energy profile. Moreover, these EP models are much more suitable and compatible with e.g. the solar energy harvesters [26].

3.2.1 UD-WCMA

This energy prediction model proposed in the literature [26] is based on the WCMA EP model but uses a time varying gain parameter G1 (n+1). This gain is adapted depending on the variations in the reference profiles stored in memory [26]. This approach sums the information from measured data and stored profiles which represent the energy patterns in the sensor nodes location to update the prediction model. UD-WCMA yields competitive prediction values and with the tuning free parameter makes it very suitable and robust against the solar harvester parameters such as presence of dust, cast shadows orientation and cloud cover. For example, the absolute error distribution of UD-WCMA is characterized by 24W/m2, which is lower than the other schemes.

3.2.2 Proposed Adaptive Linear Energy Prediction Model (Adaptive LINE-P)

The author proposes an adaptive linear energy prediction model which estimates the energy based on the weather condition rather than using a fixed parameter. The results presented in Publication 3, and summarized below, show that Adaptive LINE-P is more accurate, reliable and adaptable as compared to other EP models.

In what follows, the mathematical modelling of Adaptive LINE-P is summarized.

3.3 Sampling Operators

For the uniformly continuous and bounded $f \in C(\mathbb{R})$, the generalized sampling series are given by $(t \in \mathbb{R}; w > 0)$ as per (6),

$$(S_w f)(t) \coloneqq \sum_{k=-\infty}^{\infty} f\left(\frac{k}{w}\right) s(wt-k), \qquad (6)$$

we get the classical (Whittaker-Kotel'nikov-) Shannon sampling operator,

$$(s_{\omega}^{sinc} f)(t) \coloneqq \sum_{k=-\infty}^{\infty} f\left(\frac{k}{w}\right) sinc(wt-k). \qquad (7)$$

Let us take $w = 1$ and $t = j \in \mathbb{Z}$ in (8), then

$$(S_1 f)(j) \coloneqq \sum_{k=-\infty}^{\infty} f(k) s(j-k) \qquad (8)$$

3.3.1 Kernels

The general kernel for the sampling operators (6) is defined in the following way.

Definition 1 ([96]) if $s: \mathbb{R} \to \mathbb{C}$ is a bounded function such that

$$m_0(s) \coloneqq \sum_{k=-\infty}^{\infty} |s(u-k)| < \infty \ (u \in \mathbb{R}), \qquad (9)$$

with the absolute convergence uniform on compact subsets of $\mathbb{R}$, and

$$\sum_{k=-\infty}^{\infty} s(u-k) = 1 \ (u \in \mathbb{R}), \qquad (10)$$

now s is said to be a kernel for sampling operators (6).

The main aim is to use the generalized sampling operators (6) for predicting the signal, where the kernel function s is defined via the Fourier transform of a certain window function:

Definition 2 A function $\lambda \in C_{\mathbb{R}}$ is called a window function for a kernel of a sampling operator if $\lambda(0) = 1$ and $\lambda(2k) = 0$ for $k \in \mathbb{N}$.

Further details about the derivation of this aspect of the model can be found in Publication 5.

3.3.2 Adaptive Predictors

Adaptive predictors are needed because the energy profiles can have different properties, i.e. with different smoothness, variation, etc. For different types of profiles, there is a need for different kernels for the sampling operators. In the current approach, the author uses the following kernels:

- For smooth profiles, kernels that allow approximation order, estimates via high order of modulus of smoothness.
- For unstable profiles, kernels that provide a sampling operator with minimal (close to 1) norm.

Note: The trivial error estimate signal for additive noise is in form $||S_w|| \ ||v||$, where $||S_w||$ is the operator norm and $||v||$ is the norm of noise component, i.e. if the operator norm is equal to 4, then in the worst case, there is a 4-times amplification of the noise in the predicted energy profile.

To deal with other profiles, a kernel that provides a sampling operator with good approximation properties and small norm is needed.

In order to choose a predictor kernel, the author uses $l_1$norms of the prediction errors of previous estimates.

$\mathbf{l_1}$ norm

In this section, the author proposes a method for adaptive prediction and uses the $l_1$norms of the prediction errors. Moreover, the author chooses some kernels, which generate sampling operators with different properties (approximation order *m*, norm, etc.) and compute the predicted values using it.

For predicting the k-th element, the author chooses the kernel for which the $l_1$norm of the prediction errors for some one-sided neighborhood of the k-th element of the profile is minimal. The norms of errors are calculated in the following form:

$$||E_i(k)||1 = \sum_{j=1}^{n} \left| f(k-j) - f_{p,i}(k-j) \right|,$$

where f(k) is the measured energy in slot k and $f_{p,i}(k)$ is the predicted energy for slot k using the kernels S_i.

For a particular realization of the adaptive predictor, to cover different types of profiles, the author chooses three kernels with different approximation properties and the corresponding sampling operators, i.e., a first one with minimal norm, a second one with high order of approximation, and a third one with good approximation properties and small norm.

3.4 Compressed Energy Profiles

In this section, the author suggests a method for compressing energy profile data to address the memory size limitation of WSN nodes.

The purpose of compression is to reduce $\alpha \geq 1$ times; the author uses the following representation,

$$\bar{f}(t) = \Sigma_k f(k)\bar{S}\,(t-k),$$

where $\bar{f}$ is the compressed energy profile, f the original energy profile and $\bar{S}\,(t) \coloneqq \frac{2}{\alpha} s\,(2t/\alpha)$ the dilated kernel. Instead of *f(k)*, it is only needed to store $\bar{f}(\alpha k)$. For example, if $\alpha = 4$, then 4 times less memory is needed.

For reconstruction, the author uses an interpolating kernel $\tilde{S}$, i.e. a kernel defined using a window function, which satisfies the equality:

$$\lambda(u) + \lambda(1-u) = 1, (u \in [0,1]).$$

The reconstruction formula is as follows:

$$f(j) \approx \Sigma_k \bar{f}(\alpha k) 2\tilde{S}\,\left(\frac{2}{\alpha} j - 2k\right).$$

For a particular realization of the compression algorithm, the author takes $\alpha = 4$ and for both the kernel s and $\widetilde{S}$, he chooses the Hann kernel.

3.5 Accuracy Assessment of the Adaptive LINE-P (all cases)

Based on MAE and MSE error evaluations, the author conducted various tests by deploying solar and wind profiles available in [91]-[92], in order to evaluate the performance in terms of accuracy, robustness, and adaptability.

After the assessment of all cases of Adaptive LINE-P, Case-III yields more accurate results as compared to Case-I and Case-II. Further details about this evaluation can be found in Publication 5.

Given this, Adaptive LINE-P model (Case III) has been selected for further comparison with the state-of-the-art, as presented in the next section.

3.6 Comparison of Adaptive LINE-P (Case-III) with the State-of-the-Art

In the following, the author summarizes the evaluation of the performance of Adaptive LINE-(Case-III) along with the state-of-the-art based on the medium (61 time-slots) time period horizon of the solar energy profile SCE [91].

3.6.1 Assessment of Adaptive LINE-P (Case-III) with the Solar Energy Profile

Figure 19 shows the results for fairly consistent profiles, to observe the behavior and adaptability of the prediction models based on the medium (61 time-slots) time-period horizon. The graphical representation shows that most of the models are estimating up to the mark only for the 1^{st} day. It can be seen that for all other days, LINE-P (Case-III) starts over-estimating. UD-WCMA also starts over- estimating in all days, especially on the 12^{th} and 13^{th} of December from the 45^{th} to the 60^{th} time-slots, and 20^{th} to 50^{th} time-slots. UD-WCMA yields the worst results comparatively to the other EP models. In particular, on the 11^{th} of December, IPro-Energy model is off the chart from the 5^{th} to 10^{th} time-slots. Although gradually its estimation is approaching the real data, it then starts under-estimating after the 40^{th} until the 53^{th} time-slots. On the contrary, Adaptive LINE-P (Case-III) seems much better and most of time yields estimates close to the real data, as also shown in Publication 5.

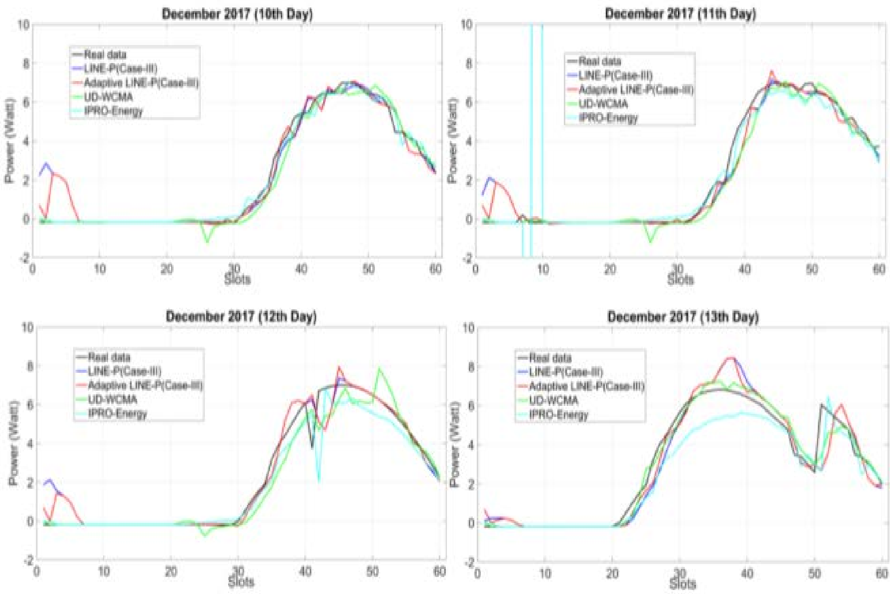

Figure 19. Graphical representation of Adaptive LINE-P (Case-III) and state-of-the-art based on the medium (22-minutes data interval) time-period horizon of solar profile with 61 time-slots in 24 hours.

For further assessment of all the prediction models, we present the estimation errors in Tables 4 and 4a by using MAE and MSE with the same SCE profile available in [91].

Table 8. Error comparison of prediction models in terms of MAE for the SCE solar energy profile (Publication 5).

MODELS	Day 1-MAE	Day 2-MAE	Day 3-MAE	Day 4-MAE	Average-MAE
LINE-P (Case-III)	0.0820	0.0945	0.0944	0.1563	0.1068
UD-WCMA	0.4280	0.3811	0.2961	0.2103	0.3288
IPRO-Energy	0.0782	0.0842	0.1745	0.2008	0.1344
Adaptive LINE-P (Case-III)	0.0802	0.0970	0.0932	0.1405	0.1027

Table 9. Error comparison of prediction models based on MSE for the SCE solar energy profile (Publication 5).

MODELS	Day 1-MSE	Day 2-MSE	Day 3-MSE	Day 4-MSE	Average-MSE
LINE-P (Case-III)	0.0348	0.0493	0.0850	0.1051	0.0685
UD-WCMA	0.5105	0.4112	0.2637	0.1451	0.3326
IPRO-Energy	0.0313	0.0351	0.1898	0.1524	0.1021
Adaptive LINE-P (Case-III)	0.0352	0.0530	0.0849	0.0905	0.0659

In relation to Tables 8 and 9, it is clearly shown that Adaptive LINE-P (Case-III) yields up to ca. 94% accuracy, which is better as compared to the other EP models.

3.6.2 Assessment of Adaptive LINE-P (Case-III) with the Wind Energy Profile

This section summarizes the comparative analysis of Adaptive LINE-(Case-III) with the state-of-the-art based on the shorter (96 time-slots in 24 hours) time period horizon for the wind energy profile Elia (Belgium's electricity transmission system operator) available in [92].

A graphical comparison is shown in Figure 20 and the MAE and MSE values are shown in Tables 10 and 11.

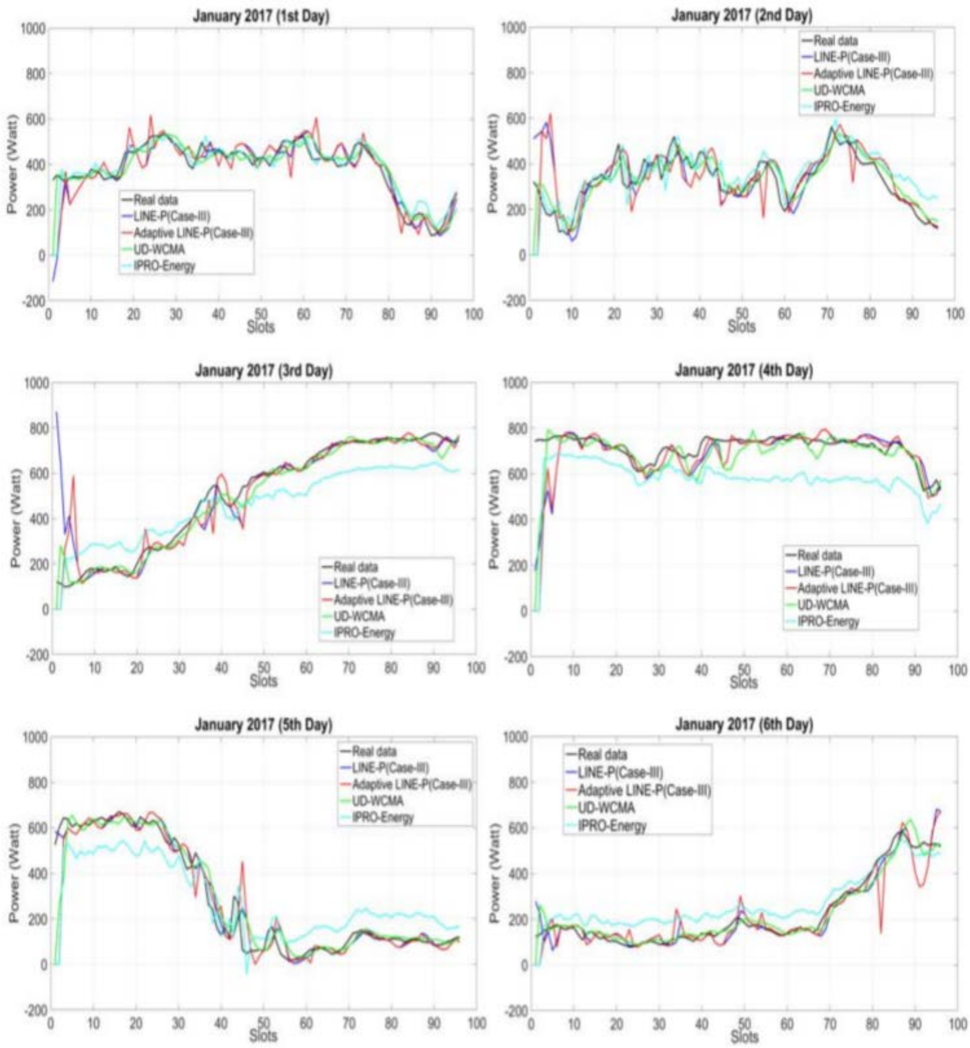

Figure 20. Graphical representation of Adaptive LINE-P (Case-III) and state-of-the-art based on the shorter (15-minutes data interval) time period horizon for the wind energy profile with 96 time-slots in 24 hours (Publication 5).

Table 10. Error comparison of the EP models in terms of MAE for the wind energy profile (Publication 5).

MODELS	Day 1-MAE	Day 2-MAE	Day 3-MAE	Day 4-MAE	Day 5-MAE	Day 6-MAE	Average-MAE
LINE-P (Case-III)	0.0349	0.0623	0.1083	0.4257	0.2294	0.1565	0.1695
UD-WCMA	0.0330	0.0879	0.1088	0.3437	0.1946	0.1279	0.1493
IPRO-Energy	0.0986	0.1907	0.1863	0.6094	3.0968	0.4993	0.7801
Adaptive LINE-P (Case-III)	0.0338	0.0569	0.1095	0.4186	0.2133	0.1594	0.16525

Table 11. Error comparison of the EPs models in terms of MSE for the wind energy profile (Publication 5).

MODELS	Day 1-MSE	Day 2-MSE	Day 3-MSE	Day 4-MSE	Day 5-MSE	Day 6-MSE	Average-MSE
LINE-P (Case-III)	0.0021	0.0065	0.0311	0.4667	0.1451	0.0545	0.1176
UD-WCMA	0.0018	0.0144	0.0415	0.3143	0.1048	0.0323	0.0845
IPRO-Energy	0.0112	0.0441	0.0936	0.5489	1.9788	0.3059	0.4970
Adaptive LINE-P (Case-III)	0.0020	0.0061	0.0292	0.4243	0.1278	0.0563	0.1076

Tables 10 and 11 show that the proposed Adaptive LINE-P (CASE-III) performs better than the other energy prediction models (error down to – 80 %) (Publication 5).

In the above section, the author compared the EPs models with two different sources, namely solar and wind data profiles; apart from a minor exception, the results show that Adaptive LINE-P (Case-III) provides the best results as compared to the other EP models.

3.7 Evaluation of the Compressed Energy Profile Method

Here, the author assesses the compressed energy profile method in two steps. Firstly, its accuracy and adaptability are verified against real data (real energy profile). Secondly, the compression method in incorporated with the two adaptive energy prediction models (Adaptive LINE-P and UD-WCMA) for further assessment against their non-compressed versions.

Generally, the compressed energy profile method is much more effective where slots are shorter. In order to verify the accuracy and adaptability of the method, the author choses wind energy profile since the wind is uncontrollable, and closer or shorter slots estimation of energy can then yield less error.

Figure 21 shows the short time–period horizon, considering 15-mins interval data, which corresponds to 96 slots in 24 hours. It is clearly visible in Figure 21 that the weather conditions are extremely inconsistent. As shown, the first two days appear consistent and productive, but the next two days have a quite low productivity in term of power generation. The last two days have even lower energy production. However, such type of variations expose the weakness of the other prediction models.

On the contrary, Adaptive and compressed LINE-P (Case-III) yields both better accuracy and reliability.

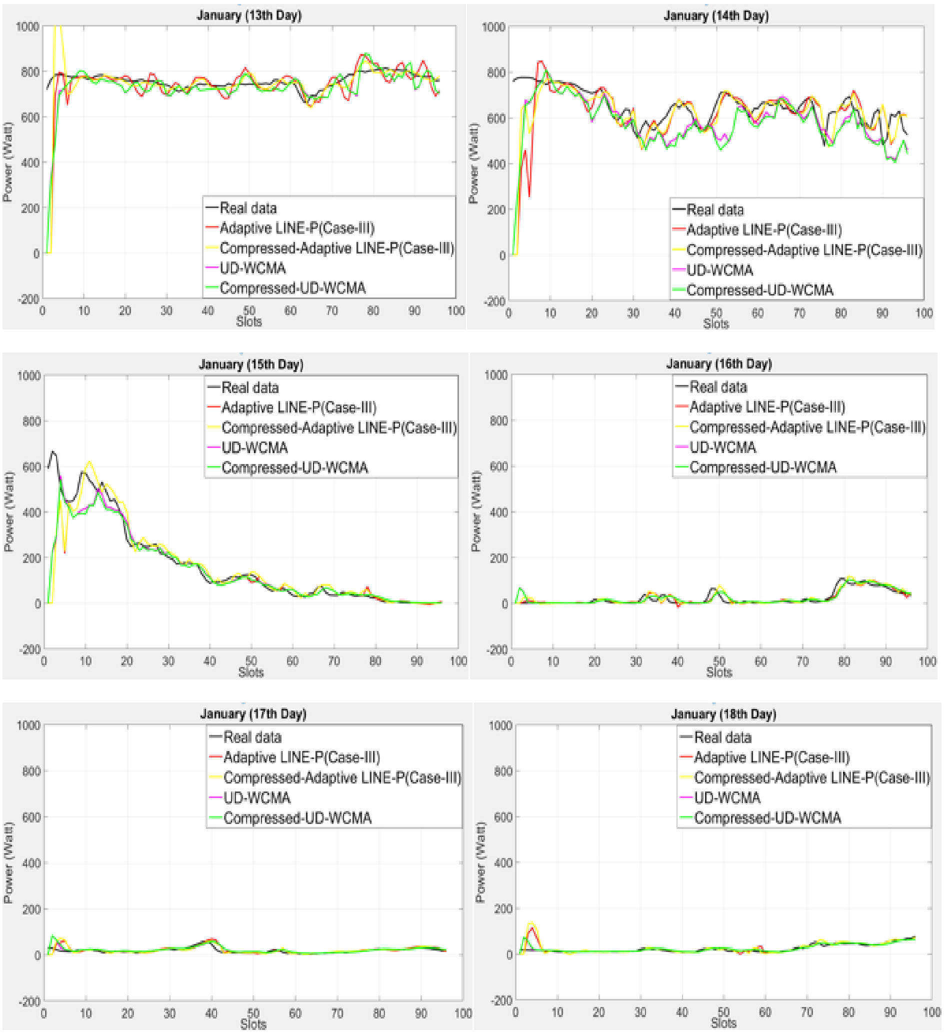

Figure 21. Graphical representation of energy prediction models with and without the compressed profile method based on the short time period horizon of the wind energy profile (Elia) (Publication 5).

In the following, the author calculates the error estimation in terms of MAE and MSE for the wind energy profile (Publication 5).

Table 12. Error estimation in terms of MAE of the prediction models with and without the compressed profile method for the wind energy profile (Publication 5).

MODELS	Day 1-MAE	Day 2-MAE	Day 3-MAE	Day 4-MAE	Day 5-MAE	Day 6-MAE	Average-MAE
Compressed - UD-WCMA	0.2005	0.0852	0.1183	1.7228	3.1929	1.5404	1.1433
Non-Compressed - UD-WCMA	0.1977	0.0884	0.1173	1.6643	3.0968	1.4999	1.1107
Compressed – Adaptive LINE-P (Case-III)	0.0182	0.0518	0.1069	0.4050	0.1908	0.1515	0.1540
Non-Compressed – Adaptive LINE-P (Case-III)	0.0338	0.0569	0.1095	0.4186	0.2133	0.1594	0.1652

Table 13. Error estimation in terms of MSE of the prediction models with and without the compressed profile method for the wind energy profile (Publication 5).

MODELS	Day 1-MSE	Day 2-MSE	Day 3-MSE	Day 4-MSE	Day 5-MSE	Day 6-MSE	Average-MSE
Compressed -UD-WCMA	0.0475	0.0120	0.0306	4.6731	13.0108	2.8090	3.4305
Non-Compressed -UD-WCMA	0.0463	0.0132	0.0304	4.4162	12.2862	2.6713	3.2439
Compressed – Adaptive LINE-P (Case-III)	0.0007	0.0053	0.0285	0.4506	0.0945	0.0495	0.1048
Non-Compressed – Adaptive LINE-P (Case-III)	0.0020	0.0061	0.0292	0.4243	0.1278	0.0563	0.1076

Tables 12 and 13 illustrate the error estimation with and without the proposed profile compression method in terms of MAE and MSE for the wind energy profile. In Table 12, it can be observed that incorporating the compressed profile method increases the MAE for UD-WCMA by +3% but decreases it for Adaptive LINE-P (CASE-III) by – 6.77% (Publication 5).

In Table 13, it can be seen that incorporating the compressed profile method increases the MAE for UD-WCMA by + 5.75 % but decreases it for Adaptive LINE-P (CASE-III) by – 2.6%. As seen earlier, the compressed energy profile method reduces the memory requirements by a factor 2 (Publication 5).

3.8 Chapter Summary

In this chapter, the author has proposed the extension of LINE-P named Adaptive LINE-P (three cases-based). This proposed model alleviates the fixed length time-slot and fixed weighting parameter. Adaptive LINE-P model chooses the weighting parameter based on the actual energy profile. Experiments have been conducted with three time-period horizons (shorter, medium and longer) on different time-slots.

The results show that the proposed adaptive prediction model is highly adaptable against sharp variations or rapid changes as compared to other adaptive and non-adaptive prediction models.

Moreover, in this chapter, the author also proposed a compressed energy profile method that can easily be incorporated with any prediction model; this method allows reducing the memory requirements by 50% and yet provides 90% accuracy.

The outcome of the experimental evaluation of Adaptive LINE-P combined with the energy profile compression illustrates that the prediction error is not significantly degraded when the proposed compressed profile method is used; thus, it offers a good trade-off between accuracy and memory requirements.

The next chapter concludes this PhD work and briefly indicates possible future work.

4. CONCLUSION

This PhD thesis touched upon several aspects related to the energy challenge in wireless sensor nodes, namely energy harvesting technologies, transient computing, energy prediction and the combination thereof. The work can be seen as an effort to the development of autonomous wireless sensor networks, and on the longer run, to energy-efficient IoT solutions.

The thesis comprised 4 chapters. After the introduction, the 1st chapter covered the architecture of WSNs, energy harvesting technologies, and related models and background information. The 2nd chapter focused on the mathematical modelling & implementation of transient computing and energy prediction model. The 3rd chapter presented the adaptive energy prediction model and the energy profile compression technique.

In particular, the author presented a combined transient computing mechanism and energy prediction model; the expected benefit of this combined approach is to help developing battery-less nodes that can be used in applications such as delay-tolerant sensor networks. The nodes can perform their computation and communication tasks as a function of the available energy.

Indeed, transient computing enables pausing/resuming the tasks when power losses occur and estimating the energy availability enables improving the system (node) performance and quality of service by pausing the tasks and sharing the information with other nodes before a power loss occurs.

The above work has been carried out not only by means of theoretical models but also by means of practical experiments involving the development of a hardware/software implementation.

The introductory chapter of this PhD thesis posed the following research questions:

1. How to rapidly evaluate the feasibility of existing and emerging energy harvesting technologies in the context of WSNs/IoT and what kind of models are sufficient to enable the above?
2. How to combine and implement the concepts of EH and TC in WSN nodes and what are the practical possibilities and limitations of such a joint approach?
3. How to design an EP model that can be used with several types of EH sources and how to reduce its computational overhead so that it can be implemented on a resource-constrained WSN node? In addition, how to further improve the EP model in terms of adaptability and reduced memory overhead?
4. How to combine and exploit EH, TC, and EP to make the best use of the available energy, i.e., control the quality of service of the application executing on a WSN network that include a WSN node solely powered by EH?

What follows briefly discusses how the contributions of this thesis provide answers or element thereof to the above questions.

Paper 1

This paper presented a system-level exploration framework named FYPSim that includes coarse-grain models of various energy harvesting technologies (including hybrid energy harvesting and battery management) and the sizing of energy storage technologies. The framework also enables comparing energy prediction algorithms (EWMA, WCMA, etc.) The exploration results with energy harvesting technology models for indoor solar, indoor air flow, and indoor radio frequency, as well as energy storage technology models for Li-Ion batteries and supercapacitors. It can be said that such coarse-grain models enable the rapid exploration of various technologies (as opposed to simulators that are based on fine-grain models that are slower to simulate), thus providing an answer to the 1st research question.

Paper 2

This paper presented the implementation of transient computing on a FRAM- based node (MSP430FR5739+CC2500) cascaded directly with three energy harvesting sources (RF, solar, thermal) without energy storage such as a battery or super capacitor. Based on various experiments, the author concluded that energy harvesting combined with transient computing in WSN nodes is indeed feasible. A limitation that was identified is the need for energy sources that can sustain the peaks of current that occur at boot time and when resuming the nodes' operations. Thus, based on the results, Paper II provides an answer to the 2nd research question.

Paper 3

This paper proposed LINE-P, a linear energy prediction model that builds upon approximation and sampling theory. LINE-P is suitable for dual-source energy harvesting. The results show that the accuracy of the solar-based and wind-based predictions is up to approximately 98% and 96%, respectively. At the same time, the proposed LINE-P model offers the best trade-off among existing energy prediction models, i.e., equivalent or better prediction accuracy at a lower complexity, which makes LINE-P is a good candidate for implementation on resource-constrained WSN nodes. Thus, this contribution provides an answer to the first part of the 3rd research question (Paper V answers the second part).

Paper 4

This paper proposed a novel approach for the combined implementation of two modalities (transient computing and energy prediction) aimed at improving the adaptability and robustness of a bidirectional communication setup comprising an energy-autonomous WSNs node. The experimental results show that the implemented modalities consume only 15% of the total memory of a node, the accuracy of the energy prediction is 90% in inconsistent weather, and the average receiving rate (reliability of the packet transmission/reception at various distances) is 94.6%. Thus, based on the proposed approach and experimental results, Paper IV provides answers to the 4th research question.

Paper 5

The paper proposed the Adaptive LINE-P (all cases) model which is an enhancement of the LINE-P model. Adaptive LINE-P incorporates an adaptive mechanism which removes the fixed-parameter issue. In addition, the paper introduced a compression technique which compresses the stored energy profile. This technique was incorporated in both Adaptive LINE-P and other existing energy prediction models. The results showed 90% accuracy in Adaptive LINE-P model along with a memory overhead reduced by 50% on solar and wind energy profiles based on shorter (96 slots in 24 hours) time-period horizon.

Thus, based on the proposed adaptive energy prediction model, energy profile compression technique and the results, Paper V provides answers to the second part of the 3rd research question.

Summary of Claims

In the following, the claims of novelty that were shown in this PhD work are listed. The claims correspond to Contributions A to E and are reflected in Papers 1-5.

Claim 1: To the best knowledge of the author, the proposed system-level framework FYPSim provides a complement to other existing WSNs simulators since it allows the rapid exploration of alternatives before their detailed simulation. This corresponds to Contribution A and Publication 1.

Claim 2: To the best knowledge of the author, the proposed mathematical model of LINE-P, based on the approximation and sampling theory, is unique in the scientific literature and offers a good trade-off between accuracy and complexity. In addition, LINE-P is designed and developed for the dual source energy profile (solar and wind); its methodology and demonstration have been shown through a practical implementation. This corresponds to Contribution C and Publication 2.

Claim 3: The author proposed a novel approach by combining two modalities (transient computing and prediction model) and demonstrated them through their implementation on a peer-to-peer setup of wireless sensor nodes. This corresponds to Contribution B to D and Publication 2 to 4. To the knowledge of the author, such an approach has not been proposed and published previously.

Claim 4: The author proposed the mathematical model of Adaptive LINE-P, which is an extension of the LINE-P model. Adaptive LINE-P is based on an adaptive weighting factor parameter, which is calculated as a function of the weather condition. This proposed prediction model is highly reliable, robust, adaptable and up to 90% accurate. To the best of knowledge of the author, the proposed energy profile compression technique that can reduce the memory overhead by up to 50% is the first of its kind. This corresponds to Contribution E and Publication 5.

Perspectives and Future work

With the technological advancement, increasing requirements and fast deployment of IoT, it is expected that the sensor nodes will deployed everywhere. This means an increased overall energy consumption even if progress can be made in terms of energy storage capacity and energy harvesting efficiency. Therefore, the proposed solution, in particular combining modalities of transient computing and energy prediction is expected to be suitable approach for cases where the delay is not critical or where monitoring is not required on a 24/7 basis.

Furthermore, the work presented in this PhD thesis could be expanded along several directions.

Firstly, energy trading between the wireless node could be considered. To do so, RF energy harvesting and RF energy transfer circuitry could be combined with a brokering mechanism that would distribute the available energy depending on the workload of the individual nodes.

Secondly, due to dense deployment of IoT, dealing with large amounts of data is creating new challenges in terms of data exchange, storage capacity, data management, computation, etc. Therefore, the traditional WSN approach may no longer be effective and thus, adding new spatial and/or temporal data prediction models to the presented work may help reducing such new burdens by reducing the amount of actual data to be transferred, stored and processed.

REFERENCES

[1] U.S. National Intelligence Council, “Disruptive Civil Technologies - six technologies with potential impacts on us interests out to 2025, Conference Report 2008-07,” http: //www.dni.gov/nic/NIC home.html, (Accessed September 2017).

[2] [Harrop2014] Harrop P., Das R., “Wireless Sensor Networks (WSN) 2014-2024: Forecasts, Technologies, Players - The New Market for Ubiquitous Sensor Networks (USN),” 2014, IDTechEx.

[3] I. F. Akyildiz, W. Su, Y. Sankarasubramaniam, and E. Cayirci, “A survey on sensor networks,” IEEE Commun. Mag., vol. 40, no. 8, pp. 102–105, 2002.

[4] C. Buratti, A. Conti, D. Dardari, and R. Verdone, “An overview on wireless sensor networks technology and evolution,” Sensors, vol. 9, no. 9, pp. 6869–6896, 2009.

[5] M. Chen, S. Gonzalez, A. Vasilakos, H. Cao, and V. C. M. Leung, “Body area networks: A survey,” Mob. Networks Appl., vol. 16, no. 2, pp. 171– 193, 2011.

[6] P. Rawat, K. D. Singh, H. Chaouchi, and J. M. Bonnin, “Wireless sensor networks: A survey on recent developments and potential synergies,” J. Supercomput., vol. 68, no. 1, pp. 1–48, 2014.

[7] Technology and Energy Assessment Report Prepared for IEA 4E EDNA. https://www.iea4e.org/document/energy-efficiency-of-the-internet-of-things-technology-and-energyassessment-report. (Accessed June 2017).

[8] H. K. Qureshi, U. Saleem, M. Saleem, A. Pitsillides, and M. Lestas, “Harvested Energy Prediction Schemes for Wireless Sensor Networks : Performance Evaluation and Enhancements,” vol, 2017.

[9]J.A.Paradiso and T.Starner,“Energy scavenging for mobile and wireless electronics,”IEEE Pervasive Computing,vol.4,no.1,pp. 18–27,2005.

[10] S. Sudevalayam and P. Kulkarni, “Energy harvesting sensor nodes: Survey and implications,”IEEE Communications Surveys & Tutorials,vol.13,no.3,pp.443–461,2011.

[11] Ma, X., Bader, S., & Oelmann, B. (n.d.). Solar Panel Modelling for Low Illuminance Indoor Conditions, 2017.

[12] J. Allen, M, Forshaw, & N. Thomas, (2017). Towards an Extensible and Scalable Energy Harvesting Wireless Sensor Network Simulation Framework, 39–42.

[13] M, Magno; L, Benini.; Gaggero, L.; la Torre Aro, J.P.; Popovici, E. A Versatile Biomedical Wireless Sensor Node with Novel Dry Surface Sensors and Interfaces. In Proceedings of the 5th IEEE International Workshop, Bari, Italy, 13–14 June 2013; pp. 217–222.

[14] W. Karlen; D. Floreano. Adaptive Sleep-Wake Discrimination for Wearable Devices. Biomed. Eng. IEEE Trans. 2011, 58, 920–926.

[15] P.Subendran; S.K.Viswanath; C.Yuen,C; C.S.Veerappan, Adaptive Transmission for Self-Sustainable Energy Harvesting Wireless Sensor Network. In Proceedings of the Frontiers of Communications, Networks and Applications (ICFCNA 2014—Malaysia), Kampar, Malaysia, 3–5 November 2014.

[16] Z.G Wan; Y.K. Tan; C.Yuen. Review on Energy Harvesting and Energy Management for Sustainable Wireless Sensor Networks. In Proceedings of the 2011 IEEE 13th International Conference on Communication Technology, Jinan, China, 25–28 September 2011; pp. 362–367.

[17] X. Xu and G. Zhang, “A Hybrid Model for Data Prediction in Real-World,” vol. 7798, no. c, pp. 1–4, 2017.

[18] A. Mehrabi, S. Member, K. Kim, and S. Member, “Maximizing Data Collection Throughput on a Path in Energy Harvesting Sensor Networks Using a Mobile Sink,” vol. 15, no. 3, pp. 690–704, 2016.

[19] J. San, M. Karthik, G. Mario, and N. E. Jerger, “The EH Model : Analytical Exploration of Energy-Harvesting Architectures,” vol. 6056, no. c, pp. 1–4, 2017.

[20] D. Balsamo; A.S. Weddell; G.V.Merrett; B. M. Al-Hashimi; D.Brunelli; L. Benini. Hibernus: Sustaining Computation during Intermittent Supply for Energy-Harvesting Systems. IEEE Embed. Syst. Lett., vol. 7, no. 1, pp. 15–18, Mar. 2015.

[21] B. Ransford; J. Sorber; Fu, K. Mementos, Mementos: System Support for Long-Running Computation on RFID-Scale Devices. ACM SIGPLAN Not. 2011, 46, 159–170.

[22] M. Hicks, “Clank: Architectural support for intermittent computation,” in 44th ISCA. ACM, 2017, pp. 228–240.

[23] D. Balsamo; A. Das; A. Weddell; D. Brunelli; B. Al-Hashimi; G. Merrett; L. Benini, Graceful Performance Modulation for Power-Neutral Transient Computing Systems. IEEE Trans. Comput. Des. Integr. Circuits Syst. 2016, 35, 738–749.

[24] B. Lucia; B. A. Ransford, Simpler, Safer Programming and Execution Model for Intermittent Systems. ACM Sigplan Not. 2015, 50, 575–585.

[25] H. Jayakumar; A. Raha; W.S. Lee; Raghunathan, V. QuickRecall: A HW/SW Approach for Computing across Power Cycles in Transiently Powered Computers. ACM J. Emerg. Technol.Comput. Syst. 2015, 12, 1–19.

[26] A. Dehwah, S. Elmetennani, C. Claudel, “UD-WCMA: An energy estimation and forecast scheme for solar powered wireless sensor networks," Jounal of Network and Computer Application, 17-25, Vol - 90, Jan 2017.

[27] S. Kosunalp, A new energy prediction algorithm for energy-harvesting wireless sensor networks with Q-Learning. IEEE Access, PP (99), 5755–5763. http://doi.org/10.1109/ACCESS.2016.2606541.

[28] A. Kensal, et al.: Power Management in Energy Harvesting Sensor Networks. ACM Transactions on Embedded Computing Systems (2007).

[29] A. Cammarano, C. Petrioli, & D. Spenza, (2012). Pro-Energy: A novel energy prediction model for solar and wind energy-harvesting wireless sensor networks. MASS 2012 - 9th IEEE International Conference on Mobile Ad-Hoc and Sensor Systems, 75–83. http://doi.org/10.1109/MASS.2012.6502504

[30] D. K. Noh, & K . Kang,(2011). Balanced energy allocation scheme for a solar-powered sensor system and its effects on network-wide performance. Journal of Computer and System Sciences, 77(5), 917–932. http://doi.org/10.1016/j.jcss.2010.08.008.

[31] A. Cammarano, C. Petrioli, & D. Spenza, (2013). Pro-Energy VLT: Poster Abstract: Improving Energy Predictions in EH-WSNS with Pro-Energy-VLT SenSys' 13, Nov 2013, ACM 978-1-4503-2027-6-13-11, http://doi.org/10.1145/2517351.2517413.

[32] D. Culler, D. Estrin, and M. Srivastava, "Overview of sensor networks," Computer (Long. Beach. Calif)., vol. 37, no. 8, pp. 41–49, 2004.

[33] M. Tubaishat and S. Madria, "Sensor networks: an overview," IEEE Potentials, vol. 22, no. 2, pp. 20–23, 2003.

[34] N. Dawood, G. M. Revel, and M. Sciences, "A Wireless Sensor Network For Intiligent Building Enegry Management Based On Multi Communication Standards – A Case Study," vol. 17, no. December 2010, pp. 43–62, 2012.

[35] T. S. Perry, "A Temporary Tattoo That Senses Through Your Skin", IEEE Spectrum, [online], http://spectrum.ieee.org/biomedical/devices/a-temporary-tattoo-that-senses-through-your-skin [Accessed: 29-May-(2015)].

[36] D. Balsamo, G V Merrett, B Zaghari, et al. Wearable and Autonomous Computing for Future Smart Cities : Open Challenges.2017.

[37] E. Ackerman, "Power Harvesting Sensor Patch Uses Your Body As a Battery", IEEE Spectrum, [online], http://spectrum.ieee.org/tech-talk/biomedical/devices/power-harvesting-sensor-patch-uses-your-body-as-a-battery, [Accessed: 16-Jan-(2016)].

[38] I. F. Akyildiz and M. C. Vuran, Wireless Sensor Networks, ser. Advanced Texts in Communications and Networking. Hoboken, NJ: John Wiley & Sons, August 2010.

[39] A. Gomez, L. Benini, L. Thiele. Designing Reliable Transient Applications.2017.

[40] S. Sudevalayam and P. Kulkarni, "Energy harvesting sensor nodes: survey and implications," IEEE Communications Surveys and Tutorials, vol. 13, no. 3, pp. 443 –461, Third quarter 2011.

[41] D. Spenza, " Towards Self-Powered Wireless Sensor Networks Computer Science by," PhD PhD thesis Department of Computer Science, SAPIENZA UNIVESITA DI ROMA, ROME, 2013.

[42] F. K. Shaikh and S. Zeadally, "Energy harvesting in wireless sensor networks: A comprehensive review," Renew. Sustain. Energy Rev., vol. 55, pp. 1041–1054, 2016.

[43] V. Raghunathan, A. Kansal, J. Hsu, J. Friedman, and M. Srivastava,"Design considerations for solar energy harvesting wireless embedded systems,"in Proceedings of the 4th International Symposium on Information Processing in Sensor Networks (IPSN 2005), Apr 15 2005, pp. 457–462.

[44] X. Jiang, J. Polastre, D. Culler, Perpetual environmentally powered sensor networks In: Fourth International Symposium on Information Processing in Sensor Networks, 2005

[45] S. Ayazian, E. Soenen, and A. Hassibi,"A photovoltaic-driven and energy-autonomous CMOS implantable sensor," in Proceedings of IEEE VLSIC 2011, June 2011, pp. 148– 149.

[46] M. Barnes, C. Conway, J. Mathews, and D. K. Arvind, "ENS: An energy harvesting wireless sensor network platform," in Proceedings of ICSNC, August 2010, pp. 83–87.

[47] V. Leonov "Thermoelectric energy harvesting of human body heat for wearable sensors," IEEE Sensors J. , vol. 13, pp. 2284-91, 2013.

[48] NA Bhatti, L. Mottola. HarvOS : Efficient Code Instrumentation for Transiently-powered Embedded Sensing. 2017.

[49] R. Heer, J. Wissenwasser, M. Milnera, L. Farmer, C. H¨opfner, and M. Vellekoop, "Wireless powered electronic sensors for biological applications,"in Proceedings of IEEE EMBC, September 2010, pp. 700–703.

[50] S. Mandal, L. Turicchia, and R. Sarpeshkar, "A low-power, battery-free tag for body sensor networks," IEEE Pervasive Computing, vol. 9, no. 1, pp. 71–77, March 2010.

[51] H. Reinisch, S. Gruber, H. Unterassinger, M. Wiessflecker, G. Hofer, W. Pribyl, and G. Holweg, "An electro-magnetic energy harvesting system with 190 nW idle mode power consumption for a BAW based wireless sensor node," IEEE Journal of SolidState Circuits, vol. 46, no. 7, pp. 1728–1741, July 2011.

[52] F. Fei, J. D. Mai, and W. J. Li, "A wind-flutter energy converter for powering wireless sensors,"Sensors and Actuators A: Physical, vol. 173, no. 1, pp. 163–171, January 2012.

[53] E. Sardini and M. Serpelloni, "Self-powered wireless sensor for air temperature and velocity measurements with energy harvesting capability," IEEE Transactions on Instrumentation and Measurement, vol. 60, no. 5, pp. 1838–1844, May 2011.

[54] Y. K. Tan and S. K. Panda, "Energy harvesting from hybrid indoor ambient light and thermal energy sources for enhanced performance of wireless sensor nodes," IEEE Transactions on Industrial Electronics, vol. 58, no. 9, pp. 4424–4435, September 2011.

[55] S. Sherrit, "The physical acoustics of energy harvesting," in Proceedings of IEEE IUS 2008, November 2008, pp. 1046–1055.

[56] F. Liu, A. Phipps, S. Horowitz, K. Ngo, L. Cattafesta, T. Nishida, and M. Sheplak, "Acoustic energy harvesting using an electromechanical Helmholtz resonator," Journal of the Acoustical Society of America, vol. 123, no. 4, pp. 1983—1990, 2008.

[57] N AUNS, Prabhakar T V, Prasad RV, Jamadagni HS. Zero Energy Network stack for Energy Harvested WSNs.

[58] A, James. F, Mathew, Thomas N,''Wireless Sensor Network Simulation Framework'', ICPE '17 Companion, April 22 - 26, 2017, L'Aquila, Italy.

[59] D. Benedetti, C. Petrioli, and D. Spenza. GreenCastalia. ENSSys '13, pages 7:1–7:6, 2013.

[60] R. Dall'Ora, U. Raza, D. Brunelli, and G. P. Picco. SensEH: From simulation to deployment of energy harvesting wireless sensor networks. IEEE LCN Workshops, pages 566–573, 2014.

[61] G. V. Merrett, N. M. White, N. R. Harris, and B. M. Al-Hashimi. Energy-aware simulation for wireless sensor networks. SECON, 2009.

[62] S. Climent, A. Sanchez, S. Blanc, J. V. Capella, and R. Ors. Wireless sensor network with energy harvesting: modeling and simulation based on a practical architecture using real radiation levels.CCPE, 28:1812–1830, 2016.

[63] J. Jeong, C. Systems, and D. Culler. A Practical Theory of Micro- Solar Power Sensor Networks. ACM Trans. Sensor Netw, 9(9), 2012.

[64] A. Didioui, C. Bernier, D. Morche, and O. Sentieys. HarvWSNet: A co-simulation framework for energy harvesting wireless sensor networks. ICNC, 2013.

[65] A. Castagnetti, A. Pegatoquet, C. Belleudy, and M. Auguin. A framework for modeling and simulating energy harvesting WSN nodes with efficient power management policies. Journal on Embedded Systems, pages 1–20, 2012.

[66] P. De Mil, B. Jooris, L. Tytgat, R. Catteeuw, I. Moerman, P. Demeester, and A. Kamerman. Design and implementation of a generic energy-harvesting framework applied to the evaluation of a large-scale electronic shelf-labeling wireless sensor network.Eurasip JWCN, 2010.

[67] Balsamo, Domenico, Weddell, S. Alex, Das, Anup, Rodriguez Arreola, Alberto, Brunelli, Davide, AlHashimi, M. Bashir, Merrett, V. Geoff. and Benini, Luca. Hibernus++: a self-calibrating and adaptive system for transiently-powered embedded devices. IEEE Transactions on Computer-Aided Design of Integrated Circuits and Systems, 35, (12), pp. 1968-1980, 2016.

[68] Zurich ETH, Sigrist L. Design Support for Energy Harvesting Driven IoT Devices. :9-10.2017.

[69] K. Ma, Y. Zheng, S. Li, K. Swaminathan, X. Li, Y. Liu, J. Sampson, Y. Xie, and V. Narayanan. 2015. Architecture exploration for ambient energy harvesting nonvolatile processors. In IEEE 21st HPCA 2015. IEEE, San Francisco, CA, USA,526–537.

[70] G V Merrett, B M Al-hashimi. Energy-Driven Computing : Rethinking the Design of Energy Harvesting Systems:960-965, 2017.

[71] T. D. Verykios, D. Balsamo, and G. V Merrett, “Exploring Energy Efficient State Retention in Transiently-Powered Computing Systems Extended Abstract,” pp. 3–4, 2017.

[72] E. Fadel et al., “A survey on wireless sensor networks for smart grid,” Comput. Commun., vol. 71, pp. 22–33, 2015.

[73] Balsamo, domenico; Elboreini, Ali; Al-Hashimi, M. Bashir; Merrett, Geoff V. Exploring ARM mbed support for transient computing in energy harvesting IoT systems. 7th IEEE International Workshop on Advances in Sensors and Interfaces (IWASI), 2017.

[74] N. A. Bhatti and L. Mottola. 2016. Efficient State Retention for Transiently- powered Embedded Sensing.In EWSN 2016. Graz, Austria, 137–148.

[75] S. Ahmed, H. Khan, and J. H. Siddiqui, “Poster Abstract : Incremental Checkpointing for Interruptible Computations,” 2016.

[76] S. Naderiparizi, A. N. Parks, Z. Kapetanovic, B. Ransford and J. R. Smith, "WISPCam: A battery-free RFID camera," 2015 IEEE Int'l Conf. RFID, San Diego, CA, 2015, pp. 166-173.

[77] A. Gomez, L. Sigrist, M. Magno, L. Benini, L. Thiele, "Dynamic energy burst scaling for transiently powered systems," in Proc. Conf. Design, Automation & Test in Europe (DATE'16), Dresden, Germany, Mar 2016.

[78] S. DeBruin, B. Campbell, and P. Dutta, "Monjolo: an energy-harvesting energy meter architecture," in Proc. ACM Conf. Embedded Networked Sensor Systems (SenSys '13), Rome, Italy, Nov 2013.

[79] D. R. Cox, "Prediction by exponentially weighted moving averages and related methods,"Journal of the Royal Statistical Society. Series B (Methodological), vol. 23, no. 2, pp. 414–422, 1961.

[80] J. R. Piorno, C. Bergonzini, D. Atienza, and T. S. Rosing,"Prediction and management in energy harvested wireless sensor nodes,"in Proceedings of Wireless VITAE 2009, May 17–20 2009, pp. 6–10.

[81] C. Moser, L. Thiele, D. Brunelli, and L. Benini,"Adaptive power management in energy harvesting systems," in Proceedings of IEEE DATE 2007, Nice, France, April 16-20, 2007, pp. 773–778.

[82] C. Bergonzini, D. Brunelli, and L. Benini,"Algorithms for harvested energy prediction in batteryless wireless sensor networks," in Proceedings of IWASI 2009, June 25–26 2009, pp. 144–149.

[83] D. K. Noh and K. Kang,"Balanced energy allocation scheme for a solar-powered sensor system and its effects on network-wide performance,"Journal of Computer and System Sciences, vol. 77, no. 5, pp. 917–932, September 2011.

[84] J. Lu, S. Liu, Q. Wu, and Q. Qiu, "Accurate modeling and prediction of energy availability in energy harvesting real-time embedded systems," in Proceedings on the 1st Green Computing Conference, ser. IEEE IGCC 2010, Chicago, IL, USA, August 15-18, 2010, pp. 469 –476.

[85] C. Moser, D. Brunelli, L. Thiele, and L. Benini, Lazy Scheduling for Energy Harvesting Sensor Nodes, ser. IFIP International Federation for Information Processing. Springer, October 2006, vol. 225, pp. 125–134.

[86] C. Moser, J. J. Chen, and L. Thiele,"Power management in energy harvesting embedded systems with discrete service levels,"in Proceedings of ACM/IEEE ISLPED 2009, 2009, pp. 413–418.

[87] C. Moser, D. Brunelli, L. Thiele, and L. Benini, "Real-time scheduling for energy harvesting sensor nodes," Real-Time Syst., vol. 37, no. 3, pp. 233–260, Dec. 2007.

[88] N. Sharma, J. Gummeson, D. Irwin, and P. Shenoy, "Cloudy computing: Leveraging weather forecasts in energy harvesting sensor systems,"in Proceedings of SECON 2010, Boston, MA, June 21–25 2010, pp. 1–9.

[89] C. Park and P. Chou, "Ambimax: Autonomous energy harvesting platform for multisupply wireless sensor nodes," in Proceedings of IEEE SECON 2006, vol. 1, Reston, Virginia, USA, September 25-28, 2006, pp. 168 –177.

[89] C. Park and P. Chou, “Ambimax: Autonomous energy harvesting platform for multisupply wireless sensor nodes,” in Proceedings of IEEE SECON 2006, vol. 1, Reston, Virginia, USA, September 25-28, 2006, pp. 168 –177.

[90] M. Magno, S. Marinkovic, D. Brunelli, E. Popovici, B. O’Flynn, and L. Benini,“Smart power unit with ultra low power radio trigger capabilities for wireless sensor networks,” in Proceedings of IEEE DATE 2012, Dresden, Germany, March 12-16, 2012, pp. 75 –80.

[91] California IOS. Our Renewables Reports Provide Important Information about Actual Renewable Energy within the ISO Grid as California Moves Towards a 33 Percent Renewable Generation Portfolio. The Reports Use Raw Data and Are not Intended to Be Used as the Basis for Operational or Financial Decisions. Available online:

http://www.caiso.com/market/Pages/ReportsBulletins/DailyRenewablesWatch.aspx (accessed on 14 July 2017).

[92] Elia. Data Download Page. Available online: http://www.elia.be/en/grid-data/data-download (accessed on 14 July 2017).

[93] Z. A. Eu, H. P. Tan, and W. K. G. Seah, “Opportunistic routing in wireless sensor networks powered by ambient energy harvesting,” Computer Networks, vol. 54, no. 17, pp. 2943–2966, December 2010.

[94] T. Zhu, Z. Zhong, Y. Gu, T. He, and Z.-L. Zhang,“Leakage-aware energy synchronization for wireless sensor networks,” in Proceedings of the 7th international conference on Mobile systems, applications, and services, ser. MobiSys ’09, New York, NY, USA, 2009, pp. 319–332.

[95] A. Cammarano, C. Petrioli, S. Member, and D. Spenza, “Online Energy Harvesting Prediction in Environmentally Powered Wireless Sensor Networks,” vol. 16, no. 17, pp. 6793–6804, 2016.

[96] P. L. Butzer, W. Splettst¨oßer, and R. L. Stens, The sampling theorems and linear prediction in signal analysis. Jahresber. Deutsch. Math-Verein 90 (1988), 1–70.

ACKNOWLEDGEMENTS

I thank Professor Toomas Rang, Head of Thomas Johann Seebeck Department of Electronics at Tallinn University of Technology, for giving me the opportunity to conduct my PhD research in his department.

I also thank my three supervisors: Professor Yannick Le Moullec, Senior Researcher Paul Annus, and Senior Researcher Gert Tamberg for their guidance, suggestions, and encouragements during my PhD studies. I am especially grateful to Senior Researcher Gert Tamberg for the pivotal role he played when he joined my supervising team.

I am thankful for my colleagues, in particular Dr. Raul Land and Mr. Eero Haldre for their technical support while conducting the experiments.

I thank my family for their constant support and encouragements that helped me throughout the research and writing of this PhD thesis.

I express my gratitude to the following entities for their financial support during my PhD studies:

- Estonian National Scholarship Programme for International Students, Researchers and Academic staff;
- IT Academy Scholarship for PhD Students of Information and Communication Technology;
- Ministry of Education and Research (Baseline Project B38 “Hardware and Software Solutions for cognitive Embedded Networks Systems”);
- ICT Doctoral School at Tallinn University of Technology.

ABSTRACT

The advent and growth of the IoT has opened new directions and challenges for the scientific community. In particular, IoT enabling devices such as wireless sensor nodes are powered by energy-limited batteries, which affects their life-time and reliability in case of intensive utilization, and eventually leads to increased maintenance requirements and related cost. Thus, researchers have investigated and proposed various solutions under the so-called energy harvesting concept. Such solutions help overcoming the limited batteries' capacities by providing a supplementary or alternative source of energy to operate e.g. smart devices, wireless sensor nodes, home appliances, industrial machine etc. The positive impact of energy harvesting in IoT enables innovative applications that are no longer hindered by the batteries limits.

However, energy harvesting poses several challenges both at the hardware and software levels when designing energy-autonomous wireless sensor nodes. Indeed, energy harvesting from the environment such as from solar, wind, thermal, RF etc sources typically exhibits intermittent characteristics. This means that the wireless sensor nodes may be left without power, which in turn impacts the application's performance in terms of e.g. connectivity and reliability.

Firstly, the author proposed a system-level framework that uses coarse-grain models of various single and hybrid energy harvesting technologies for wireless sensor nodes. Experimental results illustrate how the framework can be used to evaluate various energy harvesting sources for powering WSN nodes.

Then the author assessed the practical feasibility of powering a wireless sensor node from an energy harvesting source without energy storage. A salient feature of the work is the implementation of a transient computing mechanism on a non-volatile (FRAM-based) node. The experimental results illustrate that energy harvesting, combined with transient computing, is indeed feasible.

Next the author proposed an energy prediction model named LINE-P (Linear Energy Prediction). It builds upon sampling and approximation theory. LINE-P is more suitable for dual EH sources and various data time intervals than state-of-the-art models. The simulation results show that LINE-P's prediction accuracy is up to ca. 98% for solar energy and up to ca. 96% for wind-based prediction.

Thereafter, the author deployed a transient computing mechanism for bidirectional communication where energy harvesting is used in combination with transient computing and the LINE-P energy prediction model. This allows firing communication tasks only if sufficient and stable energy is predicted. The results for a peer-to-peer wireless setup illustrate that the combined two modalities require only 15% of the node's memory, and this proposed approach (combined) yields an average receiving rate up to 94.6%.

Finally, the author designed the Adaptive LINE-P model that addresses the fixed weighting parameter issue by calculating adaptive weighting parameters based on the stored energy profiles. In addition, a profile compression method has been proposed to reduce the memory requirements. The results illustrate that Adaptive LINE-P's accuracy is up to 90-94% and compression method can 50% reduce memory overheads.

KOKKUVÕTE

Teadlaskonnale on avanenud uued võimalused ja väljakutsed seoses asjade interneti (Internet of Things - IoT) ilmumise ja arenguga. Näiteks piiratud varuga energiaallikate kasutamine traadita võrgu sõlmedes piirab nende eluiga, vähendab usaldatavust, viib suurenenud hooldusvajaduseni ja kaasneva kuluni. Sellega seoses on teadlased uurinud energiakorje (energy harvesting) võimalusi ja pakkunud välja erinevaid lahendusi. Lisades täiendava või alternatiivse energiaallika aitavad väljapakutud lahendused ületada elektrokeemiliste allikate mahtuvusega seotud piiranguid arukates seadmetes, traadita võrgu sõlmedes, koduseadmetes, tööstusmasinates ja mujal. Energiakorje positiivne mõju lubab uuenduslikke rakendusi mida ei takista enam elektrokeemiliste allikatega seotud piirangud. Siiski on veel mitmeid väljakutseid traadita sensorsõlmede energiasõltumatuse tagamiseks, nii riistvara kui ka tarkvara vallas. Energiakorje keskkonnast, olgu see siis päikeseenergia, tuuleenergia, soojusenergia või raadiosageduslikud signaalid, on tüüpiliselt katkendliku loomuga. See tähendab, et traadita sensorsõlmed võivad jääda ilma energiata, mis omakorda mõjutab rakenduste jõudlust, ühenduvust ja usaldusväärsust.

Esmalt pakkus autor välja jämedakoelisi mudeleid kasutava süsteemitasandi raamistiku erinevate energiakorje tehnoloogiate ja nende koosluste jaoks traadita sensorsõlmedes. Katsetulemused näitavad kuidas raamistikku saab kasutada erinevate energiakorje allikate hindamiseks traadita sensorsõlmede energiaga varustamisel.

Seejärel hindas autor traadita sensorsõlme energiakorje teel toitmise teostatavust ilma energia akumuleerimiseta. Selle töö väljapaistev tulemus on transientse arvutusmeetodi implementeerimine mittevolatiilse mäluga (FRAM) võrgusõlmes. Katsetulemused näitavad et energiakorje koos transientse arvutusmeetodiga on tõepoolest teostatav.

Järgnevalt pakkus autor välja energia prognoosimise mudeli LINE-P (Linear Energy Prediction). See baseerub aproksimeerimise ja võendamise teooriatel. LINE-P on kasutatav duaalsete energiakorje allikate jaoks muutuvate ajaintervallide korral paremini kui tuntud parimad lahendused. Simulatsiooni tulemused näitavad, et LINE-P prognoosi täpsus on ligi 98% päikeseenergia korral ja ligi 96% tuuleenergia korral.

Sellele järgnevalt kasutas autor transientset arvutusmeetodit kombinatsioonis energiakorje ja LINE-P prognoosimise mudeliga kahesuunalise side jaoks. See lubab side alamülesande alustamist ainult siis kui piisav ja stabiilne energiavaru on prognoositud. Kahe sõlme vahelise traadita side katsetamise tulemused näitavad, et kaks kombineeritud meetodit nõuavad ainult 15% võrgusõlme mälust ja pakutud lahenduse keskmine vastuvõtu määr on kuni 94,6%.

Lõpuks arendas autor välja adaptiivse LINE-P mudeli, mis kasutab fikseeritud kaaluparameetrite asemel adaptiivseid kaaluparameetreid salvestatud energiaprofiilide jaoks. Lisaks pakutakse välja profiilide kokkusurumise meetod mäluvajaduse vähendamiseks. Tulemused näitavad, et adaptiivse LINE-P täpsus on kuni 90-94% ja kokkusurumine vähendab mäluvajadust 50%.

Appendix A

Publication I

Ahmed, F., Le Moullec, Y., Annus, P., Mustufa, Y.S.A. Analytical evaluation of indoor energy harvesting technologies for WSNs with FYPSim framework. 2016 International Conference on Industrial Informatics and Computer Systems (CIICS), 2016. [6] p.

Analytical Evaluation of Indoor Energy Harvesting Technologies for WSNs with FYPSim Framework

Faisal Ahmed, Yannick Le Moullec, Paul Annus
T.J. Seebeck Department of Electronics,
Tallinn University of Technology
Tallinn, Estonia
faisal@elin.ttu.ee

S. Ashad Mustufa Y.
Department of Information Engineering and Computer Science (DISI), University of Trento
Trento, Italy
syed.younus@unitn.it

Abstract— **FYPSim is a framework that enables the modeling of various energy harvesting technologies and the sizing of energy storage technologies at the system level with application to wireless sensor networks. In this paper, we present the specific features of FYPSim related to energy harvesting exploiting indoor solar, indoor air flow, and indoor radio frequency energy sources. We also describe the models used for modeling hybrid energy harvesting and battery management. Our experimental results illustrate how FYPSim can be used to evaluate the above technologies in combination with Li-Ion batteries and supercapacitors.**

Keywords—Indoor energy harvesting; Wireless sensor nodes; Photovoltaic cells; Micro turbines; RF energy.

I. INTRODUCTION

Energy harvesting (EH) is more and more commonly used for powering the nodes that compose wireless sensor networks (WSNs), whereby EH circuits collect energy from distributed sources such as solar, air flow, and radio-frequency (RF) and transform it into electrical energy.

Generally speaking, existing WSN simulators lack comprehensive coverage of energy harvesting technologies [1]. FYPSim is a framework currently under development as part of our research effort that aim at modeling EH at the system-level so as to provide WSN designers the possibility to rapidly compare design alternatives. In this paper we focus on the specific features of FYPSim related to indoor EH.

We first describe three examples of energy sources, i.e., solar, air flow, and RF, exploited in an indoor context. We also propose a hybrid model for EH based on combined indoor energy sources. We also present a battery management circuit with low current consumption that is cascaded with the storage device and the EH system. This circuit starts harvesting energy from the source(s) once the energy level in the storage device goes below a threshold voltage; it stops harvesting energy when the storage device is fully charged.

This research has been partly supported by the European Union through the European Regional Development Fund and the Estonian IT Academy Stipend Program.

978-1-4673-8743-9/16/$31.00 ©2016 IEEE

Finally, we present experimental results illustrating the capabilities of FYPSim for the three above energy sources with four different sensor types (Dresden AVR, Dresden Atmel-ARM, SenseNode, and WiSense nodes).

II. SIMULATION OF INDOOR ENERGY HARVESTING TECHNOLOGIES

Usually, energy available in indoor (ambient) environments is underestimated and often considered as ineffective; however, recent research has shown that indoor EH has the potential to power WSN nodes. For example, energy can be harvested from home appliance devices such as artificial lights, air conditioners, radiators, and washing machines; even air ventilation can be used to produce some electric power by using air micro-turbine generators [5]; yet another possibility is to exploit the fact that the human body emits energy in the form of heat all the time.

This section presents three examples of EH technologies that can be used in an indoor context, including simulation results based on mathematical models that available in the literature [1]-[3].

A. *(Indoor) Solar Energy*

Conceptually, (indoor) solar EH is based on photovoltaic cells (PV) that convert artificial light into electrical energy in the form of a direct current with no need for conversion circuitry.

In [5], the authors considered a circuit with one diode and two resistors (see Fig. 1) that is equivalent to a photovoltaic model consisting of n_s PV cells in series.

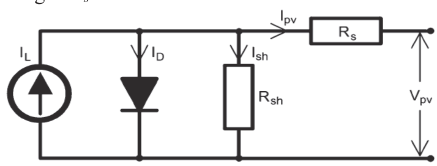

Fig. 1. Equivalent electrical circuit for a photovoltaic module [5].

Let's suppose that the shunt resistance R_{sh} is infinite and that the output of the PV module depends on the current-voltage characteristics. This can be expressed as a four parameter model described by (1) [6],

$$I_{PV} = I_L \quad I_o[\exp((V_{PV} + I_{PV}R_s)/n_sV_t) - 1] \tag{1}$$

where I_L is the current generated from light (A), I_o is the dark/reverse saturation current of the p-n diodes (1×10^{-9} A), R_s is the series resistance of the PV module, and V_t is the junction terminal voltage (V), as defined in (2),

$$V_t = \frac{kTc}{q} \tag{2}$$

where T_c is the cell absolute temperature (K), k is the Boltzmann's constant (1.3807×10^{-23} J/K), and q is the charge of an electron (1.6022×10^{-19} C) [1].

Getting the harvested power from the PV module is difficult because of the voltage-current relationship, so the value of R_s is set to a very few ohms; in addition, $I_{PV} R_s$ has to be negligible, otherwise the voltage may drop significantly [4].

In [4], the authors' formulation of the output power of a solar panel, $P_{PV}(V_{PV})$, is expressed as per (3),

$$P_{PV}(V_{PV}) = V_{PV} I_{PV} = V_{PV} I_L - V_{PV} I_o[\exp(V_{PV}/n_sV_t) - 1]$$
$$\approx V_{PV} I_{sc} - V_{PV} I_o[\exp(V_{PV}\, q / n_s\, k\, T_c)] \tag{3}$$

Note that the value of $\exp(V_{PV}/n_sV_t)$ is much greater than 1 and that the light-generated current (I_L) ≈ the short circuit current (I_{sc}) [6].

We have implemented (3) in FYPSIM and simulated the harvested power, P_{PV} as a function of V_{PV}, with standard values for the above mentioned parameters, i.e., indoor temperature T_c of 295 K, light irradiance of 480 lux, and measured I_{sc} of 74µA [1]. The results are shown in Fig 2.

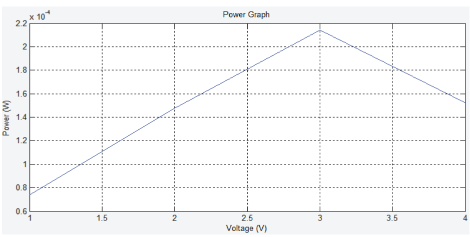

Fig. 2. Output power (P_{PV}) of the photovoltaic module for V_{PV} ranging from 1 to 4 V. The peak power is achieved for V_{PV} = 3 V.

B. (Indoor) Air Flow Energy

Nature provides us with several non-polluting energy sources, wind energy being one of them. The mechanism of a wind turbine converts the kinetic energy of the wind into mechanical energy; then a generator converts the latter into electrical energy [7].

As mentioned above, size is a key factor, so micro turbines that exploit air flows are deemed the most suitable for applications in indoor environments. Such micro turbines are capable of producing (low amount of) energy with less than 1 m/sec air velocity, as shown in Table I.

Generally, in cold places people use radiators during the winter season to keep rooms warm; this results in air movement. It is possible to calculate the corresponding air velocity by applying (4) [4],

$$V_c = 0.65[g\, L\, dt / (273 + t_e)]^{1/2} \tag{4}$$

where g is the acceleration of gravity ($9.81 m/s^2$), L is the vertical distance from the bottom of the surface (m), and ($dt = t_e - t_s$) is the difference between the radiator's surface temperature (^oC) and the room temperature (^oC).

In the following example we assume that the initial to final velocity ranges from 0.25 to 1.5 m/sec for calculating the generated power at various levels of velocity.

In [2], a mathematical model of wind power is expressed as per (5),

$$P_{avail} = 0.5(\rho \pi L^2 V^3 C_p) \tag{5}$$

German physicist Albert Betz concluded that no wind turbine can convert more than (59.3%) of the kinetic energy of the wind into mechanical energy turning a rotor; this is referred to as the power efficiency and denoted by C_p.

Specifically, (5) has been used to find the air flow power by applying standard values i.e. ρ is the air density (1.22 kg/ m^3), L is the blade length (5 cm), and C_p is the power efficiency (0.2). We have simulated the air flow power (5) in our framework (FYPSim); a screenshot of the corresponding power graph is shown in Fig 3.

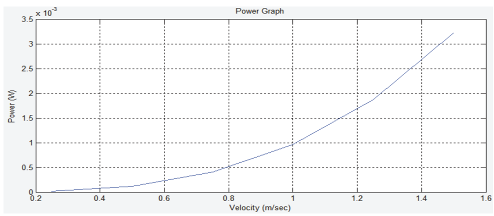

Fig. 3. Simulated wind power for an (indoor) micro turbine for velocity ranging from 0.2 to 1.5 m/sec.

As expected, the trend of the air flow power curve shown in Fig 3 is cubic. For the experiments described in Section V, we consider that the air velocity is 0.4 m/sec, yielding a harvesting power of 0.216×10^{-3} W @ 0.4 m/sec. Based on the above power value, the simulated harvested energy is 2.7 J over 24 hours, as shown in the first column of Table I.

C. Radio Frequency (Indoor) Energy

The huge deployment of RF communication devices over the last few decades makes RF energy available in many (especially urban) areas at “any time and everywhere”. Typically, the radio signals emitted by different sources, e.g. TV towers, mobile stations, and dedicated RF energy sources can be considered as RF energy transmitters; RF receivers (harvesters) can convert part of the received radio frequency signals into electrical energy.

Radio frequency energy harvesting (RFEH) can be applied in various contexts such as health monitoring systems, wireless charging systems, and wireless body area networks [7, 8]. In some implementations, a diode-based multi-stage voltage multiplier (rectifying circuit) converts the RF signal (AC) into a DC voltage [7]. The energy level of the RF signal (AC) also depends upon the distance between the emitting radio source and the RFEH circuit. Dedicated indoor RF sources possibly provides higher AC voltages, and thus DC voltages, because of typically short distances, e.g. 1.25 V @ 0.5 m [3].

In [3], the authors propose a mathematical model for an RF to DC voltage converter, as shown in (6),

$$V = 2\,[G_{ant}\,\lambda \,/\, 4\pi\, d\,(2R_e\,[Z_{rec}].P_{rf}\,(1+Q_{rf}^2))^{1/2} - V_F] \qquad (6)$$

where V is the calculated value of the output DC voltage, G_{ant} is the antenna gain (0.85 dBi), d is the distance (here we consider 0.2 to 1.5 m), $R_e\,[Z_{rec}]$ is the reactance (20 Ω), P_{rf} is the maximum available power (16.8 dBm), Q_{rf} is the quality factor (7), and V_F is the low forward voltage (150 mV).

Since [3] provides an equation for the output voltage only (i.e. not for the current, nor for the power), we assume that the value of the internal resistance R_s is 0.1 mΩ and that of the load resistance R_L (Li-Ion battery or supercapacitor) is 50 KΩ. After applying the maximum power theorem, the output DC voltage has been simulated in FYPSim and the corresponding curve plotted in Fig. 4. Assuming a scenario where d = 0.5 m, the output DC voltage is 1.25 V and the corresponding harvested energy is 2.7 J after a period of 24 hours.

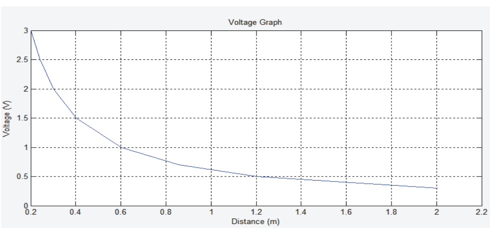

Fig. 4. Output DC voltage after conversion from RF for distances ranging from 0.2 to 2 m.

III. Modeling Hybrid Energy Harvesting Sources

As discussed above, each indoor source only produces low levels of energy. Thus, combining two or more of such sources (hybrid energy harvesting) has recently emerged as a potential way to increase the total harvestable energy. In this section, we propose to model a hybrid energy harvesting setup for the three sources discussed previously by means of (7), whereby the various energy levels are added and the sum is multiplied by a coefficient reflecting the efficiency of the combining circuit,

$$E_{HEH} = \sum_{i=0}^{n} E_i \quad \alpha = (E_s + E_{RF} + E_W) \quad \alpha \qquad (7)$$

where E_s is the harvested solar energy, E_{RF} is the RF harvested energy, E_W is the harvested air flow energy, and α efficiency coefficient.

For the example used in Section V, the hybrid harvested energy is (0.0094 + 2.7 + 2.7) * 0.59 = 3.19 J.

In order to minimize the complexity of the hybrid setup, we consider a single power management circuit referred to as battery management (for which α ranges from 0.3 to 0.8). This approach has the added benefit of avoiding several separate battery management circuits. As shown in Fig. 5, this circuit is inserted between the energy harvesters and the storage device (e.g. battery or supercapacitor) and is described in the next section.

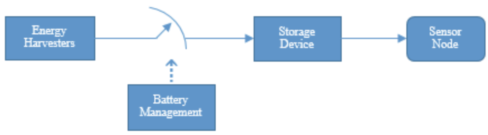

Fig 5. Block diagram illustrating that the link between the energy harvesters and the storage device is controlled by the battery management circuit.

IV. Battery Management Circuit

The circuit has been designed and simulated with LT Spice; Fig. 6 shows its schematic diagram. As seen in Fig. 6, when the battery voltage drops below the threshold value (red line), the circuit starts harvesting energy from the energy sources until the battery is fully charged (green curve). The blue curve shows the overall charging/discharging cycle.

The characteristic of the circuit can be summarized as: $V_{Battery}$ = 5.2 V, V_{Th} (threshold voltage) = 2.2 V, $V_{Out} = V_{Battery}$ when $V_{Battery} > V_{Th}$ and V_{Out} = 0 V when $V_{Battery} \leq V_{Th}$.

Furthermore, the simulation results indicate that the current consumption is very low at 630 µA.

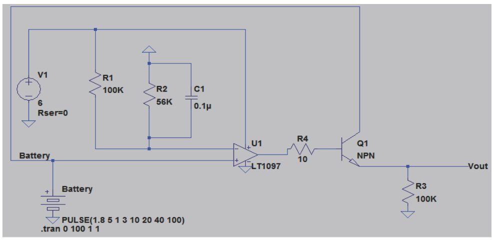

Fig. 6. Schematic diagram of the battery management circuit.

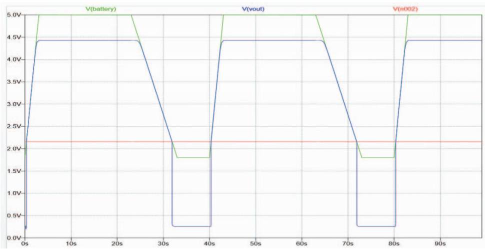

Fig. 7. Graphical presentation of the operation of the 'Battery management' circuit.

V. Experimental Results for Harvested Energy for Low Power WSN Nodes

This section presents the simulation results for the experiments conducted with FYPSim considering real-life nodes, i.e. Dresden AVR [9], Atmel ATmega , SenseNode, and WiSense [10] powered by either a Li-Ion battery (5V) or a supercapacitor (3.75V). Those experiments show how it is possible to rapidly evaluate the feasibility of using the hybrid harvesting setup described previously. The individual levels of harvestable energy are listed in Table I, whereas the level of harvestable energy for the hybrid setup is listed in the first column of Table I and Table II.

The behavior of the Dresden AVR, Atmel ATmega, SenseNode, and WiSense based nodes are simulated taking into account three different states referred to as idle, active and sleep modes, with corresponding current consumptions indicated in the first column of Tables II and III and the energy level listed in the first column of Table I.

Moreover, several duty cycle cases have been considered. Note that we consider a worst-case scenario, i.e. the batteries or supercapacitors are initially depleted. Average values for the energy production and consumption are used in all simulations.

Case A: This is a special case since the nodes are always in the sleep mode, and thus the energy consumption is minimal. Obviously, such a mode is not used continuously in practice, and the nodes have to be active at least intermittently. Nevertheless, this case can be used to evaluate the performance of the system during such inactivity periods. As can be seen in Table II and Table III, Case A yields most of the feasible combinations (positive numbers for 'Prod-Cons'), except for the Dresden AVR nodes (which has a higher energy consumption than the other nodes).

Case B: This case reflects a scenario where the nodes have a relatively light activity level (active for every 1 s out of 60 s), which can illustrate applications such as health monitoring system, slow-variation temperature monitoring, etc. As shown in Table II and Table III, the number of feasible combinations is the same as for Case A; again only Dresden AVR nodes yield to non-feasible solutions.

Case C: as compared to Case B, the nodes are now active for longer time periods, i.e. every 1.6 s out of 60 s, which corresponds to rather intensive sensing and signal processing activities. As shown in Tables II and III, the nodes consume much more energy as compared to Case A and Case B. There are now more solutions that are not feasible (Dresden AVR, ATmega) and SenseNode (the LI-Ion battery combination). For the WiSense nodes, all solutions are still feasible from a hybrid energy perspective.

Case D: this is an extreme case, which like Case A, is not expected to be continuous. It can reflect peak demand in certain applications, or applications for which sensing and/or signal processing is intensive. As can be seen in Table II and Table III, no solution is feasible for the selected hybrid energy harvesting setup.

VI. Discussion and Conclusion

We have illustrated how a designer can use FYPSim to rapidly evaluate the feasibility of hybrid energy harvesting to power WSN nodes. In the specific example, we have considered indoor solar, air flow, and RF energy sources for Dresden AVR, Atmel ATmega, SenseNode, and WiSense based WSN nodes, combined with either a Li-Ion battery or a supercapacitor.

The results tell the designer that the selected hybrid energy harvesting setup in not suitable for the Dresden AVR node, even for the least active mode (Case A); they also tell the designer that the setup is suitable for the other types of nodes for the less active modes (Case A and Case B). The results also tell the designer that for the more intensive mode (Case C), the selected hybrid energy harvesting setup is suitable for a limited number of combinations; finally, the results for the most intensive mode (Case D) illustrate the limit of the selected hybrid energy harvesting setup.

In the next phase of our research effort we will exploit the features of FYPSim for evaluating the impact of using energy harvesting on the performance of WSNs, among others at the MAC layer (e.g. LEACH protocol) and in the context of hand-over in WSNs.

TABLE II. INDIVIDUAL ENERGY HARVESTING SIMULATION RESULTS.

Indoor Solar	**Indoor RF**	**Indoor Air Flow**
Temperature in K 295@2.0V I_{sc}=74μA@480Lux	RF-DC 1.25V@0.5m	0.31x10^{-4} W@0.4 m/sec
Harvested energy: 18.8 J/m^2 0.0094 J/5cm^2@24 hours	Harvested energy: 2.7 J@24 hours	Harvested energy: 2.7 J@24 hours

TABLE II. HYBRID (INDOOR) HARVESTED ENERGY BASED AVR, ATMEL, SENSE, WI SENSE NODE POWER BY LI-ION BATTERY (5V).

Hybrid (Indoor) Harvested Energy [J] 3.19	*Operating Voltage [V]*	*Total time [300s]* *Idle [s]* *Active [s]* *Sleep [s]*	*Case A* *0* *0* *300*	*Case B* *5* *5* *290*	*Case C* *8* *8* *284*	*Case D* *0* *300* *0*
Dresden AVR current [A] $I_{active}=20*10^{-3}$ $I_{idle}=10*10^{-3}$ $I_{sleep}=10*10^{-6}$	*5*	*Node cons. (24 hours) [J]* *Req. Energy (30 days) [J]* *Prod.-Cons. (30 days) [J]*	*4.32* *129.6* *-33.9*	*220.17* *6605.28* *-6509.58*	*349.68* *10490.68* *-10394.98*	*8640* *259200* *-259104.3*
Atmel ATmega current [A] $I_{active}=0.4*10^{-3}$ $I_{idle}=0.1*10^{-6}$ $I_{sleep}=0.6*10^{-6}$	*1.8-5.5*	*Node cons. (24 hours) [J]* *Req. Energy (30 days) [J]* *Prod.-Cons. (30 days) [J]*	*0.25* *7.76* *87.92*	*3.31* *93.93* *1.76*	*4.85* *145.63* *-49.93*	*17.82* *5184* *-5088.3*
SenseNode current [A] $I_{active}=330*10^{-6}$ $I_{idle}=1.1*10^{-6}$ $I_{sleep}=0.2*10^{-6}$	*1.8-3.6*	*Node cons. (24 hours) [J]* *Req. Energy (30 days) [J]* *Prod.-Cons. (30 days) [J]*	*0.08* *2.59* *93.10*	*2.46* *74.02* *21.67*	*3.89* *116.88* *-21.18*	*142.56* *4276.8* *-4181.1*
WiSense current [A] $I_{active}=250*10^{-6}$ $I_{idle}=0.7*10^{-6}$ $I_{sleep}=0.1*10^{-6}$	*3.6*	*Node cons. (24 hours) [J]* *Req. Energy (30 days) [J]* *Prod.-Cons. (30 days) [J]*	*0.04* *1.29* *94.40*	*1.82* *55.40* *40.29*	*3* *88* *8*	*108* *3240* *-3144.3*

TABLE IIII. HYBRID (INDOOR) HARVESTED ENERGY BASED AVR, ATMEL, SENSE, WI SENSE NODE POWER BY SUPERCAPACITOR (3.75V).

Hybrid (Indoor) Harvested Energy [J] 3.19	*Operating Voltage [V]*	*Total time [300s]* *Idle [s]* *Active [s]* *Sleep [s]*	*Case A* *0* *0* *300*	*Case B* *5* *5* *290*	*Case C* *8* *8* *284*	*Case D* *0* *300* *0*
AVR current [A] $I_{active}=20*10^{-3}$ $I_{idle}=10*10^{-3}$ $I_{sleep}=10*10^{-6}$	*5*	*Node cons. (24 hours) [J]* *Req. Energy (30 days) [J]* *Prod.-Cons. (30 days) [J]*	*3.24* *97.2* *-1.5*	*165.13* *4953.96* *-4858.26*	*262.26* *7868.01* *-7772.31*	*3240* *97200* *-97104.3*
Atmel Atmega current [A] $I_{active}=0.4*10^{-3}$ $I_{idle}=0.1*10^{-6}$ $I_{sleep}=0.6*10^{-6}$	*1.8-5.5*	*Node cons. (24 hours) [J]* *Req. Energy (30 days) [J]* *Prod.-Cons. (30 days) [J]*	*0.19* *5.83* *89.86*	*2.34* *70.45* *25.24*	*3.64* *109.22* *-13.52*	*129.6* *3888* *-3792.3*
SenseNode current [A] $I_{active}=330*10^{-6}$ $I_{idle}=1.1*10^{-6}$ $I_{sleep}=0.2*10^{-6}$	*1.8-3.6*	*Node cons. (24 hours) [J]* *Req. Energy (30 days) [J]* *Prod.-Cons. (30 days) [J]*	*0.06* *1.94* *93.75*	*1.85* *55.51* *40.18*	*2.92* *87.66* *8.03*	*106.92* *3207.6* *-3111.9*
WiSense current [A] $I_{active}=250*10^{-6}$ $I_{idle}=0.7*10^{-6}$ $I_{sleep}=0.1*10^{-6}$	*3.6*	*Node cons. (24 hours) [J]* *Req. Energy (30 days) [J]* *Prod.-Cons. (30 days) [J]*	*0.03* *0.97* *94.72*	*1.38* *41.55* *54.14*	*2.19* *65.90* *29.79*	*81* *2430* *-2334.3*

REFERENCES

[1] P. Chulsung and P. H. Chou, "AmbiMax: Autonomous Energy Harvesting Platform for Multi-Supply Wireless Sensor Nodes," in Proc. 3rd IEEE Annu.Commun. Soc. SECON, 2006, vol. 1, pp. 168–177.

[2] RWE Power Renewables Mechanical and Electrical Engineering Power Industry and The Royal Academy of Engineering, "Wind Turbine Power Calculations," [Online], http://www.raeng.org.uk/publications/other/23-wind-turbine, [November 2015]

[3] Thierry Taris, Valerie Vigneras, Ludivine Fadel, "A 900 MHz RF Energy Harvesting Module," 10th IEEE International New Circuits and Systems Conference (NEWCAS 2012), Jun 2012, Montreal, Canada. pp.445 - 448, 2012.

[4] Y. K. Tan, S. K. Panda, "Energy Harvesting from Hybrid Indoor Ambient Light and Thermal Energy Sources for Enhanced Performance of Wireless Sensor Nodes," IEEE Trans. Industrial Electronics, Vol.58, No.9, Sep 2011.

[5] The Engineering Tool Box, "Convective Heat - Air Velocity and Volume of Air Flow," [Online], http://www.engineeringtoolbox.com/convective-air-flow-d_1006.html, [November 2015]

[6] A. N. Celik and N. Acikgoz, "Modelling and Experimental Verification of the Operating Current of Mono-Crystalline Photovoltaic Modules using Four- and Five-Parameter Models," Appl. Energy, vol. 84, no. 1, pp. 1–15, Jan. 2007.

[7] F. Ahmed, Y. Le Moullec, P. Annus, "Energy Harvesting Technologies - Potential Application to Wearable Health-Monitoring," 10th Conf. on Bioelectromagnetism, Estonia, June 2015.

[8] S.A. Mustufa, et al, "Design of a Smart Insole for Ambulatory Assessment of Gait," in Proc. of the 12th Int. Conf on BSN, pp.1-5, 2015.

[9] Dresden Elekronik, "User Manual Radio Modules deRFarm7-15A02 deRFarm7-25A00 deRFarm7-25A02", V1.2, 2014-04-11.

[10] The Sensor Nodes Specifications, "List of Wireless Sensor Nodes," [Online], https://en.wikipedia.org/wiki/List_of_wireless_sensor_nodes, [November 2015]

Appendix B

Publication II

Ahmed, F., Ahmed, T., Muhammad, Y., Le Moullec, Y., Annus, P. Operating wireless sensor nodes without energy storage : experimental results with transient computing. Electronics (2016) 5, 4, 89.

electronics

MDPI

Article

Operating Wireless Sensor Nodes without Energy Storage: Experimental Results with Transient Computing

Faisal Ahmed [1,*], Tauseef Ahmed [1], Yar Muhammad [2], Yannick Le Moullec [1,*] and Paul Annus [1]

[1] Thomas Johann Seebeck Department of Electronic, Tallinn University of Technology, Tallinn 12616, Estonia; Tauseef.Ahmed@ttu.ee (T.A.); paul.annus@ttu.ee (P.A.)

[2] University of Tartu, Narva College, Narva 20307, Estonia; yar.muhammad@ut.ee

* Correspondence: faisal.ahmed@ttu.ee (F.A.); yannick.lemoullec@ttu.ee (Y.L.M.); Tel.: +372-5800-7448 (F.A.)

Academic Editor: Mostafa Bassiouni

Received: 22 November 2016; Accepted: 6 December 2016; Published: 9 December 2016

Abstract: Energy harvesting is increasingly used for powering wireless sensor network nodes. Recently, it has been suggested to combine it with the concept of transient computing whereby the wireless sensor nodes operate without energy storage capabilities. This new combined approach brings benefits, for instance ultra-low power nodes and reduced maintenance, but also raises new challenges, foremost dealing with nodes that may be left without power for various time periods. Although transient computing has been demonstrated on microcontrollers, reports on experiments with wireless sensor nodes are still scarce in the literature. In this paper, we describe our experiments with solar, thermal, and RF energy harvesting sources that are used to power sensor nodes (including wireless ones) without energy storage, but with transient computing capabilities. The results show that the selected solar and thermal energy sources can operate both the wired and wireless nodes without energy storage, whereas in our specific implementation, the developed RF energy source can only be used for the selected nodes without wireless connectivity.

Keywords: WSN; energy harvesting; transient computing

1. Introduction

Advances in semiconductor technology has given birth to low-power, miniaturized computing units (microcontrollers, DSPs, (nano)-FPGAs), and radio modules. Such circuits are commonly used for implementing the nodes in wireless sensor networks (WSN) and, more generally, in the internet of things (IoT). On the other hand, and although new battery technologies (e.g., hydrogen fuel cells) are being developed and promise new performance levels, those available today are not always sufficient when it comes to filling the gap between the physical size, capacity, and energy requirements of the computing and communication modules of the nodes.

Furthermore, for some applications, it is sometimes not possible to include a battery or super-capacitor in the nodes due to stringent physical constraints or for maintenance reasons (for example, it may be impossible to access a node integrated in a physical structure and replace its energy storage unit if the battery fails or once its maximum number of charge/discharge cycles have been reached, in the case of e.g., intensive and/or very-long term applications) [1].

Thus, many research efforts strive at designing (A) architectural solutions that effectively reduce energy consumption in the processing and communication modules, and (B) energy harvesting (EH) solutions that can complement, or even replace, the energy storage units of the nodes for, e.g., autonomous systems, leading to the concept of transient computing (TC) discussed later on.

In the context of WSN nodes, the idea of using EH emerged in the late 1990s [2] and refers to the various techniques that allow collecting energy from the environment (solar, thermal, radio frequency

(RF), etc.) and use it to recharge and/or complement energy storage units, such as rechargeable batteries or super-capacitors, especially in the context of fully-autonomous WSN nodes and/or for prolonging the lifespan of battery-powered WSN nodes. EH, aided by energy prediction or estimation, has led to a service-oriented infrastructure supporting a broad range of applications such as IoT and cyber-physical systems by optimizing the energy consumption and balancing the traffic load to increase the nodes' lifetime.

Nevertheless, EH remains challenging in many cases (e.g., for wearable sensors) due to strict form factor constraints and usability concerns [3,4].

Examples of EH used in wearable WSNs include the research proposed in [1] where the authors conducted real-world scenario experiments and achieved 550 µW for an indoor photovoltaic source and 98–250 µW for a thermal source with 3° and 5° temperature gradients, respectively. Several works have been proposed to minimize the RF energy requirements of the devices with different techniques, such as at the physical layer [4,5], MAC, routing algorithms, and duty cycle [6–9]. In [10], the authors used solar and wind energy harvesters and interfaced them with an ultralow power WSN hardware infrastructure that is suitable for long-term wireless structural health monitoring (WSHM).

RF-EH is an emerging alternative among the numerous energy harvesting techniques. Indeed, many RF transmitters (TV towers, mobile base stations, wireless access points, and even dedicated RF transmitters) have been deployed in the past decades; RF energy can, thus, be considered as easily available in many places [11], especially in indoor environments [12]. RF-EH has found applications in wireless charging, wireless body area networks, surveillance, and cognitive radio networks [13,14] with quality of service (QoS) constraints. Harvesting such energy is typically achieved by means of a so-called rectenna, connected to the WSN nodes, that converts a share of the available energy of the RF signal into electrical energy. Such rectennas are typically composed of an antenna and matched voltage multiplier/rectifying circuitry tuned to the radio frequency of interest; such a setup converts the RF signal to a DC voltage. In particular, dedicated indoor RF sources possibly provides higher AC voltages and, thus, DC voltages, because of typically short distances between the energy source and the nodes, e.g., 1.25 V @ 0.5 m [11]. Furthermore, when it comes to large-scale wireless networks, simulation results [15] indicate that RF-EH can increase the lifetime of a network by up to 70% while maintaining adequate quality of service. Simulation results presented in [16] suggest that RF-EH can increase the lifetime of randomly-deployed dense cooperative WSNs up to 69%.

In [17] the authors focused on a solar energy harvester and energy management, in combination with a new energy forecast model for WSNs. In [18], the authors proposed a hybrid energy harvesting concept based on wind, solar, and chemical energy, which can be used for both simultaneous and individual harvesting processes.

As illustrated above, a large body of research related to EH for WSNs and the IoT has been published in the literature; the interested reader can refer to, e.g., [19] for a recent overview.

That being said, there is still room for research in this field. For example, it has recently been suggested in [3] to combine the concepts of EH and TC. The overall idea stems from the fact that harvested energy is typically fluctuating and intermittent, possibly leaving the WSN nodes without power (even if they include a battery or super-capacitor since these can possibly reach a discharged state). Another argument behind TC is to enable the design and implementation of WSN nodes that operate without an energy storage unit (for e.g., size or maintenance issues, as mentioned earlier).

Such WSN nodes operating with energy storage, but complemented with TC, are suitable for, e.g., applications that do not require permanent monitoring, or that are tolerant to delays (e.g., storing data locally and transmitting it when energy is again available), or that are tolerant to missing data (such missing data can sometimes be compensated for by means of spatial or temporal correlation techniques).

A critical issue in TC is stopping (ideally pausing) and restarting (ideally resuming) computations depending on the available power. For this, several methods, such as checkpointing [20,21] and dynamic power management [22], have been recently proposed. They all rely on the use of microcontrollers that feature non-volatile memory, i.e., flash or more recently ferroelectric RAM (FRAM), to enable saving and restoring the state and data of the node.

One of the first research effort related to TC is the Mementos approach, proposed by Ransford et al. [20]. It turns general computing programs into interruptible versions that are 'protected' from frequent power cuts by means of a checkpointing mechanism that saves and restores the context data and program into flash memory on a periodic basis. Although this mechanism adds an overhead in terms of execution time, it enables suspending the execution when the voltage reaches a given threshold and resuming when the voltage rises sufficiently again. In effect, this type of approach enables spreading computation over time as a function of the available energy.

As a follow-up to the above, DINO ("Death Is Not an Option") [23] adds support for dealing with the inconsistency between volatile and non-volatile data that may occur due to frequent interrupts. Another novelty in DINO is the use of a microcontroller based on FRAM instead of Flash memory. The reported execution-time overhead for DINO is between 1.8× and 2.7×.

Further improvements to TC have been proposed in Hibernus [21]. The key idea here is to replace the periodic checkpointing by an ad-hoc technique, whereby the microcontroller enters the save mode only when the power supply voltage falls to a given threshold (detected by means of a comparator). Hibernus significantly reduces the number of checkpoints and, thus, reduces the execution time and energy overheads by 76%–100% and 49%–79%, respectively, as compared to Mementos.

QuickRecall [24] goes one step further by using the FRAM in a unified mode (i.e., containing the instructions, data, and saves); thus, the RAM is not used, which can reduce execution time and energy consumption since there are no data transfers between the FRAM and the RAM.

Recently, Balsamo et al. [22] have developed a TC method that adapts the power consumption of energy-storage-less devices dynamically by means of dynamic frequency scaling (DFS), which allows handling energy fluctuations in a finer manner. In addition to a threshold for detecting power cuts, two extra thresholds are used to help decide if the voltage and frequency of the FRAM-based microcontroller should be decreased or increased. Tests conducted on Fast Fourier Transform (FFT), Cycling Redundancy check (CRC), and Rivest, Shamir, and Adleman (RSA) algorithms together with solar and micro-turbine energy harvesters show that it is not only possible to adjust the performance of the microcontroller but also to effectively reduce the number of save and restore phases since the microcontroller is allowed to run in a lower performance mode when the available power is reduced.

Whereas transient computing has been demonstrated on microcontrollers (mostly without wireless connectivity features), the literature still lacks reports on experiments with wireless-enabled sensor nodes. The purpose of this paper is to share findings and experimental results obtained when three EH sources (solar, thermal, and RF) are used to power both wired and wireless sensor nodes without energy storage, and evaluate the practical feasibility of TC for WSNs.

The main contributions presented in this paper are:

(A) The practical implementation of three EH sources combined with a TC method on FRAM wireless sensor nodes, and
(B) The assessment of the practical feasibility of such combinations.

In particular, it is shown that for the selected EH sources and nodes, the solar and thermal energy sources can power both non-wireless and wireless sensor nodes without energy storage, whereas in our specific implementation, the developed RF energy source can only be used for the selected nodes without wireless connectivity.

2. Materials and Methods

2.1. Energy Modeling

Before evaluating the practical feasibility of EH combined with TC, we briefly review the fundamentals of the three selected EH sources and related analytical models. These models are used to obtain baseline references against which the actual EH sources can be compared (including both indoor and outdoor environments for the solar energy source).

2.1.1. Solar Energy

Visible light can be converted into electrical energy via solar panels that are typically constructed from crystalline silicon cells (i.e., multicrystalline and monocrystalline silicon). Outdoor solar harvesting is a highly explored area and provides a higher value of energy [1]. However, ambient (mostly indoor) solar energy is not exploited as much since it generally provides less energy [25]. In [26], a formulation of the output power of a solar panel, P_{PV} (V_{PV}), is expressed as per Equation (1):

$$P_{PV}\ (V_{PV}) = V_{PV}\ I_{PV} = V_{PV}\ I_L - V_{PV}\ Io\ [\exp\ (V_{PV}/n_s\ V_{t)}\ -1] \approx V_{PV}\ Isc - V_{PV}\ Io\ [\exp\ (V_{PV}\cdot q/n_s\cdot k\cdot Tc)] \quad (1)$$

where V_{PV} is the output voltage, I_{PV} is the output current, I_L is the light-generated current, Io is the dark/reverse saturation current of the p-n diodes, n_s is the number of series solar cells, V_t is the junction terminal thermal voltage, q is the charge of the electron, k is Boltzmann constant, and Tc is the ambient temperature.

2.1.2. Thermal Energy

Thermoelectric generators (TEGs) exploit the Seebeck effect to produce electrical energy. TEGs are typically constructed from n-type and p-type semiconductors that are connected in series, which are combined with thermal ceramics in parallel. By connecting a load of resistance R_L to the TEG, an electric current I_{TEG} flows in accordance to the temperature difference. In [26], a model is proposed for a TEG energy harvester. The corresponding model equation is showed in Equation (2):

$$P_{TEG}(V_{TEG}) = V_{TEG} \times I_{TEG} = \frac{\left(V_{TEG} \times \mathrm{n} \times \alpha \times (T_H - T_C) - V_{TEG}{}^2\right)}{\mathrm{R_s,\ TEG}} \quad (2)$$

where n is the number of thermocouples, α is the Seebeck's coefficient, R_s, TEG is the internal resistance, and ΔT is the temperature difference (T_H–T_C, where T_H is the temperature of the hot side and T_C is temperature of cold side).

2.1.3. Radio-Frequency Energy

RF-EH devices are typically composed of an antenna matched to either a single or multiple frequency bands, combined with an impedance-matching circuit tuned to the targeted frequencies, followed by a voltage amplitude multiplier, e.g., as in the diode based, multi-stage voltage multiplier proposed in [11]. In addition to the quality of the matching circuit, an important limiting factor in RF-EH is the distance between the emitting radio source and the RF-EH circuit. In [11], an analytical model of an RF to DC voltage converter is proposed and expressed by Equations (3) and (4):

$$\mathrm{V} = 2\ [G_{ant}\ \lambda/4\pi\ d\ (2R_e\ [Z_{rec}].P_{rf}\ (1+Q_{rf}{}^2))\ ½ - V_F] \quad (3)$$

where V is the output voltage of the RF-EH circuit which performs the RF to DC conversion, G_{ant} is the antenna gain, d is the distance, R_e (Z_{rec}) is the reactance, P_{rf} is the maximum available power, Q_{rf} is the quality factor, and V_F the low forward voltage.

$$V_{out} = \frac{nV_0}{nR_0 + R_L} = \frac{V_0}{\frac{R_0}{R_L} + \frac{1}{n}} \quad (4)$$

where V_0 (i.e., V in Equation (3)) is the input of the voltage multiplier, R_0 is the internal resistance, R_L is the load resistance, n is the number of stages, and V_{out} is the output voltage.

The above sections briefly reviewed the three EH sources used in this work. As mentioned earlier, various approaches combining TC and EH have been proposed in the literature. However, such approaches have not been widely experimented in practice, especially when actual radio modules are included; what follows describes our experimental setup for conducting such experiments; our results are then presented in Section 3.

2.2. Experimental Setup

The experimental setup consists of the hardware listed below.

- One MSP-EXP430G2 Launchpad kit (used as a temperature sensor node without wireless connectivity);
- Two EZ430-RF2500 kits (used as temperature sensor nodes with wireless connectivity);
- Two MSP-EXP430FR5739 kits with CC2500 evaluation module kit (used as sensor nodes with wireless connectivity and non-volatile FRAM memory);
- One Linear Technology DC2080A energy harvesting multi source demo board including solar (Panasonic AM-5412) and TEG (CUI INC CP85438) energy sources, as well as an input for our self-developed RF-EH source;
- One self-developed RF-EH board (900 MHz matching network and five-stage voltage multiplier architecture);
- Two Kent Electronics log periodic printed circuit board antennas (850 MHz to 6500 MHz);
- One SMA 100 A Signal Generator—9 KHz to 6 GHz (used as an RF transmitter);
- One Jameco PS 613 DC Power Supply;
- One PRT-13781 solar panel (13.5 cm × 11.2 cm) and 3.3 V voltage regulator;
- One Hewlett Packard 34401A Multimeter for measuring the current;
- One Fluke 123 industrial scope meter for observing and measuring the voltages;
- One TES 1335 light meter for measuring the illuminances.

The schematic of the self-developed RF-EH board is shown in Figure 1; the corresponding photograph is shown in Figure 2.

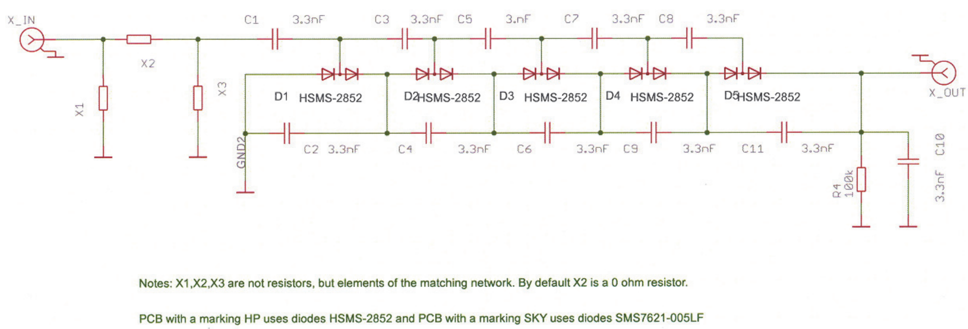

Figure 1. Schematic diagram of the self-developed RF-EH (five-stage voltage multiplier).

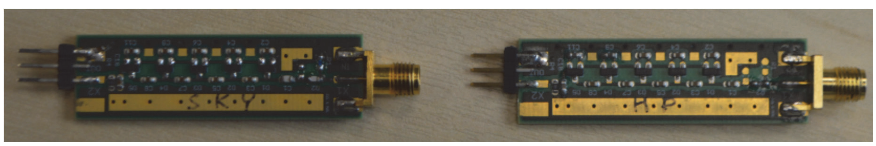

Figure 2. Photograph of the two variants of the self-developed RF-EH circuit based on HP and SKYWORK manufactured diodes.

The code running on the MSP-EXP430FR5739 kits is the device-to-device example provided in the SimpliciTI RF protocol package from Texas Instrument. This package was ported to the MSP-EXP430RF5739 board by following the guidelines provided in [27]. The code has then been modified to implement a TC method. For this, "Compute through Power Loss Utility (CTPL)" from Texas Instrument was used [28]. It contains a set of functions for implementing the strategy, shown in Figure 3.

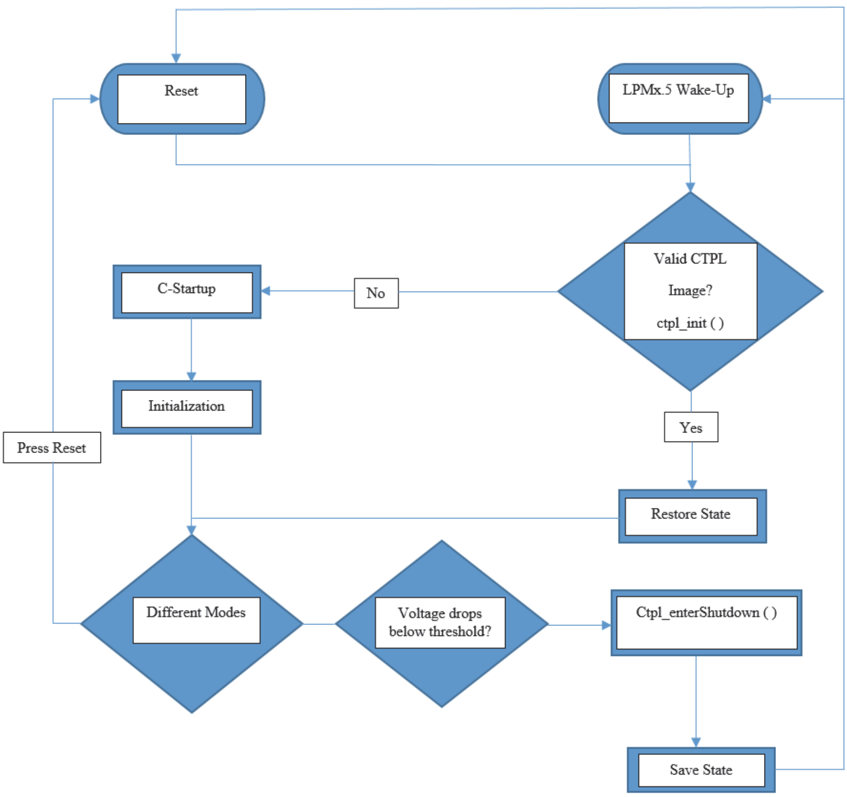

Figure 3. Selected parts of Texas Instrument's Compute through Power Loss Utility strategy used for implementing TC. The Ctpl_enterShutdown () function is triggered when the power supply voltage drops below the threshold. Adapted from [28].

In a first set of experiments, the DC2080A board (with onboard solar panel, onboard TEG, and external RF energy harvester) was used. Each energy path (corresponding to the various sources) on the DC2080A board includes a voltage step-up converter and power manager. The three energy sources were first evaluated individually by configuring jumpers on the DC2080A board and then in a simple hybrid mode by means of OR-ring diodes. Several experiments were run with and without the small onboard capacitors (12 × 100 µF, configured via a jumper). These small onboard capacitors are not considered as 'real' energy storage (which would be implemented by e.g., supercapacitors or batteries). In a second set of experiments, the PRT-13781 solar panel and 3.3 V voltage regulator were used.

For the experiments with the MSP-EXP430FR5739 kits, a reference voltage (coming from the EH source through a voltage divider) is fed to the microcontroller pin 1.5, as can been seen in Figure 4. The proper operation of the CTPL utility has been verified by defining CTPL_BENCHMARK in the compiler and assembler predefined symbols, which enables toggling a pin to indicate that the CTPL function has been triggered (pin 4.0 in our case); this toggling pattern is shown in Figure 5. A photograph of the experimental setup is shown in Figure 6.

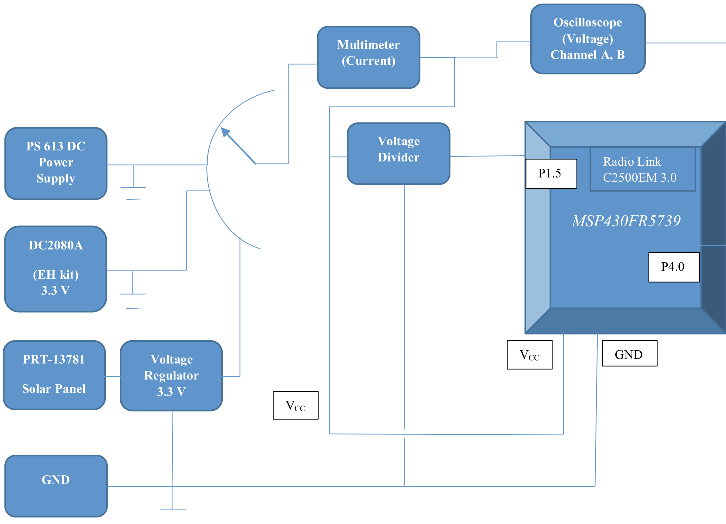

Figure 4. Block diagram of the experimental setup used to test TC with the FRAM-based microcontroller and radio link. It is possible to switch between a regulated DC power supply, energy harvesting kit (with onboard solar and TEG sources and external RF source), and the external solar panel. When the reference voltage on P1.5 lowers down to the value set in software, the ctpl_enterShutdown () software function is triggered; this can be verified on P4.0.

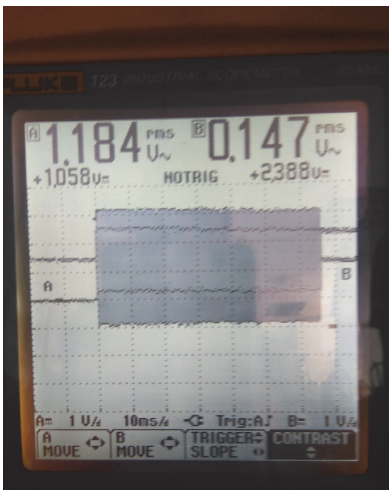

Figure 5. Illustration of the toggling pattern. The threshold value is set in software to 2.5 V; thus, when the voltage drops below (here captured at 2.388 V), the state and data of the microcontroller is saved. This is followed by the toggling pattern that indicates the end of the CTPL function (the ctpl_enterShutdown () function continues to toggle the pin while waiting for the device to enter a BOR).

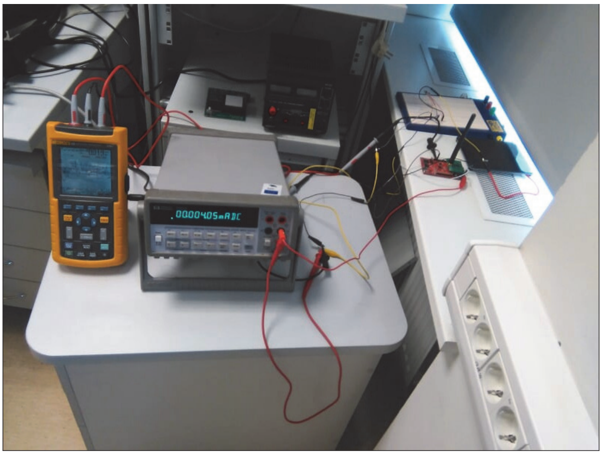

Figure 6. Photograph of the experimental setup. Here, the external solar panel is used to power the FRAM-based microcontroller. The regulated DC power supply and multi-source EH kit can be seen in the background.

3. Experimental Results

3.1. Powering the Nodes with RF-EH

We have first characterized the DC output voltage of the self-developed RF-EH (by means of the Kent Electronics log periodic printed circuit board antennas and SMA 100 A Signal Generator) and compared the measurements with the analytical models (described in Section 2.1.3). As shown in Figure 7, both simulated and measured output DC voltages peak at 900 MHz (the matching frequency) and, to a lesser degree, at 1.8 GHz. As can also be observed, although their orders of magnitude are similar, the simulated and measured curves do not fit perfectly. This can be explained by the fact that the selected analytical model is not sufficiently realistic since it does not take the conversion efficiency into account; in future work a model, such as the one proposed in [16], could be used instead.

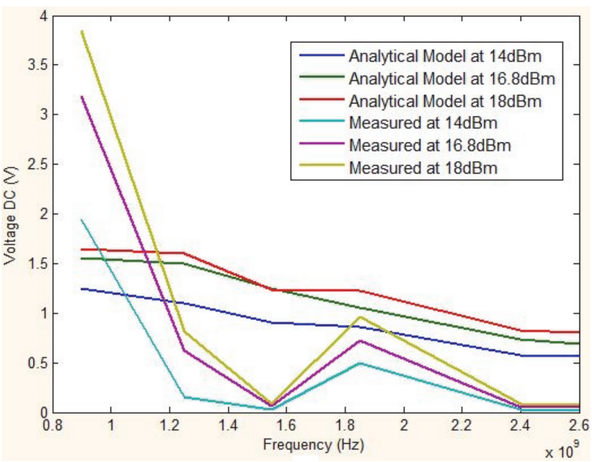

Figure 7. Analytical model and measured output voltages for the RF-EH (five-stage voltage multiplier) at 5 cm, without a load.

We have then used the RF-EH circuit to power the MSP-EXP430G2 kit (configured as a wired temperature sensor). Figures 8 and 9 show the output DC voltage for frequencies ranging from 900 MHz up to 2.6 GHz for five different RF levels (10, 12, 14, 16.8, and 18 dBm) with 2 cm and 5 cm distances between the transmitting (TX) and receiving (RX) antennas, respectively. As expected, the maximum output voltage is achieved at the matching frequency (900 MHz). It can also be seen that there is another smaller peak at 1.85 MHz for all input levels. The experimental results (first row in Table 1) show that the energy provided by the self-developed RF-EH board is sufficient to power the MSP-EXP430G2 kit configured as a wired temperature sensor with a distance of 5 cm and 18 dBm.

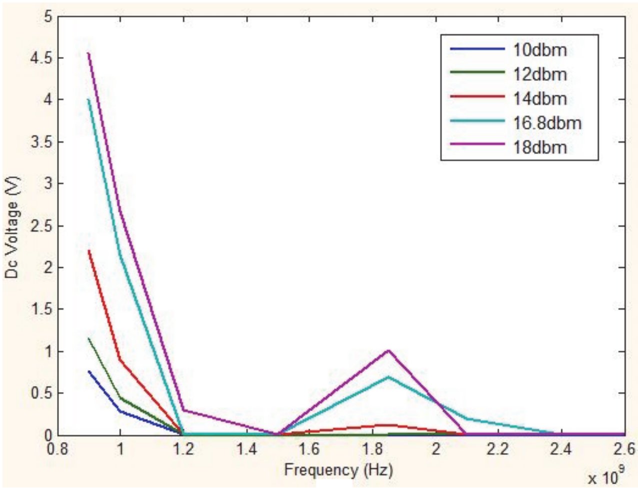

Figure 8. DC voltage at the fifth stage of the self-developed RF-EH board when powering the MSP-EXP430G2 kit. The distance between the TX and RX antennas is 2 cm.

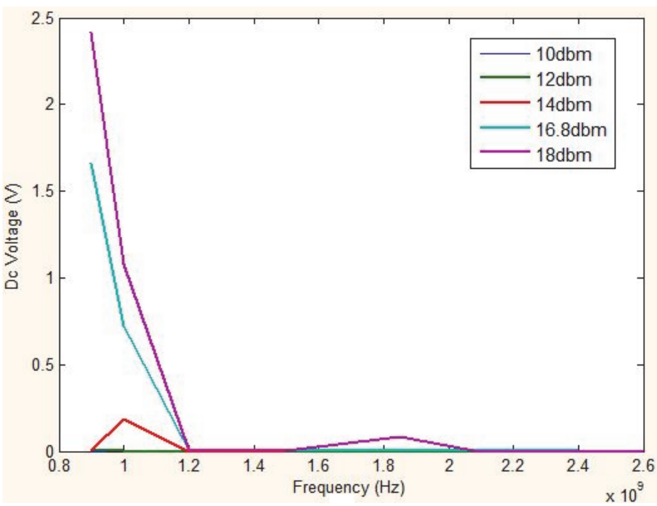

Figure 9. DC voltage at the fifth stage of the self-developed RF-EH board when powering the MSP-EXP430G2 kit. The distance between the TX and RX antennas is 5 cm.

Table 1. Measured voltage and current values with different nodes powered by the RF, solar, and TEG energy harvesters.

EH Technology	Node's Voltage [V]; Current [mA] MSP-EXP430G2	Node's Voltage [V]; Current [mA] EZ430-RF2500	Node's Voltage [V]; Current [mA] MSP-EXP430FR5739+CC2500
RF (900MHz@5 cm, 18 dBm)	1.83; 0.029	0.89; 2.21	0.001; 0.0
Solar (Panasonic AM-5412)	3.2; 0.24	3.23; 0.19	See Table 2 for values
TEG (CUI INC P85438)	3.0; 0.25	2.8; 0.182	2.35; 0.66

We have then used the RF-EH board to power the nodes that feature wireless connectivity (EZ430-RF2500 and MSP-EXP430FR5739 kits with CC2500 evaluation module kit). The experimental results show that the RF-EH board does not provide sufficient energy to operate the nodes featuring wireless connectivity, even whilst the small onboard capacitors are enabled. This is essentially due to the peak current that is required when the nodes boot and try to form or join the wireless network, which makes the voltage drop below the minimum operating voltage of the microcontrollers. However, the self-developed RF-EH is used for illustration purposes only and could be replaced by a more efficient one.

3.2. Powering the Nodes with the Onboard Solar Source

This experiment makes use of the onboard solar panel (3 cm $\times$ 5 cm) in a well-lighted office environment; it powers the three different types of nodes, one at a time. The experimental results (second row in Table 1) show that the solar energy source is able to boot and operate the three types of nodes (including with wireless connectivity), even whilst the small onboard capacitors are disabled.

Moreover, specific experiments have been conducted with the MSP-EXP430FR5739+CC2500 kits which were powered by alternative sources instead of those reported in Table 1. The two kits are programmed as a transmitter and a receiver. The results are presented in Table 2. The sources are (i) a fixed power supply and (ii) the onboard solar panel. Tests have been conducted both with and without wireless activity. Due to the low ambient illuminance, extra lamps had to be used to boot the nodes (measured at 9.98K LUX). As can be seen for the transmitter case, the current increases quite a lot when the radio in on, leading to a voltage drop. The same does not happen for the receiver.

Table 2. First to fourth rows: measured voltage and current for the MSP-EXP430FR5739+CC2500 used as a transmitter. Fifth to eighth rows: measured voltage and current for the MSP-EXP430FR5739+CC2500 used as a receiver, both with the fixed power supply and the onboard solar panel (3 cm $\times$ 5 cm).

Source [V]	Node Input [V]	Node Output [V]	Node Input [mA]
Main 3.3	3.33	2.5	2, No Radio
Main 3.3	3.33	2.5	37, With Radio
Solar EH	3.327	3.325	2, No Radio
Solar EH	2.185	2.167	29, With Radio
Main 3.3	3.3	3.106	2, No Radio
Main 3.3	3.3	3.106	20, With Radio
Solar EH	3.326	3.211	2.11, No Radio
Solar EH	3.324	3.112	20, With Radio

3.3. Powering the Nodes with the PRT-13781 Solar Panel

As seen above, it is difficult to boot the MSP-EXP430FR5739+CC2500 kits with the onboard solar panel, mostly due to the peak current when booting. Thus, further experiments were also conducted with the larger PRT-13781 solar panel (13.5 $\times$ 11.2 cm); the results for the transmitter and receiver are presented in Table 3.

Table 3. First and second rows: measured voltage and current for the MSP-EXP430FR5739+CC2500 used as a transmitter. Third and fourth rows: measured voltage and current for the MSP-EXP430FR5739+CC2500 used as a receiver, with the larger solar panel (13.5 cm × 11.2 cm).

Parameters	Case I (Outdoor Light)	Case II (Indoor Light)	Case III (Sharp Lamp Indoor Light)
Light Intensity [LUX]	5.36 K	1.46 K	9.98 K
Voltage [V] and Current [mA] without radio	3.06 2.46	3.10 2.00	3.5 2.16
Voltage [V] and Current [mA] with radio	3.0 20.0	3.09 22.0	3.5 22.16
Voltage [V] and Current [mA] without radio	3.0 2.16	3.10 2.00	3.5 2.16
Voltage [V] and Current [mA] with radio	2.91 19.98	3.09 22.0	3.5 22.16

3.4. Powering the Nodes with the TEG Source

In this experiment, the analytical model (described in Section 2.1.2) and the measured output voltage of the onboard TEG EH are compared. The results shown in Figure 10 indicate that the orders of magnitude and overall trends are similar but not matching perfectly. This can be explained by the fact that some of the required parameters are not provided in the datasheet of the TEG module and had to be estimated.

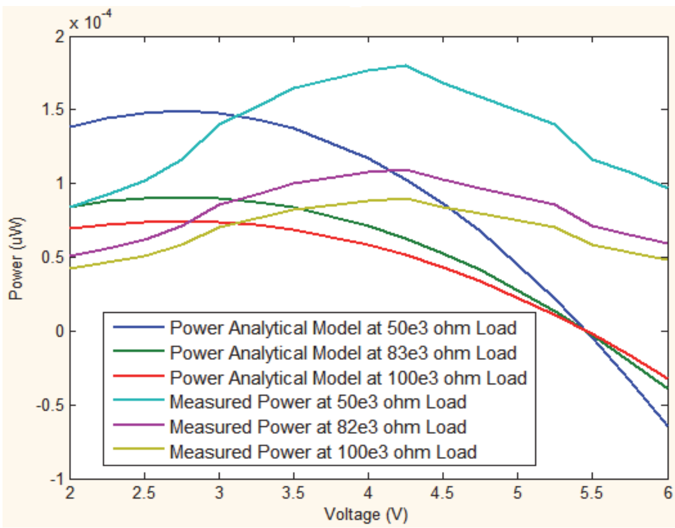

Figure 10. Analytical model and measured power for the TEG-EH source with different loads.

Furthermore, the TEG EH source was used to power the three different nodes, one at a time. Keeping the palm of the hand on the TEG module gradually increased the temperature and, consequently, the output voltage, as shown in Figure 11 for the EZ430-RF2500 kit (used as a temperature sensor node with wireless connectivity). Due to this gradual start, it was necessary to use the small onboard capacitors to boot the nodes. The experimental results (third row in Table 1) show that whilst the TEG-EH does not provide as much energy as the onboard solar panel, it is also able to operate all three types of nodes (one at a time).

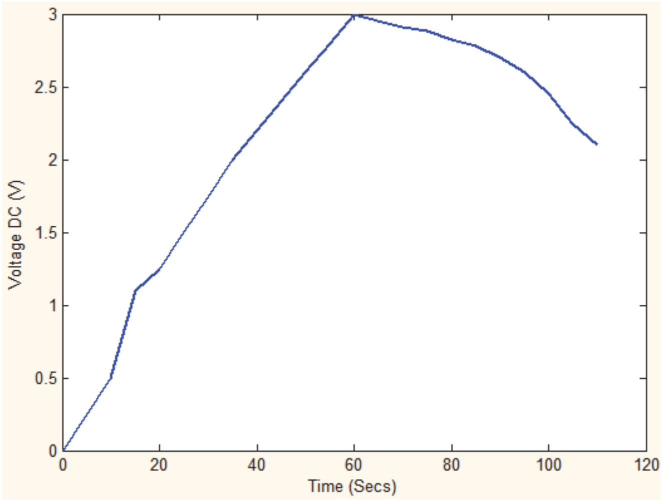

Figure 11. Output voltage of the TEG module over time, when heated with the palm of the hand.

4. Concluding Remarks

Our practical experimental results show that EH combined with TC in WSN nodes is feasible. However, a number of conditions have to be met to makes this possible.

One of them is to implement a mechanism that allows pausing and resuming computations on the nodes depending on the available power. The results show that for simple applications, such as the one used in our experiments, a lightweight method like CTPL combined with a FRAM-based microcontroller is sufficient.

Another condition is to have energy sources that are powerful enough to power the nodes. The experimental results show that it is possible to boot and operate WSN nodes solely on certain harvested energy sources (in our case: solar, thermal, or hybrid), but not on others (in our case: RF and an onboard solar panel in ambient conditions). The experimental results also confirmed that the peak currents can be problematic, not only for booting the nodes but also for resuming computations after a power cut. Although adding extra capacitors might alleviate the problem, this would somehow defeat the whole purpose of operating WSN nodes without energy storage units.

Generally speaking, the experimental results are positive, but also highlight the need for careful dimensioning of the EH sources and the save/restore method. For those applications that are more complex or more demanding, it would most likely be needed to use more sophisticated methods, such as the ones discussed in the introduction; this is a possible topic for future work.

Another topic that needs to be further investigated is the impact that TC has on the application that runs on the WSN nodes in terms of quality of services (QoS) and quality of experience (QoE), especially for a large number of nodes. For this, it would be best to begin with simulations to evaluate metrics, such as delay, latency, throughput, and jitter in a system where the nodes are on and off at different times. Despite the fact that, in general, such patterns are expected to degrade the QoS and QoE, it might be possible to apply some of the methods and techniques developed for delay-tolerant networking and disruption-tolerant networking (although the memory and bandwidth overheads would have to be minimized significantly).

Acknowledgments: This work has been supported in part by TUT baseline project B38 and IT Academy stipend program. This project has also received funding from the European Union's Horizon 2020 research and innovation programme under grant agreement No 668995. This material reflects only the authors' view and the EC Research Executive Agency is not responsible for any use that may be made of the information it contains. We are also very thankful to Dr. J. Ojarand, Mr. M. Reidla, Mr. M. Lavrov and Mr. M. Rist for their technical support throughout the experiments.

Author Contributions: F. Ahmed, T. Ahmed and Y. Le Moullec designed and performed the experiments and analyzed the results; P. Annus and Y. Muhammad provided hardware resources and helped analyze the results. All authors participated in the paper writing...

Conflicts of Interest: The authors declare no conflict of interest. The founding sponsors had no role in the design of the study; in the collection, analyses, or interpretation of data; in the writing of the manuscript, and in the decision to publish the results.

References

1. Magno, M.; Brunelli, D.; Sigrist, L.; Andri, R.; Cavigelli, L.; Gomez, A.; Benini, L. InfiniTime: Multi-sensor wearable bracelet with human body harvesting. *Sustain. Comput. Inform. Syst.* **2016**, *11*, 38–49. [CrossRef]
2. Chandrakasan, A.; Amirtharajah, R.; Goodman, J.; Konduri, G.; Kulik, J.; Rabiner, W.; Wang, A. Design Considerations for Distributed Microsensor Systems. In Proceedings of the IEEE 1999 Custom Integrated Circuits Conference, Cat. No.99CH36327, San Diego, CA, USA, 19 May 1999; pp. 279–286.
3. Arreola, A.R.; Balsamo, D.; Das, A.K.; Weddell, A.S.; Brunelli, D.; Al-Hashimi, B.M.; Merrett, G.V. Approaches to Transient Computing for Energy Harvesting Systems: A Quantitative Evaluation. In Proceedings of the 3rd International Workshop on Energy Harvesting & Energy Neutral Sensing Systems—ENSsys '15, Seoul, Korea, 1–4 November 2015; pp. 3–8.
4. Jelicic, V.; Magno, M.; Brunelli, D.; Bilas, V.; Benini, L. Benefits of Wake-up Radio in Energy-Efficient Multimodal Surveillance Wireless Sensor Networks. *Sens. J.* **2016**, *14*, 3210–3220. [CrossRef]
5. Jelicic, V.; Magno, M.; Brunelli, D.; Bilas, V.; Benini, L. Analytic Comparison of Wake-up Receivers for WSNs and Benefits over the Wake-on Radio Scheme. In Proceedings of the 7th ACM Workshop on Performance Monitoring and Measurement of Heterogeneous Wireless and Wired Networks, Paphos, AA, Cyprus, 21–25 October 2012; pp. 99–106.
6. Magno, M.; Benini, L.; Gaggero, L.; la Torre Aro, J.P.; Popovici, E. A Versatile Biomedical Wireless Sensor Node with Novel Dry Surface Sensors and Interfaces. In Proceedings of the 5th IEEE International Workshop, Bari, Italy, 13–14 June 2013; pp. 217–222.
7. Karlen, W.; Floreano, D. Adaptive Sleep-Wake Discrimination for Wearable Devices. *Biomed. Eng. IEEE Trans.* **2011**, *58*, 920–926. [CrossRef] [PubMed]
8. Subendran, P.; Viswanath, S.K.; Yuen, C.; Veerappan, C.S. Adaptive Transmission for Self-Sustainable Energy Harvesting Wireless Sensor Network. In Proceedings of the Frontiers of Communications, Networks and Applications (ICFCNA 2014—Malaysia), Kampar, Malaysia, 3–5 November 2014.
9. Wan, Z.G.; Tan, Y.K.; Yuen, C. Review on Energy Harvesting and Energy Management for Sustainable Wireless Sensor Networks. In Proceedings of the 2011 IEEE 13th International Conference on Communication Technology, Jinan, China, 25–28 September 2011; pp. 362–367.
10. Magno, M.; Boyle, D.; Brunelli, D.; Flynn, B.O.; Popovici, E.; Member, S.; Benini, L. Hybrid Energy Supply. *IEEE Trans. Ind. Electron.* **2014**, *61*, 1871–1881. [CrossRef]
11. Taris, T.; Vigneras, V.; Fadel, L. A 900 MHz RF Energy Harvesting Module. In Proceedings of the 10th IEEE International New Circuits and Systems Conference (NEWCAS 2012), Montreal, QC, Canada, 17–20 June 2012; pp. 445–448.
12. Georgiou, O.; Mimis, K.; Halls, D.; Thompson, W.H.; Gibbins, D. How Many Wi-Fi APs Does it Take to Light a Lightbulb? *IEEE Access* **2016**, *4*, 3732–3746. [CrossRef]
13. Lu, X.; Wang, P.; Niyato, D.; Kim, D.I.; Han, Z. Wireless Networks with RF Energy Harvesting: A Contemporary Survey. *IEEE Commun. Surv. Tutorials* **2014**, *17*, 757–789. [CrossRef]
14. Mustufa, Y.S.A.; Barton, J.; Flynn, B.O.; Davies, R.; McCullagh, P.; Zheng, H. Design of a Smart Insole for Ambulatory Assessment of Gait. In Proceedings of the 12th International Conference on BSN, Cambridge, MA, USA, 9–12 June 2015; pp. 1–5.
15. Mekikis, P.V.; Lalos, A.S.; Antonopoulos, A.; Alonso, L.; Verikoukis, C. Wireless energy harvesting in two-way network coded cooperative communications: A stochastic approach for large scale networks. *IEEE Commun. Lett.* **2014**, *18*, 1011–1014. [CrossRef]

16. Mekikis, P.V.; Antonopoulos, A.; Kartsakli, E.; Lalos, A.S.; Alonso, L.; Verikoukis, C. Information Exchange in Randomly Deployed Dense WSNs with Wireless Energy Harvesting Capabilities. *IEEE Trans. Wirel. Commun.* **2016**, *15*, 3008–3018. [CrossRef]
17. Zhang, P.; Tan, H.; Xiao, G.; Yi, Yu. Maximizing Lifetime in Clustered WSN s with Energy Harvesting Relay: Profiling and Modeling. In Proceedings of the 2015 IEEE Tenth International Conference on Intelligent Sensors, Sensor Networks and Information Processing (ISSNIP), Singapore, 7–9 April 2015; pp. 1–6.
18. Wu, Y.; Zhong, X.; Wang, X.; Yang, Y.; Wang, Z.L. Hybrid Energy Cell for Simultaneously Harvesting Wind, Solar, and Chemical energies. *Nano Res.* **2014**, *7*, 1631–1639. [CrossRef]
19. Shaikh, F.K.; Zeadally, S. Energy harvesting in wireless sensor networks: A comprehensive review. *Renew. Sustain. Energy Rev.* **2016**, *55*, 1041–1054.
20. Ransford, B.; Sorber, J.; Fu, K. Mementos. Mementos: System Support for Long-Running Computation on RFID-Scale Devices. *ACM SIGPLAN Not.* **2011**, *46*, 159–170. [CrossRef]
21. Balsamo, D.; Weddell, A.S.; Merrett, G.V.; Al-Hashimi, B.M.; Brunelli, D.; Benini, L. Hibernus: Sustaining Computation during Intermittent Supply for Energy-Harvesting Systems. *IEEE Embed. Syst. Lett.* **2015**, *7*, 15–18. [CrossRef]
22. Balsamo, D.; Das, A.; Weddell, A.; Brunelli, D.; Al-Hashimi, B.; Merrett, G.; Benini, L. Graceful Performance Modulation for Power-Neutral Transient Computing Systems. *IEEE Trans. Comput. Des. Integr. Circuits Syst.* **2016**, *35*, 738–749. [CrossRef]
23. Lucia, B.; Ransford, B. A Simpler, Safer Programming and Execution Model for Intermittent Systems. *ACM Sigplan Not.* **2015**, *50*, 575–585. [CrossRef]
24. Jayakumar, H.; Raha, A.; Lee, W.S.; Raghunathan, V. QuickRecall: A HW/SW Approach for Computing across Power Cycles in Transiently Powered Computers. *ACM J. Emerg. Technol.Comput. Syst.* **2015**, *12*, 1–19. [CrossRef]
25. Ahmed, F.; le Moullec, Y.; Annus, P. FYPSim: Evaluation Tool for Solar-based Energy Harvesting for WSNs. *Int. J. Bioelectromagn.* **2015**, *17*, 75–86.
26. Tan, Y.K.; Panda, S.K. Energy Harvesting From Hybrid Indoor Ambient Light and Thermal Energy Sources for Enhanced Performance of Wireless Sensor Nodes. *IEEE Trans. Ind. Electron.* **2011**, *58*, 4424–4435. [CrossRef]
27. Texas Instrument. MSP430 SimpliciTI Porting Guidelines. 2014. Available online: http://processors.wiki.ti.com/index.php/MSP430_SimpliciTI_Porting_Guidelines (accessed on 26 September 2016).
28. Texas Instrument, Intelligent System State Restoration after Power Failure with Compute through Power Loss Utility. 2015. Available online: http://www.ti.com/lit/ug/tidu885/tidu885.pdf (accessed on 26 September 2016).

Appendix C

Publication III

Ahmed, F., Tamberg, G., Le Moullec, Y., Annus, P. Dual-source Linear Energy Prediction (LINE-P) model in the context of WSNs. Sensors (2017) 17, 7, 1666.

sensors

MDPI

Article

Dual-Source Linear Energy Prediction (LINE-P) Model in the Context of WSNs

Faisal Ahmed [1,*], Gert Tamberg [2,*], Yannick Le Moullec [1,*] and Paul Annus [1]

[1] Thomas Johann Seebeck Department of Electronic, Tallinn University of Technology, Tallinn 12616, Estonia; paul.annus@ttu.ee

[2] Department of Cybernetics, Tallinn University of Technology, Tallinn 12616, Estonia

* Correspondence: faisal.ahmed@ttu.ee (F.A.); gert.tamberg@ttu.ee (G.T.); yannick.lemoullec@ttu.ee (Y.L.M.); Tel.: +372-5800-7448 (F.A.)

Received: 12 May 2017; Accepted: 14 July 2017; Published: 20 July 2017

Abstract: Energy harvesting technologies such as miniature power solar panels and micro wind turbines are increasingly used to help power wireless sensor network nodes. However, a major drawback of energy harvesting is its varying and intermittent characteristic, which can negatively affect the quality of service. This calls for careful design and operation of the nodes, possibly by means of, e.g., dynamic duty cycling and/or dynamic frequency and voltage scaling. In this context, various energy prediction models have been proposed in the literature; however, they are typically compute-intensive or only suitable for a single type of energy source. In this paper, we propose Linear Energy Prediction "LINE-P", a lightweight, yet relatively accurate model based on approximation and sampling theory; LINE-P is suitable for dual-source energy harvesting. Simulations and comparisons against existing similar models have been conducted with low and medium resolutions (i.e., 60 and 22 min intervals/24 h) for the solar energy source (low variations) and with high resolutions (15 min intervals/24 h) for the wind energy source. The results show that the accuracy of the solar-based and wind-based predictions is up to approximately 98% and 96%, respectively, while requiring a lower complexity and memory than the other models. For the cases where LINE-P's accuracy is lower than that of other approaches, it still has the advantage of lower computing requirements, making it more suitable for embedded implementation, e.g., in wireless sensor network coordinator nodes or gateways.

Keywords: WSN; energy harvesting; transient computing

---

1. Introduction

Although improvements have been made in the domain of energy storage (e.g., supercapacitor and lithium battery), those storage devices still have numerous shortcomings such as size, installation, maintenance and cost, especially for WSNs nodes [1]. In this context, energy harvesting is an increasingly popular approach used for powering wireless sensor network (WSN) nodes. Various energy harvesting methods and techniques have been proposed and developed over the last decade [2]; such approaches are typically used to complement more traditional energy storage devices such as rechargeable batteries and supercapacitors, or even to replace them all together as in battery-less nodes that operate according to the principles of transient computing [3].

However, energy sources such as solar and wind are characterized by significant variations and intermittence; thus, it is challenging to guarantee that the WSN nodes always have the necessary energy to operate. In turn, this can negatively impact the quality of service of the application. In the worst case, some nodes might temporarily run out of energy. To alleviate this issue, on-line mechanisms such as dynamic duty cycling and/or dynamic frequency and voltage scaling can be used to modulate the energy consumption of the WSN node according to the available energy.

In this context, energy prediction plays a vital role to deal with questions such as "when is the next power loss going to happen?" and "What will happen when the data transmission/reception is performed although energy has not been predicted properly?" In addition, "Will WSNs operation provides satisfactory QoS by using energy prediction, specifically if used together with transient computing?" The importance of energy prediction in WSNs is also highlighted by recent works such as [4] which proposes a forecast algorithm applicable to solar-powered WSNs and also demonstrates its practical implementation using real WSN nodes, as well as [5] which focuses on a wind energy prediction model. In particular, the accuracy of the prediction or forecast model is deemed significant, especially in the case of autonomous WSNs for which proper operation relies on the available energy predictions [4].

Moreover, research shows that, at least as of today, a node's radio chip consumes the largest amount of energy as compared to computation and sensing operations [3]. Proper management of radio consumption can be more effective if the microcontroller of a WSN node can be programmed in such a way that it performs the transmission/reception operations in accordance to the predicted energy availability.

Furthermore, other causes of energy wastage in the WSN nodes are idling, listening, etc. As a solution, a node remains in the idle state and wakes up when the energy is predicted and performs transmission/receiving at that time. Energy prediction can be seen as an alternative solution [3], which can control the computation and communication operations in the WSN nodes, although energy optimizations techniques can also be applied with modifications, e.g., in the MAC (media access control) protocol [6].

For better performance of the autonomous WSN nodes, energy prediction concept is essential because prediction at different data time intervals provides more accuracy, realistic results, and allows executing the tasks when energy has been properly estimated [7].

Although it could be argued that energy prediction in the context of energy harvesting technologies for WSNs is now quite mature, few energy prediction models provide accurate results at a low computational complexity cost. In fact, energy prediction for autonomous WSNs is still not extensively explored, which calls for further research. Most of the prediction models use as much as possible the energy history (e.g., past records) for accuracy [7] or by employing rather computational complex models to reduce the error estimation. On the contrary, in this article, we propose three different sub-cases of an energy prediction model, named LINE-P, which considers very few values for predicting energy from past records. Furthermore, most proposed energy prediction models are suitable for solar energy or wind energy only; to accommodate the emergence of multi-source energy harvesting, the proposed LINE-P model supports dual-source (solar and wind) WSNs harvesters.

The main contributions presented in this paper are:

1. An overview of existing fixed weighting factor based energy prediction models.
2. A proposal for a symmetrical kernel-based model (LINE-P) for dual-source (solar and wind) which estimates the value on three different data time intervals, i.e., shorter, medium and longer. Indeed, although different prediction models have been proposed in the literature to forecast solar or wind energy availability, most are based on a fixed weighting factor. However, the fixed weighting factor is incompatible with the solar powered WSNs because each solar panel has a different set of parameters [4]. On the other hand, the symmetric kernels have simple computation of the dot product in a potentially infinite dimensional feature space by means on the kernel function. In addition, symmetric kernels have a simpler structure than non-symmetric kernels.
3. A comparison of the proposed LINE-P model against state-of-the-art energy prediction models (fixed weighting factor) for solar and wind-based energy sources. We validate our model by using real datasets (energy profiles) and comparing the performance of the various models by means of classical error estimation techniques, showing their accuracy and complexity in terms of execution time and space (memory).

Before looking at the details of the existing and proposed models, what follows briefly discusses solar and wind energy; these two sources as used for the experimental results described in the second part of this paper.

1.1. Solar Energy

In consumer applications, the concept of solar energy harvester came up in the late 1980s [8], as illustrated by many applications such as calculators and electronic games that were powered by means of solar harvested technology. Solar energy harvesting converts light and heat from the sun into electricity. Nevertheless, the direction of the solar panel is very crucial; i.e., two co-located harvesters at different angles produce different amounts of energy. In addition, indoor solar energy harvesting is generally speaking less exploited as it generates less energy [8].

Both outdoor and indoor solar energy harvesting can potentially power a system for relatively long durations, although due to their uncertainties (either varying weather or varying indoor illumination patterns), neither can be used very in a dependable way, especially when considering autonomous and transient computing based nodes.

1.2. Wind Energy

Nature provides us many non-polluting energy sources, including wind. Three key elements affect the amount of energy that can be harvested from wind, i.e., wind speed, air density and shaft area. A small change in these elements causes large differences in the net amount of energy, either positively or negatively. It has also been shown that no wind turbine converts more than 59.3% of the kinetic energy of the wind into mechanical energy [8].

1.3. Datasets

In order to design the proposed energy prediction model, as well as to evaluate and compare its performance, several datasets have been used. Significantly, solar and wind technology are varying and intermittent by nature. For solar energy, we considered two different data time intervals, shorter and medium; since wind energy is very uneven, a longer data time interval is better for improving the prediction accuracy. However, a longer time interval (more number of slots) requires more space.

To fulfill the different data time interval requirements, we obtained datasets from trusted sources for different locations.

From the California ISO (Folsom, CA, USA), we selected three datasets for solar energy, Southern California Edison Company (SCE, Rosemead, CA, USA), Pacific Gas and Electric Company (PG&E, San Francisco, CA, USA), San Diego Gas & Electric Company (SDG&E, Santa Ana, CA, USA), and one dataset for wind energy [9].

Shorter, medium and longer data time intervals of 22, 60 and 15 min, consisting of 24, 61 and 96 slots in 24 h, respectively, have been used. Furthermore, data from NREL's Solar Radiation Research Laboratory (SRRL, Washington, DC, USA) [10] were used for one solar energy profile (shorter data time interval).

Finally, we used one profile for wind energy from Elia (Belgium's electricity transmission system operator) [11] specifically for longer data time interval.

2. Materials and Methods

In the context of WSNs, few prediction models for solar and very few for wind energy exist. This section comprises two parts: in the first one, the state of the art related to solar and wind based energy prediction models is discussed in detail; and, in the second part, we describe and discuss the proposed LINE-P model.

2.1. Solar-Based Energy Prediction Models

Solar energy is considered on short-term intervals for accurate prediction purposes, i.e., a day is divided into slots ranging from one minute to several hours [12]. For example, in [12], a day is divided into 24 slots (an hour equal to one slot).

2.1.1. Exponential Weighted Moving Average (EWMA)

EWMA [13] is one of the popular prediction models in the domain of WSNs. Several models have then been proposed to extend EWMA [6,13,14]. EWMA predicts the solar energy based on the energy profile of the previous day along with the historical average of real data [15]. EWMA has been discussed in [6] and is expressed as:

$$X(i) = \alpha X(i-1) + (1-\alpha)x(i) \tag{1}$$

where $x(i)$ denotes the value of the real energy. EWMA is dependent on the weighting factor α, which ranges from 0 to 1, and $x(i)$, which expresses the real energy. EWMA works very well on longer slots and if the weather is consistent. However, EWMA is not suitable for shorter slots and generates large errors for alternate sunny and cloudy days [15].

Complexity of EWMA: In this work, we are interested in comparing the complexity (in terms of running time) of various energy estimation methods. For this, we present the Big-O notation for each of them, starting with that of EWMA for a single estimation value. Since in Equation (1) the number of multiplication operations are constant and one addition operation is performed, the complexity in terms of running time is denoted by $T(n)$; i.e., $T(n) = 2$, thus the Big-O for EWMA is $O(2)$.

2.1.2. Weather Conditioned Moving Average (WCMA)

WCMA is an extension of EWMA that works on short-term prediction by accounting for the mean of the previous day's energy as well as the mean of the current day's energy [14]. WCMA is proposed in [6] and expressed as:

$$E(d, n+1) = \alpha E(d, n) + GAP_K(1-\alpha)M_D(d, n+1) \tag{2}$$

The estimation yielded by WCMA is more accurate and has a lower computational complexity as compared to EWMA [16]. In Equation (2), α is a weighting factor similar to that used in Equation (1), $E(d, n)$ is the harvested energy of the previous slot, $M_D(d, n+1)$ is the mean of the D past days at $n + 1$ sample of the day, and GAP_K is a new factor which reflects the solar condition in the present day on the base of the previous day [15], and $E(d, n+1)$ is represent predicted energy for the next slot. In [15], the authors presented a comparative analysis of EWMA with WCMA and found higher accuracy for WCMA based on four different day profiles. Considering $K = 3$ and $\alpha = 0.7$ for both models, the mean square error (MSE) and mean absolute error (MSA) of WCMA is less than that of EWMA, i.e., 5% and 7%, respectively.

Complexity of WCMA: WCMA introduces the GAP_K factor that depends on the present and previous days, so GAP_K complexity in terms of running time is $T(n) = n^2\ (k + 1)$, where n is the length of the vector and k is the number of previous days. $M_D(d, n+1)$ is the mean of the past days, so it is $T(n) = nk$. The total complexity of WCMA in terms of running time is $T(n) = k\ (n^2 + 1)$ and with the Big-O notation it is $O(n^2)$, whereas the other parameters are negligible.

2.1.3. Accurate Solar Energy Allocation (ASEA)

ASEA is also based on EWMA. In [16], the author realized the importance of short-term conditions, and designed the ASEA model keeping in mind situations where the weather is extremely unpredictable such as in the northern part of Europe, etc. To address the above problem, the authors of

ASEA introduced the parameter ψ as a weighting factor. It is based on the ratio between the harvested energy and real energy data, based on the previous slots. For example, when ψ is smaller than 1, it indicates bad weather or other issues.

The ASEA model is expressed as:

$$E(d,n) = E(d,n).\psi;\ where\ \psi = \frac{H(d,n-1)}{E(d,n-1)} \tag{3}$$

where E is the predicted value of EWMA and H is the harvested energy.

Moreover, ψ is calculated at the start of each slots, and then multiplied with EWMA for the ASEA prediction values. In [17] the authors have checked the performance of ASEA on the summer season; usually the weather was consistent at that time. However, we have verified the performance of ASEA by utilizing three different data profiles (for three different months, i.e., in August, October and December) and we found that ASEA is not always closer to real data than WCMA, as Figure 1 illustrates for the month of December on the dataset presented in [9].

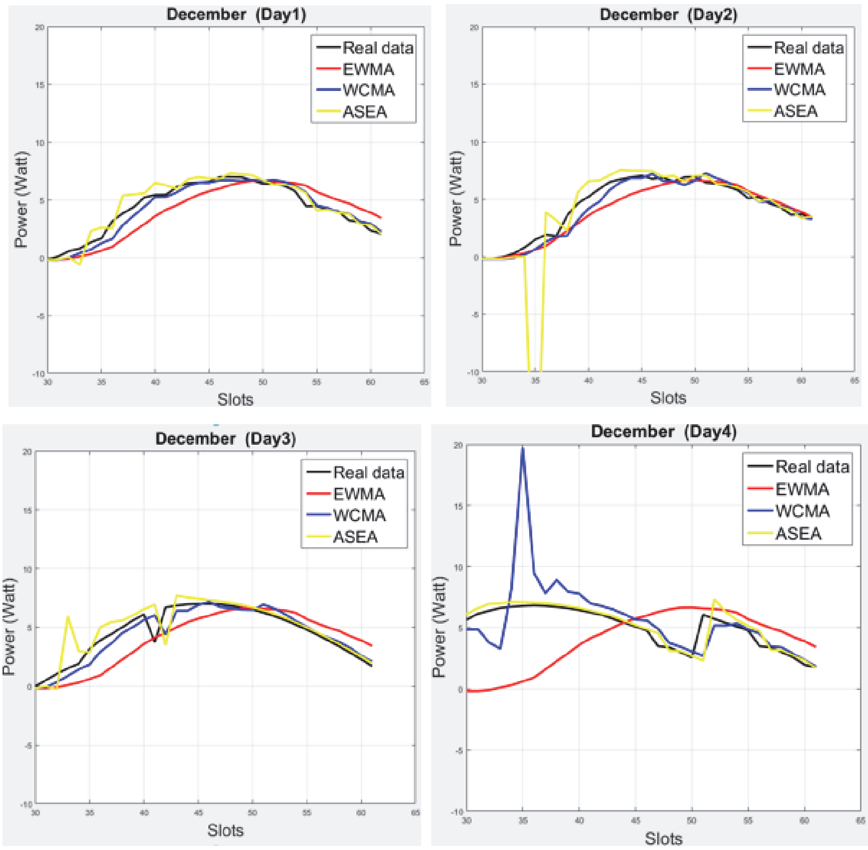

Figure 1. Graphical comparison of three energy prediction models (EWMA, WCMA, and ASEA) with real solar energy data for four different days in December. While the three models can follow the general trend of the real data, none of them can deal with all illumination variations due to inconsistent weather conditions.

Complexity of ASEA: ASEA introduces the ψ factor which has $T(n) = 1$. This is then multiplied with the value of EWMA as can be seen in Equation (3). Thus, the total complexity of ASEA in terms of execution time is $T(n) = 2$. The Big-O notation of ASEA is $O(2)$.

2.1.4. A Solar Energy Algorithm with Q-Learning (QL-SEP)

QL-SEP is a solar energy prediction model that has been recently proposed in [12]. It uses the historical data of past days and as well as most recent weather condition from the present day. In [12], the author assumes that solar energy is based on a periodic cycle and they thus equally divide each day into many slots. QL-SEP also uses the feature of EWMA for the current solar condition. Furthermore, the author introduces a daily ratio (DR) parameter. DR is the average of the energy either increasing or decreasing in the previous slots. DR can be computed as:

$$DR = \frac{\sum_{i=1}^{N}(P_e(i).R(i).i)}{\sum i}. \tag{4}$$

In Equation (4), P_e expresses the prediction error, R is the reliability level and i is the index. R is the key factor which represents the current reward (status) [12]. Suppose the harvested energy H is that of the prediction energy of EWMA as shown in Expression (5):

$$\frac{|H - P|}{P} \tag{5}$$

Therefore, if the result of Equation (5) is positive, then R is considered as +1, otherwise -1, when calculating R for each slot. In addition, the value of R changes the status of r as per γ which is the learning rate with the value of 0.1 in [12]. These parameters are applied in Equation (6) to calculate the Q-value:

$$Q_{t+1}(s) = Q_t(s) + \gamma(r - Q_t(s)) \tag{6}$$

After calculating the Q-values, DR is obtained as:

$$DR = \frac{\sum_{i=1}^{N}\left(\frac{|H-P|}{P}\right).Q(i).i}{\sum i} \tag{7}$$

Finally, the QL-SEP predicts the energy based on DR and EWMA, as expressed in Equation (8):

$$E_{\text{QL-SEP}} = E_{\text{EWMA}}(1 + DR) \tag{8}$$

In [12], the author evaluates the QL-SEP models on real-life solar data over a one-year period and achieves better estimation comparatively to EWMA, ASEA, and Pro-Energy. However, QL-SEP is designed for longer slots; for instance, each day is divided into 24 slots [12], which is not suitable if the weather changes rapidly and continuously; furthermore, to get accurate results, a significant number of computations are required since the device running the prediction modeling has to perform the calculations for EWMA and then for QL-SEP.

Complexity of QL-SEP: In Equation (8), DR is dependent on the Q-value, as can be seen in Equation (7), so the complexity in terms of running time of DR is $T(n) = (2n + 1)q$. Then, for obtaining the final value of QL-SEP, this is multiplied with EWMA. Now, $T(n) = (4n + 2)q$, and the Big-O notation of QL-SEP is $O(n)$; the other parameters are negligible.

2.1.5. Pro-Energy Prediction Model (Suitable for Solar and Wind)

Pro-Energy (PROfile Energy prediction model) predicts energy based on the past days [12]. The Pro-Energy model is designed for multi-source (solar and wind) and is recommended for short and medium slots in a given day. Pro-energy matches the information of the current day with the most similar day among the pool of stored energy profiles. In addition, Pro-energy predicts the next value with the combination of the next slot in the stored profile noted in the last slot [14].

The energy for the current day is calculated as:

$$E(d,n) = \alpha H + (1-\alpha)E_{\mathrm{MS}} \tag{9}$$

where H is the harvested energy in the previous slot and E_{MS} is the observed energy for the most similar day. For evaluating the similarity between the previous day and the current day, the mean absolute error (*MAE*) of each day from previous to current slot is calculated and stored in K. The smallest *MAE* of any day is considered as the most similar day [14]. For multiple profiles, E_{MS} is replaced with a weighted profile (*WP*) that is computed as:

$$WP = \frac{\sum_{j=0}^{P} w_j.E_{sj}}{P-1} \tag{10}$$

Pro-energy combines multiple energy profiles in order to get better estimates for different data time intervals. In Equation (10), P represents the profiles, *MAE* of each day is stored in E, and w_j is calculated as:

$$w_j = 1 - \frac{MAE\ (E_{sj}, C)}{\sum_{j=1}^{P} MAE\ (E_{sj}, C)} \tag{11}$$

where C is the current day. By inserting Equation (11) into Equation (10), and for multiple profiles, Equation (9) becomes Equation (12), i.e., the energy prediction model of Pro-Energy:

$$E(d,n) = \alpha H + (1-\alpha)WP \tag{12}$$

In [14], the authors evaluate the performance of Pro-energy by deploying TelosB nodes with Solar PV and wind micro-turbines energy harvesters along with datasets from the US National Renewable Energy Laboratory. Their results show 60% better prediction than EWMA and WCMA.

Complexity of Pro-Energy: The Pro-Energy model expressed in Equation (12) is based on multiple profiles and requires a significant number of computations. K stores the mean absolute error (*MAE*) of previous and current slots, so its complexity in terms of running time in relation to w_j is $T(n) = (k+1)^2$ and that of WP is $T(n) = n$. Overall, the running time complexity of Pro-energy is $T(n) = (k+1)^2 n$, i.e., higher than that of the previously analyzed models because of the squaring factor. The Big-O notation of the Pro-Energy model is $O((k+1)^2)$.

3. Proposed Dual-Source (Solar and Wind) Linear Energy Prediction) Model (LINE-P)

In this section, we discuss the proposed linear energy prediction model, of which the aim is to reduce the computational complexity while maintaining similar accuracy as compared to the other models.

In order to predict the amount of the harvested energy in the next time slot, we propose a class of methods based on sampling operators. We suppose that the energy profile E can be expressed as:

$$E(t) = E^*(t) + \overrightarrow{E}(t) \tag{13}$$

where E^* is a smooth trend and $\overrightarrow{E}$ represents fluctuations. Our aim is to construct a predictor that on the one hand is good for approximation of smooth trends expressed by E^* and, on the other hand, is not so sensitive to fluctuations expressed by $\overrightarrow{E}$. In our approach, we use results of approximation and sampling theory. In the following, we provide a short overview of those results.

3.1. Sampling Operators

For the uniformly continuous and bounded $f \in C(\mathbb{R})$, the generalized sampling series are given by $(t \in \mathbb{R}; w > 0)$ as Equation (14), i.e., a summation of function values with sampling kernel,

$$(S_w f)(t) := \sum_{k=-\infty}^{\infty} f\left(\frac{k}{w}\right) s(wt - k), \tag{14}$$

where $s \in C(\mathbb{R})$ is a kernel function (see Definition 1 below).

If the kernel function, used in sampling series is the cardinal sine or sinc function, as:

$$s(t) = sinc(t)\frac{\sin \pi t}{\pi t},$$

we get the classical Whittaker-Kotel'nikov-Shannon sampling operator:

$$\left(s_w^{sinc} f\right)(t) := \sum_{k=-\infty}^{\infty} f\left(\frac{k}{w}\right) sinc(wt - k), \tag{15}$$

Let us take $w = 1$ and $t = j \in \mathbb{Z}$ in Equation (14), then

$$(S_1 f)(j) := \sum_{k=-\infty}^{\infty} f(k)s(j - k), \tag{16}$$

The idea to replace the *sinc* kernel $sinc(\cdot) \notin L^1(\mathbb{R})$ by another kernel function $s \in L^1(\mathbb{R})$ appeared first in [18], where the case $s(t) = (sinc(t))^2$ was considered. A systematic study of sampling operators (14) for arbitrary kernel functions was initiated in 1977 at the RWTH Aachen University by Butzer and his students [19–21].

In [20], Section 4 describes why we should be motivated to use the generalized sampling operators (Equation (14)) and also describes the general convergence theorems and convergence theorems with rates.

3.2. Kernels

The general kernel for the sampling operators (Equation (14)) is defined in the following way. Definition 1 [20] if $s : \mathbb{R} \to \mathbb{C}$ is a bounded function such that:

$$m_0(s) := \sum_{k=-\infty}^{\infty} |s(u - k)| < \infty \; (u \in \mathbb{R}), \tag{17}$$

with the absolute convergence uniform on compact subsets of $\mathbb{R}$, and

$$\sum_{k=-\infty}^{\infty} s(u - k) = 1 \; (u \in \mathbb{R}), \tag{18}$$

Now, s is said to be a kernel for sampling operators (14).

The objective of this paper is to use results from [22,23] for signal prediction with the generalized sampling operators ((Equation (14)), when the kernel function s is defined via the Fourier transform of certain even window function $\lambda \in C_{[-1,1]}$, $\lambda(0) = 1$, $\lambda(u) = 0 \; (|u|) \geq 1$. More precisely, our kernel function is defined by the Equation (19),

$$\mathrm{s}(t)\mathrm{s}\;(\lambda; t) := \int_0^1 \lambda(u)\cos(\pi t u)du. \tag{19}$$

This approach generates even kernels. For some cases, asymmetric kernels are more appropriate. In this case, we use a general window function $\lambda : [-1, 1] \to \mathbb{C}$ and define the kernel in the Equation (20),

$$\mathrm{s}(t) := \mathrm{s}\,(\lambda; t) := \frac{1}{2}\int_{-1}^{1} \lambda(u) \exp(-i\pi t u) du. \tag{20}$$

In [24], we considered the general cosine window:

$$\lambda_{C,\mathrm{a}}(u) := \sum_{k=0}^{n} a_k \cos k\pi u \; (n \in \mathbb{N},\; \mathrm{a} = (a_0, a_1, \ldots, a_n)), \tag{21}$$

provided:

$$\sum_{k=0}^{\lfloor \frac{n}{2} \rfloor} a_{2k} = \sum_{k=0}^{\lfloor \frac{n+1}{2} \rfloor} a_{2k-1} = \frac{1}{2}. \tag{22}$$

We get the Hann window, if we take $n = 1$ in (21) and Blackman window, if n = 2 and $a_0 = a$ in Equation (21). For $n \in \mathbb{N}$, there exists a choice of parameters, which allows us to have the order of approximation of the corresponding sampling operators estimated by $\omega_{2n}\left(f; \frac{1}{w}\right)x$ [19]. Another choice of the parameter vector $a = a^*$ in Equation (21), where the parameter vector $a \in \mathbb{R}^{n+1}$ has components $a_0^* = \frac{1}{2^{2n}} \begin{pmatrix} 2n \\ n \end{pmatrix}$ and $a_k^* = \frac{1}{2^{2n-1}} \begin{pmatrix} 2n \\ n-k \end{pmatrix}$ for $k = 1, 2, \ldots, n$, gives us by Equation (19) a family of rapidly decreasing kernels $s_{H,2n} = O(|t|^{2n+1})$ (see [24] for corresponding operator norms and [25–27] for truncation errors).

The general cosine window generates a linear combination of translated sinc-functions. We can use instead of the general cosine window a window in the Equation (23),

$$\lambda_{E,\mathrm{a}}(u) := \sum_{k=-n}^{n} a_k e^{ik\pi u} \; (n \in \mathbb{N},\; \mathrm{a} = (a_{-n}, a_{-n+1}, \ldots, a_n)) \in \mathbb{R}^{2n+1}, \tag{23}$$

provided:

$$\sum_{k=-\lfloor \frac{n}{2} \rfloor}^{\lfloor \frac{n}{2} \rfloor} a_{2k} = \sum_{k=1-\lfloor \frac{n+1}{2} \rfloor}^{\lfloor \frac{n+1}{2} \rfloor} a_{2k-1} = \frac{1}{2}. \tag{24}$$

If we use Equation (20), we get a corresponding kernel in the Equation (25),

$$s_{E,\mathrm{a}}(t) = \sum_{k=-n}^{n} a_k \mathrm{sinc}(t-k), \tag{25}$$

which is indeed a kernel in terms of Definition 1, because Condition (24) guarantees that we have Equation (18) and that $m_0(s_{E,a})$ is bounded. Let $w = 1$ and $t = j \in \mathbb{Z}$ in Equation (14), then for a kernel $s_{E,a}$ we get

$$(S_{1;E,\mathrm{a}}f)(j) := \sum_{k=-\infty}^{\infty} f(k) s_{E,\mathrm{a}}(j-k) = \sum_{k=-n}^{n} a_k f(t-k). \tag{26}$$

3.2.1. Approximation Error Estimates

We estimate the approximation error in terms of modulus of smoothness. The classical modulus of smoothness ([28], p. 76) is defined for any $\delta > 0$ by

$$\omega_k(f; \delta)c := \sup_{|h| \le \delta} ||\Delta_h^k f(\cdot)||C,\, f \in C(\mathbb{R}),$$

where the one-side difference in respect to increment h is given by:

$$\Delta_h^k f(x) = \sum_{l=0}^{k} (-1)^{k-l} \left(\begin{array}{c} k \\ l \end{array} \right) f(x + lh). \tag{27}$$

Modulus of smoothness is a neat measure of the structural properties of a function. As we can see from the definition, the modulus of smoothness is related to the derivative of the function. We can estimate the *r*-th modulus of smoothness using the *r*-th derivative of a function. Our aim is to construct a predictor in the form of a sampling operator that has approximation error estimate via modulus of smoothness of high order. Such predictors are good for the approximation of smooth trends (i.e., trends with high order continuous derivatives).

We proved in [23] a theorem about the approximation properties of the Blackman–Harris sampling operators, defined by the general cosine window (Equation (21)).

3.2.2. Theorem 1 [23]

For $C_{w,a}\left(a \in \mathbb{R}^{n+1}\right)$, let $l, 1 \leq l \leq n$ be fixed. If l = 1 or for every j = 1, . . . , $l - 1$

$$\sum_{k=1}^{n} a_k k^{2j} = 0,$$

then, for $f \in C(\mathbb{R})$, we have estimated order of the approximation,

$$||C_{w,a} f - f|| \leq M_{a,l}\, \omega_{2l}\left(f; \frac{1}{w}\right).$$

Then, constant $M_{a,l}$ is independent of f and w.

For the sampling operators, defined by the general exponent window in Equation (23), we need to prove an analogous theorem. Because we need to use samples from the past to predict the current value, we give a theorem for one-sided kernels, i.e., we use a parameter vector a such that $a_k = 0$ for $k \leq 0$.

3.2.3. Theorem 2 [23]

For $S_{w;E,a}$ with $\left(a \in \mathbb{R}^{n+1}\right)$ such that $a_k = 0$ for $k \leq 0$, let $l, 1 \leq l \leq n$ be fixed.
If l = 1 or for every j = 1, . . . , $l - 1$

$$\sum_{k=1}^{n} a_k k^{2j} = 0, \tag{28}$$

and for every j = 1, . . . , l

$$\sum_{k=1}^{k} (-1)^k a_k k^j = 0, \tag{29}$$

then, for $f \in C(\mathbb{R})$, we have estimated order of the approximation,

$$||S_{w;E,\mathrm{a}} f - f|| \leq M_{a,l}\, \omega_l\left(f; \frac{1}{w}\right). \tag{30}$$

Then, constant $M_{a,l}$ is independent of f and w. In [21], Theorem 2 has been proven.

3.2.4. Good Kernels for Prediction

Theorem 3 [28]

Let $s \in C(\mathbb{R})$ be a kernel. Then, $\{s_w\}_{w>0}$ defines a family of bounded linear operators from $C(\mathbb{R})$ into itself with the operator norm $||S_w|| \equiv ||S_w||c \to c$, satisfying

$$||S_w|| = \sup_{u\in\mathbb{R}} \sum_{k=-\infty}^{\infty} |s(u-k)| < \infty \ (w > 0).$$

If we suppose that the energy profile E can be represented in form

$$E(t) = E^*(t) + \overrightarrow{E}(t),$$

where E^* is a smooth trend and $\overrightarrow{E}$ represents fluctuations, then we have

$$(S_w E)(t) = (S_w E^*)(t) + (S_w \overrightarrow{E})(t),$$

and the error of predicting the trend is

$$|(S_w E)(t) - (S_w E^*)(t)| = |(S_w \overrightarrow{E}(t)| \leq \sup_t |\overrightarrow{E}(t)| \ ||S_w||.$$

The last estimate indicates that for good prediction we need to choose a sampling operator with a small norm. If the trend is smooth [18], we need for good approximation a kernel with approximation error estimate via high order of approximation.

We choose a symmetric kernel (Equation (25)) with the parameter vector

$$\mathrm{b} := \left\{-\frac{11}{2560}, -\frac{11}{256}, -\frac{23}{320}, \frac{25}{256}, \frac{167}{512}, \frac{25}{128}, 0, \frac{25}{128}, \frac{167}{512}, \frac{25}{256}, -\frac{23}{320}, -\frac{11}{256}, -\frac{11}{2560}\right\}$$

The symmetric kernels have simpler computation and structure than non-symmetric kernels.

For this b-kernel, we have Theorem 1, and, for a-kernel, we use Theorem 2, which provides estimates of the error of approximation via modulus of smoothness order 4. This kernel also has a good decay and a small operator norm, close to the minimal possible value of the norm for a kernel with such order of approximation.

We choose a one-sided kernel (Equation (25)) with the parameter vector

$$\mathrm{a} := \left\{0, 0, 0, 0, 0, 0, 0, \frac{3}{8}, \frac{15}{16}, \frac{1}{2}, -\frac{3}{8}, -\frac{3}{8}, -\frac{1}{16}\right\}$$

In the following, we construct predictors as sampling operators in Equation (26) with kernels using those parameter vectors.

4. Prediction

We define three predictors using sampling operators in Equation (26). For the first case, we use the previous samples from the same day and the information from one of the previous days, closest to the current day. Because the symmetric kernels give better order of approximation, we use in our predictor a symmetric kernel with parameter vector b. For measure of the closeness and error correction, we use a one-sided kernel with parameter vector a.

For the second case, we use only the previous samples from the same day and a one-sided kernel. The third case is a simplified version of the first case. Instead of the one-sided kernel, we use a part of the main symmetric kernel for measure of the closeness and error correction.

4.1. Case-I

If we have the samples $f_l(l = 1, \ldots, k)$ from k previous days, then we can use this information for more complex prediction method. The parameter vector b defines a symmetric kernel, the parameter vector a, where $a_k = 0$ for $k \leq 0$, generates a one-sided kernel with the corresponding sampling operator (Equation (26)), yielding Equation (31),

$$(S_{PREDI;\mathrm{b}}f)(j) := \sum_{k=1}^{m} b_k f(j-k) + \sum_{k=-m}^{0} b_k\, f_l(j-k) + CDIF_{PREDI;\mathrm{a;b};l}(j), \tag{31}$$

where the correction term $CDIF_{PREDI;\mathrm{b}}$ is in Equation (32),

$$CDIF_{PREDI;\mathrm{a;b};l}(j) := CT_{PREDI;\mathrm{a;b}} \left(\sum_{k=1}^{n} a_k f(k-i) - \sum_{k=1}^{n} a_k\, f_l(j-k) \right), \tag{32}$$

with the multiplier $CT_{PREDI;\mathrm{b}}$ as:

$$CT_{PREDI;\mathrm{a;b}} := \sum_{k=-m}^{0} b_k. \tag{33}$$

We choose from the k previous days the Day l for which the absolute value of the correction term $CDIF_{PREDI;b;l}$ is minimal and take the values f_l from that day. Finally, Equation (31) is used to estimate the energy based on the next time slot, specifically for LINE-P (Case-I), and Equations (32) and (33) are the substitution factors of Equation (31).

Time Complexity of LINE-P Case-I: Typically, LINE-P case-I is dependent to the two parameters length of the kernel vector (m, n) and the number of previous days (k). The running time complexity of the correction term Equation (32) is $T(n) = 2nk$. Thus, the total running time complexity of Equation (31) for a single value estimation is $T(n) = 2(nk + m) + 1$. The Big-O notation of the LINE-P Case-I is $O(n)$.

4.2. CASE-II

Generally, most prediction models predict energy based on the previous days, but here we propose a model which works with only n previous samples from the same day. For instance, if we suppose we do not have the samples from the previous days and have only few previous samples of the same day, in that case we can use those samples from the past to determine the current value of the function t. We can use the sampling operators (Equation (26)) with one-sided kernels where $a_k = 0$ for $k \leq 0$, i.e.,

$$(S_{PREDII;\mathrm{a}}f)(j) := \sum_{k=1}^{m} a_k f(j-k). \tag{34}$$

Here, Equation (34) is used for LINE-P (Case-II).

Time Complexity of LINE-P Case-II: LINE-P case-II is dependent to one parameter i.e., m. The running time complexity of LINE-P case-II is $T(n) = n$. Its notation in Big-O is $O(n)$.

4.3. CASE-III

Specifically, in this case, if we have samples similar to in Case-I, the parameter vector b defines a symmetric kernel with the corresponding sampling operator (Equation (26)), yielding Equation (35).

$$(S_{PREDIII;\mathrm{b}}f)(j) := \sum_{k=1}^{m} b_k f(j-k) + \sum_{k=-m}^{0} b_k\, f_l(j-k) + CDIF_{PREDIII;\mathrm{b};l}(j), \tag{35}$$

where the correction term $CDIF_{PREDIII;\mathrm{b}:l}$ is in Equation (36),

$$CDIF_{PREDIII;\mathrm{b};l}(j) := CT_{PREDIII;\mathrm{b}} \left(\sum_{k=1}^{m} b_k f(j-k) - \sum_{k=1}^{m} a_k\, f_l(j-k) \right), \tag{36}$$

with the multiplier $CT_{PREDIII;\mathrm{b}}$

$$CT_{PREDIII;\mathrm{b}} := \frac{\sum_{k=-m}^{0} b_k}{\sum_{k=1}^{m} b_k}. \tag{37}$$

We choose from the k previous days the day l for which the absolute value of the correction term $CDIF_{PREDIII;b;l}$ is minimal and take the values f_l from that day.

Here, Equation (35) is used for LINE-P (Case-III).

Complexity of LINE-P Case-III: LINE-P Case-III is dependent on two parameters, i.e., the length of the kernel vector (m) and number of previous days (k). Considering the correction term (Equation (36)) and its time complexity which is $T(n) = 2mk$, now the total running time complexity of Equation (36) is $T(n) = m(2k + 1) + 1$. Its notation in Big-O is $O(m)$.

5. Performance Comparison of LINE-P Model with the State-of-the-Art on Real Solar-Based Data Profiles

We evaluate the performance of the proposed LINE-P model (all three cases) based on solar profiles (datasets) in comparison with the state-of-the-art models by means of: (i) graphical representations along with real datasets; and (ii) calculating two types of errors.

5.1. Graphical Comparison of the Models for Solar Energy

In this section, we present the comparative analysis of the simulation results of all above-mentioned solar models, including LINE-P. They are examined on 22- and 60-min interval data corresponding to a medium case of 61 slots, and a longer case of 24 slots in 24 h, respectively. We show their graphical behavior in comparison with the real profiles (datasets) available in [9,10].

Figure 2 illustrates the medium interval, considering 22-min interval data. As can be seen in the subplots, solar energy varies quite a lot, as shown here for the month of December. However, most proposed energy prediction models rely on the smaller number of slots (longer interval), as shown in the state-of-the-art and in Figure 2. The first four days appear quite consistent, but the next two days yields low energy production; such variations make that some of the models does not work properly in this situation. For example, for the fifth and sixth days, the predictions coming from the EWMA and QL-SEP models are quite off the real data. Another example is that ASEA collapses from the second day because it is not meant for medium and shorter slots. On the other hand, Figure 1 shows that ASEA is able to yield suitable predictions for longer intervals. As can also be observed, in any weather situation, all three cases of LINE-P provide predictions very close to the real dataset.

As illustrated above the authors deploy real datasets [10] in all above models for the graphical comparison and use longer interval (24 slots) in a day. However, as Figure 3 shows, some of the models yield worst predictions such as EWMA, WCMA, Pro-Energy and QL-SEP. In addition, ASEA is also not an appropriate for this kind of datasets situation. On the contrary, LINE-P Case-I and Case-III provide more realistic and accurate values than the other models. Furthermore, among the three cases of LINE-P, Case-III performs better than Case-I and Case-II. In addition, note that, for certain days, Case-II yields over predictions.

In a nutshell, Figures 2 and 3 clearly show that the proposed LINE-P model (all cases) are slots independent (adjustable based on the profiles) both for medium and short data intervals, as well as more reliable than the other models.

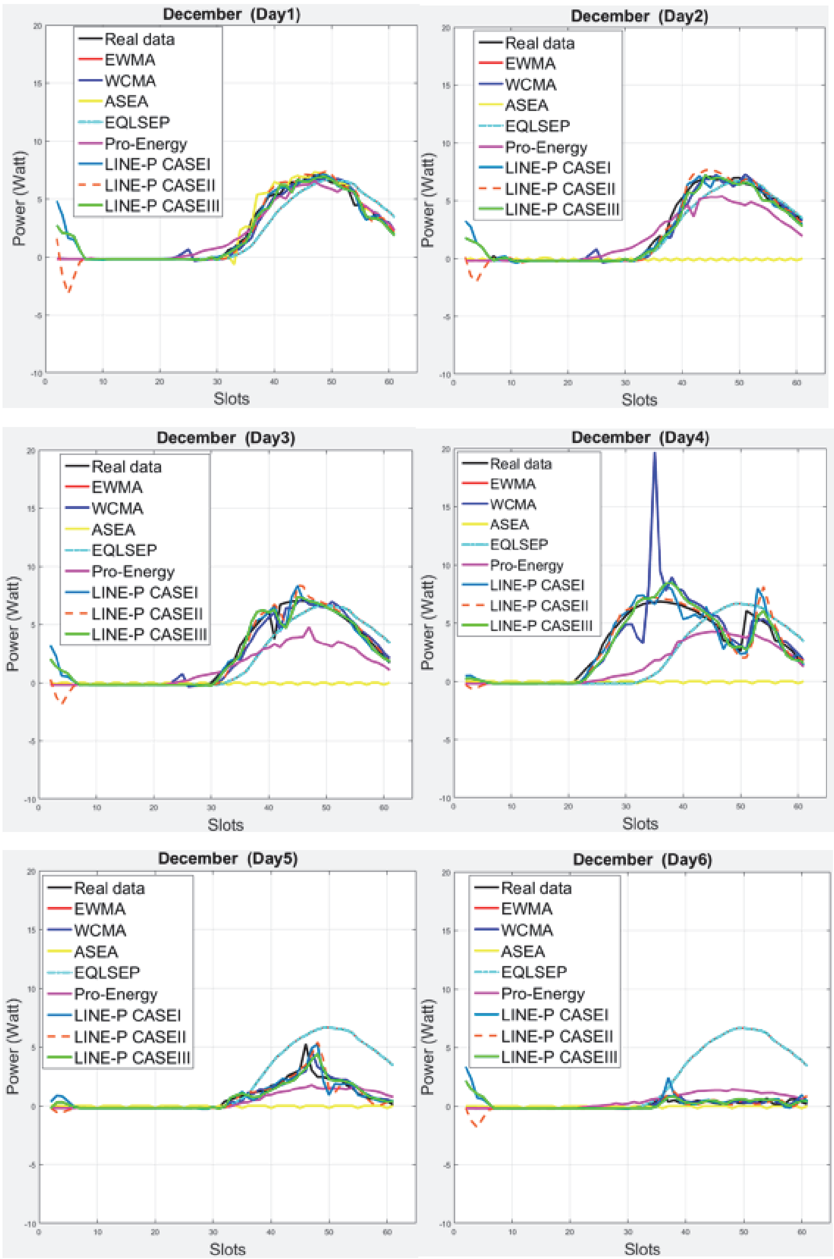

Figure 2. Graphical comparison of the obtained predictions for all energy prediction models (including the proposed LINE-P cases) for medium interval-based (61 slots) solar energy in December. Solar energy variations are troublesome for some of the models (e.g., EWMA and QL-SEP models on the 5th and 6th days, and ASEA on the 2nd day). On the other hand, ASEA is able to yield suitable predictions for longer intervals. In any weather situation, all three cases of LINE-P provide predictions very close to the real dataset.

In the next section, the above graphical analysis is complemented by a mathematical error comparison in terms of mean square error and mean absolute error.

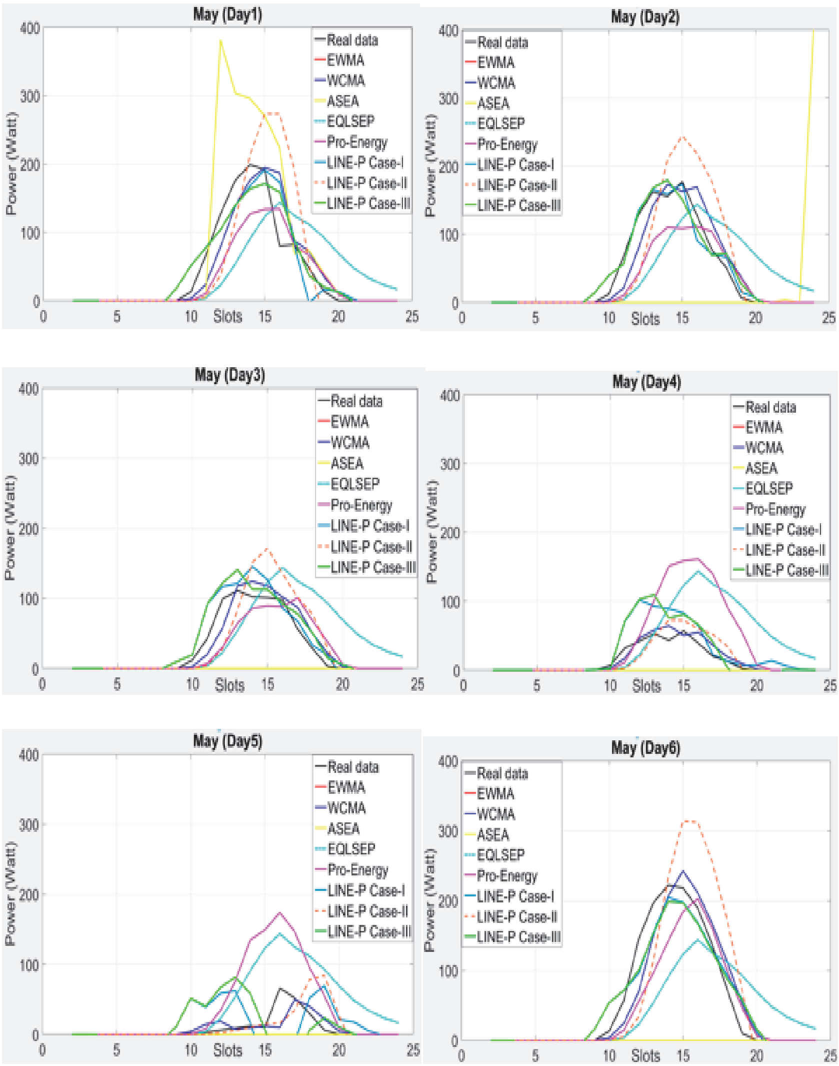

Figure 3. Graphical comparison of the obtained predictions for all models (including the proposed LINE-P cases) for longer interval-based (24 slots) solar energy in May. Here, even ASEA is not always able to deal with energy variations; in contrast, LINE-P Case-I and Case-III provide more realistic and accurate values.

5.2. Error Comparison of the Models for Solar Energy

Mean square error (MSE) and mean absolute error (MAE) have been consider for comparing the error of each of model. To find the error in each model, we have used solar-based (SDG&E) [9] dataset (see Figure 3). We considered a medium interval (61 slots) in 24 h. As can be seen in Table 1, LINE-P (all cases) have the lowest error as compared to the other models. In addition, it is clearly visible that LINE-P Case-I and Case-III have lower MAE in all the days, as shown in Table 2.

Table 1. MSE of the LINE-P (all cases) and other prediction models for solar energy.

Prediction Model	1st Day MSE	2nd Day MSE	3rd Day MSE	4th Day MSE	Average MSE
EWMA	0.0169	0.0831	0.0546	0.0757	0.05757
WCMA	0.0029	0.0074	0.0215	0.0102	0.0105
ASEA	0.0081	0.4998	0.6539	0.6974	0.04648
QL-SEP	0.0169	0.0831	0.0546	0.0757	0.0575
Pro-Energy	0.0046	0.0395	0.0189	0.0299	0.02322
LINE-P (Case-I)	0.0032	0.0102	0.0388	0.0144	0.01665
LINE-P (Case-II)	0.0040	0.0125	0.0461	0.0181	0.020175
LINE-P(Case-III)	0.0038	0.0074	0.0296	0.0105	0.012825

Table 2. MAE of the LINE-P (all cases) and other prediction models for solar energy.

Prediction Model	1st Day MAE	2nd Day MAE	3rd Day MAE	4th Day MAE	Average MAE
EWMA	0.0820	0.2060	0.1588	0.2109	0.16442
WCMA	0.0388	0.0522	0.0863	0.0681	0.06135
ASEA	0.0472	0.5865	0.6379	0.6938	0.49135
QL-SEP	0.0820	0.2060	0.1588	0.2109	0.16442
Pro-Energy	0.0459	0.1493	0.0916	0.1319	0.104675
LINE-P (Case-I)	0.0426	0.064	0.1170	0.0743	0.074675
LINE-P (Case-II)	0.0407	0.0714	0.1279	0.0891	0.082275
LINE-P(Case-III)	0.0459	0.0574	0.0967	0.0682	0.06705

6. Performance Comparison of LINE-P Model with Pro-Energy Models on Real Wind-Based Data Profiles

Pro-Energy is suitable for both types of energy harvester (solar and wind) or multi-source harvesters [14,29]. Similarly, we designed LINE-P (all cases) keeping in mind dual-source EH (solar and wind). Furthermore, for the performance evaluation in terms of accuracy and robustness of the model, we have examined the proposed LINE-P with two different profile lengths (time slots) and conducted various experiments. We found very low error in LINE-P (all cases), as shown in Figures 4 and 5. The previous section compared the performance of all models for solar energy; in what follows, we compare the performance of LINE-P and Pro-Energy for wind energy.

6.1. Graphical Representation of LINE-P and Pro-Energy Models for Wind Energy

The performance of the proposed LINE-P and of the existing Pro-Energy models have been examined for wind energy harvesting on a short 14.25-min data time interval of 90 slots in 24 h. Figure 4 shows their graphical behavior against the real profiles (i.e., US Department of energy [9] and National Laboratory of Research [10]). Figure 4 shows that for a 10-days dataset (real data), LINE-P (all cases) yields better results than Pro-Energy in most cases. Moreover, we also used a 15-min shorter data time interval of 96 slots in 24 h from another dataset [11]; the results shown in Figure 5 confirm that generally speaking, LINE-P performs better and more precisely than Pro-Energy. For example, the prediction yielded by Pro-Energy model in both Figures 4 and 5 are over/under estimated for certain days. On the other hand, LINE-P (all cases), especially LINE-P Case-III, yields more vigorous, less complexity, compatible and accurate predictions.

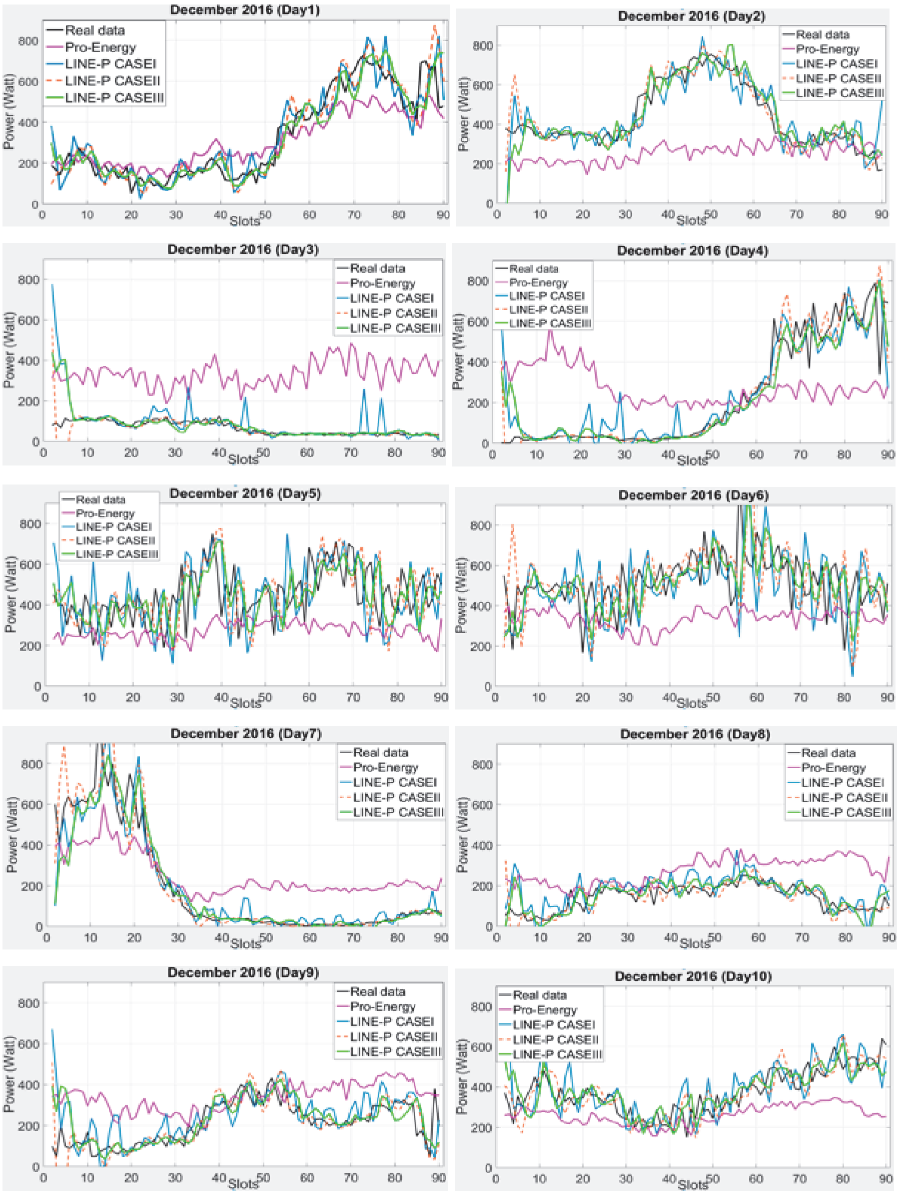

Figure 4. Graphical comparison of the obtained predictions for LINE-P (all cases) and Pro-Energy for shorter interval-based (90 slots) wind energy in December for dataset [9]. Generally speaking, LINE-P yields more accurate estimates than Pro-Energy.

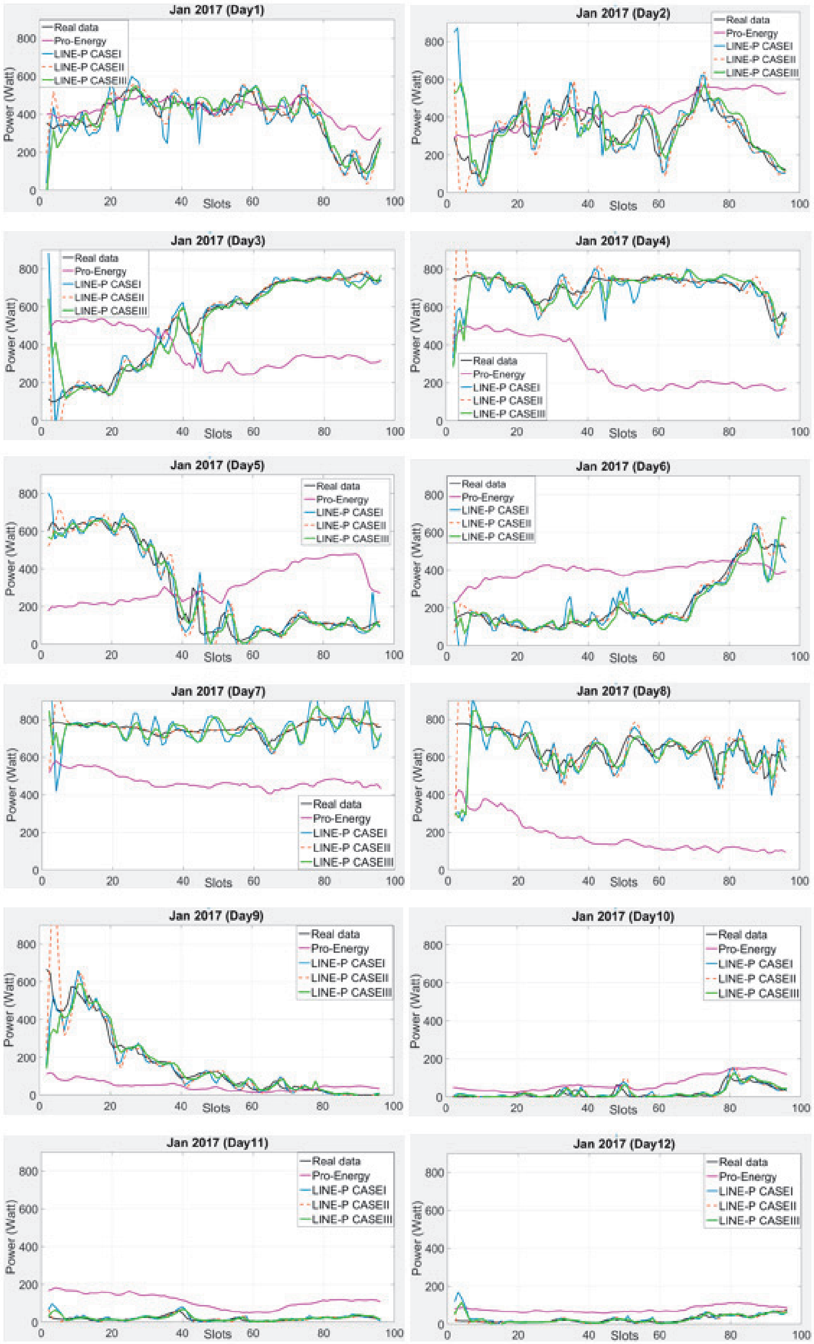

Figure 5. Graphical comparison of the obtained predictions for LINE-P (all cases) and Pro-Energy for shorter interval-based (96 slots) wind energy in December (12 days) and dataset [11]. Generally speaking, the estimates provided by LINE-P are more accurate than those of Pro-Energy.

6.2. Error Comparison of the Models for Wind Energy

We also use MSE and MAE to compare the prediction errors of Pro-energy and LINE-P (all cases). In this case, we use datasets [11] to evaluate the prediction error. The results shown in Table 3 indicate that in general the prediction errors of LINE-P (all cases) are lower than that of Pro-Energy. From the results shown in Table 3, it is concluded that LINE-P (all cases) prediction values are very close to real data; especially Case-III is very effective and accurate.

Table 3. Average MSE and MAE over 10 days for LINE-P (all cases) and Pro-Energy.

Prediction Models	10 Days MSE	10 Days MAE
Pro-Energy	0.777	0.238
LINE-P (Case-I)	0.028	0.038
LINE-P (Case-II)	0.021	0.031
LINE-P(Case-III)	0.018	0.032

6.3. Comparison of the Time Complexities

Table 4 shows the time complexity and Big-O notation for all prediction models. ASEA and EWMA have constant complexity ($O(2)$), whereas WCMA and Pro-Energy have quadratic complexities ($O(n^2)$ and $O((k+1)^2)$, respectively). QL-SEP and LINE-P (all cases) have linear complexity ($O(n)$ and $O(m)$).

Considering both the prediction performance of all models and their respective complexities, it can be said that the proposed LINE-P approach offers the best trade-off, i.e., equivalent or better prediction accuracy than the best existing models at a lower complexity. This means that LINE-P is a good candidate for embedded implementation on resource-constrained platforms such as WSN nodes/coordinators where CPU usage and energy consumption are critical.

Table 4. Time Complexity of the LINE-P (all cases) and the other prediction models. Note: In some models, we consider m and k times rather than n times.

Prediction Models	Time Complexity $T(n)$	Big-O Notation $O(n)$
EWMA	$T(n) = 2$	$O(2)$
ASEA	$T(n) = 2$	$O(2)$
WCMA	$T(n) = k(n^2 + 1)$	$O(n^2)$
Pro-Energy	$T(n) = (k+1)^2 n$	$O((k+1)^2)$
QL-SEP	$T(n) = (4n + 2)$q	$O(n)$
LINE-P Case-I	$T(n) = 2(nk + m) + 1$	$O(n)$
LINE-P Case-II	$T(n) = n$	$O(n)$
LINE-P Case-III	$T(n) = m(2k + 1) + 1$	$O(m)$

6.4. Comparison of Space (Memory) Requirements

The proposed LINE-P model performs well as compared to the other models in terms of prediction error, and at the same time has small memory requirements. A higher number of slots N means memory overhead for a given predictor. For instance, assuming $N = 48$ and D (previous days) = 20, WCMA requires almost 4 kB of memory to store the matrix of $N \cdot D$ for an energy prediction [29]. On the contrary, LINE-P (Case-I) and (Case-III) use only require $N = 13$ and $D = 4$. Similarly, LINE-P (Case-II) only require $N = 8$ and $D = 1$. Thus, LINE-P models' memory overheads are approximately 90% and 70% lower than for WCMA and Pro-Energy models, respectively.

7. Conclusions and Perspectives

We presented LINE-P (three cases-based) prediction model for dual-source (solar and wind energy harvesting) which is suitable for many possible data time intervals, e.g., shorter, medium and longer, as opposed to previous models that are only recommended for a particular data time interval (resulting in degraded predictions when slightly different conditions occur).

The proposed LINE-P (Case-I) predicts the energy based on the previous and current days. LINE-P (Case-II) predicts the energy according to the current days in case of missing data. LINE-P (Case-III) is a simplified version of LINE-P (Case-I): instead of the one-sided kernel, we use a part of the main symmetric kernel for measuring the closeness and error correction. Furthermore, LINE-P model allows adjusting or resizing of the kernels, making it compatible with solar powered WSNs. On the contrary, most of the solar-based prediction models exploit a fixed weighting parameter factor (α), which is incompatible with the solar harvesters due to their different parameter characteristics.

In addition, LINE-P's principle means that it is associated with low computational and reduced memory overheads, making it suitable for implementation on WSN nodes/coordinators.

Several datasets have been considered to evaluate the prediction performance and error of the models. We found that LINE-P model provides low errors, for either solar or wind energy sources. In terms of MSE and MAE, the predictions are approximately 98% accurate for the LINE-P model Case-III for solar energy, and around 96% accurate for wind-based prediction.

As future work, we plan to extend LINE-P with adaptive features and compare its performance against those of UD-WCMA (adaptive tuning of the weighting factor) [4] and Pro-Energy-VLT (adaptive timeslots granularity) [5].

We also plan to integrate the proposed LINE-P model with our recent work on transient computing for WSNs, e.g., to dynamically control the execution patterns of the nodes depending on the available energy. In particular, we will develop an adaptive prediction model which will use the appropriate kernels according to the energy profiles; if the uncertainty thereof is high, then the model will use the non-sensitive kernels; on the other hand, if the energy profiles are smooth, then sensitive kernel will be used for higher prediction accuracy.

Acknowledgments: This work has been supported in part by TUT baseline project B38 and IT Academy stipend program. This project has received funding from the European Union's Horizon 2020 research and innovation program under grant agreement No 668995. This material reflects only the authors' view and the EC Research Executive Agency is not responsible for any use that may be made of the information it contains.

Author Contributions: Faisal Ahmed and Gert Tamberg designed the model, performed the simulations, and analyzed the results. Yannick Le Moullec and Paul Annus helped analyze the results. All authors participated in the paper writing.

Conflicts of Interest: The authors declare no conflict of interest.

References

1. Wu, F.; Rüdiger, C.; Yuce, M.R. Real-Time Performance of a Self-Powered Environmental IoT Sensor Network System. *Sensors* **2017**, *17*, 282. [CrossRef] [PubMed]
2. Balsamo, D.; Weddell, A.S.; Merrett, G.V.; Al-Hashimi, B.M.; Brunelli, D.; Benini, L. Hibernus: Sustaining Computation during Intermittent Supply for Energy-Harvesting Systems. *IEEE Embed. Syst. Lett.* **2015**, *7*, 15–18. [CrossRef]
3. Ahmed, F.; Ahmed, T.; Muhammad, Y.; Le Moullec, Y.; Annus, P. Operating Wireless Sensor Nodes without Energy Storage: Experimental Results with Transient Computing. *Electronics* **2016**, *5*, 89. [CrossRef]
4. Dehwah, A.; Elmetennani, S.; Claudel, C. UD-WCMA: An energy estimation and forecast scheme for solar powered wireless sensor networks. *J. Netw. Comput. Appl.* **2017**, *90*, 17–25. [CrossRef]
5. Kosunalp, S. An energy prediction algorithm for wind-powered wireless sensor networks with energy harvesting. *Energy* **2017**, in press. [CrossRef]
6. Alam, M.M.; Berder, O.; Menard, D.; Anger, T.; Sentieys, O. A hybrid model for accurate energy analysis of WSN nodes. *Eurasip J. Embed. Syst.* **2011**, *4*. [CrossRef]

7. Piorno, J.R.; Bergonzini, C.; Atienza, D.; Rosing, T.S. Prediction and Management in Energy Harvested Wireless Sensor Nodes. In Proceedings of the 1st International Conference on Wireless Communication, Vehicular Technology, Information Theory and Aerospace & Electronic Systems Technology, Aalborg, Denmark, 17–20 May 2009. [CrossRef]
8. Ahmed, F.; Le Moullec, Y.; Annus, P.; Ashad, S. Analytical Evaluation of Indoor Energy Harvesting Technologies for WSNs with FYPSIM Framework. In Proceedings of the International Conference on Industrial Informatics and Computer Systems (CIICS), Shariah, United Arab Emirates, 13–15 March 2016; pp. 1–6.
9. California IOS. Our Renewables Reports Provide Important Information about Actual Renewable Energy within the ISO Grid as California Moves Towards a 33 Percent Renewable Generation Portfolio. The Reports Use Raw Data and Are not Intended to Be Used as the Basis for Operational or Financial Decisions. Available online: http://www.caiso.com/market/Pages/ReportsBulletins/DailyRenewablesWatch.aspx (accessed on 14 July 2017).
10. Stoffel, T.; Andreas, A. *NREL Solar Radiation Research Laboratory (SRRL): Baseline Measurement System (BMS); Golden, Colorado (Data)*; NREL/DA-5500-56488; National Renewable Energy Laboratory: Golden, CO, USA, 15 July 2017.
11. Elia. Data Download Page. Available online: http://www.elia.be/en/grid-data/data-download (accessed on 14 July 2017).
12. Kosunalp, S. A new energy prediction algorithm for energy-harvesting wireless sensor networks with Q-Learning. *IEEE Access* **2016**, *4*, 5755–5763. [CrossRef]
13. Kensal, A.; Hsu, J.; Zahedi, S.; Srivastava, M.B. Power Management in Energy Harvesting Sensor Networks. *ACM Trans. Embed. Comput. Syst.* **2007**, *6*, 32. [CrossRef]
14. Cammarano, A.; Petrioli, C.; Spenza, D. Pro-Energy: A novel energy prediction model for solar and wind energy-harvesting wireless sensor networks. In Proceedings of the 2012 IEEE 9th International Conference on Mobile Adhoc and Sensor Systems, Las Vegas, NV, USA, 8–11 October 2012; pp. 75–83.
15. Ahmed, F.; Le Moullec, Y.; Annus, P. FYPSim: An estimation framework for energy harvesting and energy prediction for WSNs. In Proceedings of the 2016 IEEE International Conference on Consumer Electronics-Taiwan, Nantou, Taiwan, 27–29 May 2016; pp. 1–2.
16. Noh, D.K.; Kang, K. Balanced energy allocation scheme for a solar-powered sensor system and its effects on network-wide performance. *J. Comput. Syst. Sci.* **2011**, *77*, 917–932. [CrossRef]
17. Bergonzini, C.; Brunelli, D.; Benini, L. Algorithms for harvested energy prediction in battery less wireless sensor networks. In Proceedings of the 3rd International Workshop on Advances in Sensors and Interfaces, Trani, Italy, 25–26 June 2009; pp. 144–149.
18. Tamberg. On some truncated Shannon sampling series. *Sampl. Theory Signal Image Process.* **2013**, *12*, 21–32.
19. Butzer, P.L.; Nessel, R.J. Fourier analysis and approximation, Vol. 1. In *Reviews in Group Representation Theory, Part A (Pure and Applied Mathematics Series, Vol. 7)*; Dornhoff, L., Ed.; Marcel Dekker Inc.: New York, NY, USA, 1971.
20. Butzer, P.L.; Schmeisser, G.; Stens, R.L. An introduction to sampling analysis. In *Information Technology: Transmission, Processing, and Storage*; Marvasti, F., Ed.; Springer: New York, NY, USA; pp. 17–121.
21. Kivinukk, A.; Tamberg, G. On window methods in generalized Shannon sampling operators. In *New Perspectives on Approximation and Sampling Theory*; Zayed, A., Schmeisser, G., Eds.; Applied and Numerical Harmonic Analysis; Springer: Cham, Switzerland, 2014; pp. 63–86.
22. Kivinukk, A.; Tamberg, G. On sampling series based on some combinations of sinc functions. *Proc. Estonian Acad. Sci. Phys. Math.* **2002**, *51*, 203–220.
23. Kivinukk, A.; Tamberg, G. On Blackman-Harris windows for Shannon sampling series. *Sampl. Theory Signal Image Process.* **2007**, *6*, 87–108.
24. Butzer, P.L.; Splettstößer, W.; Stens, R.L. *The Sampling Theorems and Linear Prediction in Signal Analysis*; Lehrstuhl A für Math., Rheinisch-Westfälische Techn. Hochsch.: Aachen, Germany, 1986; pp. 1–70.
25. Graf, O.; Tamberg, G. On generalized Blackman-Harris sampling operators. In Proceedings of the International Conference on Sampling Theory and Applications (SampTA), Tallinn, Estonia, 3–7 July 2017; in press.
26. Stens, R.L. Sampling with generalized kernels. In *Sampling Theory in Fourier and Signal Analysis: Advanced Topics*; Higgins, J.R., Stens, R.L., Eds.; Oxford University Press: New York, NY, USA, 1999.

27. Tamberg, G. On truncation error of some generalized Shannon sampling operators. *Numer. Algorithms* **2010**, *55*, 367–382. [CrossRef]
28. Theis, M. Über eine interpolationsformel von de la Vallee-Poussin. *Math. Z.* **1919**, *3*, 93–113. [CrossRef]
29. Cammarano, A.; Petrioli, C.; Spenza, D. Improving Energy Predictions in EH-WSNS with Pro-Energy-VLT. In Proceedings of the 11th ACM Conference on Embedded Networked Sensor Systems, Roma, Italy, 11–13 November 2013; p. 41.

Appendix D

Publication IV

Ahmed, F., Kervadec, C., Le Moullec, Y., Tamberg, G., Annus, P. Autonomous Wireless Sensor Networks: Implementation of Transient Computing and Energy Prediction for Improved Node Performance and Link Quality. The Computer Journal (2018) (under reviewed for second round).

Autonomous Wireless Sensor Networks: Implementation of Transient Computing and Energy Prediction for Improved Node Performance and Link Quality

Faisal Ahmed, Corentin Kervadec, Yannick Le Moullec, Gert Tamberg, and Paul Annus

Abstract

Over the last decades, research and development in energy harvesting significantly changed the traditional way of powering electronic devices, as exemplified by the emergence of battery-less wireless sensor nodes. In contrast to existing works that consider energy prediction and transient computing separately, we present a novel approach for the joint implementation of these two modalities aimed at improving the adaptability and robustness of applications running on battery-less nodes. The proposed approach performs online energy measurements and store them as energy profiles. Based on these, we use our recently proposed LINE-P (Case-II) model to estimate the energy availability in the near future. These energy estimates are exploited in a transient computing mechanism that manages the operation of the nodes, in particular their wireless communication functions. We present an implementation thereof for a peer-to-peer application on FRAM-based wireless sensor nodes (TI MSP430FR5739 MCU and TI CC2500 transceiver) that operate without energy storage. In a first set of experiments, the nodes are powered by a power supply programmed to mimic the intermittent nature of harvested energy; in a second set, they are powered by a solar panel yielding real data sets (profiles) at 1, 5, and 10-minute data intervals. The experimental results show how the proposed combined transient computing and energy prediction approach addresses various issues such as time failure of the node and system shutdown, as well as how the link quality and overall performance of the peer-to-peer application are improved.

Keywords: *Transient computing; Energy harvesting; Battery-less, Autonomous system; Link quality and jitter.*

1 Introduction

Although advances have been achieved in terms of storage capacity (power source), e.g. supercapacitors or lithium batteries, these storage devices have numerous shortcomings. These are related to installation/maintenance, physical constraints (e.g. size, weight), and safety risks due to their electrochemical properties, especially when it comes to wireless sensor network (WSN) nodes. The explosive growth of IoT and WSN also raises environmental concerns. In [1], the global electricity consumption of network-enabled devices is reported to have reached 615 TWh in 2013. In addition, this demand is estimated to raise up to 1140 TWh by 2025, which will be 6% of total global electricity consumption. Furthermore, it is expected that there will be 23 billion battery-powered IoT devices in 2025. The annual estimation of the global battery consumption is almost 12 billion batteries in 2025. It is also worth noting that the manufacturing of a battery requires 40 to 500 times its actual energy capacity. Thus, the manufacturing of IoT batteries is expected to yield a further burden of 2 TWh of energy consumption in 2025.

Energy harvesting (EH) changes the two above-mentioned dynamics and brings significant improvements in the energy capabilities of embedded systems such as wireless sensor network (WSN). EH introduces various paths of research for prolonging the life-span of WSN nodes, typically in the form of a buffered temporary energy storage, or directly (i.e. battery-less), which enables devices to be more energy-autonomous. Recent research results illustrate that energy harvesting is not capacity-limited anymore [2]; EH, either used as a substitute or as a direct power source for WSN nodes is highly beneficial [3].

However, due to its intermittent nature, EH is highly unpredictable and variable. For example, weather, light intensity, and the time of the day greatly affect how much and when energy can be obtained from a photovoltaic

(PV) panel. Finding a good trade-of between performance, adaptability, and robustness for achieving an acceptable quality of service is challenging.
One approach to deal with this is to use accurate sets of energy prediction models to dynamically control and modulate the operation of the wireless sensor nodes as a function of the instantaneous and near-future available energy.
Transient computing (TC) is another recent paradigm designed to deal with the intermittent behavior of EH. TC is an umbrella term that encompasses various methods that allow pausing and resuming a node's operations with limited loss of information; this is typically achieved by means of various strategies for saving/restoring the context and data of a node by exploiting non-volatile memory technologies such as FRAM.

TC and energy prediction have been studied mostly independently in the scientific literature. Given their respective potentials, the overall purpose of this work is twofold, namely i) to propose a novel joint approach that combines those two modalities and ii) to evaluate its practical impact in terms of performance, adaptability and robustness of applications running on battery-less sensor nodes that are solely powered through EH.

In this paper, we address several concerns related to the design and implementation of the above modalities. The first one is related to the choice of the energy prediction model. Most of the existing prediction models are based on long records of past values; however, these are unfeasible in real implementations due to the limited memory of the WSN nodes. The second one is related to the connectivity of the nodes, i.e. how to properly restore the state of the WSN nodes and re-establish the connectivity after a power failure using TC?

This paper emphasizes the real-life implementation and evaluation of our proposed solutions to the above issues. The details thereof are presented in Section 3 and Section 4, respectively. However, we first briefly introduce the system-level setup (for a single WSN node) shown in Figure 1. In our work, the heart of a WSN node is a microcontroller that feature FRAM (i.e. non-volatile) memory combined with a radio transceiver. The WSN node does not include an energy storage device; instead, the energy harvester is used as the sole powering source. In [4] we evaluated the practical feasibility of TC on a single node basis by deploying three different energy harvesters (RF, thermal and solar); such an approach is improved and re-implemented in this work. In addition, we recently proposed the so-called set of linear energy prediction models (LINE-P) in [5]; one of these (Case-II) is modified and implemented in this work. We also implement a peer-to-peer wireless application whereby two modalities are integrated and evaluated in terms of link quality features for instance jitter, packet receiving ratio and energy consumption.

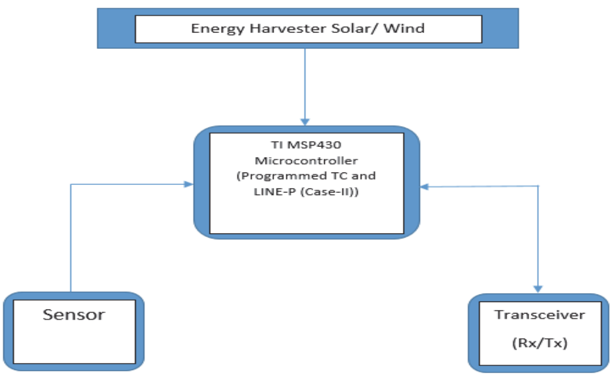

Figure 1. System-level illustration of the joint implementation of the both modalities (TC and LINE-P (Case-II)) into a WSN node solely powered by an energy harvester.

Contributions

The main contributions presented in this paper are summarized as follows:

A) A TC-based mechanism for reducing the negative impact of power losses in battery-less WSN nodes is designed and implemented. In brief, this mechanism allows 1) ending communication tasks properly before a shutdown occurs due to a loss of power, as well as 2) resuming them after a wake up (i.e. when energy is again available). This mechanism consists of four main steps. Upon an imminent loss of power, 1) a node informs its peer that it will not be able to continue the communication task and 2) the TC mechanism saves the state of the microcontroller. Once energy is again available, 3) the state of the microcontroller is restored, the SPI communication with the radio transceiver is re-initialized, and the radio transceiver is reconfigured, and 4) the link protocol is restarted and communication with the peer is resumed.

B) To improve the energy efficiency of the above system, we adapt and implement an energy prediction model. To summarize, this model is used to predict how much energy will be available in the next time period and allows firing a communication task only if a sufficiently high and stable amount of energy is predicted for the given time period. By doing so, less communication tasks are interrupted, i.e. less communication errors happen and thus less energy is wasted due to re-transmissions.

C) The feasibility and efficiency of the joint TC and energy prediction modalities are evaluated in practice, both in a controlled setup using a programmable power supply to mimic the intermittent behavior of harvested energy, as well as in non-controlled setup using a solar panel exposed to natural light. The results show that the two implemented modalities consume only 15% of the total memory of a node and the accuracy of LINE-P (Case-II) is 98% in a consistent weather and 90% in inconsistent weather (e.g. rapidly changing sunny and cloudy conditions), respectively. In addition, the results illustrate that the joint modalities provide improved adaptability and robustness, e.g. up to 94.6% average receiving rate.

2 Related Work

Several methods have been proposed to minimize the power consumption and management of WSNs in the literature. In [6] the authors proposed an extended ad hoc on-demand distance vector (EAODV) routing method based on distributed minimum transmission (DMT) multicast routing. Similarly, in [7] a multicast routing method with minimum transmission for multicast routing algorithms is presented. In [8], the authors proposed an unequal clustering routing protocol considering energy balancing based on network partition and distance (UCNPD), i.e. unequal clustering based on network partition and distance for the WSN. Their simulation results demonstrate that the protocol efficiently decreases the speed of the nodes death. In [9], an energy-balanced routing method, FA-EBRM, based on forward-aware factor is proposed; in [10] the authors present a clustering routing method based on predictive energy consumption efficiency (PECE), this method works in two stages: firstly cluster formation and secondly stable data transfer for WSNs.

In [11] the authors proposed a RFID anti-collision method that improves the efficiency of the system. In [12] the authors proposed a local-world theory where an uneven clustering weighted evolving model of WSNs is designed. Their experimental data shows that the WSNs share robustness and reduce the probability that successive node breakdowns occur. In [13] the authors simulation results show that their new MAC protocol can supply better network service under low energy consumption and transmission delay. Their experimental results indicate that their method is effective and very useful for transmission of big-data bio-medical image in the context of WSNs. In [14] the authors discussed a protocol which is based on a low duty cycle energy-efficient MAC for WSNs and is adaptively updated based on the estimated nodes wake-up time. Their experimental results show that the improved protocol reduces the network energy consumption and improves the adaptability of the network. In [15], the authors proposed a fusion approach with coding based on spherical coordinate domain (SCD) in WSNs for transmission of big-data medical image. Other works that use spherical coordinate domain in medical imaging are [16], [17].

In [18] the authors deal with the data collection problem in the domain of WSNs. They designed a kind of optimization of sparse matrix. Their results show that their approach reduces the collection frequency and costs less energy as compared to general method.

Apart from the traditional low power consumption methods discussed above, researchers are increasingly proposing autonomous WSNs that operate on the available energy directly from the energy harvester. In what follows we discuss the operating principle of TC that allows dealing with the intermittent nature of EH.

2.1 Transient Computing

The intermittent nature of EH, especially when used to power battery-less WSN nodes, makes that the execution of both computations and communication tasks will be interrupted and resumed depending on the available energy. During the last few years, a number of TC approaches have been proposed in the scientific literature. They can broadly be classified as software-based and hardware-assisted approaches. In either case, a non-volatile memory such as Flash or FRAM is used to store a snapshot of the state and/or data of the microcontroller during the power-loss. Once power is again available, the snapshot is restored and execution either restarts, or preferably, resumes.

A) Software-based TC approaches consist of trigger points and checkpoints that are strategically inserted in the source code and periodically evaluated. When energy is deemed too low (typically by evaluating the voltage of the energy device), a snapshot of the state and/or data of the microcontroller is taken. After a loss of power, the latest valid snapshot is restored and the corresponding tasks or blocks of codes are restarted. The major drawbacks of such approaches are i) deciding where to insert the trigger points and checkpoints in the code, ii) the code size overheads for those points and the restore mechanisms, and iii) the execution time overheads caused by creating the snapshots, restoring them, and the re-execution of tasks or blocks of code that got included in the snapshot even though they completed before a loss of power.

B) Hardware-assisted TC approaches make use of e.g. hardware comparators that detect an imminent loss of power and trigger the snapshot mechanism. Those approaches do not require to periodically evaluate the available energy; this significantly reduces or completely avoids the need for software trigger points and checkpoints and reduces or avoids the unnecessary re-execution of full tasks or blocks of code as done in the software-based approaches.

TC approaches have previously been discussed in e.g. [4]. To avoid duplication, we hereby only summarize the main features of various TC approaches, see Table 1.

Table 1. Summary of the main features of various TC approaches

Work	SW-based or HW-assisted	Key feature	Platform
Mementos [17], 2011	SW	Checkpoints placed at a compile-time.	MSP430F1232, Flash
Dino [18], 2015	SW	Continuation of Mementos, ensures coherence between volatile and non-volatile data.	MSP430FR5969, FRAM
Hibernus [19], 2015	HW	Uses a hardware comparator to detect imminent loss of power.	MSP430(unspecified), FRAM
QuickRecall [20], 2015	HW	FRAM is used as a unified memory.	MSP430FR5739, FRAM
Hibernus++ [21], 2016	HW	Dynamic adaptation of the hibernate and restore thresholds according to both the energy source variations and the system load properties. However, requires additional circuitry.	MSP430FR5739, FRAM
HarvOS [22], 2017	SW	Operates at compile-time, allow transiently powered devices to complete a given workload with 68% fewer checkpoints on average, compared to existing approaches.	STM32L152RE (ARM Cortex M3), FLASH
ARM mbed support [23], 2017	HW	Integrates TC approaches into mbed OS. Enables multiplatform and TC as a service above IoT application protocols.	NXP FRDM-KL05Z (ARM Cortex-Mo+), Flash
TI CTPL [24], 2015	HW	Similar principles as that of Hibernus. Designed and supplied by TI.	MSP430FRxx series, FRAM
This work	HW	*Combines TC (TI CTPL) and Energy prediction (LINE-P (Case II), see Section 2.2).*	*MSP430FR5739, FRAM*

In Table 1, we have summarized the state of the art related to transient computing; in what follows we briefly discuss the existing state of the art related to energy prediction models.

2.2 Energy Prediction models

Energy prediction in itself remains an active research topic. Energy prediction (sometimes called energy estimation) deal with unpredictable and non-controllable energy sources such as solar, wind, etc.; this is a critical issue, which raises many questions. Recent research in energy prediction has enhanced the accuracy and minimized the error chances; this thus enables very useful tools to support e.g. power management strategies and link quality in the context of WSNs.

Usually, the idea of energy prediction can be applicable in a broad range of scenarios. In [25], the authors focus on solar energy harvester and its energy management that includes a new energy forecast approach (based on Arima and Garch models) for WSNs. In [26], a solar-based prediction model is presented for structural health monitoring.

In [27], the authors show that prediction strategies that use weather forecasts are more accurate than those based on the past and are capable of improving the performance of a variety of systems. However, in this article the authors have limited scope, which is only energy prediction model.

Recently in [28] the authors proposed aggregated and compression schemes for solar powered WSNs. A node continually aggregates and compresses sensed data, but only transmits it when it expects to receive more energy. However, this approach is based on a fixed energy source (battery) rather than battery-less (autonomous node) and their work is lacking with real time implementation.

An overview of existing proposed energy prediction models, that can support dynamic power management such as those mentioned above, is presented in Table 2.

Table 2. Summary of various energy prediction models

Prediction models	**Time Interval (Slots)**	**Mathematical Expression**	**Source of Harvester**
EWMA [28], 2007	Longer (60 mins)	$X(i) = \alpha X(i-1) + (1-\alpha)x(i)$ where the weighting factor α ranges from 0 to 1 and $x(i)$ expresses the real energy.	Solar
WCMA [29], 2012	Longer (60 mins)	$E(d, n+1) = \alpha E(d, n) + GAP_K(1 - \alpha)M_D(d, n+1)$ where E is the predicted value of EWMA, $M_D(d, n+1)$ is the mean of D past days at n+1 sample of the day, and GAP_K is a factor which reflects the solar condition in the present day on the base of the previous.	Solar
QL-SEP [30], 2016	Longer (60 mins)	$E_{\text{QL-SEP}} = E_{\text{EWMA}}(1 + DR)$ Daily ratio (DR) parameter.	Solar
Pro-Energy (PROfile Energy [31], 2012	Longer/Medium (60/30 mins)	$E(d, n) = \alpha H + (1-\alpha)E_{\text{MS}}$ where H is the harvested energy in the previous slot and E_{MS} is the observed energy for the most similar day.	Dual–Source (Solar/Wind)

2.2.1 LINE-P (Case-II)

In [5] we have presented LINE-P (linear energy prediction model) which is designed and developed based on the sampling and approximation theory. Moreover, it is applied not only in signal processing but also compression techniques [34].

In [5] we have shown that LINE-P (Case-II) has a lower complexity and higher energy efficient as compared to other energy prediction models. In this article, we have implemented LINE-P (Case-II) [5] combined with TC. LINE-P (Case-II) performs energy estimation based on the n previous samples from the same day. In particular, Case II is dependent on only single variable, i.e. a.

$$(S_{PREDII;\mathrm{a}}f)(j) := \sum_{k=1}^{m} a_k f(j-k)$$

Here, samples $f_l(l = 1, \dots, k)$ are from the k previous days and a is the parameter vector where $a_k = 0$ for $k \leq 0$.

2.3 Solar Energy

Solar energy is a very popular energy source among the research community, especially for the case of energy prediction for either WSNs or other applications. Indeed, solar energy is one of the promising technologies for which relatively efficient energy harvesters exist; the efficiency of modern solar PVs makes that they can provide more power/energy than other sources, as illustrated in Figure 2 [35].

Nevertheless, solar energy also exhibits an uncontrollable (intermittent) behaviour. Although it is obvious that no energy is produced at night for outdoor solar energy harvesters, there can be illumination variations and drops during day time as well due to changing weather conditions. It is quite difficult to predict this behaviour accurately and on the long term; for example, solar energy was examined only for one-time scheduler level for 60 minutes data interval in 24 hours [35].

Thus, solar energy is well suited for experimenting with TC in combination with energy prediction algorithms for autonomous WSNs nodes.

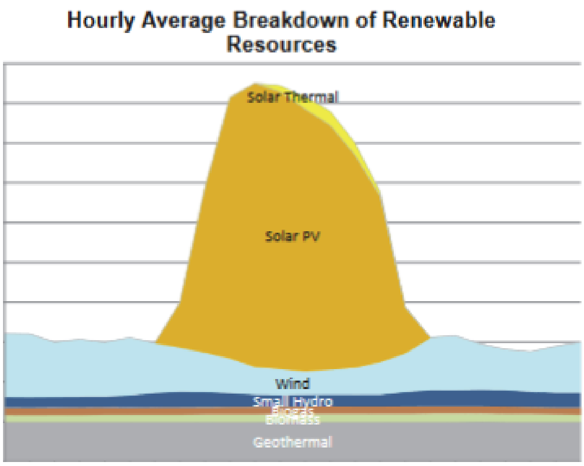

Figure 2. Illustrate the production of renewable energies across the one day [35].

The above sections briefly discussed the TC approaches and energy prediction models, and summarized their state of the art, along with the solar energy source. As mentioned earlier, most of the prediction models are impractical to implementation due to the large memory required to store the history data, as well as heavy computations. In the following section, the design and implementation of TC and LINE-P (Case-II) are presented.

3) Design and Implementation of the joint TC and energy prediction approach

3.1) TC mechanism

Our proposed design and implementation builds upon the embedded software utilities and API (application programming interface) for FRAM-based microcontrollers provided by Texas Instruments in [12]. In particular, the package "Compute through Power Loss Utility (CTPL)" contains the function "ctpl_enterShutdown ()" that allows entering into shutdown mode after saving onboard peripherals, stack and CPU context into FRAM. A hardware comparator (Comparator D of the MSP430FR5739) is used to detect when the power supply goes below a programmable threshold (here V = 2,5V), and then triggers an interrupt calling the ctpl enterShutdown() function. The backup image is restored after a power up or a shutdown timeout. As described later on, this function has to be called strategically when a loss of power is imminent or when it is predicted that not enough energy will be available to complete a communication task properly.

The basic architecture of our experimental setup is identical to that of [4]. The additional setup consists in establishing the network between an EH-powered Node (A) and another Node (B) as peer-to-peer for wireless bidirectional communication, as well as incorporating TC with the energy prediction model on Node (A).

In addition to CTPL, we use SimpliciTI which is a lightweight and low-power network protocol suitable for small RF networks; it is available as a library from Texas Instrument [36] and we have ported it to the MSP430FR5739 board as per the guidelines provided in [37].

Proper operation of wireless communication tasks that uses the SimplicitTI protocol requires initialization before starting the communication. In our case, SimpliciTI is reinitialized at every wake up of a node. This is mostly due to the fact that the radio component (TI CC2550) is an external device and thus its configuration cannot be saved and restored with CTPL; therefore, it has to re-configured upon restoring power.

Given the intermittent nature of the EH source and the fact that Node (A) operates without any energy storage, power can be lost at any time; the main challenge is to end the communication just before shutdown and start it again after the wake up of the node. In order to create link quality between Node (A) and (B) in the peer-to-peer network, we identified three main issues that should be addressed in our work:

1) In case of low energy and before entering into shutdown mode, a node is supposed to update its peer that communication will not be continued. This activity requires a few clock cycles, thus the saving mechanism should be started early enough.
2) The TC mechanism does not support saving the configuration of the radio device. Thereafter each wake-up following a loss of power, the SPI communication between the node and the radio must be re-initialized, and the CC2500 registers need to be re-configured.
3) Finally, in order to re-establish the communication, the link protocol has to be relaunched after the restarting of the node.

Figure 3 shows how the TC mechanism has been modified in order to solve the issues raised by the communication. Among others, we added a semaphore (Wake-up semaphore) which is set at the end of the TC routine. It is used by the main state machine to know when a waking up has just happened (See the state machine in Figure 3).

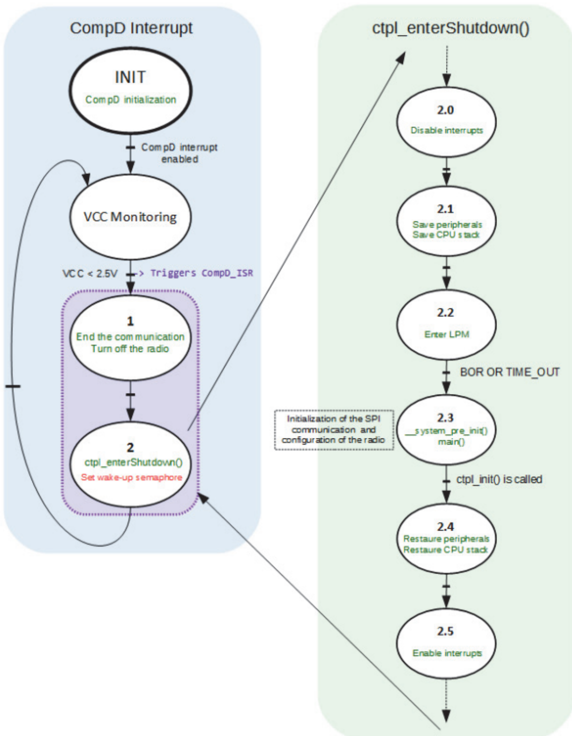

Figure 3. State machine of the TC mechanism allowing *proper* wireless communication.

In the following subsection, the implementation of LINE-P (Case-II) in combination with TC is discussed.

3.2) Combining TC and LINE-P (Case-II) energy prediction model

As discussed earlier, checkpointing methods are less efficient since they periodically evaluate the possible imminent loss of power. An advantage of using energy prediction in combination with TC is that it is not only possible to detect imminent loss of power but also to better decide whether or not to fire a task depending on the predicted amount of energy for the next period of time. In our case, energy prediction provides information about much energy will be available for the next period of time. This allows the system to start communicating only when a sufficiently high amount of energy is predicted for a stable period of time. In that case, the communication will be more efficient since less errors due to power losses will occur.

The energy prediction model used in this work builds upon the three cases proposed in [37]. Given the resource constraints of the nodes used in this work, we selected LINE-P Case II since it is the less computational-intensive of the three. Nevertheless, in order to reduce the memory footprint of the model to allow it to fit inside the FRAM memory of the MSP430FR5739 (16KB), we had to scale and a normalize the kernel coefficients used in the prediction model, thereby replacing float multiplications by integer ones. This allows saving five kilo-bytes of memory (see Table 3a in the results section), but slightly reduces the accuracy of the model.

During the experiments, real data has been used; thus, live-data of Vcc must be recorded and stored in a buffer on the node. The prediction is based on the last 6 values recorded (according to the time prediction scale, so that a one minute prediction is based on the last 6 minutes).

The time prediction of the energy prediction model is configurable. However, as a node is not using any energy storage, a short-term prediction (between one and ten minutes) is needed to provide enough adaptability to the system. The impact of the time prediction is further discussed in the experimental section.

Figure 4 illustrates the modified version of the TC mechanism. A time-out protection is used in order to avoid a node being blocked in the "communicate" state. If a node has not received a message for a chosen time period (for instance 15 seconds), it has to end the communication and start the link protocol again.

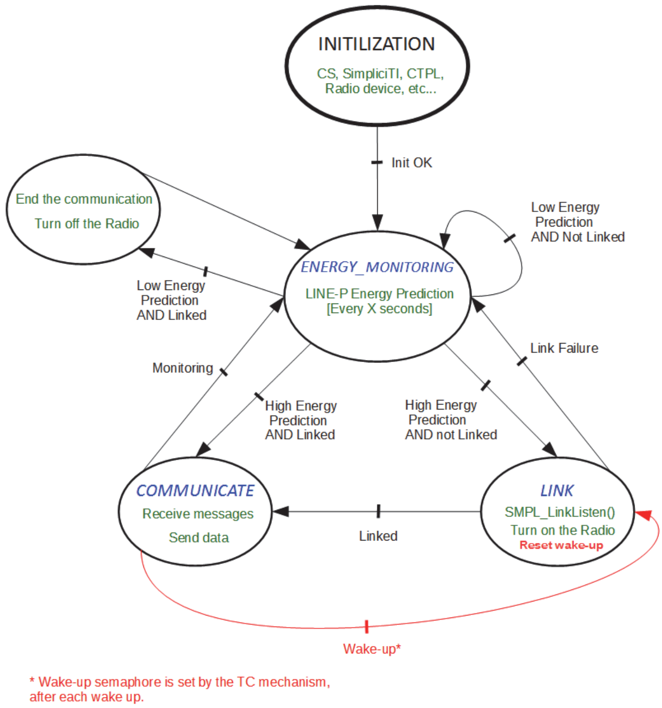

Figure 4. Diagram of the state machine integrating TC, energy prediction, and wireless communication.

Figure 5 illustrates the behaviour of the system according to Vcc. In order to decide whether or not to perform communication, a configurable threshold voltage (here set to 2.9V) has been set to verify whether energy is low or high. As shown in the figure, the TC mechanism has limited time to perform the save. If the voltage decreases too quickly, it will not be able to perform this correctly. This limit is further discussed in the experimental section.

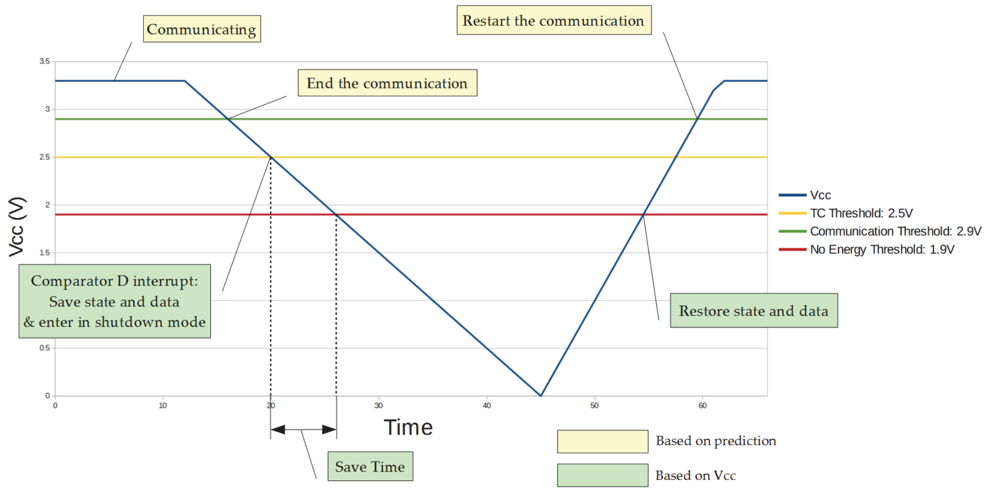

Figure 5. Illustration the node energy level and its packets sending capacity at certain Vcc (voltages).

3.3) Experimental Setup

In order to assess the proper operation and performance of the proposed combined TC and energy prediction mechanism described above, the following elements have been used to conduct the experiments.

- Two EXP-MSP430FR5739 kits with CC2500 radio device (used as sensor node with wireless connectivity and non-volatile FRAM memory);
- One PRT-13781 solar panel (13.5 cm * 11.2 cm) and 3.3V voltage regulator;
- One Hewlett Packard 34401A Multimeter for measuring the current;
- One Velleman PS 613 DC power supply;
- One FLUKE 123 industrial scope meter for observing and measuring the voltage;
- One programmable energy supply (using LabView) for simulating an energy harvester for the set of controlled-experiments.
- SimpliciTI (TI), simple low-power RF network protocol;
- FRAM utilities (TI), FRAM embedded software utilities for MSP ultra-low-power microcontrollers.

Figure 6 shows the diagram of the hardware setup for the peer-to-peer network. In the first part of the network, a solar panel (source) provides power directly to Node (A). For power stability, a voltage regulator and a low pass filter have been deployed between the power supply and the microcontroller to get a 3.3 DC voltage. The solar panel size (13.5 cm * 11.2 cm) can deliver up to 7 V. The maximum power it can produce is 2 Watt with a voltage of 6 V. The characteristics diagram shown in Figure 7a and 7b are measured under various conditions such as sunny day, cloudy day, and half an hour before sunset. The FLUKE 123 industrial scope meter is used for observing and measuring the voltage provided by the solar panel through the voltage regulator and the low pass filter. The current consumption of the node using EH is measuring by the Hewlett Packard 34401A Multi-meter.

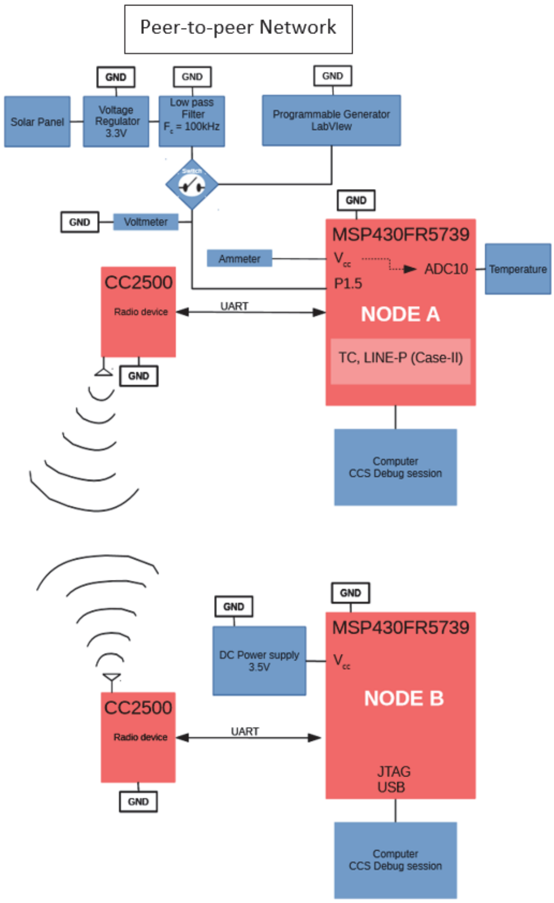

Figure 6. Diagram of the peer-to-peer network. Note: for controlled-experimental purposes, a programmable power supply have been used for certain experiments (instead of the solar panel).

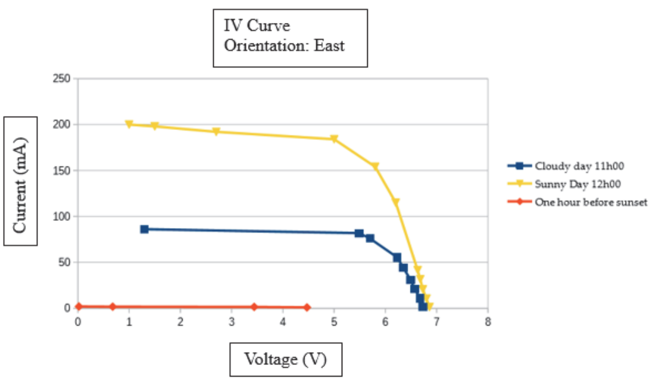

Figure 7a. Current-voltage (IV) curve of the solar panel.

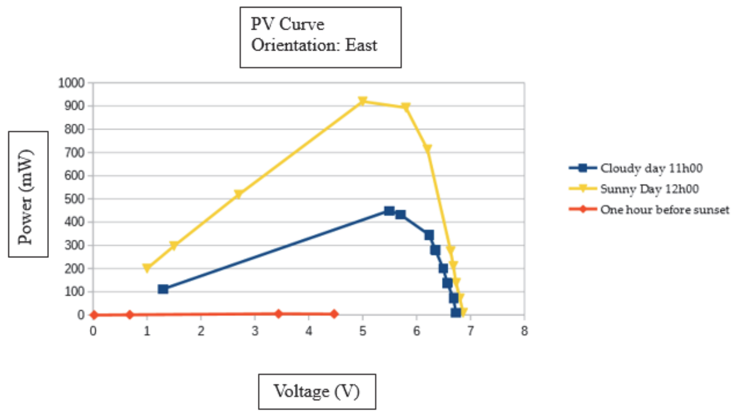

Figure 7b. Power-voltage (PV) curve of the solar panel.

Finally, Figure 8a and 8b are photographs of the complete peer-to-peer network experimental setup. Figure 8a shows the two nodes composed of EXP-MSP430FR5739 kits fitted with CC2500 RF modules, as well as the solar panel. The nodes are programmed with the peer-to-peer application that runs on top of the combined TC and energy prediction approach described above. Figure 8b shows the connection between Node (B) and the programmable DC power supply.

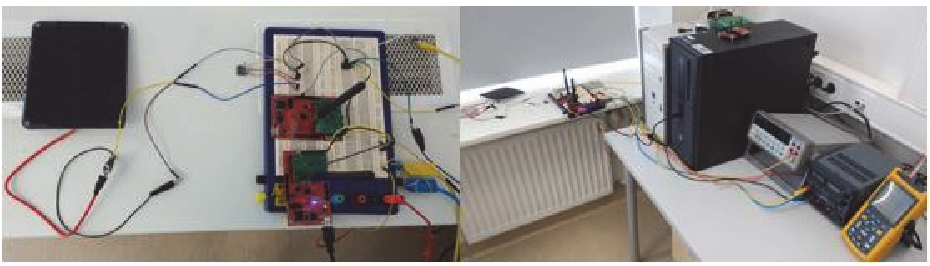

a. b.

Figure 8. Figure 8a: Node (A) programmed with TC and LINE-P (Case-II) energy prediction and powered by solar energy harvester. Figure 8b: Node (B) is powered by DC power supply.

In the next section, the results and performance are presented and discussed.

4) Results and Evaluation

In this section, we show the experimental results for the peer-to-peer network based on both modalities, i.e. TC and LINE-P (Case-II) energy prediction model; in particular, we evaluate its performance with the following aspects:

I) Verification of the system (node) shutdown activity and saving data successfully;
II) Evaluation of the memory footprint of the node before and after deploying TC and LINE-P (Case-II) model;
III) Accuracy of the LINE-P (Case-II) model, by comparing the measured and predicted energies;
IV) Scenario-based experiments and comparative analysis between programmable power supply and solar panel for the network performance;
V) Evaluation of the link quality and reliability of the network.

The next section presents the evaluation part of the proposed solution with respect to the TC mechanism.

I) Verification of the system (node) shutdown activity and saving data successfully

When TC is implemented, in case of low energy the system should be able to save the data successfully before entering the shutdown mode. To verify this, we use the benchmark feature of CTPL, which toggles a pin of the microcontroller when it enters the shutdown mode.

Figure 9 is a snapshot taken on the oscilloscope; due to insufficient amount of energy the node enters the shutdown mode but, before this, the registers of the microcontroller are saved in its FRAM memory. Afterwards, once the energy will be available again, the node restarts, restores the registers values from the FRAM and resumes its operations.

One limitation of the TC mechanism is that if the voltage decreases sharply, i.e. more than 4.8 volts/sec, then the loss of power cannot be detected and no save will take place.

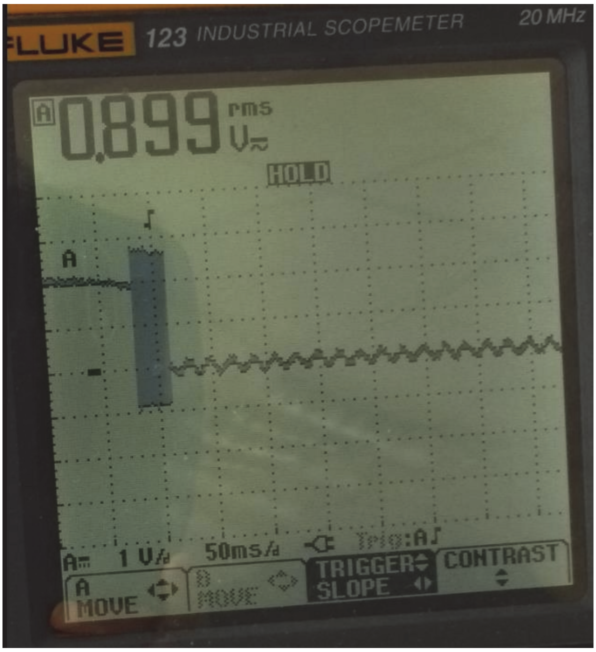

Figure 9. Illustrating the node behaviour in case of low harvesting energy.

In the following section, we evaluate the node's memory footprint by deploying TC and energy prediction model (Case-II) simultaneously.

II) Memory footprint of the node before and after deploying TC and LINE-P (Case-II) model

In [21], we presented the LINE-P (Case-II) model and showed, through simulations, that (Case-II) has the lowest complexity. This case has therefore been selected for implementation on the resource constrained microcontroller. The implementation also makes use of integer multiplications instead of float ones (as briefly discussed in Section 3). As shown in Table 3a, this allows reducing the memory footprint of LINE-P (Case-II) from 6.5 KB to 1.5 KB.

Table 3b shows the memory footprint for i) Simplicity only, ii) Simplicity with TC, and iii) Simplicity with TC and LINE-P (Case-II) energy prediction. As can be seen in the table, the overall memory footprint is 14414 bytes, which closely fits inside the available memory (91%).

Table 3a. Memory footprint of LINE-P (CASE-II) using float or integer (scaled) multiplications

	Float multiplications	Integer (scaling) multiplications
LINE-P (Case II)	6.5 KB	1.5KB

Table 3b. Memory footprint of Simplicity on TI MSP430FR5739-based node with and without TC and LINE-P (Case-II).

Simpliticiti	Simpliticiti (TC)	Simpliticiti (TC and LINE-P (Case-II))
FRAM: 12114 bytes (76%)	FRAM: 13950 bytes (88%)	FRAM: 14414 bytes (91%)

III) Accuracy of the LINE-P (Case-II) model, by comparing between measured and predicted energy

In order to validate the accuracy of the LINE-P (Case-II) model, we have conducted several experiments in different weather conditions. For instance, Figure 10a illustrates the graphical difference between the measured energy and the predicted energy on a sunny day. For further evaluation, the classical method mean absolute error (MAE) has been used to calculate the percentage error. The corresponding results for Figure 10a can be viewed in Figure 10b. Similarly, the results shown in Figure 11 and 12 are for partially cloudy and cloudy weather, respectively

Furthermore, Figures 10a, 11 and 12 represent the predicted data based only on the six previous values of real data for minimizing utilization of the memory. Each slot duration is four minutes and the energy is predicted based on next 16 minutes. Therefore, the predicted value of the slot 17 have been computed at slot 7 and compared with real value of Slot 11.

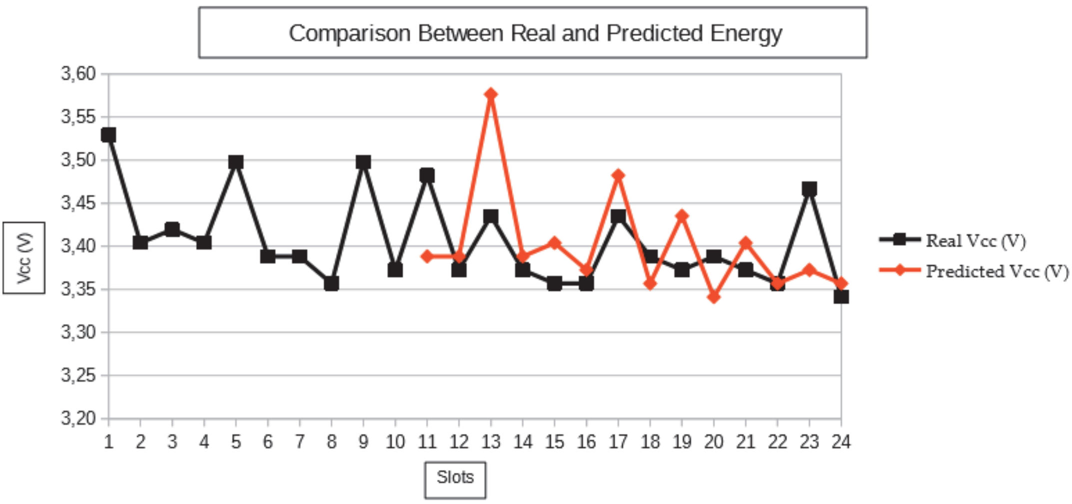

Figure 10a. Graphical comparison between real and predicted energy on a sunny day.

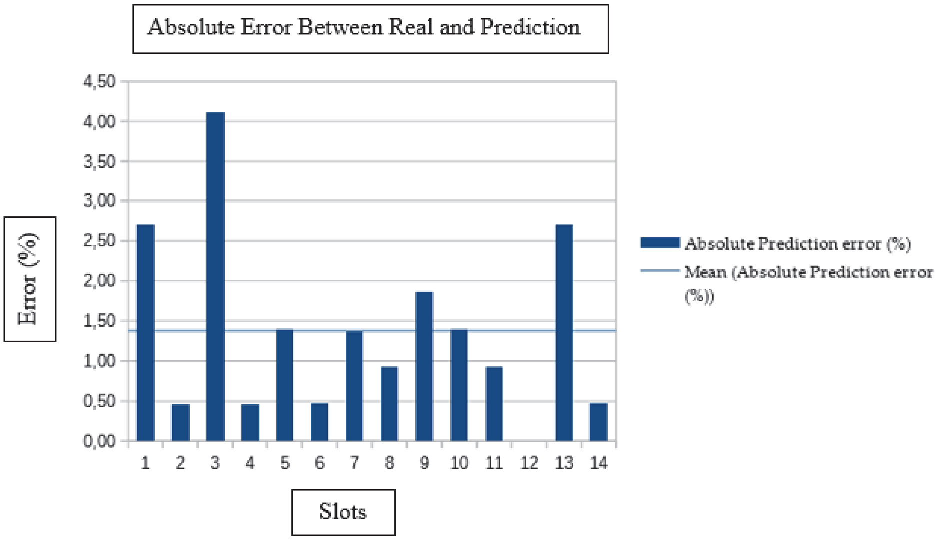

Figure 10b. Mean absolute error percentage between the real and estimated energy for a sunny day.

Figure 10b, shows that the MAE between real and predicted energy on a sunny day is approximately 1.38 %, which is deemed very good.

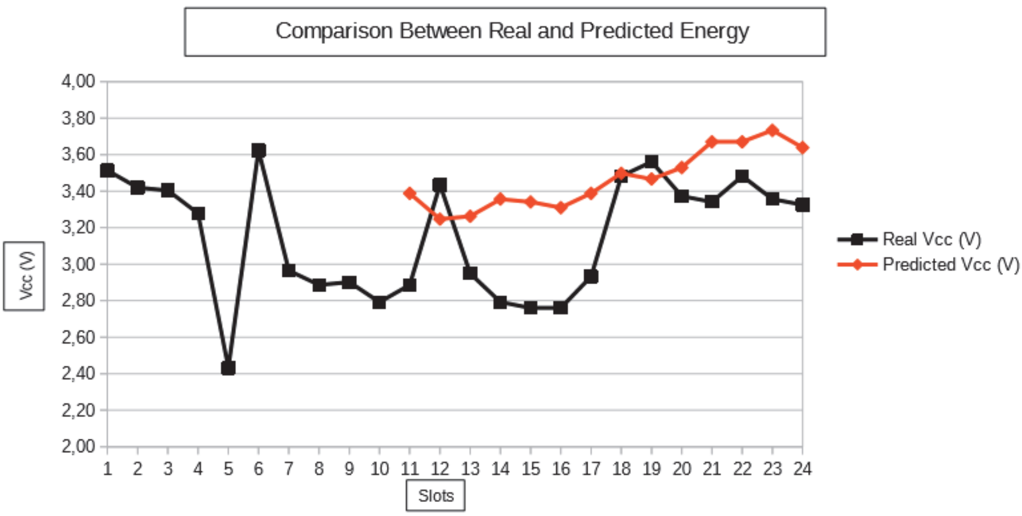

Figure 11. Graphical comparison between real and predicted energy for a partially cloudy day.

Due to more intermittent characteristics of a partially cloudy day, the probability of error increases. The calculated MAE for Figure 11 is approximately 10%.

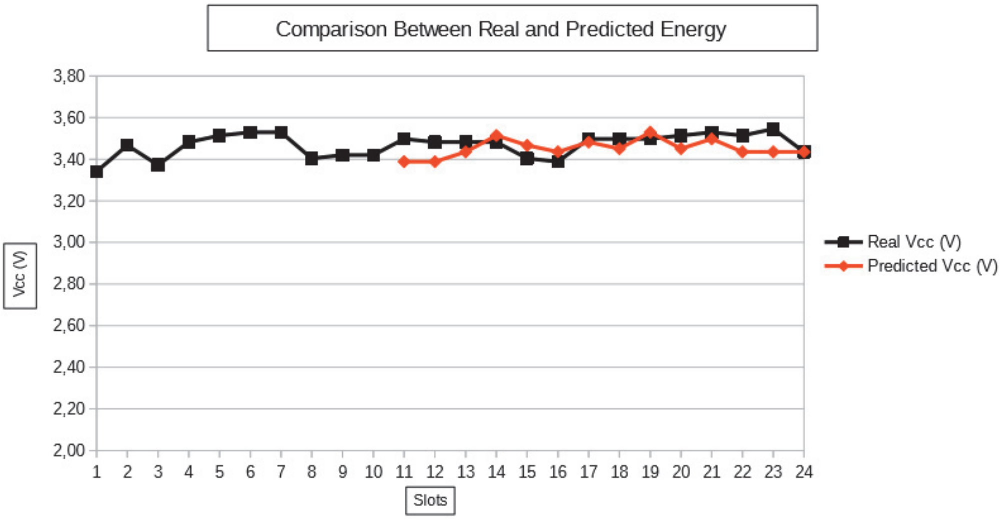

Figure 12. Graphical comparison between real and predicted energy for a cloudy day.

Figure 12 shows consistency in weather, thus the probability of error in prediction values is very low, i.e. 1.57%. Significantly, the accuracy of the proposed approach is deemed to range from very good to acceptable. Given this, using energy prediction can have a positive impact in terms of network performance and link quality since it allows firing a communication task only when enough energy is predicted to be available.

IV) Scenario-based experiments and comparative analysis between the programmable power supply and solar panel for the network performance.

In this subsection we present various experiments and their results which are based on a programmable power supply and a solar panel.

A) The programmable power-supply has been used to mimic an energy harvester so as to study the behaviour of the system for different situations. To mimic the intermittent pattern of a real energy harvester, we use a programmable power supply. LabVIEW has been used to program the power; this enables studying the behaviour of the energy prediction-based system through different energy scenarios.

Scenario I is based on a 20 minutes duration and the voltage varies between 2.7 V and 3.5 V. At the 9th minute, a loss of power occurs, i.e., the voltage decreases quickly to 0 V and thereafter increases sharply to 3.5 V, as shown in Figure 13.

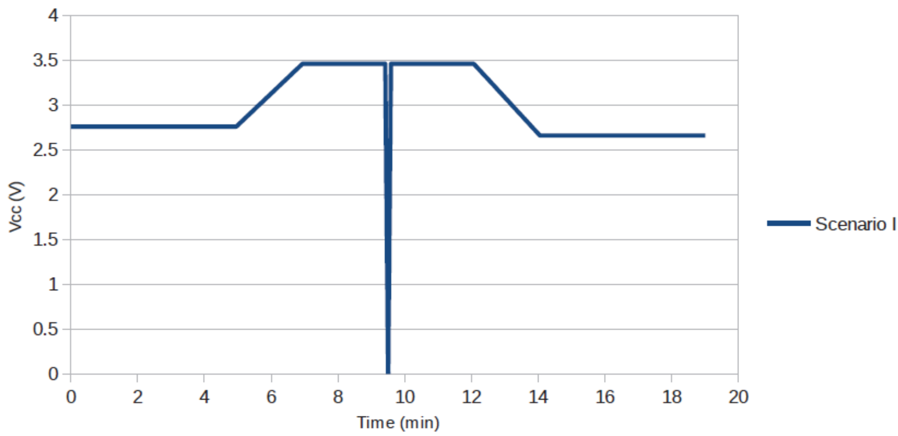

Figure 13. Voltage variation for Scenario I, including a loss of power at the 9th minute.

As compared to the previous scenario, Scenario II includes more fluctuations between 2.7 V and 3.5 V but no power loss; the duration of experiment is 12 minutes, as shown in figure 14.

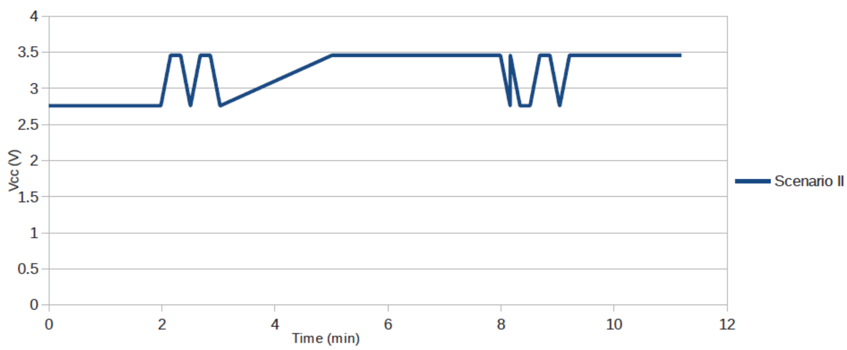

Figure 14. Illustrated the more variation between 2.7 to 3.5V.

Scenarios I and II are considered as case studies; next the corresponding behaviours of the system is presented for 1, 5 and 10 minutes data time-intervals.

Scenario I for 1-minute prediction performed every 30 seconds

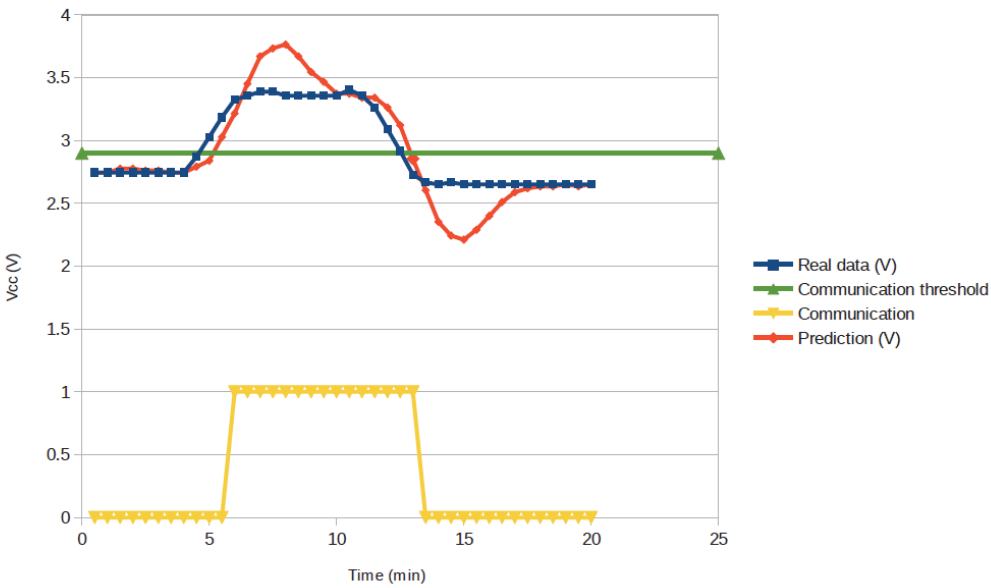

Figure 15. Behaviour of the system corresponding to scenario I, for 1-minute prediction performed every 30 seconds.

In Figure 15, energy prediction has been performed every 30 seconds and Vcc recorded every 30 seconds by the node. If the predicted energy goes above the 2.9 V threshold, then the system starts the communication (in the figure, '1' indicates active communication), otherwise it stops it. The results are consistent with the expected behaviour of the system. In this scenario the prediction model is not very useful; nevertheless, this scenario illustrates that the TC mechanism works properly since despite the loss of power, the system is able to end and restart the communication.

Scenario II

As shown in Figure 16, Scenario II includes more voltage variations. The behaviour of the system is tested with four cases, namely without energy prediction and for 1, 5 and 10 minutes energy predictions. LINE-P (Case-II) model is based on the six previous slots. Thus, a 1 minute prediction is based on the last 6 minutes; similarly, a 5 minutes prediction relies on the last 30 minutes, and a ten minutes prediction is based on the last hour, respectively.

Figure 16 shows the system behaviour for Scenario II with no energy prediction case. Since no energy prediction is performed, the system controls the communication based only on the current value of voltage. The system is adaptive and very sensitive against the variations. As illustrated in the figure at 11:00 and 13:00, the communication is stopped although the voltage increases again just after the power loss.

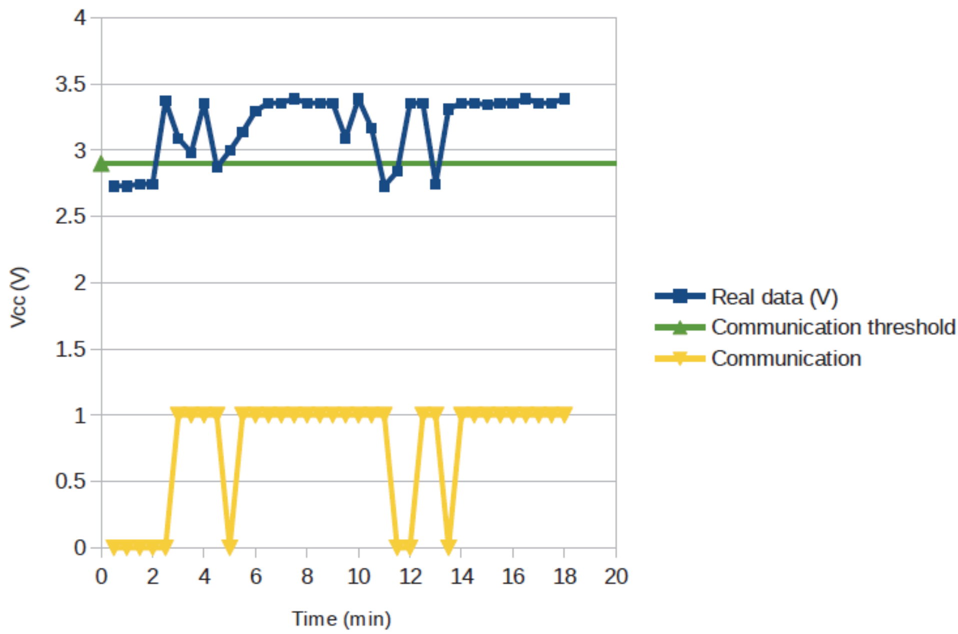

Figure 16. Behaviour of the system for Scenario II without energy prediction.

Figure 17 shows the system behaviour for Scenario II with a 1-minute energy prediction. In this case, we observed that the prediction model itself is not given enough time for performing the energy prediction. This case is very similar with the previous no energy prediction case; again, the system is adaptive and sensible against the variations.

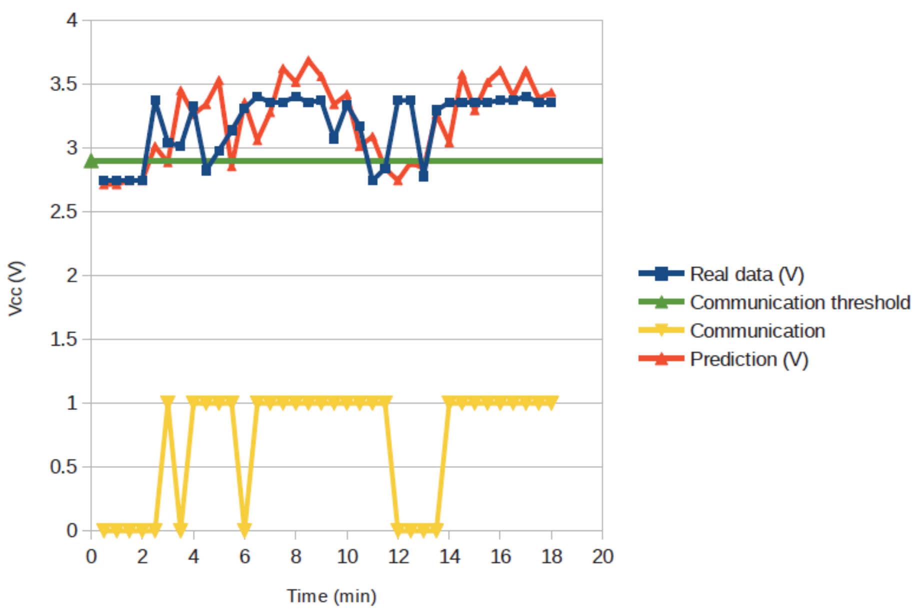

Figure 17. Behavior of the system for Scenario II with a 1-minute energy prediction.

Figure 18 shows the system behaviour for Scenario II with a 5 minutes energy prediction. In this case, it can be observed that the prediction model is now given enough time, in this case 5 minutes; as a result, the communication time is higher since prediction time is higher. Power losses at 11:00 and 13:00 illustrate this point, because despite these, the system continues to communicate. Thus, the system is more robust and stable against the variations; the price to pay is that it is less adaptive.

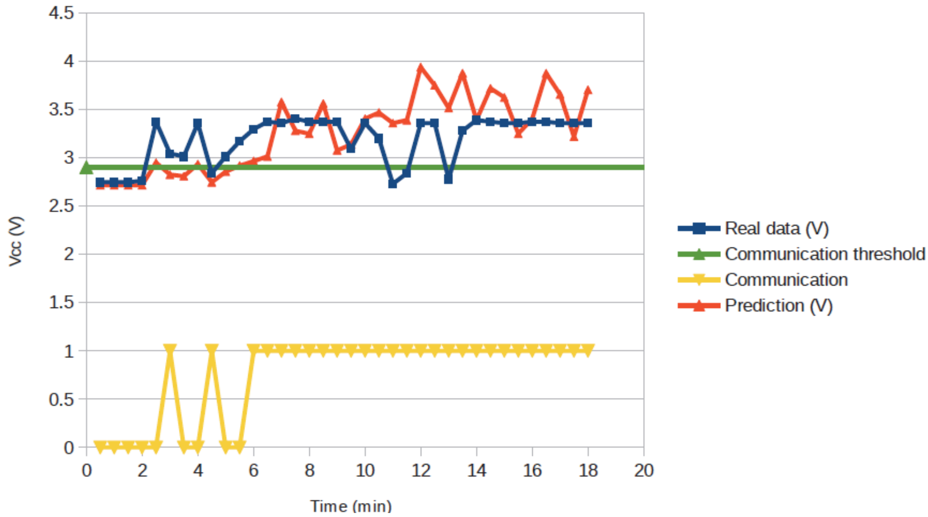

Figure 18. Behaviour of the system for Scenario II with a 5 minutes energy prediction.

Figure 19 shows the system behaviour for Scenario II with a 10-minute energy prediction. In this case, the experiment shows long and stable communication, although the energy prediction is very close to communication threshold and a decrease of a few millivolts would stop the communication. However, the waiting time for a stable communication is longer than in the previous case as shown in Figure 19 at 13:00. Thus, this specific case illustrates that for such a long prediction time, the system is not adaptive enough.

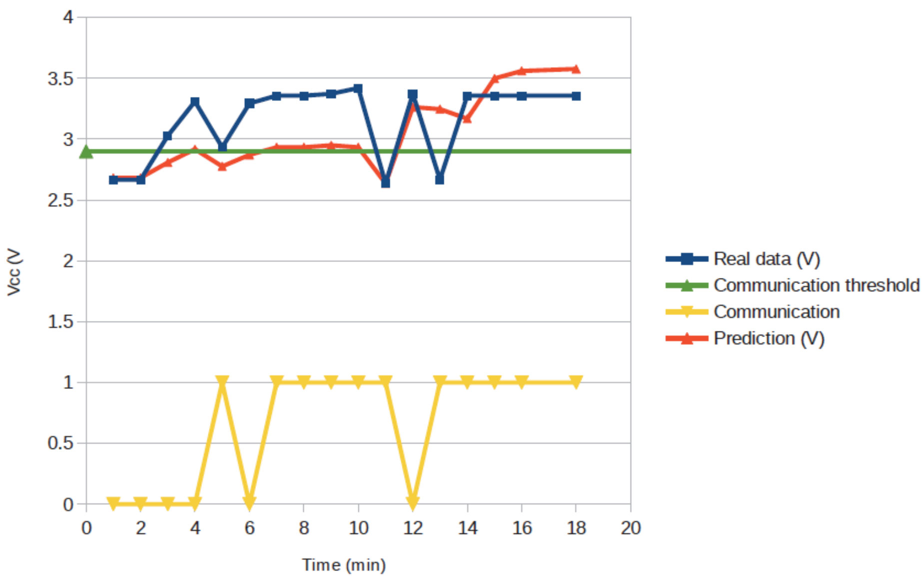

Figure 19. Behaviour of the system for Scenario II with a 10 minutes energy prediction. Note: In this case, Vcc is recorded and predicted every 1 minute instead of every 30 seconds.

Through the above various observations, it can be said that either too short or too long slots are not beneficial for the energy prediction model in order to achieve stability in the communication.

B) Experiments with the solar panel

After experimenting with the programmable power supply, we used the solar panel to power the node, again without any energy storage device. Figure 20 shows the behaviour of the system with a 1-minute energy prediction, in sunny conditions. The behaviour of the system is as expected as per the previous experiments with the programmable power supply. Thus, the node is communicating for a longer period and it is deemed more reliable and stable for the same length of prediction time (1-minute).

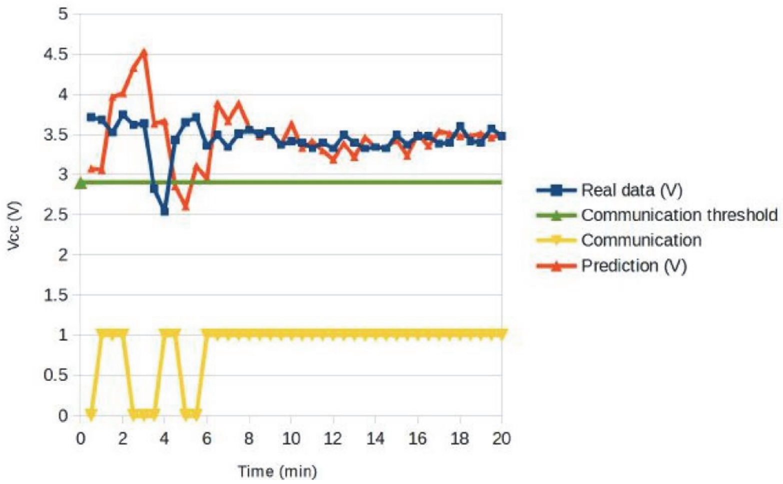

Figure 20. *Behaviour* of the system using the solar panel with a 1-minute energy prediction *under sunny conditions*.

Next, we repeated the experiment under cloudy conditions. The corresponding results are shown in Fig. 21.
In this case, the solar panel provided insufficient power, though very close to threshold voltage. We observed that when the node is communicating, its consume more current. However, once the communication is established, thereafter the current consumption increases and the voltage decreases, which causes the system to repeatedly start and end the communication.

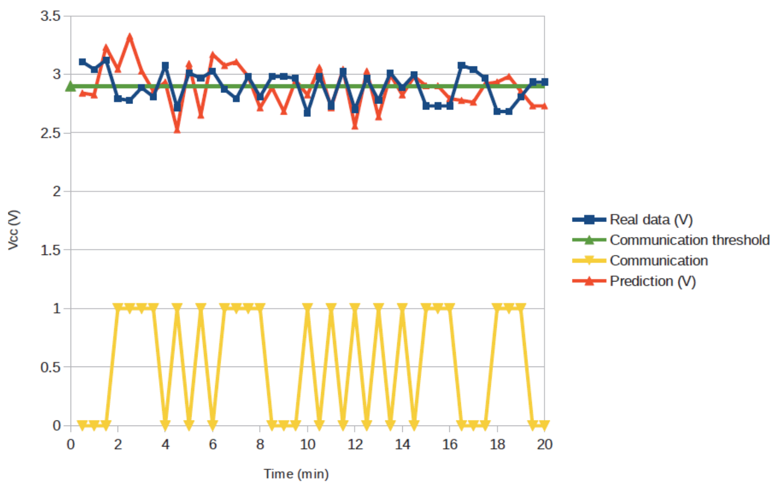

Figure 21. Behaviour of the system with a 1-minute energy prediction, using the solar panel as the energy harvester under cloudy conditions.

V) Evaluation of link quality and reliability of the network by measuring the jitter and ratio at various distance.

In order to achieve efficient energy, we exploit a solar energy harvester as a power source. Moreover, the implementation of both modalities, i.e. TC along with LINE-P (CASE-II) energy prediction model simultaneously is expected to be effective and to improve the system performance and link quality based on the energy prediction. The peer-to-peer link quality can be viewed from two levels, i.e. application specific level and network level.

In this section, we evaluate the network performance at certain distances by observing three features, namely jitter, ratio of packets transmission and energy consumption. Usually, in peer-to peer networks, the coverage area is based on the 4 hops count [23]. However, in this scenario, the network has no hops. Thus, it is interesting to evaluate whether or not the variation of distance can make a difference or influences the communication between two nodes in terms of power consumption. Usually, ensuring reliability and link quality requires many mechanisms. However, here the application is not very critical (environment monitoring system). In addition, in this scenario, the reliability is evaluated in terms of the average receiving ratio. Therefore, delays in the transmission are not so critical. Table 4 presents the jitter, average receiving ratio of the packets, and the power consumption of the node at various distances. Similarly, Table 5 shows the current consumption and power consumption of the node without deployment of TC and LINE-P for certain states of the node.

Table 4. Peer-to-peer network performance based on the average receiving rate at various distances.

Distance (m)	Jitter (ms)	Average receiving rate (%)	Power Consumption (mW)
0.3	20.9	94.6	66.7
1	20.9	94.6	66.7
3	20.9	94.6	66.9
6	20.9	94.6	70.2

As can be observed in Table 1, only power consumption is affected by distance. Both the jitter and average receiving rate are constant and their values quite acceptable for such a non-critical application. On the contrary, the power consumption of the node without the deployment of TC and LINE-P while establishing the link and the transmission is 60 mW, which can be observed in Table 5.

Table 5. Power consumption of the node without TC and LINE-P modalities for various states.

State	Current Consumption (mA)	Power Consumption (mW) at Vcc = 3V
Idle	2	6
Linking	20	60
Communicating	20	60

By deploying both TC and LINE-P (Case-II) model into the peer-to-peer network does not require much more power; as can be seen in Table 4 and Table 5, the difference in power consumption of the node is very low. Actually, both modalities improved the link quality. In addition, jitter and power consumption are definitely affected, due to the decreasing amount of harvested energy and longer distance. In the context of network performance and reliability, all the packets were received successfully, which can be seen in the Table 4.

VI) Discussion and Conclusion

We have demonstrated and evaluated the hardware-based implementation of both modalities (TC and LINE-P (CASE-II) energy prediction model). As our experiments have shown, the TC mechanism, on an individual basis, plays an important role for the performance of the node and helps mitigating issues such as power loss by saving and restoring the microcontroller registers in its FRAM memory. However, TC itself operates with the instantaneous energy only, neither estimating the availability of energy nor performing the tasks accordingly.

Indeed, if the voltage decreases too rapidly, (4.9 volts/sec or above in our case) then the TC mechanism will not be performed at all. In addition, in case of decreasing energy, the node should to stop a communication task.

To deal with this, we added an energy prediction model in the system. Our experiments have shown that by adding energy prediction in the TC-enabled system, the node can now predict the availability of the energy for the next time slot. Thereafter, it can take the decision to fire or stop a task based on the estimated energy. In particular, it can only communicate when the energy is higher than the energy threshold, which provides link quality, reliability and system stability. Furthermore, energy prediction can improve the robustness against the variation in power. The experiments also show that several parameters such as the communication threshold, sampling period, prediction time, and the power capacity of the harvester influence the behaviour of the system. On the other hand, the energy prediction model calculation requires some CPU-time and consume a small amount of energy. Finally, it was noted that the energy prediction model has its own limits and is not able to perform very well in highly changing weather.

In conclusion, and to the best of our knowledge, the practical implementation of the joint TC and energy prediction has not been shown previously and a novel approach for autonomous WSN nodes has been presented in this paper. The results illustrates the benefits of the proposed approach, e.g. an average receiving rate of 94.6% at various distances between the nodes for various power variation scenarios. Furthermore, by conducting various experiments and utilizing real energy datasets of the solar energy, the results show that the proposed solution provides 90-98% accuracy of the predicted energy, depending upon the weather conditions.

Usually, if harvested energy is greater than 0 but insufficient to power the node or more, then this harvested energy is wasted. Therefore, in our upcoming work, we will consider wireless power transfer between autonomous nodes so that unused harvested energy can be shared among the nodes. We also plan to integrate the wireless power transfer concept with the proposed TC and energy prediction to enhance the operating time of the nodes as much as possible.

Acknowledgements: Project B38 at TUT and the Estonian IT Academy stipend program have supported this research. This project has received funding from the European Union's Horizon 2020 research and innovation program under grant agreement No 668995. We are also thankful to Raul land and Eero Haldre for their technical support while conducting the experiments.

Author Contributions: Faisal Ahmed initiated the idea of using the two modalities simultaneously. Faisal Ahmed developed the initial C code and Corentin Kervadec implemented the code on the MSP430FR5739 node. Faisal and Corentin Kervadec designed the experiments. Yannick Le Moullec, Gert Tamberg and Paul Annus helped analyse the results. All authors participated in the paper writing.

Conflicts of Interest: The authors declare no conflict of interest.

References

[1] IEA 4E EDNA. (2017). Technology and Energy Assessment Report. Vienna, Austria.

[2] Ma, X., Bader, S., & Oelmann, B. (n.d.), (2016), Solar Panel Modelling for Low Illuminance Indoor Conditions.

[3] Allen, J., Forshaw, M., & Thomas, N, (2017), Towards an Extensible and Scalable Energy Harvesting Wireless Sensor Network Simulation Framework, 39–42.

[4] Ahmed, F., Ahmed, T., Muhammad, Y., Le Moullec, Y., & Annus, P. (2016). Operating Wireless Sensor Nodes without Energy Storage: Experimental Results with Transient Computing. Electronics, 5(4), 89.

[5] Ahmed, F., & Tamberg, G. Le Moullec Y., Annus P. (2017). Dual-Source Linear Energy Prediction (LINE-P) Model in the Context of WSNs. MDPI, Sensors, 17(7), 66.

[6] Song X D,Wang X,(2015). Extended AODV Routing Method Based on Distributed Minimum Transmission (DMT) for WSN. International Journal of Electronics and Communications,

69(1):371-381.

[7] Degan Zhang, Guang Li, Ke Zheng, (2014). An energy-balanced routing method based on forward-aware factor for Wireless Sensor Network. IEEE Transactions on Industrial Informatics, 2014,10(1):766-773.

[8] Si Liu,Ting Zhang, (2017). Novel Unequal Clustering Routing Protocol Considering Energy Balancing Based on Network Partition & Distance for Mobile Education, Journal of Network and Computer Applications,88(15):1-9. DOI:10.1016/j.jnca.2017.03.025

[9] Degan Zhang, Guang Li, Ke Zheng, (2014). An energy-balanced routing method based on forward-aware factor for Wireless Sensor Network. IEEE Transactions on Industrial Informatics, 10(1):766-773.

[10] Xiang Wang, Xiaodong Song, (2015). New Clustering Routing Method Based on PECE for WSN. EURASIP Journal on Wireless Communications and Networking,2015,2015(162):1-13. DOI: 10.1186/s13638-015-0399-x

[11] Degan Zhang, Xiang Wang, Xiaodong Song, (2014). A Novel Approach to Mapped Correlation of ID for RFID Anti-collision. IEEE Transactions on Services Computing,7(4):741-748.

[12] Yanan Zhu, (2012). A new constructing approach for a weighted topology of wireless sensor networks based on local-world theory for the Internet of Things (IOT). Computers & Mathematics with Applications, 64(5):1044-1055.

[13] Zhao C P, (2012). A new medium access control protocol based on perceived data reliability and spatial correlation in wireless sensor network. Computers & Electrical Engineering, 38(3):694-702.

[14] Zhou S, Ya-meng Tang, (2017). A low duty cycle efficient MAC protocol based on self-adaption and predictive strategy, Mobile Networks & Applications. DOI: 10.1007/s11036-017-0878-x.

[15] Li W B, (2016). Novel Fusion Computing Method for Bio-Medical Image of WSN Based on Spherical Coordinate.Journal of Vibroengineering,18(1):522-538.

[16] X J Kang,(2012). A novel image de-noising method based on spherical coordinates system, EURASIP Journal on Advances in Signal Processing, (110):1-10 DOI:10.1186/1687-6180-2012-110.

[17] Xiang Wang, Xiaodong Song. New Medical Image Fusion Approach with Coding Based on SCD in Wireless Sensor Network.Journal of Electrical Engineering & Technology, 2015,10(6):2384-2392.

[18] Ma Z, (2016). A Novel Compressive Sensing Method Based on SVD Sparse Random Measurement Matrix in Wireless Sensor Network. Engineering Computations,33(8):2448 - 2462.

[19] Ransford, B.; Sorber, J.; Fu, K. Mementos (2011). Mementos: System Support for Long-Running Computation on RFID-Scale Devices. ACM SIGPLAN Not, PP 159–170.

[20] Lucia, B.; Ransford, B, (2015). A Simpler, Safer Programming and Execution Model for Intermittent Systems. ACM Sigplan Not, PP 575–585.

[21] D. Balsamo, A. S. Weddell, G. V. Merrett, B. M. Al-hashimi, D. Brunelli, and L. Benini, (2015), Hibernus: Sustaining Computation during Intermittent Supply for Energy-Harvesting Systems. 7(1):1–4.

[22] H. Jayakumar, A. Raha, and V. Raghunathan, (2014). QUICKRECALL: A low overhead HW/SW approach for enabling computations across power cycles in transiently powered computers. Proc. IEEE Int. Conf. VLSI Des., pages 330–335.

[23] Balsamo, Domenico, Weddell, Alex S., Das, Anup, Rodriguez Arreola, Alberto, Brunelli, Davide, Al-

Hashimi, Bashir M., Merrett, Geoff V. and Benini, Luca, (2016), Hibernus++: a self-calibrating and adaptive system for transiently-powered embedded devices IEEE Transactions on Computer-Aided Design of Integrated Circuits and Systems, 35, (12), pp. 1968-1980.

[24] Naveed Anwar Bhatti and Luca Mottola, (2017), "HarvOS: Efficient Code Instrumentation for Transiently-powered Embedded Devices," International Conference on Information Processing in Sensor Networks (IPSN).

[25] Balsamo, domenico; Elboreini, Ali; Al-Hashimi, Bashir M; Merrett, Geoff V, (2017) Exploring ARM mbed support for transient computing in energy harvesting IoT systems. 7th IEEE International Workshop on Advances in Sensors and Interfaces (IWASI).

[26] FRAM utilities, by Texas Instruments, (2017).

[27] P. Zhang, H.Tan, G. Xiao, Yu. Yi, (2015)“Maximizing Lifetime in Clustered WSN s with Energy Harvesting Relay: Profiling and Modeling,” pp. 1–6.

[28] J. R. Piorno, C. Bergonzini, D. Atienza, and T. S. Rosing, (2009) “Prediction and Management in Energy Harvested Wireless Sensor Nodes,” Proc. 1st Int. Conf. Wirel. Commun. Veh. Technol. Inf. Theory Aerosp. Electron. Syst. Technol. Wirel. VITAE, pp. 6–10.

[29] Wu, Fan, Christoph Rüdiger, and Mehmet Yuce, (2017). “Real-Time Performance of a Self-Powered Environmental IoT Sensor Network System.” Sensors 17(2):282.

[30] Energy, I, (2017). Adaptive Data Aggregation and Compression to Improve Energy Utilization in Solar-Powered Wireless Sensor Networks. Sensors, 17(7), 66.

[31] J. R. Piorno, C. Bergonzini, D. Atienza, and T. S. Rosing, (2009) “Prediction and Management in Energy Harvested Wireless Sensor Nodes,”1st Int. Conf. Wirel. Commun. Veh. Technol. Inf. Theory Aerosp. Electron. Syst. Technol. Wirel. VITAE 2009, pp. 6–10.

[32] Kosunalp, S, (2016) A new energy prediction algorithm for energy-harvesting wireless sensor networks with Q-Learning. IEEE Access, 4, 5755–5763.

[33] Cammarano, A.; Petrioli, C.; Spenza, D, (2012). Pro-Energy: A novel energy prediction model for solar and wind energy-harvesting wireless sensor networks. In Proceedings of the IEEE 9th International Conference on Mobile Adhoc and Sensor Systems, Las Vegas, NV, USA, 8–11; pp. 75–83.

[34] Ahmed, F., & Tamberg, G., Le Moullec Y., Annus P. (2017). Adaptive LINE-P: an adaptive Line Energy Prediction Model for Wireless Sensor Networks Nodes. MDPI, Sensors, 17(7), 66.

[35] California IOS, (2017). Our Renewables Reports Provide Important Information about Actual Renewable Energy within the ISO Grid as California Moves Towards a 33 Percent Renewable Generation Portfolio. The Reports Use Raw Data and Are not Intended to Be Used as the Basis for Operational or Financial Decisions.

[36] SimpliciTI Compliant Protocol Stack, (2017).

[37] Texas Instrument. MSP430 SimpliciTI Porting Guidelines, (2014).

Appendix E

Publication V

Ahmed, F.; Tamberg, G.; Le Moullec, Y.; Annus, P. Adaptive LINE-P: An Adaptive Linear Energy Prediction Model for Wireless Sensor Network Nodes. Sensors 2018, 18, 1105. .

sensors

MDPI

Article

Adaptive LINE-P: An Adaptive Linear Energy Prediction Model for Wireless Sensor Network Nodes

Faisal Ahmed [1,*], Gert Tamberg [2], Yannick Le Moullec [1,*] and Paul Annus [1]

1 Thomas Johann Seebeck Department of Electronics, Tallinn University of Technology, Tallinn 12616, Estonia; paul.annus@ttu.ee

2 Department of Cybernetics, Tallinn University of Technology, Tallinn 12616, Estonia; gert.tamberg@ttu.ee

* Correspondence: faisal.ahmed@ttu.ee (F.A.); yannick.lemoullec@ttu.ee (Y.L.M.); Tel.: +372-5800-7448 (F.A.)

Received: 15 February 2018; Accepted: 29 March 2018; Published: 5 April 2018

check for updates

Abstract: In the context of wireless sensor networks, energy prediction models are increasingly useful tools that can facilitate the power management of the wireless sensor network (WSN) nodes. However, most of the existing models suffer from the so-called fixed weighting parameter, which limits their applicability when it comes to, e.g., solar energy harvesters with varying characteristics. Thus, in this article we propose the Adaptive LINE-P (all cases) model that calculates adaptive weighting parameters based on the stored energy profiles. Furthermore, we also present a profile compression method to reduce the memory requirements. To determine the performance of our proposed model, we have used real data for the solar and wind energy profiles. The simulation results show that our model achieves 90–94% accuracy and that the compressed method reduces memory overheads by 50% as compared to state-of-the-art models.

Keywords: WSN; energy harvesting; energy prediction

1. Introduction

1.1. Energy Harvesting and Prediction Models

Energy harvesting (EH) is a promising technology that became a hot topic in the scientific community during the last few decades; however, EH is still a least explored area, especially at the micro and nano power levels. In particular, EH at the micro level is quite useful to power ultra-low-power sensor nodes. EH introduces various paths of research for prolonging the lifespan of wireless sensor network (WSN) nodes, either as an energy harvester with buffered energy storage (e.g., battery or super-capacitor) or directly (e.g., without energy storage) for autonomous devices. Several EH approaches, presented in the literature, exploit solar, wind, or thermal energy.

EH is a good alternative solution for those applications that are implemented once and become operational for longer periods; examples include environmental monitoring, structural monitoring, etc. Furthermore, WSN applications can benefit from EH to extend the life of the node or network [1]. Generally, numerous methods associated with EH have been discussed in the literature. These include energy-aware protocols, duty cycle management, task scheduling, transient computing (TC) in stand-alone mode (which performs transmission when the energy is available with or without any power source battery), data prediction [2], as well as mobility, which can reduce the power consumption if mobility incurs low overheads [3].

According to the literature, EP plays an important role for EH in the context of WSNs. Energy prediction for non-controllable energy source seeks to provide information about the upcoming available energy based on past records (profiles) and/or current values. EP mechanisms increase the system's efficiency [4] because they enable more careful utilization of the available energy as well as the dynamic execution of tasks depending upon the estimation of the energy available in the next time slots. Given the importance of EP, it is necessary to propose accurate sets of energy prediction models in order to increase the performance and other important processes for better quality of service.

In this article, we first briefly recall the limitations of most existing EP models due to the fixed-weighting parameter issue; thereafter, we suggest a solution with an adaptive weighting factor based on the energy profiles. In [5], we discussed how most of the energy prediction models such as EWMA, WCMA, ASEA, PRO-Energy, QL-SEP, and LINE-P (all cases) are dependent on a fixed weighting parameter; however, these solutions are not always suitable for real implementations with many various types (and hence characteristics) of e.g., solar energy harvesters.

In addition, the proposed Adaptive LINE-P (all cases) model estimates the energy over three different time periods, namely shorter, medium, and longer, and uses variable-length timeslots. The proposed prediction model improves the prediction accuracy and minimizes the error between the harvested energy and stored profiles. Furthermore, in this article we propose a compression method that reduces the size of the stored energy profiles by 50% in order to reduce memory overheads.

1.2. Contribution

Our contribution can be summarized as follows:

- We propose and evaluate enhancements to the existing LINE-P (all cases) model; we name the resulting new model "Adaptive LINE-P (all cases)"; namely,
  - we propose an adaptive parameter to address the fixed weighting parameter issue that is found in most existing energy prediction models, specifically when targeting solar energy harvesters;
  - we propose a profile compression technique that can be integrated in any energy prediction model.
- Our results show that the proposed enhancements achieve up to 98% accuracy (non-compressed profile) and up to 90% accuracy but with a 50% reduction of the memory requirements when using the compressed profile method, as compared to the state of the art.

The rest of the article is formulated as follows. Related work is presented in Section 2. The proposed Adaptive LINE-P (all cases) is detailed in Section 3. The comparative performance evaluation of the models is discussed in Section 4. Finally, we briefly conclude in Section 5.

2. Materials and Methods

Here, we discuss the state of the art regarding the fixed kernel parameter issue, variable length time slots, and dynamic or adaptive energy prediction models related to the domain of WSNs.

2.1. Non-Adaptive Energy Prediction Models

In [5] the authors presented three cases of LINE-P (linear energy prediction model) that are based on the sampling and approximation theory. The authors showed that LINE-P (all cases) is more accurate, has a lower complexity, and is energy-efficient in terms of computation as compared to other non-adaptive EP models.

However, the above comparison did not include the latest extensions, namely Pro Energy VLT and IPro-Energy. Thus, in this sub-section we first briefly introduce LINE-P and then discuss Pro Energy VLT and IPro Energy.

2.1.1. LINE-P

We first briefly introduce LINE-P. The detailed mathematical derivations can be found in [5].

Linear Energy Prediction LINE-P (Case I)

The main aim when designing LINE-P was to minimize the computational complexity while maintaining similar accuracy to other models.

If we have the samples $f_l (l = 1, \dots, k)$ from k previous days, we utilize this information as the basis for EP. Here, vector b defines a symmetric kernel and the parameter vector a, where $a_k = 0$ for $k \leq 0$, generates a one-sided kernel with the correspondent sampling operator:

$$(S_{PREDI;b}f)(j) := \sum_{k=1}^{m} b_k f(j-k) + \sum_{k=-m}^{0} b_k \, f_l(j-k) + CDIF_{PREDI;a;b;l}(j), \tag{1}$$

where the correction term $CDIF_{PREDI;b}$ in Equation (1) is given as

$$CDIF_{PREDI;a;b;l}(j) := CT_{PREDI;a;b}(\sum_{k=1}^{n} a_k f(k-i) - \sum_{k=1}^{n} a_k \, f_l(j-k)), \tag{2}$$

with the multiplier $CT_{PREDI;b}$ defined as:

$$CT_{PREDI;a;b} := \sum_{k=-m}^{0} b_k. \tag{3}$$

Equation (1) is used to estimate the energy based on the next time slot, specifically for LINE-P (Case I), and Equations (2) and (3) are the substitution factors of Equation (1).

Linear Energy Prediction LINE-P (Case II)

In this case, we proposed a model that performs energy estimation with only n previous samples from the same day. This case is dependent on only one variable, i.e., a:

$$(S_{PREDII;a}f)(j) := \sum_{k=1}^{m} a_k f(j-k). \tag{4}$$

Linear Energy Prediction LINE-P (Case III)

The third case is similar to Case I; the only difference is in $CT_{PREDIII;b}$ as shown in Equation (7).

$$(S_{PREDIII;b}f)(j) := \sum_{k=1}^{m} b_k f(j-k) + \sum_{k=-m}^{0} b_k \, f_l(j-k) + CDIF_{PREDIII;b;l}(j), \tag{5}$$

where the correction term $CDIF_{PREDIII;b:l}$ is in Equation (6),

$$CDIF_{PREDIII;b;l}(j) := CT_{PREDIII;b} \, (\sum_{k=1}^{m} b_k f(j-k) - \sum_{k=1}^{m} b_k \, f_l(j-k)), \tag{6}$$

with the multiplier $CT_{PREDIII;b}$

$$CT_{PREDIII;b} := \frac{\sum_{k=-m}^{0} b_k}{\sum_{k=1}^{m} b_k}. \tag{7}$$

We select, from the k previous days, day l for which the absolute value of the correction term $CDIF_{PREDIII;b;l}$ is minimal and consider the values f_l from that day.

2.1.2. Pro-Energy-VLT

In this subsection, Pro-Energy-VLT is discussed. In [6], the authors presented Pro-Energy with variable-length timeslots (Pro-Energy-VLT), based on the Pro-Energy model. In particular, the author proposed a perceptually important point (PIP) technique to calculate the variable size timeslots such as 30, 60, and 90 min [6], as compared to their original design, which was fixed to 30-min data intervals [6]. The authors revealed that Pro-energy-VLT increases the prediction accuracy while reducing the memory and the energy overhead of energy forecasting [6]. However, the authors used two fixed weighting factors α and γ in their algorithms to estimate energy for the next time slot over short and medium data intervals. As mentioned earlier, such a fixed tuning parameter is not compatible with various solar energy harvesters with different characteristics.

2.1.3. IPro-Energy

We now discuss IPro-Energy, which is also based on the Pro-Energy model. In [7], the authors of IPro-energy highlighted its two main features. Firstly, IPro-Energy uses a weighted profile (WP) technique to compensate for inconsistency in the weather behavior. Secondly, the authors showed that the model has a low complexity in terms of execution time, and low requirements in terms of storage data. We have conducted a simulation test of IPro-energy and compared its results with Pro-Energy; we found that, indeed, IPro-Energy yields better results than Pro-Energy, as shown in Figure 1. In order to quantify the prediction error, we have used two classical measures, namely MAE (mean absolute error) and MSE (mean square error), as shown in Table 1.

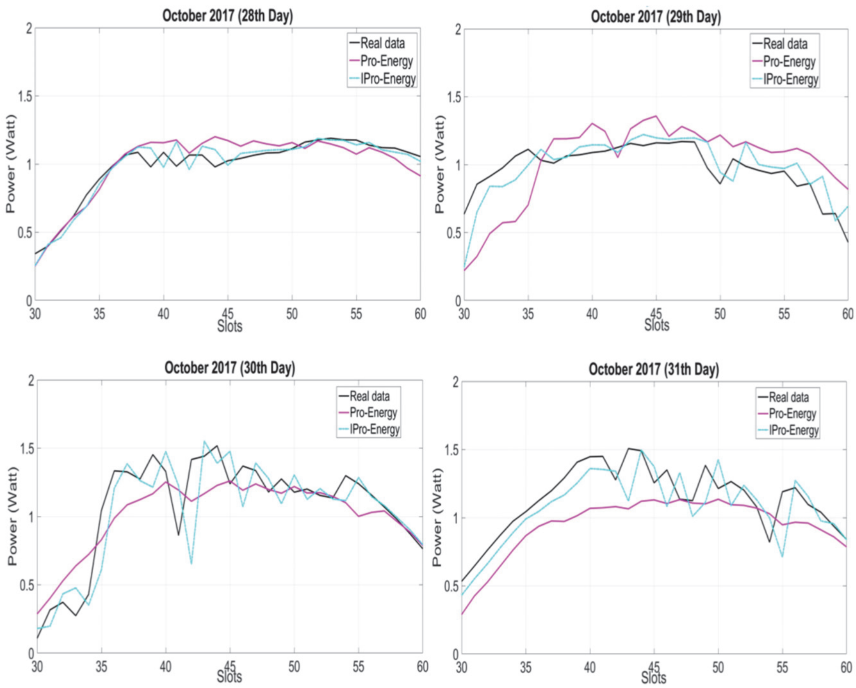

Figure 1. Illustration of a four-day comparative analysis of IPro-Energy with Pro-Energy.

Table 1. Prediction error in terms of MAE and MSE for IPro-Energy and Pro-Energy.

Energy Prediction Model	MAE (Mean Absolute Error)	MSE (Mean Square Error)
IPro-Energy	0.09915	0.0608
Pro-Energy	0.15875	0.1665

Although the results yielded by IPro-Energy are better than those of Pro-Energy, the former relies on a more complex model and the execution times are much higher than those of Pro-Energy.

This is because both the basic Pro-Energy model and the new features of IPro-Energy have to be executed. In particular, IPro-Energy introduces an additional weighting factor, W_f, which lies at [0, 1]. Thereafter, based on W_f and the r weighting factor (which has a 0.5 fixed value), the authors calculated the smarting factor (S) in Equation (8). Then, for predicting the energy based on the next timeslots, Equation (8) is inserted into Equation (9):

$$S = r\left(\frac{(C_t - C_{t-1})}{(C_t + C_{t-1})/2}\right) C_{t-1}. \tag{8}$$

The expected energy is denoted by C_{t+i} for the timeslot t+i of the current day,

$$C_{t+i} = W_f C_t + \left(\left(1 - W_f\right) WP_{t+i}\right) + S, \tag{9}$$

where WP is expressed as a combination of the previously observed most similar days.

Apart from the fixed parameter weighting factor-based models, there are several ANN-based algorithms available in the literature that estimate the energy based on a short-term energy prediction. In [8], the authors proposed a method for an adaptive neural network model. They used sliding window training with window sizes of three, four, and five months' data. In particular, their simulation results show that the five-month window size was the best simulation. In addition, they show that it is good to have a larger window size for training purposes as fewer data decreases the prediction quality. However, even a window size of three months of data would be too big for the microcontroller's (MSP430FR5739 and MSP430G2) memory targeted in our work and in [9] it was concluded that such ANN-based models are not adaptive and not more reliable than EWMA and WCMA algorithms.

There are others approaches to reducing the energy consumption and management in WSNs that work by estimating the energy, i.e., route selection schemes [9] and adaptive duty cycling [10]. Furthermore, in [11] the authors investigate the distributed sampling rate adaptation method in the multi-sensor implemented wireless devices to assign data capturing tasks among them based on the remaining energy network participation and correlations. In addition, they proposed effective mechanisms to utilize the ability of wireless devices to monitor a few selected points in a certain area. In [12], the authors present joint channel selection and routing schemes for multi-channel WSNs that apply duty cycling to sustain energy. The experimental tests and simulation show that the proposed schemes reduce overhearing by approximately 60% with two channels without affecting network performance. Furthermore, the researchers exploited some other techniques for minimizing energy consumption, for instance data compression and source coding [13], transmitting power control and distributed sampling rate adaptation for WSNs [14].

In the following, we discuss adaptive parameter weighting factor-based models for solar energy harvesting in the context of WSNs.

2.2. Adaptive Energy Prediction Model

In this section we discuss UD-WCMA, the only dynamic or adaptive weighting factor-based EP model that aims at better tracking variations in the generated energy (due to, e.g., weather conditions).

UD-WCMA [15] is developed based on the WCMA structure; it introduces a time-varying weighting parameter $G_1(n+1)$. This gain is adapted depending on the variations in the reference profiles stored in the memory. In addition, the energy prediction is ensured by combining the information collected from the last observations $\theta(n)$ with the mean value $\mu_d(n+1)$ of the harvested energy from the stored profiles.

Mathematical expression of the dynamic schemes in the UD-WCMA prediction model is as follows:

$$\hat{x}\,(n+1) = G_1(n+1)\theta(n) + [1 - G_1(n+1)]GAPu_d(n+1), \tag{10}$$

where

$$G_1(n+1) = \frac{\sigma(n+1)}{2(\sigma(n+1)+\sigma_1(n+1))}. \tag{11}$$

In Equation (10) σ represents the standard deviation of the irradiance levels of the stored profiles at time $n + 1$ with respect to the mean value. Subsequently, σ_1 is also a standard deviation that indicates the energy variation in the stored profiles between the time slots n and $n + 1$. They are defined, for $i = \{1, \ldots, d\}$, by:

$$\sigma(n+1) = \sqrt{\frac{1}{d}\sum\nolimits_{i=1}^{d}(x_i(n+1) - u_d(n+1))^2} \tag{12}$$

and

$$\sigma_1(n+1) = \sqrt{\frac{1}{d}\sum\nolimits_{i=1}^{d}(\Delta_{1i}(n+1) - u_d(n+1))^2}, \tag{13}$$

where

$$\Delta_{1i}(n+1) = x_i(n+1) - x_i(n) \tag{14}$$

and

$$u_1(n+1) = \frac{1}{d}\sum\nolimits_{i=1}^{d}\Delta_{1i}(n+1). \tag{15}$$

In order to further increase the accuracy and robustness of the model, especially for dealing with inconsistent weather, the author in [15] proposed replacing the last observation $\theta(n)$ with a weighted linear combination of the last observation and the closest energy pattern in memory denoted by $x_i(n+1)$. Moreover, the linear combination is weighted by an adaptive factor $G(n + 1)$ depending on the variation of the current day measurements, as follows:

$$\hat{x}(n+1) = G_1(n+1)[G(n+1)\theta(n) + 1 - G(n+1)x_i(n+1)] + (1 - G_1(n+1))GAPu_d(n+1), \tag{16}$$

where

$$G_1(n + 1) = G_1(n + 1) + G_2(n + 1) \tag{17}$$

and

$$G_2(n+1) = \frac{\sigma(n+1)}{2(\sigma(n+1)+\sigma_2(n+1))}. \tag{18}$$

In Equation (18), $\sigma_2(n+1)$ represents the standard deviation of the variations in the solar irradiance measurement vector θ between continuous time steps along a window of size K. Consequently, the vector of consecutive variations defined by $\Delta_2(n+1)$ is given by:

$$\Delta_{2k}(n+1) = \theta(n+1-k) - \theta(n-k),\ k = 1, \ldots, k-1. \tag{19}$$

Thus, the corresponding mean and standard deviation are defined by:

$$u_2(n+1) = \frac{1}{k-1}\sum\nolimits_{k=1}^{k-1}\Delta_{2k}(n+1) \tag{20}$$

and

$$\sigma_2(n+1) = \sqrt{\frac{1}{k-1}\sum\nolimits_{k=1}^{k-1}(\Delta_{2k}(n+1) - u_2(n+1))^2}. \tag{21}$$

3. Proposed Multi-Source Adaptive Linear Energy Prediction Model (Adaptive LINE-P)

As described above, LINE-P is designed and developed based on sampling theory and approximation; we propose a novel adaptive linear energy prediction model (named Adaptive LINE-P), of which the main purpose is to add adaptive weighting to LINE-P. Rather than using a fixed weighting parameter, which makes it difficult to reflect the different properties of energy harvesters such as solar-based ones, Adaptive LINE-P is based on energy profiles, which improves the accuracy, adaptability, and reliability of the energy predictions.

We first present the Adaptive LINE-P model and evaluate its basic performance. Thereafter, we compare its performance against that of Pro-Energy, Pro-Energy-VLT, IPro-Energy, and UD-WCMA. We used four datasets of traces of harvested energy. These datasets are from trusted sources, and taken from different locations of the USA and Europe. Furthermore, three datasets for solar energy, i.e., Southern California Edison Company (SCE, Rosemead, CA, USA), Pacific Gas and Electric Company (PG&E, San Francisco, CA, USA), and San Diego Gas & Electric Company (SDG&E, Santiago, CA, USA) [16] are used; we also selected one dataset for wind energy from Elia (Belgium-based power generation company, Brussels, Belgium) [17].

3.1. Sampling Operators

Let us suppose that a function f is defined for every point of some domain D and has series representation there in the form:

$$f(t) := \sum_{k=-\infty}^{\infty} f(t_k) s_k(t),$$

in which $\{t_k\}$ is a collection of points of D and $\{s_k\}$ is some set of suitable expansion functions. Such an expansion is called a sampling series. The function f is represented in its entirety in terms of its values, that is samples, at a discrete subset of its domain. For the uniformly continuous and bounded $f \in C(\mathbb{R})$, the generalized sampling series are given by $(t \in \mathbb{R}; w > 0)$ as per Equation (22),

$$(S_w f)(t) := \sum_{k=-\infty}^{\infty} f\left(\frac{k}{w}\right) s(wt - k), \tag{22}$$

where $s \in C(\mathbb{R})$ is a kernel function.

If the kernel function used in the sampling series is the cardinal sine, defined in the form:

$$s(t) = \sin\mathrm{c}(t) := \frac{\sin \pi t}{\pi t},$$

we get the classical (Whittaker-Kotel'nikov-) Shannon sampling operator,

$$\left(S_w^{\sin\mathrm{c}} f\right)(t) := \sum_{k=-\infty}^{\infty} f\left(\frac{k}{w}\right) \sin\mathrm{c}(wt - k). \tag{23}$$

Let us take $w = 1$ and $t = j \in \mathbb{Z}$ in Equation (22), then

$$(S_1 f)(j) := \sum_{k=-\infty}^{\infty} f(k) s(j - k). \tag{24}$$

3.2. Kernels

The general kernel for the sampling operators Equation (22) is expressed below.

Definition 1. ([18]) *If* $s : \mathbb{R} \to \mathbb{C}$ *is a bounded function such that the absolute moment*

$$m_0(s) := \sum_{k=-\infty}^{\infty} |s(u - k)| < \infty (u \in \mathbb{R}), \tag{25}$$

with the absolute or positive convergence uniform on compact subsets of $\mathbb{R}$*, and we have a partition of unity*

$$\sum_{k=-\infty}^{\infty} s(u-k) = 1 \ (u \in \mathbb{R}), \tag{26}$$

then s is called a kernel for sampling operators Equation (22).

The conditions in Definition 1 guarantee that the series in Equation (22) converges for $f \in C(\mathbb{R})$; moreover, we have uniform convergence

$$\|(S_w f) - f\| \to 0, (w \to \infty)$$

for any $f \in C(\mathbb{R})$. We estimate the speed of the convergence of sampling operators in terms of the modulus of smoothness ω_r ($r \in \mathbb{N}$) (see [18–22]) in the form

$$\|(S_w f) - f\| = M\omega_r\left(f, \frac{1}{w}\right),$$

where M is a positive constant. If we have an estimate in terms of a high order of modulus of smoothness, then the sampling operator rapidly converges for smooth signals.

The main aim of this article is to use for signal prediction the generalized sampling operators Equation (22), where the kernel function s is defined through the Fourier transform of a certain window function:

Definition 2. *A function* $\lambda \in C(\mathbb{R})$ *is called a window function for a kernel of a sampling operator if* $\lambda(0) = 1$ *and* $\lambda(\pm 2k) = 0$ *for* $k \in \mathbb{N}$.

Our kernel function is defined by the equality

$$s(t) := s\ (\lambda; t) := \frac{1}{2}\int_{-\infty}^{\infty} \lambda(u)\ \exp(-i\pi t u) du. \tag{27}$$

A special case of the kernel function are M-bandlimited kernels, defined by Equation (27), using window functions $\lambda(u) = 0$ ($|u| \geq M > 0$). We consider the case $M = 1$, i.e., with kernels defined using window functions $\lambda \in C_{[-1,1]}, \lambda(0) = 1,\ \lambda(u) = 0$ ($|u| \geq 1$). If the window function is an even function, then we get an even kernel:

$$s(t) = \int_0^1 \lambda(u)\cos(\pi t u) du. \tag{28}$$

Generally, for some cases, non-symmetric kernels are more suitable. In such cases, we prefer the general window function $\lambda \in C_{[-1,1]}$ and define the kernel in the form

$$s(t) = \frac{1}{2}\int_{-1}^{1} \lambda(u)\ \exp(-i\pi t u) du. \tag{29}$$

These sorts of kernels arise in conjunction with window functions widely use in applications (e.g., [23–26]), particularly in signal analysis. Many kernels can be defined by Equation (28), e.g.,

(1) $\lambda(u) = 1$ represents the sine function;

(2) $\lambda_j(u) := \cos\ \pi\left(j + \frac{1}{2}\right)u,\ j = 0, 1, 2, \ldots$ defines the Rogosinski-type kernel (see [20]), in the form

$$r_j(t) := \frac{1}{2}(\sin c\left(t + j + \frac{1}{2}\right) + \sin c\left(t - j - \frac{1}{2}\right)) \tag{30}$$

$$= \frac{\frac{(-1)^j}{\pi}\left(j+\frac{1}{2}\right)}{\left(j+\frac{1}{2}\right)^2 - t^2}\cos\pi t. \tag{31}$$

Powers of the Hann window (see [25], Equation (25));

$$\lambda_{H,m}(u) := \cos^m\left(\frac{\pi u}{2}\right) \tag{32}$$

give a general Hann kernel in the form

$$s_{H,m}(t) = 2^{-m}\frac{\Gamma(1+m)}{\Gamma(1+\frac{m}{2}-t)\Gamma(1+\frac{m}{2}+t)}, \tag{33}$$

where Γ is the Euler gamma function.

If $m = 1$, we get the Hann kernel:

$$s_H(t) = \frac{(\sin c(t-1) + 2\sin c(t) + \sin c(t+1))}{4}. \tag{34}$$

(3) The general cosine window

$$\lambda_{C,a}(u) := \sum_{k=0}^{n} a_k \cos k\pi u, \tag{35}$$

illustrates the Blackman–Harris kernel (see [20]),

$$s_{C,a}(t) := 1/2\sum_{k=0}^{n} a_k(\sin c(t-k) + \sin c(t+k)), \tag{36}$$

provided (here and following $\lfloor x \rfloor$ is the largest integer less than or equal to $x \in \mathbb{R}$):

$$\sum_{k=0}^{\lfloor \frac{n}{2} \rfloor} a_{2k} = \sum_{k=0}^{\lfloor \frac{n+1}{2} \rfloor} a_{2k-1} = \frac{1}{2}. \tag{37}$$

We get the Hann window if we take $n = 1$ in Equation (35), and the Blackman window if $n = 2$ and $a_0 = a$ in Equation (35). For $n \in \mathbb{N}$ there exists a choice of parameters that allows us to have the order of approximation of the corresponding sampling operators estimated by high ($2n$) order of modulus of smoothness $\omega_{2n}\left(f; \frac{1}{w}\right)x$ (cf. [20]). Another possibility for the parameter vector $a = a^*$ in (35), where the parameter vector $a^* = \left(a_0^*, a_1^*, \ldots, a_n^*\right) \in \mathbb{R}^{n+1}$ has components $a_0^* = \frac{1}{2^{2n}}\begin{pmatrix} 2n \\ n \end{pmatrix}$ and $a_k^* = \frac{1}{2^{2n-1}}\begin{pmatrix} 2n \\ n-k \end{pmatrix}$ for $k = 1, 2, \ldots, n$, gives us by Equation (28) a family of rapidly decreasing kernels $s_{H,2n} = O(|t|^{2n+1})$ (see [21] for corresponding operator norms and [22] for truncation errors).

The general cosine window generates a linear combination of translated sine-functions; rather than the general cosine window, a window in the form Equation (38) can be used:

$$\lambda_{E,a}(u) := \sum_{k=-n}^{n} a_k e^{ik\pi u}\ (n \in \mathbb{N},\ a = (a_{-n}, a_{-n+1}, \ldots,\ a_n)) \in \mathbb{R}^{2n+1}, \tag{38}$$

provided

$$\sum_{k=0}^{\lfloor \frac{n}{2} \rfloor} a_{2k} = \sum_{k=1}^{\lfloor \frac{n+1}{2} \rfloor} a_{2k-1} = \frac{1}{2}. \tag{39}$$

If we use Equation (29), we get a corresponding kernel in the form of Equation (40):

$$s_{E,a}(t) = \sum_{k=-n}^{n} a_k \sin\mathrm{c}(t-k), \tag{40}$$

which fulfills the properties of a kernel in terms of Definition 1, because the condition in Equation (39) guarantees that we have Equation (26) and that $m_0(s_{E,a})$ is bounded. Let us take $w = 1$ and $t = j \in \mathbb{Z}$ in Equation (22), then for kernel $s_{E,a}$ we get

$$(S_{1;E,a}f)(j) := \sum_{k=-\infty}^{\infty} f(k)s_{E,a}(j-k) = \sum_{k=-n}^{n} a_k f(t-k). \tag{41}$$

Comment on Approximation Error Estimates

The reader can refer to this section in [5] for a short discussion of approximation error estimates. Note, for the case at hand: if we have for some r ($r \in \mathbb{N}$), an estimate of speed of convergence in terms of modulus of smoothness ω_r, then the sampling series representation is exact for polynomials with a maximal power less than or equal to (r + 1).

3.3. Adaptive Predictors

We need adaptive predictors because the energy profiles can have different properties, i.e., with different smoothness, variation, etc. For different types of profiles we need different kernels for the sampling operators. In the current approach, we use the following kernels:

- For smooth profiles, kernels allow approximation order, estimates through high order of modulus of smoothness.
- For unstable profiles, the kernel provides a sampling operator with minimal (close to 1) norm.

Note: The trivial error estimate signal for additive noise is in the form $||S_w||\cdot||v||$, where $||S_w||$ is the operator norm and $||v\ ||$ is the norm of the noise component, i.e., if the operator norm is equal to 4, then in the worst case, we have 4-fold amplification of the noise in the predicted energy profile.

We deal with other profiles with a kernel that provides a sampling operator with good approximation properties and a small norm.

In order to choose the predictor kernel, we use l_1 norms of the prediction errors of previous estimates.

3.4. l_1 Norm

Now, we propose a method for adaptive prediction. We use the l_1 norms of the prediction errors. Moverover, we choose some r ($r \in \mathbb{N}$) kernels s_i (i = 1, 2, . . . , r) that generate sampling operators with different properties (approximation order, norm, etc.) and compute the predicted values using it.

For predicting the k-th element, we choose the kernel for which the l_1 norm of the prediction errors for some one-sided neighborhood of the k-th element of the profile is minimal. We compute for the k-th element norms $||E_i(k)||1$ of errors in the following form:

$$||E_i(k)||1 = \sum_{j=1}^{n} |f(k-j) - f_{p,i}(k-j)|,$$

where $f(k)$ is the measured energy in slot k and $f_{p,i}(k)$ is the predicted energy for slot k using the kernels s_i.

For particular realization of the adaptive predictor, to cover different types of profiles, we choose three kernels with different approximation properties. We have corresponding sampling operators, a first one with minimal norm, a second one with a high order of approximation, and a third one with good approximation properties and a small norm.

3.5. Compressed Profiles

In this section, we suggest a method for compressing profile data to address the memory size limitation of WSN nodes. This is expressed as

$$\overline{f}(t) = \Sigma_k f(k)\overline{S}(t-k),$$

where $\overline{f}$ is the compressed profile, f the original profile, and $\overline{S}(t) := \frac{2}{\alpha}s\ (2t/\alpha)\ (\alpha > 0)$ the dilated kernel. Instead of $f(k)$ we store $\overline{f}(\alpha k)$. For example if $\alpha = 4$, we use one-quarter of the memory.

For reconstruction, we use an interpolating kernel $\overline{S}$, i.e., a kernel defined using a window function that satisfies the equality

$$\lambda(u) + \lambda(1-u) = 1,\ (u \in [0,1]).$$

The reconstruction formula is as follows:

$$f(j) \approx \Sigma_k \overline{f}(\alpha k) 2\overline{S}\left(\frac{2}{\alpha}j - 2k\right).$$

For efficient realizations we need to choose a reconstruction kernel, which allows us to compute a good enough reconstruction with a minimal number of operations; for the compression part the kernel may be more complicated, because we need to compress the profile only once a day.

For a particular realization of the compression algorithm, we take $\alpha = 4$ and for both the kernel s and $\overline{S}$, we choose the Hann kernel (Equation (34)), which adds for reconstruction only three multiplications for every day in one prediction step.

In what follows, we check the accuracy of Adaptive LINE-P (all cases). Thereafter, we can determine which of the cases is predicted best in terms of numerical value and suitable for further comparison with the state of the art.

3.6. Accuracy Evaluation of the Adaptive LINE-P (All Cases) Based on the MAE and MSE

In this section we seek to find which of the three cases of Adaptive LINE-P model provides the most accuracy, robustness, lower errors, and adaptability in case of frequent changes in the energy source. In order to quantify the error in each case of Adaptive LINE-P, we consider two source energy profiles (solar and wind) and conduct various evaluations by means of MAE and MSE measures.

We have conducted two tests based on the two sources, namely, solar (SDG&E energy profile) and wind (Elia energy profile). Tables 2 and 3 show the MAE and MSE for Adaptive LINE-P (all cases) for SDG&E energy profile for six individual days, as well as the average. Similarly, Tables 4 and 5 show the MAE and MSE for Adaptive LINE-P (all cases) for Elia energy profile.

Table 2. Error comparison of adaptive LINE-P (all cases) based on the MAE for SDG&E solar energy profile.

MODELS	MAE (Day 1)	MAE (Day 2)	MAE (Day 3)	MAE (Day 4)	MAE (Day 5)	MAE (Day 6)	Average MAE
Adaptive LINE-P (Case I)	0.0632	0.1071	0.1575	0.0969	0.0597	0.0382	0.0871
Adaptive LINE-P (Case II)	0.0591	0.1148	0.1993	0.1239	0.0869	0.0554	0.1065
Adaptive LINE-P (Case III)	0.0634	0.0887	0.1486	0.0902	0.0523	0.033	0.0793

Table 3. Error comparison of adaptive LINE-P (all cases) based on the MSE for SDG&E solar energy profile.

MODELS	MSE (Day 1)	MSE (Day 2)	MSE (Day 3)	MSE (Day 4)	MSE (Day 5)	MSE (Day 6)	Average MSE
Adaptive LINE-P (Case I)	0.0212	0.0649	0.1462	0.0588	0.0184	0.0069	0.0527
Adaptive LINE-P (Case II)	0.0180	0.0698	0.2402	0.0769	0.0356	0.0207	0.0768
Adaptive LINE-P (Case III)	0.0161	0.0395	0.1287	0.0537	0.0133	0.0065	0.0429

Table 4. Error comparison of adaptive LINE-P (all cases) based on the MAE for Elia wind energy profile.

MODELS	MAE (Day 1)	MAE (Day 2)	MAE (Day 3)	MAE (Day 4)	MAE (Day 5)	MAE (Day 6)	Average MSE
Adaptive LINE-P (Case I)	0.0984	0.1455	0.0494	0.0391	0.1192	0.0806	0.0887
Adaptive LINE-P (Case II)	0.0902	0.1598	0.0343	0.0295	0.1481	0.0754	0.0895
Adaptive LINE-P (Case III)	0.0955	0.1444	0.0474	0.0322	0.1137	0.0921	0.0875

Table 5. Error comparison of adaptive LINE-P (all cases) based on the MSE for Elia wind energy profile.

MODELS	MSE (Day 1)	MSE (Day 2)	MSE (Day 3)	MSE (Day 4)	MSE (Day 5)	MSE (Day 6)	Average MSE
Adaptive LINE-P (Case I)	0.0185	0.0410	0.0070	0.0038	0.0445	0.0129	0.0212
Adaptive LINE-P (Case II)	0.0149	0.0484	0.0027	0.0019	0.0597	0.0106	0.0230
Adaptive LINE-P (Case III)	0.0156	0.0412	0.0031	0.0021	0.0431	0.0211	0.0210

Tables 2–5 illustrate that, among all cases of Adaptive LINE-P model, Case III yields more accurate estimates as compared to Case I and Case II (error down by between −1% and −44%). Given this, Adaptive LINE-P model (Case III) has been selected for further comparison with the state of the art, as presented in the next section.

4. Comparative Analysis of Adaptive LINE-P (Case III, Non-Compressed Profiles) with the State of the Art

In this section, we assess the performance of Adaptive LINE-P (Case III) against that of UD-WCMA (the only other adaptive energy prediction model available in the literature) and against that of LINE-P (Case III) and IPro-energy (deemed the best two non-adaptive energy prediction models). Note that although we refer to LINE-P (Case III) and IPro-energy as non-adaptive, they are able to model energy variations, but they do not include specific adaptation mechanisms as in Adaptive LINE-P and UD-WCMA.

The comparison is based on short, medium, and longer time period horizons. The classification of the time periods and their graphical representations are extracted from the real datasets available in [16,17]. For the longer time period, we consider 30 time slots; for the medium and shorter time periods we used 61 and 96 time slots in 42-, 22-, and 15-min data intervals in 24 h, respectively.

As far as the longer time period is concerned, by deploying real implementation of energy prediction, we have found that a longer time period such as a 1-h data interval is not sufficiently adaptive and feasible, specifically for those regions where the weather changes frequently. Therefore, we have reduced the data interval time from 60 to 42 min and conducted experiments based on 42-, 22-, and 15-min time periods.

In addition, we present the evaluation of the model based on the same two error measures as in Section 2, i.e., MSA and MSE; thereafter, we assess their time complexities and finally the analysis of the proposed compression technique.

4.1. Graphical Representation of Adaptive LINE-P (Case III) as Compared to the State of the Art Based on Longer, Medium, and Shorter Time Period Horizons

For the assessment of all the prediction models, we present the estimation errors in Tables 6 and 7 by using MAE and MSE with the same profile PG&E available in [16].

Table 6. Error comparison of prediction models based on MAE for the PG&E solar energy profile.

MODELS	MAE (Day 1)	MAE (Day 2)	MAE (Day 3)	MAE (Day 4)	MAE (Day 5)	MAE (Day 6)	Average MAE
LINE-P (Case III)	0.0269	0.0315	0.0188	0.0189	0.0138	0.0141	0.0206
UD-WCMA	0.0407	0.0686	0.0685	0.0330	0.0194	0.0312	0.0435
IPRO-Energy	0.0070	0.0861	0.0645	0.0526	0.0252	0.0310	0.0443
Adaptive LINE-P (Case III)	0.0251	0.0370	0.0150	0.0210	0.0171	0.0155	0.0217

Table 7. Error comparison of prediction models based on the MSE by deploying PG&E solar profile.

MODELS	MSE (Day 1)	MSE (Day 2)	MSE (Day 3)	MSE (Day 4)	MSE (Day 5)	MSE (Day 6)	Average MSE
LINE-P (Case III)	0.0037	0.0040	0.0018	0.0017	0.0011	0.0008	0.0021
UD-WCMA	0.0063	0.0184	0.0429	0.0040	0.0017	0.0034	0.0127
IPRO-Energy	0.0002	0.0267	0.0127	0.0037	0.0027	0.0032	0.0082
Adaptive LINE-P (Case III)	0.003	0.0086	0.0013	0.0037	0.0015	0.0011	0.0032

Tables 6 and 7 illustrate that adaptive LINE-P (Case III) yield less error comparatively to the other prediction models, except LINE-P (Case III), although the error difference between adaptive LINE-P and non-adaptive LINE-P is negligible. Actually, the estimation error is also dependent on the profile; in another profile, we have found higher error in non-adaptive LINE-P (Case III) than adaptive LINE-P.

To obtain the results shown in Figure 2, we have used a PG&E profile [16] for the solar energy to assess the adaptive LINE-P (Case III) and the state-of-the-art models based on longer (30 time slots) time period horizon. Figure 2 shows that the profile corresponds to highly consistent weather; all together, all days are nearly identical.

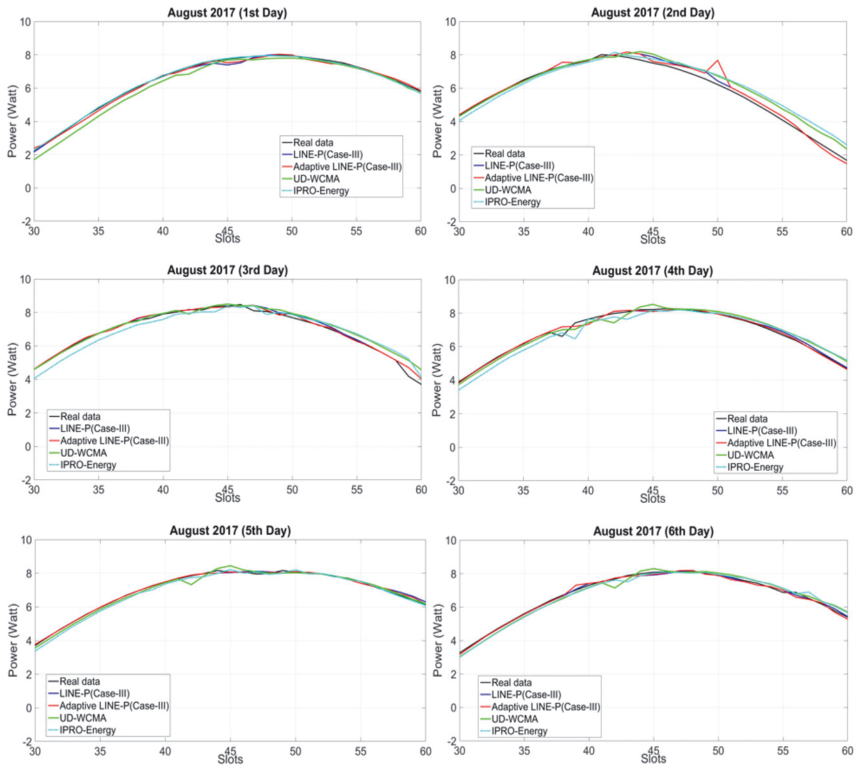

Figure 2. Graphical representation of Adaptive LINE-P (Case III) and state of the art based on the longer (42-min data interval) time period horizon for the solar profile with 30 time slots in 24 h.

However, some of the EP models are unable to predict the energy with full accuracy. For instance, UD-WCMA overestimates the energy on all six days. Even though for the first day it starts by underestimating, after the 40th time slot it estimated the real data well; after the 50th time slot it starts overestimating again. Therefore, this overestimation may indicate that UD-WCMA is not sufficiently adaptable, even for consistent profiles.

Similarly, IPRO-Energy starts by underestimating at all days (except for the first day), but as compared to UD-WCMA, IPRO-Energy is better at modeling energy variations. Although IPRO-Energy and LINE-P (Case III) provide adequate results, both are based on a fixed weighting parameter factor; thus, they are not well suited for various types of solar energy harvesters, as mentioned earlier in the paper. On the other hand, Adaptive LINE-P (Case III) is not dependent on any fixed weighting parameter; it performs predictions on the adaptive weighting factor based on the profiles. Furthermore, we observe in Figure 2 (for all days) that the adaptive LINE-P (Case III) is highly accurate. Thus, for this energy profile, Adaptive LINE-P provides both accuracy and adaptability.

In the following, we evaluate the performance of Adaptive LINE (Case III) along with the state of the art based on the medium (61 time slots) time period horizon of the solar energy profile SCE [16].

For further assessment of all the prediction models, we present the estimation errors in Tables 8 and 9 by using MAE and MSE with the same profile SCE available in [16].

Table 8. Error comparison of the prediction models based on MAE for the SCE solar energy profile.

MODELS	MAE (Day 1)	MAE (Day 2)	MAE (Day 3)	MAE (Day 4)	Average MAE
LINE-P (Case III)	0.0820	0.0945	0.0944	0.1563	0.1068
UD-WCMA	0.1088	0.1347	0.1881	0.0979	0.1323
IPRO-Energy	0.0782	0.0842	0.1745	0.2008	0.1344
Adaptive LINE-P (Case III)	0.0802	0.0970	0.0932	0.1405	0.1027

Table 9. Error comparison of the prediction models based on MSE for the SCE solar energy profile.

MODELS	MSE (Day 1)	MSE (Day 2)	MSE (Day 3)	MSE (Day 4)	Average MSE
LINE-P (Case III)	0.0348	0.0493	0.0850	0.1051	0.0685
UD-WCMA	0.0559	0.0797	0.1509	0.0465	0.0832
IPRO-Energy	0.0313	0.0351	0.1898	0.1524	0.1021
Adaptive LINE-P (Case III)	0.0352	0.0530	0.0849	0.0905	0.0659

In relation to Tables 8 and 9, it is shown that adaptive LINE-P (Case III) has less error possibility as compared to the other prediction models.

Figure 3 shows the results for fairly consistent profiles, to see the behavior and adaptability of the prediction models based on the medium (61 time slots) time period horizon. The graphical representation shows that most of the models are estimating up to the mark only in the first day. It can be seen that in all other days, LINE-P (Case III) starts overestimating. UD-WCMA also starts overestimating in all days, especially on the 12th and 13th of December from the 45th to the 60th time slots, and 20th to 50th time slots. UD-WCMA yields the worst results comparative to the other prediction models. Furthermore, on 11th December, the IPro-Energy model is off the chart from the fifth to the 10th time slots. Although gradually its estimation is approaching the real data, it then starts underestimating from the 40th until the 53rd time slots. On the contrary, Adaptive LINE-P (Case III) seems much better and most of the time yields estimates close to the real data.

In addition, we have assessed Adaptive LINE-P (Case III) comparative to the state of the art based on the graphical representation and classical error-calculating methods (MSA and MSE), as presented in what follows.

Figure 4 shows the comparison of Adaptive LINE-P (Case III) and the state of the art for the SDG&E solar energy profile. This profile exhibits very low power production throughout the figure. In addition, this profile is for cloudy days with lots of variation. This kind of profile is a real challenge for the prediction models; indeed, too much fluctuation and extremely sharp variation-based weather is difficult to predict accurately and requires continuous adaptation. As can be observed, most of the models, especially from the second to the fourth days, are overestimating. Moreover, UD-WCMA shows poor prediction for all the days. Furthermore, due to rapid changes in the profile, IPRO-Energy underestimates on the 30th and 31st of October, but once the profile becomes smooth IPRO-Energy predicts well until the end of profile, especially in the last two days. LINE-P (Case III) and Adaptive LINE-P (Case III) overestimate from the 30th to 40th time slots in all days. Thereafter, it can be observed that Adaptive LINE-P (Case III) also shows robustness and predicts accurately as compared to LINE-P (Case III) and the state of the art.

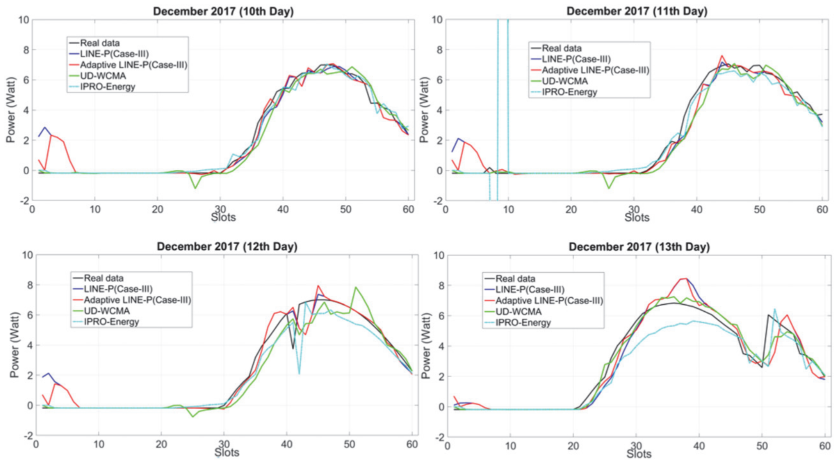

Figure 3. Graphical representation of Adaptive LINE-P (Case III) and state of the art based on the medium (22-min data interval) time period horizon of the solar profile with 61 time slots in 24 h.

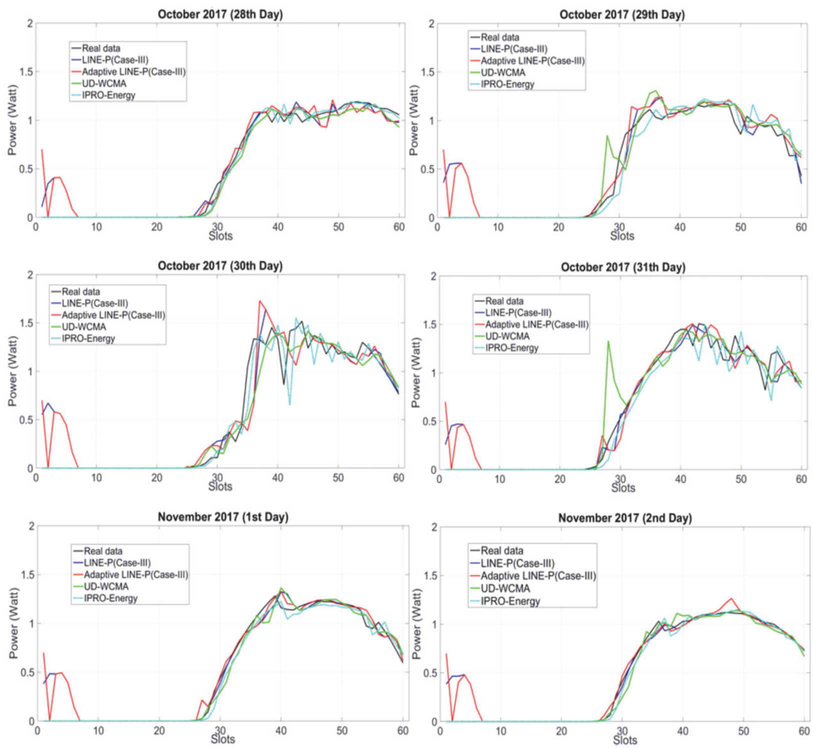

Figure 4. Graphical representation of Adaptive LINE-P (Case III) and the state of the art based on the medium (22-min data interval) time period horizon for the solar energy profile with 61 time slots in 24 h.

For further assessment of all the prediction models, we also present the estimation errors in Tables 10 and 11 by using MAE and MSE with the same profile SDG&E available in [16].

Table 10. Error comparison of the prediction models based on MAE for the SDG&E solar energy profile.

MODELS	MAE (Day 1)	MAE (Day 2)	MAE (Day 3)	MAE (Day 4)	MAE (Day 5)	MAE (Day 6)	Average MAE
LINE-P (Case III)	0.0619	0.0841	0.1432	0.0910	0.0668	0.0362	0.0805
UD-WCMA	0.0625	0.1224	0.1376	0.1409	0.1392	0.1381	0.1234
IPRO-Energy	0.0467	0.1053	0.1305	0.1141	0.0733	0.0418	0.0852
Adaptive LINE-P (Case III)	0.0645	0.0861	0.1486	0.0976	0.0525	0.0366	0.0809

Table 11. Error comparison of the prediction models based on MSE for the SDG&E solar energy profile.

MODELS	MSE (Day 1)	MSE (Day 2)	MSE (Day 3)	MSE (Day 4)	MSE (Day 5)	MSE (Day 6)	Average MSE
LINE-P (Case III)	0.0156	0.0392	0.1378	0.0417	0.0193	0.0066	0.0433
UD-WCMA	0.0160	0.1040	0.1185	0.1220	0.1386	0.1281	0.1045
IPRO-Energy	0.0115	0.0555	0.1150	0.0615	0.0198	0.0091	0.0454
Adaptive LINE-P (Case III)	0.0161	0.0395	0.1287	0.0537	0.0133	0.0065	0.0429

For this kind of energy profile, we found that in terms of MAE, Adaptive LINE-P (Case III) yields less errors than IPRO Energy and UD WCMA (between ca. −5% and ca. −34%), and is almost identical to LINE-P (Case III) (+0.5%). In terms of MSE, Adaptive LINE-P (Case III) yields lower error as compared to all other energy prediction models (between −5.5% and ca. −59%). In addition, Adaptive LINE-P (Case III) model is highly adaptive, as can be observed in Figure 4. However, LINE-P and IPRO-Energy also show good estimations, but they still suffer from the fixed weighting parameter issue, which was discussed earlier.

Results for Wind Energy

In what follows, we compare Adaptive LINE (Case III) with the state of the art based on the shorter (96 time slots in 24 h) time period horizon for the wind energy profile Elia available in [11].

As shown in Figure 5, it can be observed that LINE-P (Case III) initially overestimates and then approaches the real data. Similar to the solar energy case, UD-WCMA predictions are rather far from the real data. Most of the time, it can be seen that it starts with an overestimation if the real data increases; on the other hand, if the real data decreases, then its behavior changes completely and underestimates, especially in the last two days in Figure 4. IPRO-Energy is also not yielding very good estimates. It is clearly visible in Figure 4 that both UD-WCMA and IPRO-Energy are not suitable for uncontrollable energy sources on the shorter time period horizon. On the other hand, Adaptive LINE-P (Case III) shows robustness, adaptability, suitability for variable-length time slots, and accuracy. If the profiles are changing frequently, then UD-WCMA and IPRO-Energy are not as accurate as Adaptive LINE-P (Case III). In addition, the Adaptive LINE-P (Case III) model is highly adaptable, as can be observed in Figure 5.

In the following section, we compute the accuracy of the adaptive LINE-P (Case III) by means of the MAE and MSE for the wind energy profile.

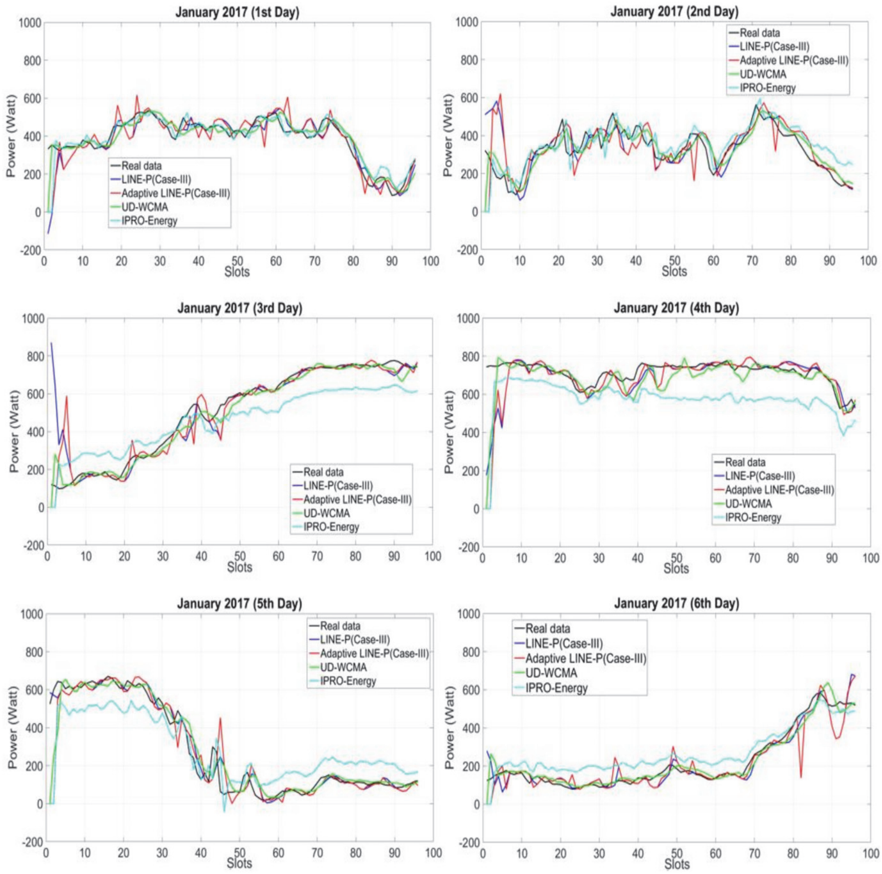

Figure 5. Graphical representation of Adaptive LINE-P (Case III) and state of the art based on the shorter (15-min data interval) time period horizon for the wind energy profile with 96 time slots in 24 h.

4.2. Accuracy Assessment of the Energy Prediction Models Based on the MAE and MSE for Solar and Wind Energy Profiles

In this section, we examine the models based on the multiple (solar and wind) energy profiles. In order to calculate the error possibility in Adaptive LINE-P (Case III) and the other energy prediction models, we consider the PG&E solar energy profile available in [16].

Tables 12 and 13 illustrate that the results provided by Adaptive LINE-P (Case III) have less errors as compared to the other prediction models (down by up to −82%), with the exception of LINE-P (Case III) (+50%) in terms of MSE (Table 13).

Table 12. Error comparison of the energy prediction models in terms of MAE for the solar energy profiles.

MODELS	MAE (Day 1)	MAE (Day 2)	MAE (Day 3)	MAE (Day 4)	MAE (Day 5)	MAE (Day 6)	Average MAE
LINE-P (Case III)	0.0269	0.0315	0.0188	0.0189	0.0138	0.0141	0.0206
UD-WCMA	0.0407	0.0686	0.0685	0.0330	0.03476	0.03688	0.047
IPRO-Energy	0.0070	0.0861	0.0645	0.0526	0.0252	0.0310	0.044
Adaptive LINE-P (Case III)	0.0251	0.037	0.0150	0.0210	0.0171	0.0155	0.0217

Table 13. Error comparison of the energy prediction models in terms of MSE for the solar energy profile.

MODELS	MSE (Day 1)	MSE (Day 2)	MSE (Day 3)	MSE (Day 4)	MSE (Day 5)	MSE (Day 6)	Average MSE
LINE-P (Case III)	0.0037	0.0040	0.0018	0.0017	0.0011	0.0008	0.0021
UD-WCMA	0.0049	0.0184	0.0429	0.0040	0.0329	0.0372	0.0233
IPRO-Energy	0.0002	0.0267	0.0127	0.0037	0.0027	0.0032	0.0082
Adaptive LINE-P (Case III)	0.003	0.0086	0.0013	0.0095	0.0015	0.0011	0.0041

Next, we deal with Elia wind energy profile [17] to see the possible errors in Adaptive LINE-P (Case III) as compared to the state of the art.

Similarly, Tables 14 and 15 show that the proposed Adaptive LINE-P (CASE III) performs better than the other energy prediction models (error down by up to ca. −78% in terms of MAE and MSE). In the above section, we have compared the energy prediction models with two different sources, namely solar and wind data profiles; apart from a minor exception, the results show that Adaptive LINE-P (Case III) provides the best results as compared to the other energy prediction models.

In the next section, we evaluate the performance of the proposed compressed profile method as compared to the state of the art.

Table 14. Error comparison of the energy prediction models in terms of MAE for the wind energy profile.

MODELS	MAE (Day 1)	MAE (Day 2)	MAE (Day 3)	MAE (Day 4)	MAE (Day 5)	MAE (Day 6)	Average MAE
LINE-P (Case III)	0.0349	0.0623	0.1083	0.4257	0.2294	0.1565	0.1695
UD-WCMA	0.0330	0.0879	0.1088	0.3437	0.1946	0.1279	0.1493
IPRO-Energy	0.0986	0.1907	0.1863	0.6094	3.0968	0.4993	0.7801
Adaptive LINE-P (Case III)	0.0338	0.0569	0.1095	0.4186	0.2133	0.1594	0.16525

Table 15. Error comparison of the energy prediction models in terms of MAE for the wind energy profile.

MODELS	MSE (Day 1)	MSE (Day 2)	MSE (Day 3)	MSE (Day 4)	MSE (Day 5)	MSE (Day 6)	Average MSE
LINE-P (Case III)	0.0021	0.0065	0.0311	0.4667	0.1451	0.0545	0.1176
UD-WCMA	0.0018	0.0144	0.0415	0.3143	0.1048	0.0323	0.0845
IPRO-Energy	0.0112	0.0441	0.0936	0.5489	1.9788	0.3059	0.4970
Adaptive LINE-P (Case III)	0.0020	0.0061	0.0292	0.4243	0.1278	0.0563	0.1076

5. Comparison of the Compressed Profile Method with the State of the Art Based on the Shorter Time Period Horizon

Here, we assess the compressed profile method in two steps. Firstly, in order to verify its accuracy and adaptability, we compare it with the real data (real profile), see Figures 6 and 7. Secondly, we incorporate the method with the two adaptive energy prediction models (Adaptive LINE-P and UD-WCMA) for further assessment against their non-compressed versions, as well as against the real data.

In all experiments, we use the shorter (96 time slots) time period horizon in 24 h. We check the accuracy of the compressed profile method against the graphical representation and a MAE and MSE as well.

5.1. Graphical Representation of the Compressed Profile Method and Its Error Estimation as Compared to the Real Data (a Real Dataset) Based on the Solar Energy Profile

In Figure 6, the energy profile reflects consistent weather; however, there are certain variations in each day. In this figure, the accuracy remains at a high level, though some lack in adaptability against the sharp variation is visible on all days (except on the third day).

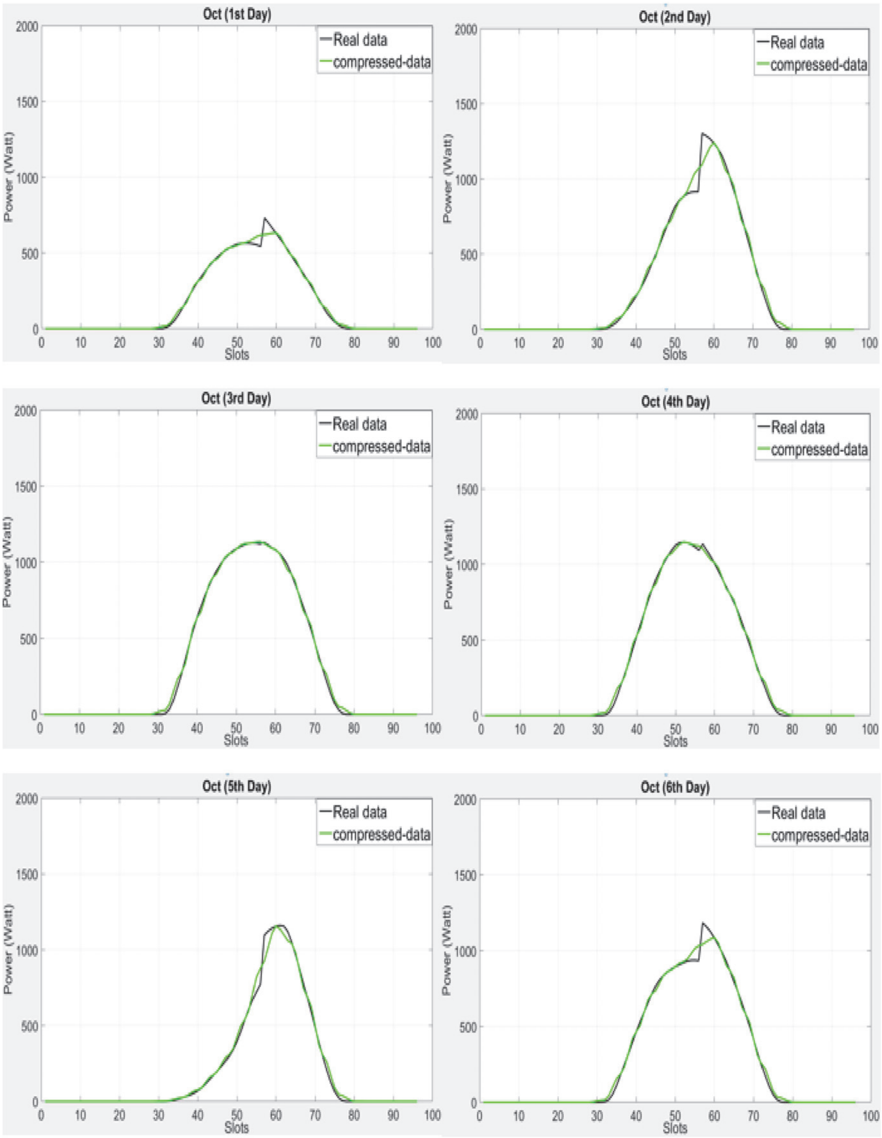

Figure 6. Graphical representation of compressed profile method against the real data based on the shorter (15-min data interval) time period horizon of solar energy profile (Elia) with 96 time slots in 24 h.

For further analysis of the proposed compressed profile method, we incorporate it into UD-WCMA and adaptive LINE-P (Case III) models to validate its accuracy when used with those models. In addition, we have used the same energy profile [17] to compare the error estimation with the non-compressed UD-WCMA and adaptive LINE-P (Case III) as well. The results for the solar energy profile are presented in Section 5.2 and those for the wind energy profile in Section 5.3.

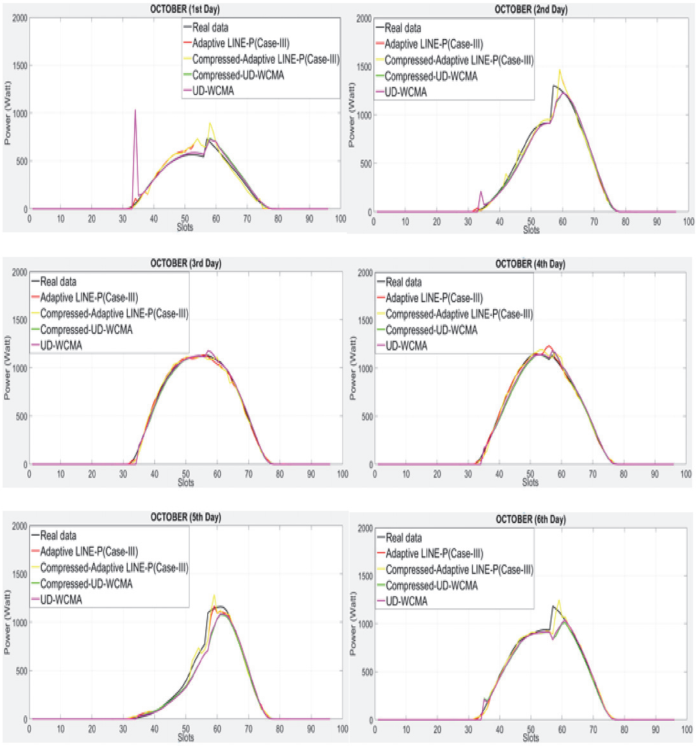

Figure 7. Graphical representation of the compressed profile method against the real data based on the shorter (15-min data interval) time period horizon of solar profile with 96 time slots in 24 h.

5.2. Error Estimation with and without Compression Method in UD-WCMA and Adaptive LINE-P (Case III) for the Solar Energy Profile

Furthermore, Tables 16 and 17 illustrate the error estimation with and without the proposed profile compression method in terms of MAE and MSE for the solar energy profile.

Table 16. Error estimation MAE of the prediction models with and without the compressed profile for the solar energy profile.

MODELS	MAE (Day 1)	MAE (Day 2)	MAE (Day 3)	MAE (Day 4)	MAE (Day 5)	MAE (Day 6)	Average MAE
Compress-Method	0.0471	0.0550	0.0248	0.0283	0.0608	0.0432	0.0432
Compressed-UD-WCMA	0.1225	0.0719	0.0265	0.0430	0.1046	0.0649	0.0722
Non-Compressed-UD-WCMA	0.1138	0.0697	0.0241	0.0407	0.1130	0.0588	0.0700
Compressed-Adaptive LINE-P (Case III)	0.1327	0.0687	0.0305	0.0360	0.0771	0.0431	0.0646
Non-Compressed-Adaptive LINE-P (Case III)	0.1315	0.0793	0.0264	0.0258	0.0677	0.0398	0.0617

Table 17. Error estimation MSE of the prediction models with and without the compressed profile for the solar energy profile.

MODELS	MSE (Day 1)	MSE (Day 2)	MSE (Day 3)	MSE (Day 4)	MSE (Day 5)	MSE (Day 6)	Average MSE
Compress-Method	0.0121	0.0177	0.0022	0.0024	0.0202	0.0087	0.0105
Compressed–UD-WCMA	0.3549	0.0298	0.0030	0.0077	0.0833	0.0351	0.0856
Non-Compressed-UD-WCMA	0.3528	0.0324	0.0025	0.0055	0.0818	0.0316	0.0844
Compressed-Adaptive LINE-P (Case III)	0.0691	0.0306	0.0033	0.0052	0.0342	0.0156	0.0263
Non-Compressed-Adaptive LINE-P (Case III)	0.1315	0.0302	0.0022	0.0046	0.0293	0.0152	0.0355

It can be observed that incorporating the compressed profile method increases the MAE for UD-WCMA and Adaptive LINE-P (CASE III) by ca. +3.14% and +4.7%, respectively. Interestingly, it can also be seen that incorporating the compressed profile method increases the MSE by ca. +1.4% for UD-WCMA and decreases it by ca. −26% for Adaptive LINE-P. As seen earlier in the paper, the compressed profile method reduces the memory requirements by a factor of 2, thus offering a good trade-off between accuracy and memory requirements. In the following, we further evaluate the compressed profile method with the graphical representation as well as with MAE and MSE based on the wind energy profile.

5.3. Error Estimation with and without Compression Method in UD-WCMA and Adaptive LINE-P (Case III) for the Wind Energy Profile

Here, we use the wind energy profile to evaluate the performance of the compressed profile method as compared to the real data in terms of the graphical view.

Figure 8 exhibits extremely inconsistent weather; moreover, the last three days show low power productivity. As can been observed in the figure, the compressed profile method shows stability (smoothness) rather than adaptability, especially on 14th and 15th January, due to sharp variation; however, approaching the profile's end, we see the robustness of the compressed profile method.

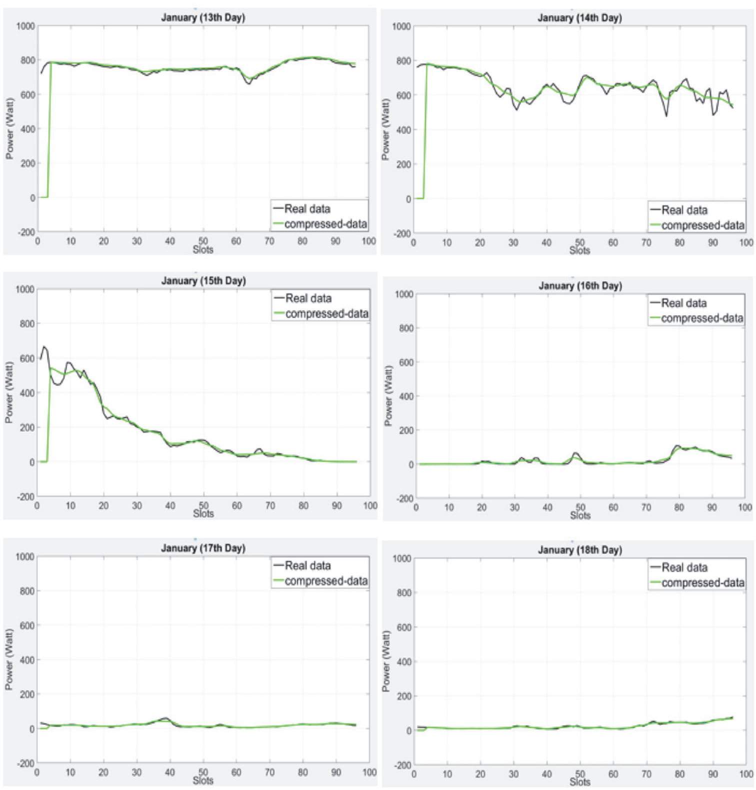

Figure 8. Graphical representation of the compressed profile method against the real data based on the shorter (15-min data interval) time period horizon of wind profile (Elia) with 96 time slots in 24 h.

In the following, we present the prediction error of the compressed profile method in terms of MAE and MSE for the wind energy profile.

5.4. Graphical Representation of the Prediction Model with and without the Compressed Profile Method for the Wind Energy Profile

In the following, we calculate the error estimation in terms of MAE and MSE for the wind energy profile.

In Figure 9 we observed that the proposed compressed profile method integrated with Adaptive LINE-P (Case-III) and UD-WCMA shows stability and accuracy similar to the non-compressed Adaptive LINE-P (Case-III) and UD-WCMA; however, we calculated minor error in the compressed method as compared to the non-compressed method.

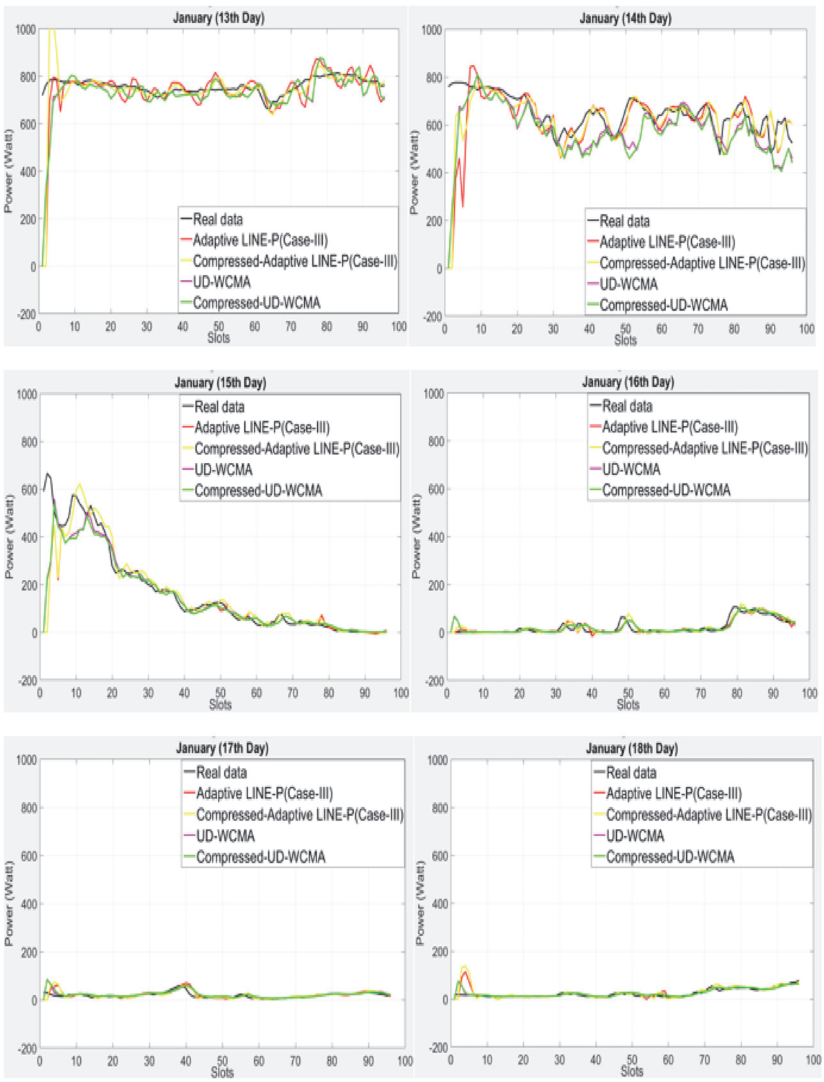

Figure 9. Graphical representation of energy prediction models with and without the compressed profile method based on the short time period horizon of the wind energy profile (Elia).

As can be observed in Tables 18 and 19, the MAE and MSE values are of the same order of magnitude as for the solar energy profile (Tables 16 and 17). Next, for further evaluation, we apply the same profile we used above for the compressed profile method into the UD-WCMA and Adaptive Line-P (CASE III) energy prediction models and then compare their results without adding the compression feature.

Table 18. Error estimation in terms of MAE of the prediction models with and without the compressed profile method for the wind energy profile.

MODELS	MAE (Day 1)	MAE (Day 2)	MAE (Day 3)	MAE (Day 4)	MAE (Day 5)	MAE (Day 6)	Average MAE
Compressed-profile	0.0089	0.0303	0.0577	0.2216	0.1189	0.0704	0.0846
Compressed-UD-WCMA	0.0761	0.1186	0.0431	0.0424	0.0997	0.0797	0.0766
Non-Compressed-UD-WCMA	0.0757	0.1179	0.0425	0.0405	0.1008	0.0799	0.0762
Compressed-Adaptive LINE-P (Case III)	0.0813	0.1322	0.0435	0.0280	0.1137	0.0921	0.0818
Non-Compressed-Adaptive LINE-P (Case III)	0.0955	0.1444	0.0474	0.0322	0.1120	0.0927	0.0873

Table 19. Error estimation in terms of MSE of the prediction models with and without the compressed profile method for the wind energy profile.

MODELS	MSE (Day 1)	MSE (Day 2)	MSE (Day 3)	MSE (Day 4)	MSE (Day 5)	MSE (Day 6)	Average MSE
Compressed-profile	0.0001	0.0019	0.0088	0.1146	0.0398	0.0107	0.0293
Compressed-UD-WCMA	0.0102	0.0233	0.0039	0.0038	0.0267	0.0132	0.0135
Non-Compressed-UD-WCMA	0.0101	0.0230	0.0038	0.0035	0.0267	0.0132	0.0133
Compressed-Adaptive LINE-P (Case III)	0.0145	0.0405	0.0065	0.0016	0.0432	0.0333	0.0232
Non-Compressed-Adaptive LINE-P (Case III)	0.0186	0.0456	0.0074	0.0021	0.0441	0.0336	0.0252

In addition, Tables 18 and 19 illustrate the error estimation with and without the proposed profile compression method in terms of MAE and MSE for the wind energy profile. In Table 18, it can be observed that incorporating the compressed profile method increases the MAE for UD-WCMA by ca. +0.52% but decreases it for Adaptive LINE-P (CASE III) by ca. −6.3%.

In Table 19, it can be seen that incorporating the compressed profile method increases the MAE for UD-WCMA by +1.5% but decreases it for Adaptive LINE-P (CASE III) by ca. −7.93%. As seen earlier in the paper, the compressed profile method reduces the memory requirements by a factor of 2. In line with the results shown for the solar energy profile (Tables 16 and 17), the results for the wind energy profile show that that the proposed compressed profile method offers a good trade-off between accuracy and memory requirements.

6. Conclusions

We have presented Adaptive LINE-P (three cases-based) prediction model for multi-source (solar and wind) energy sources. The proposed model is independent of the fixed length time slot and fixed weighting parameter. We have conducted experiments with three time period horizons (shorter, medium, and longer) with different time slots. Adaptive LINE-P model chooses the weighting parameter based on the actual energy profile. We have conducted numerous experiments with real datasets, and for the error evaluation we have used the MAE and MSE error calculating method. The results show that Adaptive LINE-P, especially (Case III), is 90–94% accurate (depending on the weather). In addition, our prediction model is highly adaptable against sharp variations as compared to other adaptive and non-adaptive prediction models. Most of the time, the proposed Adaptive LINE-P model yields estimates with less errors, except in a few cases, depending on the energy profile. Nevertheless, this is a small (and relatively rare) price to pay as compared to the general gains offered by the adaptive feature of the model. Moreover, we proposed a compressed profile method that can easily be incorporated into any prediction model; this method allows us to reduce the memory requirements by 50% and provides 90% accuracy.

In the future, we plan to work on the data prediction concept, which is also one of promising solution for saving energy. This concept can be applied to cases where the data are identical for longer time periods, for instance temperature and humidity, specifically in the domain of WSNs.

Acknowledgments: This research was partly supported by the TUT baseline project B38 and the IT Academy stipend program. This project has received funding from the European Union's Horizon 2020 research and innovation program under grant no. 668995. This material reflects only the authors' view and the EC Research Executive Agency is not responsible for any use that may be made of the information it contains.

Author Contributions: F.A. and G.T. designed the model, performed the simulations, and analyzed the results; Y.L.M. and P.A. gave feedback on the models and helped analyze the results. All authors participated in the paper writing.

Conflicts of Interest: The authors declare no conflict of interest. The founding sponsors had no role in the design of the study; in the collection, analyses, or interpretation of data; in the writing of the manuscript, and in the decision to publish the results.

References

1. Shahzad, F.; Sheltami, T.R. An Efficient MAC Scheme in Wireless Sensor Network with Energy Harvesting (EHWSN) for Cloud Based Applications. In Proceedings of the 2015 IEEE 40th Local Computer Networks Conference Workshops (LCN Workshops), Clearwater Beach, FL, USA, 26–29 October 2015; pp. 783–788.
2. Xu, X.; Zhang, G. A Hybrid Model for Data Prediction in Real-World Wireless Sensor Networks. *IEEE Commun. Lett.* **2017**. [CrossRef]
3. Mehrabi, A.; Kim, K. Maximizing data collection throughput on a path in energy harvesting sensor networks using a mobile sink. *IEEE Trans. Mob. Comput.* **2016**, *15*, 690–704. [CrossRef]
4. Kosunalp, S. A new energy prediction algorithm for energy-harvesting wireless sensor networks with Q-Learning. *IEEE Access* **2016**, *4*, 5755–5763. [CrossRef]
5. Ahmed, F.; Tamberg, G.; Le Moullec, Y.; Annus, P. Dual-Source Linear Energy Prediction (LINE-P) Model in the Context of WSNs. *Sensors* **2017**, *17*, 1666. [CrossRef] [PubMed]
6. Cammarano, A.; Petrioli, C.; Spenza, D. Online Energy Harvesting Prediction in Environmentally Powered Wireless Sensor Networks. *IEEE Sens. J.* **2016**, *16*, 6793–6804. [CrossRef]
7. Qureshi, H.K.; Saleem, U.; Saleem, M.; Pitsillides, A.; Lestas, M. Harvested Energy Prediction Schemes for Wireless Sensor Networks: Performance Evaluation and Enhancements. *Wirel. Commun. Mob. Comput.* **2017**, *2017*, 6928325.
8. Ismail, M.J.; Ibrahim, R.; Ismail, I. Adaptive Neural Network Prediction Model for Energy Consumption. In Proceedings of the 2011 3rd International Conference on Computer Research and Development, Shanghai, China, 11–13 March 2011; pp. 109–113.
9. Bergonzini, C.; Brunelli, D.; Benini, L. Algorithms for harvested energy prediction in batteryless wireless sensor networks. In Proceedings of the 2009 3rd International Workshop on Advances in sensors and Interfaces, Trani, Italy, 25–26 June 2009; pp. 144–149.
10. Kim, Y.; Shin, H.; Cha, H. Y-MAC: An energy-efficient multi-channel mac protocol for dense wireless sensor networks. In Proceedings of the 7th International Conference on Information Processing in Sensor Networks, St. Louis, MO, USA, 22–24 April 2008; IEEE Computer Society: Washington, DC, USA, 2008; pp. 53–63.
11. Pal, A.; Kant, K. On the Feasibility of Distributed Sampling Rate Adaptation in Heterogeneous and Collaborative Wireless Sensor Networks. In Proceedings of the 2016 25th International Conference on Computer Communication and Networks (ICCCN), Waikoloa, HI, USA, 1–4 August 2016.
12. Pal, A.; Nasipuri, A. Distributed Routing and Channel Selection for Multi-Channel Wireless Sensor Networks. *J. Sens. Actuator Netw.* **2017**, *6*, 10. [CrossRef]
13. Tang, C.; Raghavendra, C.S. *Compression Techniques for Wireless Sensor Networks*; Springer: Boston, MA, USA, 2004; pp. 207–231.
14. Pal, A.; Soibam, B.; Nasipuri, A. A distributed power control and routing scheme for rechargeable sensor networks. In Proceedings of the 2013 IEEE Southeastcon, Jacksonville, FL, USA, 4–7 April 2013.
15. Dehwah, A.; Elmetennani, S.; Claudel, C. UD-WCMA: An energy estimation and forecast scheme for solar powered wireless sensor networks. *J. Netw. Comput. Appl.* **2017**, *90*, 17–25. [CrossRef]

16. California Distributed Generation Statistics. Available online: http://www.caiso.com/market/Pages/ReportsBulletins/DailyRenewablesWatch.aspx (accessed on 4 April 2018).
17. Grid Data Download. Available online: http://www.elia.be/en/grid-data/data-download (accessed on 4 April 2018).
18. Butzer, P.L.; Splettstößer, W.; Stens, R.L. *The Sampling Theorems and Linear Prediction in Signal Analysis*; Lehrstuhl A für Math., Rheinisch-Westfälische Techn. Hochsch.: Aachen, Germany, 1986; Volume 328.
19. Kivinukk, A.; Tamberg, G. Subordination in generalized sampling series by Rogosinski-type sampling series. In Proceedings of the 1997 International Workshop on Sampling Theory and Applications, Aveiro, Portugal, 16–19 June 1997; pp. 397–402.
20. Kivinukk, A.; Tamberg, G. On Blackman-Harris windows for Shannon sampling series. *Sampl. Theory Signal Image Process.* **2007**, *6*, 87–108.
21. Kivinukk, A.; Tamberg, G. On Sampling Series based on Some Combinations of Sinc Functions. *Proc. Est. Acad. Sci. Phys. Math.* **2002**, *51*, 203–220.
22. Tamberg, G. On truncation error of some generalized Shannon sampling operators. *Numer. Algorithms* **2010**, *55*, 367–382. [CrossRef]
23. Albrecht, H.H. A family of cosine-sum windows for high resolution measurements. In Proceedings of the IEEE International Conference on Acoustics, Speech and Signal Processing, Salt Lake City, UT, USA, 7–11 May 2001; pp. 3081–3084.
24. Blackman, R.B.; Tukey, J.W. *The Measurement of Power Spectra*; Wiley-VCH: New York, NY, USA, 1958.
25. Harris, F.J. On the use of windows for harmonic analysis with the discrete Fourier transform. *Proc. IEEE* **1978**, *66*, 51–83. [CrossRef]
26. Meikle, H. *A New Twist to Fourier Tansforms*; John Wiley & Sons: Berlin, Germany, 2004.

CURRICULUM VITAE

Personal data

Name: Faisal Ahmed

Date of birth: 16.03.1980

Place of birth: Pakistan

Citizenship: Pakistan

Contact data

Address: 104 B, Raja 4D, 12611 Tallinn, Estonia

Phone: +372 58007448

E-mail: Faisal.Ahmed@ttu.ee

Education

Educational Institution	Year	Education
Tallinn University of Technology, Estonia	2014 – 2018	PhD, Electronics and Telecommunication
Blekinge Institute of Technology, Sweden	2006 – 2007	MSc (Master of Electrical Engineering)
Usman Institute of Technology, Karachi, Pakistan	1999 – 2004	B.E (Computer System Engineering)
PECHS Education Foundation Govt College, Karachi, Pakistan	1996 – 1998	Pre-Engineering (Intermediate)

Language competence

Urdu: Native

English: Fluent

Professional employment

2012-2014 Lecturer at IQRA University, Pakistan.

2010-2012 Network Administrator at Venus Pakistan, Pakistan.

ELULOOKIRJELDUS

Isikuandmed

Nimi: Faisal Ahmed

Sünniaeg: 16.03.1980

Sünnikoht: Pakistan

Kodakondsus: Pakistan

Kontaktandmed

Aadress: 104 B, Raja 4D, 12611 Tallinn, Estonia

Telefon: +372 58007448

E-mail: Faisal.Ahmed@ttu.ee

Hariduskäik

Haridusasutus	Aasta	Haridus
Tallinna Tehnikaülikool	2014 – 2018	PhD, elektroonika ja telekommunikatsioon
Blekinge Institute of Technology	2006 – 2007	Magister, info- ja telekommunikatsiooni-tehnoloogia
Usman Institute of Technology	1999 – 2004	Bakalaureus, arvutisüsteemid
PECHS Education Foundation Govt College, Karachi	1996 – 1998	Keskharidus

Keelteoskus

Urdu: emakeel

English: Kõrgtase

Teenistuskäik

2012-2014 õppejõud IQRA Ülikoolis, (Pakistan)

2010-2012 võrguadministraator, ettevõttes Venus Pakistan, (Pakistan)